UNIVERSITY OF CALIFORNIA
RIVERSIDE

Cellular, Molecular, and Circuit Mechanisms of Pathophysiology in Mouse Models of Fragile X Syndrome

A Dissertation submitted in partial satisfaction
of the requirements for the degree of

Doctor of Philosophy

in

Biomedical Sciences

by

Maham Rais

September 2021

Dissertation Committee:
Dr. Iryna M. Ethell, Chairperson
Dr. Khaleel A. Razak
Dr. Devin K. Binder

The Dissertation of Maham Rais is approved:

_____

_____

_____

Committee Chairperson

University of California, Riverside

Acknowledgements

Dr. Jonathan W. Lovelace, whose EEG findings of impaired resting gamma in forebrain excitatory neuron specific *Fmr1* KO mice provided the basis for this research. Klaus Nave (Göttingen, Germany) and Joshua Sanes (Harvard University, Boston, Massachusetts) for providing breeding pairs of Nex1(NeuroD6)-Cre mice. Dr. David Nelson (Baylor College of Medicine, Houston, Texas) for providing *Fmr1*^{Flox} and *Fmr1*^{FloxNeo} mice. Arnold Palacios, Xinghao S. Shuai, Steven Bishay, and Walker Woodard for assistance in generating and maintaining the mouse lines. Dr. Khaleel A. Razak for allowing me the use of his EEG surgery setup, and Dr. Devin K. Binder for access to the EEG recording rig. Dr. David Carter for advice on confocal microscopy. Dr. Patricia S. Pirbhoy, Dr. Anna O. Kulinich, Dr. Jeffrey Rumschlag, Samantha N. Sutley, Jamiela Kokash, and Stephen Brookshire for technical support. ASN Neuro and Cerebral Cortex, for the publication of much of the data presented here.

This work was supported by the National Institute of Health and the National Institute of Neurological Disorders and Stroke National Research Service Award Fellowship (1F31NS117178-01).

Dedication

I would like to thank my advisor Dr. Iryna Ethell for all her guidance, support and encouragement. When I joined her lab I had no experience in neuroscience research, but the motivation, direction and drive she gave me allowed me to learn a wide range of techniques and instilled a lasting interest in neuroscience and neurodevelopmental disorders. I would like to thank my dissertation committee members: Dr. Khaleel A. Razak and Dr. Devin K. Binder for taking time to advise me and provide me with instrumental feedback on my project. I would also like to thank all the members of the Ethell, Razak, and Binder labs for all their support in the completion of my dissertation research project.

I could not have completed my dissertation without the help of my family and friends. To my husband, Mark Wiley, who has been my rock from day one. Thank you for being my pillar of strength and support as I navigated through the highs and lows of my PhD. I would never have been able to complete this journey without you. To my parents, thank you for always encouraging me in my academic pursuits and for all the sacrifices you made to help me get to this stage of my life. To my sister, Joham Rais, thank you for always believing in me and lifting me up during the trying times of my dissertation research. And lastly, to my cat, Ivy, who is the light of my life and fills our home with an incredible amount of love and joy every day.

ABSTRACT OF THE DISSERTATION

Cellular, Molecular, and Circuit Mechanisms of Pathophysiology
in Mouse Models of Fragile X Syndrome

by

Maham Rais

Doctor of Philosophy, Graduate Program in Biomedical Sciences
University of California, Riverside, September 2021
Dr. Iryna M. Ethell, Chairperson

Fragile X Syndrome (FXS) is a neurodevelopmental disorder and the leading known genetic cause of autism spectrum disorder (ASD). Approximately 96% of individuals with ASD and FXS experience improper processing of sensory stimuli. Possible mechanisms attributed to this hyperarousal state include altered excitatory and inhibitory balance and impaired synaptic development. How these developmental changes impair sensory processing, neural responses and functions remain unclear. The major goal of my dissertation project is to identify the developmental mechanisms underlying the pathophysiology of FXS. Our previous studies have shown that elevated levels of Matrix Metalloproteinase-9 (MMP-9) contribute to the hyper-responsiveness of auditory cortex in *Fmr1* KO mice by affecting perineuronal net (PNN) formation around parvalbumin (PV)-expressing inhibitory interneurons. Abnormal development of PV neurons most likely contributes to abnormal electroencephalography (EEG)-based phenotypes of auditory hypersensitivity in the *Fmr1* KO mice that are remarkably similar

to those seen in humans with FXS. However, how the expression of *Fmr1* in different cell types shapes normal cortical responses during circuit development is not known.

Therefore, I investigated whether the disruption of communication between excitatory neurons and inhibitory PV cells was sufficient to trigger abnormal phenotypes using several mouse models. In the first part of this study, cell-specific deletion of *Fmr*1 was achieved in cortical excitatory neurons during early embryonic development. I demonstrated that embryonic deletion of *Fmr1* from cortical excitatory neurons did indeed trigger PV cell loss, abnormal cortical responses, and behavioral phenotypes in the auditory cortex of *Fmr1* KO mice. In the second part of this study, I examined whether conditional deletion (cOFF) or re-expression (cON) of *Fmr1* in excitatory neurons during the critical postnatal day (P)14-P21 period of PV cell development is sufficient to trigger or prevent abnormal phenotypes. Our results indicate that postnatal deletion or re-expression of FMRP in excitatory neurons is sufficient to elicit or ameliorate structural and functional cortical deficits as well as abnormal behavioral phenotypes in mice, informing future gene re-expression studies about appropriate treatment window and providing a new insight into the mechanism of cortical circuit dysfunctions in FXS. Lastly, with the discovery of FMRP in astrocytes, coupled with a role of astrocytes in synaptic function and inhibition in particular, it is possible that astrocytes contribute, in some capacity, to the impaired inhibition and circuit hyperexcitability seen in FXS. Therefore, in the third part of this study, I aimed to determine whether astrocyte-specific deletion of *Fmr1* during critical developmental period of inhibitory circuit maturation would alter GABAergic signaling and PV cell development leading to cortical

hyperexcitability and behavioral alterations. Our results demonstrate a profound role of astrocytic FMRP in the development of inhibitory circuits and shaping normal inhibitory responses.

Table of Contents

List of Figures

List of Tables

Abbreviations

AuC: Auditory cortex

Akt: Protein kinase B

ASD: Autism spectrum disorders

CA1: Cornu Ammonis 1region of the hippocampus

CPP: Critical period plasticity

cKO: Conditional knock out

CNS: Central nervous system

E/I: excitatory/inhibitory

ECM: extracellular matrix

EEG: Electroencephalogram

Ex: Excitatory neuron

FC: Frontal cortex

Fmr1: Fragile X mental retardation 1 gene

FMRP: Fragile X mental retardation protein

FXS: Fragile X Syndrome

GABA: γ-Aminobutryic acid

GAPDH: Glyceraldehyde 3-phosphate dehydrogenase

GFAP: Glial fibrillary acidic protein

ITPC: inter-trial phase coherence

KO: knock out

mGluR5: Metabotropic glutamate receptor 5

MMP-9: matrix metalloproteinase-9

mTOR: Mammalian target of rapamycin

P14-21: postnatal day 14-21

PNN: perineuronal nets

PSD95: postsynaptic density protein 95

PV: Parvalbumin

Pyr: Pyramidal neurons

STP: single trial power

vGAT: Vesicular GABA transporter

vGlut1:Vesicular glutamate transporter 1

WT: wild type

Chapter 1 – Introduction

Fragile X Syndrome (FXS) is a neurodevelopmental disorder that leads to intellectual deficits. It is the leading known genetic cause of autism spectrum disorder (ASD). ASD and FXS individuals exhibit deficits in social behavior, delays in language development, and sensory over-responsivity. In fact, approximately 96% of individuals with ASD and FXS experience improper processing of sensory stimuli. Possible mechanisms attributed to this hyperarousal state include altered excitatory and inhibitory balance and impaired synaptic development. These alterations arise early in development and lead to lifelong disability. How these developmental changes impair sensory processing, neural responses and functions remain unclear. The major goal of my dissertation research is to identify the developmental mechanisms underlying cortical hyperexcitability in FXS. Our understanding of how different cell types contribute to the cortical deficits observed in FXS and the time period during which these deficits manifest may offer relatively simple measures to correlate neural responses/behavior with cellular mechanisms and allow for the development of more targeted therapies.

Fragile X Syndrome (FXS)

Fragile X Syndrome (FXS) is the most prevalent cause of inherited intellectual disability and is a leading genetic cause of autism (Crawford, Acuña, & Sherman, 2001). FXS affects 1 in 4,000 boys and 1 in 8,000 girls and is caused by the silencing, deletion, or loss-of-function mutation of the *FMR1* gene. As a result, its protein product, Fragile X Mental Retardation Protein (FMRP), is either not expressed or is non-functional (Okray et al., 2015; Sutcliffe et al., 1992; Verkerk et al., 1991). FMRP is an mRNA-binding

protein (Ashley, Wilkinson, Reines, & Warren, 1993) that regulates several aspects of mRNA metabolism such as nuclear export, transport to synaptic terminals, activity-dependent ribosome stalling and protein translation (Bagni & Greenough, 2005; Bassell & Warren, 2008; Darnell et al., 2011; Laggerbauer, Ostareck, Keidel, Ostareck-Lederer, & Fischer, 2001; Santoro, Bray, & Warren, 2012).

FMRP regulates translation of mRNAs at synapses, some of which encode proteins involved in synaptic plasticity (V. Brown et al., 2001; Zalfa et al., 2003). The absence of FMRP leads to the dysregulation of protein translation and increased protein synthesis (Bear, Huber, & Warren, 2004; Darnell & Klann, 2013), which may contribute to altered metabotropic glutamate receptor 5 (mGluR5) signaling resulting in exaggerated long-term depression (LTD) in the hippocampus (Huber, Gallagher, Warren, & Bear, 2002). FMRP also negatively regulates matrix metalloproteinase-9 (MMP-9) translation in neurons (Dziembowska et al., 2013; Dziembowska & Wlodarczyk, 2012; Janusz et al., 2013), and MMP-9 levels are elevated in FXS (Bilousova et al., 2009; Gkogkas et al., 2014; Sidhu, Dansie, Hickmott, Ethell, & Ethell, 2014). mGluR5 and MMP-9 may mediate changes in synaptic functions by signaling through the PI3K/Akt/mTORC1 and MEK/ERK pathways to increase cap-dependent translation (Antion, Hou, Wong, Hoeffer, & Klann, 2008; Banko, Hou, Poulin, Sonenberg, & Klann, 2006; Ferraguti, Baldani-Guerra, Corsi, Nakanishi, & Corti, 1999; Gallagher, Daly, Bear, & Huber, 2004; Hou et al., 2006; Hou & Klann, 2004; Klann & Dever, 2004; Ronesi & Huber, 2008; Sharma et al., 2010). Recent data suggest that FMRP may also regulate the activity of these translational control pathways directly through its other targets, such as

phosphatidylinositide-3-kinase enhancer (PIKE), phosphatase and tensin homolog (PTEN), neurofibromin 1 (NF1), and tuberous sclerosis 2 (TSC2), which regulate phosphatidylinositide-3-kinase (PI3K) and mammalian target of rapamycin complex 1 (mTORC1) signaling (Enriquez-Barreto & Morales, 2016; Sato, 2016; Sharma et al., 2010). In addition, extracellular signal-regulated kinase 1 (ERK1), all three eukaryotic translation initiation factor 4 G (eIF4G) isoforms, eukaryotic translation elongation factor 1 and 2 (eEF1 and eEF2), argonaute proteins (Ago1/2), and Dicer are FMRP targets and their dysregulation may contribute to enhanced neuronal translation in FXS (Cheever & Ceman, 2009; Darnell et al., 2011; Muddashetty et al., 2011) (**Figure 1.1**).

Dysregulated PI3K/mTOR signaling, enhanced mGluR5-dependent LTD, increased MMP-9 activity and reduced activity of the voltage and Ca^{2+} activated K^{+} (BKCa or BK) channel may contribute to the immature dendritic spine morphology in rodent models of FXS (Hou & Klann, 2004; Hu et al., 2008; Huber, Kayser, & Bear, 2000; Nimchinsky, Oberlander, & Svoboda, 2001; Sidhu et al., 2014; Vanderklish & Edelman, 2002). In mice, FMRP may also regulate neuronal branching (Galvez, Gopal, & Greenough, 2003) as well as dendritic spine development (Nimchinsky et al., 2001). Consistent with animal work, clinical studies revealed alterations in dendritic spine number and morphology in the cortex of FXS humans, with a prevalence of immature dendritic spines (Hinton, Brown, Wisniewski, & Rudelli, 1991; Irwin et al., 2001) (**Figure 1.1**). In fact, dendritic abnormalities are consistent anatomical correlates of intellectual disability (Kaufmann & Moser, 2000). Although most of FMRP activity is considered to be related to the regulation of synaptic functions (Darnell et al., 2011;

Edbauer et al., 2010; Y. Q. Zhang et al., 2001), little is known about how the synaptic alterations in the absence of FMRP may lead to deficits in neurophysiology and behavior in humans with FXS. Abnormal dendritic spine development alone cannot explain increased cortical excitability observed in FXS.

FMRP loss increases network-level hyperexcitability in the rodent cortex through impaired inhibition and altered neural synchrony (Gonçalves, Anstey, Golshani, & Portera-Cailliau, 2013; Y. Zhang et al., 2014). The *Fmr1* KO mouse shows decreased GABA receptor levels, decreased GABA synthesis, increased GABA catabolism, and overall decreased GABAergic input in many regions of the brain (Adusei, Pacey, Chen, & Hampson, 2010; Curia, Papouin, Séguéla, & Avoli, 2009; D'Hulst et al., 2006; D'Hulst et al., 2009; El Idrissi et al., 2005; Liu et al., 2013; Selby, Zhang, & Sun, 2007). FMRP was also shown to regulate neuronal excitability through the direct interactions with several ion channels, such as sodium-activated potassium channel Slack, presynaptic N-type voltage-gated calcium channels and calcium-activated potassium BK channels (M. R. Brown et al., 2010; Deng et al., 2013; Ferron, Nieto-Rostro, Cassidy, & Dolphin, 2014; Hébert et al., 2014; Myrick et al., 2015; Y. Zhang et al., 2012). The enhanced excitability is associated with neurological symptoms observed in FXS, such as hypersensitivity, hyperarousal, hyperactivity, anxiety, and seizures (Braat & Kooy, 2015; Penagarikano, Mulle, & Warren, 2007) (**Figure 1.1**). However, limited knowledge of the neuronal circuits underlying complex behaviors, such as anxiety and communication deficits, have hindered the progress in translating the results of the mouse studies into successful clinical trials. Potential mechanisms of altered neuronal circuit excitability and

how these changes might impact sensory perception and behavior in FXS are beginning to be understood. In this review, we bring together clinical, functional, and neuroanatomical studies that outline auditory, visual, and somatosensory processing deficits in FXS and how understanding these mechanisms using pre-clinical studies in animal models can help our search for new therapeutic applications in FXS.

Animal models of FXS

To understand the molecular and cellular pathogenesis of FXS, the disease has been successfully modeled in rodents (Bakker et al., 1994; Eadie et al., 2009; Hamilton et al., 2014), Drosophila (Pan, Woodruff, Liang, & Broadie, 2008) and zebrafish (den Broeder et al., 2009). The mouse *Fmr1* gene product shows 97% homology to human FMRP (Ashley, Sutcliffe, et al., 1993). The *Fmr1* knockout (KO) mouse model was generated with phenotypes similar to those observed in human FXS patients, like progressive macroorchidism (Bakker et al., 1994) and abnormal dendritic spine development (Nimchinsky et al., 2001). *Fmr1* KO mice also demonstrate impaired cognitive functions and aberrant behaviors (Hayashi et al., 2007; Yan, Rammal, Tranfaglia, & Bauchwitz, 2005). More robust cognitive deficits have been identified in studies of memory extinction that include inhibitory avoidance paradigm, trace fear conditioning and lever-press escape/avoidance tasks (Brennan, Albeck, & Paylor, 2006; Dölen et al., 2007; Eadie et al., 2009; Hayashi et al., 2007; Zhao et al., 2005). Susceptibility to age-dependent audiogenic seizures is another reproducible phenotype observed in *Fmr1* KO mice (Chen & Toth, 2001; Dölen et al., 2007; Yan et al., 2005). The mouse FXS model is also tractable for electrophysiology experiments to define the

synaptic alterations associated with FXS. *Fmr1* KO hippocampal neurons show enhanced metabotropic glutamate receptor (mGluR5) dependent long-term depression (LTD) (Huber et al., 2002). Other studies have shown deficits in long-term potentiation (LTP) in the hippocampus, cortex and the lateral amygdala (Desai, Casimiro, Gruber, & Vanderklish, 2006; Larson, Jessen, Kim, Fine, & du Hoffmann, 2005; Li, Pelletier, Perez Velazquez, & Carlen, 2002; Volk, Pfeiffer, Gibson, & Huber, 2007; Wilson & Cox, 2007; Zhao et al., 2005), suggesting alterations in synaptic plasticity that may underlie deficits in experience-dependent brain functions in FXS.

The development of the *Fmr1* KO rat model allows for modeling more complex cognitive and social behaviors associated FXS (Hamilton et al., 2014). It also provides an opportunity for comparison of phenotypes across mammalian species that result from FMRP deletion. Similar to mouse studies, mGluR-LTD was enhanced in *Fmr1* KO rats, whereas mGluR LTP was significantly decreased at both cortical and thalamic inputs to the lateral amygdala (Jackson, 2017). Adult *Fmr1* KO rats also showed disrupted cortical processing of auditory stimuli (Engineer et al., 2014), recapitulated spine density and synaptic plasticity defects observed in mouse models, and displayed deficits in hippocampal forms of associative recognition memory (Till et al., 2015), and novel social interaction phenotypes (Hamilton et al., 2014). Juvenile *Fmr1* KO rats exhibit abnormal cortical state regulation that begins at ages equivalent to human birth (Berzhanskaya et al., 2017). Despite largely normal patterns of spontaneous activity during the first two postnatal weeks before eye opening, *Fmr1* KO rats exhibit signs of mild hyper-excitability during the third and fourth postnatal weeks, including an increase in the

visually-evoked firing of excitatory neurons and reduced firing of inhibitory neurons (Berzhanskaya et al., 2017).

Similar to the rodent models of FXS, the fruit fly (Drosophila) is a powerful genetic model organism for study of FXS. The single FMRP homolog, dFMRP, is well conserved to human FMRP with respect to its functional amino acid motifs (Wan, Dockendorff, Jongens, & Dreyfuss, 2000) and RNA-binding properties (Darnell et al., 2005). The fly FXS model system has collectively yielded much insight into the cognitive, behavioral and morphological phenotypes associated with FXS. Morphological analyses of fly neurons have identified defects in axons and dendrites of specific neuronal subsets, in particular in the neuromuscular junction (NMJ) and the mushroom body. In the absence of *dFmr1* activity, the axons within the NMJ display significant increase in synaptic boutons and branching (Y. Q. Zhang et al., 2001). Neurons in the mushroom body, a brain area that is required for short-term and long-term memory, are also affected in *dFmr1* mutants (McBride et al., 1999; Pascual & Préat, 2001; Zars, Fischer, Schulz, & Heisenberg, 2000). Moreover, long-term memory defects have been reported in *dFmr1* mutants using olfactory-based assays (Bolduc, Bell, Cox, Broadie, & Tully, 2008). dFMRP has also been shown to be necessary for long-term, but not short-term olfactory habituation, as indicated by an olfactory avoidance task (Sudhakaran et al., 2014). Electrophysiology analysis also shows defects in synaptic transmission in the optic lobe (Y. Q. Zhang et al., 2001). In addition to axonal, dendritic and synaptic transmission defects, male *dFmr1*-null flies also have enlarged testes, a phenotype that is observed in both FXS humans and *Fmr1* KO mice (Y. Q. Zhang et al., 2004). Similar to *Fmr1* KO

mice (J. Zhang et al., 2008), *dFmr1*-null flies lack the ability to maintain a normal circadian rhythm when placed in total darkness, and exhibit erratic patterns of locomotor activity (Dockendorff et al., 2002; Inoue et al., 2002; Morales et al., 2002; Xu, Poidevin, Han, Bi, & Jin, 2012). They also lack interest in courtship (Dockendorff et al., 2002), a social impairment similar to that found in autism. Furthermore, FXS flies exhibit strongly impaired olfactory behaviors. The absence of dFMRP results in reduced olfactory attraction and aversion. Calcium imaging data show that antennal lobe projection neurons have broader odor tuning in *dFmr1* flies, leading to reduced specificity in odor coding and alterations in olfactory representations. Consistent with these results, lateral inhibition across olfactory glomeruli, as well as the inhibitory connections between local interneurons and projection neurons are impaired in *dFmr1* flies (Franco, Okray, Linneweber, Hassan, & Yaksi, 2017). This suggests that absence of dFMRP leads to defective lateral inhibition across olfactory glomeruli, which, in turn, results in impaired odor coding and olfactory behaviors. Thus, the fly FXS model displays significant social, cognitive, and sensory deficits that can be used to examine the underlying mechanisms.

Zebrafish is a more recent animal model that has shown potential as a complementary vertebrate model in studying the pathophysiology of FXS. The adult zebrafish FMRP shares 72% amino acid identity with human FMRP, and is highly expressed in the brain, including in the telencephalon, diencephalon, metencephalon and cerebellum, and spinal cord (van 't Padje et al., 2005). In adult zebrafish, *Fmr1* KO produces the anxiolytic-like responses of increased exploratory behavior in light/dark and open-field tests and avoidance learning impairment, indicating that hyperactivity and

anxiety can be also tested in *Fmr1* KO zebrafish. Furthermore, electrophysiological recordings from telencephalic slice preparations of *Fmr1* KO zebrafish displayed markedly reduced LTP and enhanced LTD compared to wild-type counterparts (Ng, Yang, & Lu, 2013). Animal models of FXS have a great potential for elucidating mechanisms underlying cognitive, behavioral and morphological phenotypes associated with FXS, as well as pre-clinical studies.

Auditory hypersensitivity and underlying mechanisms

Auditory hypersensitivity is common in humans with FXS and mouse models of FXS (S. E. Rotschafer & Razak, 2014; Sinclair, Oranje, Razak, Siegel, & Schmid, 2017). Notably, studies indicate abnormalities in auditory processing in people with FXS (Castrén, Pääkkönen, Tarkka, Ryynänen, & Partanen, 2003; Rojas et al., 2001; Schneider et al., 2013; St Clair, Blackwood, Oliver, & Dickens, 1987; Van der Molen et al., 2012a, 2012b). Tone-evoked responses measured using magnetic fields are higher in the auditory cortex of humans with FXS (Rojas et al., 2001). Increased activation of left hemispheric circuitry, including superior temporal gyrus, was observed in FXS subjects during auditory temporal discrimination task (Hall, Walter, Sherman, Hoeft, & Reiss, 2009). To assess sensory-cognitive processing in humans with FXS, various event-related brain potential (ERP) techniques have been employed. ERPs reflect the activity of neuronal populations in response to specific sensory-cognitive processes and can be detected using electro-encephalograms (EEG) and magneto-encephalograms (MEG) (Luck, 2014). A relatively simple auditory stimulus can elicit a N1 wave in the auditory cortex. Auditory ERP studies report abnormally high amplitude of the N1 wave in response to tones, and

reduced habituation to repeated sound in FXS (Castrén et al., 2003; Ethridge et al., 2016; Rojas et al., 2001; Schneider et al., 2013; Van der Molen et al., 2012a, 2012b). FXS patients also exhibit increased gamma frequency band power during resting state. This increased gamma activity is believed to be linked to increased neural excitability, and examining the relationship of alpha and theta band activity with gamma band activity might provide system-level understanding about the altered balance between excitatory and inhibitory activity (J. Wang et al., 2017). Furthermore, a recent study shows that humans with FXS demonstrate a marked reduction in the ability to synchronize evoked high-frequency neural activity to time varying signals suggesting impairments in underlying neural generators involved in sensory processing (Ethridge et al., 2017). These data indicate a 'noisy resting state' of sensory cortex in people with FXS that may lead to abnormal synchronization of evoked responses. Auditory cortex processing abnormalities that arise early in development may contribute to higher order auditory functional deficits such as language deficits seen in FXS and autism (Barnes et al., 2009; Finestack, Richmond, & Abbeduto, 2009; Nieto Del Rincón, 2008; J. E. Roberts, Mirrett, & Burchinal, 2001; T. P. Roberts et al., 2011). However, very little is known about development of EEG/MEG abnormalities and correlations with language development in humans.

Fmr1 KO mice also exhibit abnormal pre-pulse inhibition and auditory startle responses, with greater startle responses than WT mice to low intensity (80 dB) white noise bursts and decreased responses to high intensity (120 dB) white noise bursts (Nielsen, Derber, McClellan, & Crnic, 2002). *Fmr1* KO mice are also acoustically

hypersensitive and are prone to audiogenic seizures (Chen & Toth, 2001; Frankland et al., 2004; Miller et al., 1999; Nielsen et al., 2002), suggesting enhanced excitability in the auditory system. Intense auditory stimuli (>100 dB SPL) induces a period of wild running, clonic – tonic seizing, and can result in the death of the animal (Chen & Toth, 2001; Dansie et al., 2013; Musumeci et al., 2000; Musumeci et al., 2007). Reintroduction of FMRP to *Fmr1* KO mice significantly reduces audiogenic seizure susceptibility (Musumeci et al., 2007). In addition, the audiogenic seizure phenotype of *Fmr1* KO mice is prevented by the systemic administration of the mGluR5 receptor antagonist, MPEP (Yan et al., 2005). Enhanced susceptibility to audiogenic seizures is a robust phenomenon in *Fmr1* KO mice and is one of the most widely used outcome measures in pre-clinical drug discovery studies. The auditory brainstem expresses high FMRP levels (Y. Wang et al., 2014) and abnormal sensory processing at the level of the auditory brainstem may underlie the enhanced susceptibility to audiogenic seizures. FMRP interactions with sodium-activated potassium channel Slack in the auditory brainstem and its ability to regulate Slack activity may also explain increased excitability in the auditory brainstem of *Fmr1* KO mice (M. R. Brown et al., 2010). In addition, *Fmr1* KO mice show enhanced acoustic startle responses (Chen & Toth, 2001; Frankland et al., 2004; Nielsen et al., 2002; Yun et al., 2006). Abnormal habituation of acoustic startle responses, which is accompanied with hypersensitivity or hyposensitivity to sensory stimuli, was also shown to be dependent on BK channel functions (Zaman et al., 2017). BK channels can directly interact with FMRP and their functions are affected by the loss of FMRP (Deng et al., 2013), whereas the upregulation of BK channel activity in a mouse model of FXS was

shown to normalize the enhanced glutamate release and excessive epileptiform activity (Deng & Klyachko, 2016). However, the mechanisms by which the absence of FMRP in the specific brain areas, such as brainstem or cortex leads to the enhanced excitability need to be further studied in order to better understand the epileptic phenotype of FXS.

In vivo recordings from the auditory cortex show that the abnormal cortical processing may underlie auditory hypersensitivity in *Fmr1* KO mouse (S. Rotschafer & Razak, 2013). First, single unit recordings show that cortical neurons respond to tones with more action potentials in *Fmr1* KO mice than WT neurons in both adults (S. Rotschafer & Razak, 2013) and P21 mice (Wen et al., 2017). The increased responses are due to prolonged firing of action potentials well after stimulus offset. Second, there is also increased variability of spike timing, broader frequency receptive fields and reduced spectrotemporal selectivity in the *Fmr1* KO cortex. The broader receptive fields mean that more neurons will be activated synchronously for any given sound in the KO cortex. Third, recordings from KO mice cortex to repeated sound presentation shows reduced habituation of response amplitudes. Together these findings suggest that hypersensitivity arises due to a 'triple hit' – increased response per neuron, more number of responsive neurons and reduced habituation of responses.

Remarkably similar EEG phenotypes are also present in Fmr1 KO mice and humans with FXS (Jonathan W Lovelace, Ethell, Binder, & Razak, 2018; Sinclair, Featherstone, et al., 2017; Sinclair, Oranje, et al., 2017). Lovelace *et al.* recorded EEG signals from both auditory and frontal cortex of awake, freely moving mice and compared the WT and *Fmr1* KO genotypes. They identified increased gamma power in

baseline EEG, reduced evoked phase synchronization to auditory stimuli in the gamma band and larger ERP N1 component amplitudes in the KO mice (Jonathan W Lovelace et al., 2018). These data are essentially identical to findings in humans with FXS (Ethridge et al., 2017; J. Wang et al., 2017). Together these data support the notion that there is a milieu of 'noisy resting state' in the auditory cortex in FXS in addition to the triple hit mentioned earlier giving rise to auditory hypersensitivity.

Most studies on humans with FXS have focused on older children and/or adolescents. However, abnormalities in auditory processing may arise from altered critical period plasticity during development. In the auditory cortex, *Fmr1* KO mice show abnormal critical period plasticity in response to developmental tone exposure (Kim, Gibboni, Kirkhart, & Bao, 2013), which effectively reduces activity- or experience-evoked responses of neuronal networks. The impaired sound exposure-induced cortical map plasticity in the *Fmr1* KO mice may extend into adulthood affecting stability of auditory circuits and may underlie the abnormalities found in the adult auditory cortical responses (S. Rotschafer & Razak, 2013). We have proposed a specific mechanism for development of auditory hypersensitivity in the *Fmr1* KO mice (Wen et al., 2017). Impaired development of parvalbumin (PV)-expressing inhibitory interneurons may underlie abnormal auditory processing in *Fmr1* KO mice via MMP-9-dependent regulation of perineuronal nets (Wen et al., 2017). In normal brain, the development of PV interneurons is implicated in shaping critical period plasticity, stabilization of synaptic networks and network synchronization (Hensch, 2005; Jeevakumar & Kroener, 2016), whereas perineuronal net loss around PV cells is associated with abnormal critical

period plasticity and reduced excitability of PV cells (Balmer, 2016; Lensjø, Lepperød, Dick, Hafting, & Fyhn, 2017; Pizzorusso et al., 2002). The formation of perineuronal nets, which consists of extracellular matrix proteins, coincides with the closure of critical period plasticity window creating a non-permissive environment for new synapse growth and structural plasticity. A disruption of extracellular matrix affects the stability of existing circuits and opens critical period plasticity window, which may underlie auditory hyperexcitability in FXS (Happel & Frischknecht, 2016). Studies have reported higher MMP-9 activity in *Fmr1* KO mouse brains and humans with FXS, suggesting that MMP-9 dysregulation may contribute to FXS-associated deficits (Bilousova et al., 2009; Gkogkas et al., 2014; Sidhu et al., 2014). The increased MMP-9 activity may delay the maturation of cortical circuits and extend critical period plasticity past the normal developmental window affecting the maturation of functional circuits.

The role of MMP-9 up-regulation in FXS symptoms is supported by the fact that the genetic reduction of MMP-9 activity in the brain of *Fmr1* KO mice restored auditory responses and the formation of perineuronal nets around PV cells in the *Fmr1* KO mice to WT levels (Wen et al., 2017). MMP-9 deletion in the *Fmr1* KO mice also reversed ERP N1 amplitude habituation deficits (J. W. Lovelace et al., 2016). As genetic deletion of MMP-9 can also reverse FXS-associated behaviors in *Fmr1* KO mice (Bilousova et al., 2009; Sidhu et al., 2014), MMP-9 is an attractive therapeutic target to reduce sensory deficits in FXS and potentially other FXS-associated behaviors. Indeed, minocycline, which beside its antibiotic effects, inhibits MMP-9, has emerged as a potential treatment for FXS (Bilousova et al., 2009; Dansie et al., 2013; Dziembowska et al., 2013; Leigh et

al., 2013; Paribello et al., 2010; S. E. Rotschafer & Razak, 2014; Schneider et al., 2013; Yau et al., 2018). In humans with FXS, minocycline can reduce MMP-9 levels, reverse auditory ERP deficits and improve FXS-associated behaviors (Dziembowska et al., 2013; Leigh et al., 2013; Paribello et al., 2010; Schneider et al., 2013). However, several adverse effects of minocycline, such as stained teeth, skin pigmintation, gastrointestinale disturbance, drug-induced lupus and autoimmune hepatitus, are associated with its antibiotic properties, limiting its chronic use in humans (Abe et al., 2003; Akin, Miller, & Tucker, 1998; Ang, Zimmerman, & Malkin, 2002; A. Cascio et al., 2004; Edition, 1994; Eisen & Hakim, 1998; LaPorta, Nikitakis, Sindler, & Reynolds, 2005; Lawson, Amos, Bulgen, & Williams, 2001; Porter & Harrison, 2003; Sánchez, Rogers, & Sheridan, 2004; Schlienger, Bircher, & Meier, 2000; Shepherd, 2002; Shetty, 2002; Smith & Leyden, 2005; Teitelbaum, Perez-Atayde, Cohen, Bousvaros, & Jonas, 1998; Tournigand et al., 1999). Therefore, there is an unmet need in developing novel, potent and selective MMP-9 inhibitors to treat auditory hypersensitivity associated with FXS and potentially other neurodevelopmental disorders associated with sensory hypersensitivity, such as autism.

Taken together, studies of auditory processing and sensitivity in humans with FXS and *Fmr1* KO mice show remarkable overlap in phenotypes, providing a translation relevant framework for both mechanism and drug discovery. It must be noted that FMRP is expressed in multiple nuclei of the auditory system (Zorio, Jackson, Liu, Rubel, & Wang, 2017), and cortical processing deficits may be intrinsic to cortical changes and/or inherited from subcortical sites (Garcia-Pino, Gessele, & Koch, 2017; S. E. Rotschafer & Cramer, 2017; S. E. Rotschafer, Marshak, & Cramer, 2015; Strumbos, Brown,

Kronengold, Polley, & Kaczmarek, 2010). How multiple regions of the auditory system contribute to symptoms that range from hypersensitivity to language and communication deficits is not understood and is an important direction for future studies. The availability of mouse models in which the protein can be removed from specifc neuron types, regions and time points will aid such future studies.

Visual-motor deficits

A prominent feature of the FXS neurobehavioral phenotype is diminished performance on neuropsychological tasks that assess visual-motor function. Visuomotor dysfunction have been described for tasks that require drawing skills (Crowe & Hay, 1990; Freund & Reiss, 1991), tasks that involve manipulation of blocks to construct abstract designs (Cornish, Munir, & Cross, 1999; Crowe & Hay, 1990) and tasks requiring psychomotor coordination (Cornish et al., 1999). Although these tasks are multifactorial in nature and the performance affected by many causes, visual-motor ability is a common feature. This led to the hypothesis that the visual-motor deficiencies observed in FXS may reflect underlying neuroanatomical and functional abnormalities specific to the thalamic component of one of the two main parallel visual pathways called the magnocellular (M) pathway (Kogan, Boutet, et al., 2004). Dysfunctions of the pathway may lead to impaired visually guided actions requiring the manipulation of objects, further explaining why individuals with FXS perform poorly on a variety of neuropsychological tasks that have a visual-motor component.

Additional behavioral studies in infants and toddlers with FXS have documented impairments in processing texture-defined motion stimuli (Farzin, Whitney, Hagerman,

& Rivera, 2008), temporal flicker (Farzin, Rivera, & Whitney, 2011), perceiving the ordinality of sequences of numerical displays (Owen, Baumgartner, & Rivera, 2013), and the ability to maintain the identity of dynamic object information during occlusion (Farzin & Rivera, 2010). Impaired performance has also been demonstrated on tasks requiring inhibitory control (Scerif, Cornish, Wilding, Driver, & Karmiloff-Smith, 2007) as well as numerical reasoning (Murphy, Mazzocco, Gerner, & Henry, 2006; Rivera, Menon, White, Glaser, & Reiss, 2002). One possible reason behind the visual-spatial and numerical deficits seen in FXS is disruption of the so-called dorsal stream (occipito-parietal visual pathway, projecting to the posterior-lateral parietal cortex, which processes information involved in guiding actions, including spatial location and motion) with relative sparing of the ventral stream (occipito-temporal visual pathway, projecting to the inferior temporal cortex, which processes object features such as form and color) (Milner & Goodale, 2006; Ungerleider, 1982). Because of its relatively prolonged time course of development (Atkinson, 2002), the dorsal stream is thought to be particularly vulnerable to atypical development in a number of disorders, including FXS (Farzin & Rivera, 2010; Kogan, Bertone, et al., 2004).

Vision integration is affected in humans with FXS with alteration of spatiotemporal visual processing, reduction of contrast sensitivity for visual stimuli presented at high temporal frequencies, and visual sensitivity for both static and moving images (Farzin et al., 2011; Kogan, Boutet, et al., 2004). These deficits may be associated with a delayed development in the primary visual cortex as seen in the model of FXS pre-mutation (Berman, Murray, Arque, Hunsaker, & Wenzel, 2012). However, before being

integrated at the cortex level, the visual signals are detected, processed and transmitted by the retina. *Fmr1* deficiency has been shown to affect retinal function, with abnormal wiring of neuronal connections and synaptic destabilization in the retina leading to similar cellular and functional phenotypes as seen in the brain (Rossignol et al., 2014). Since animal behaviors rely on sensory processing (which allows mice to integrate environmental stimuli and to adapt their action), this makes one wonder how far retinal defects, as opposed to cortical processing defects, are involved in the recorded behavioral impairments seen in *Fmr1* KO mice, like visuospatial deficits, diminished performance on neuropsychological tasks that assess visuomotor function, and impairments in processing texture-defined motion stimuli.

Enhanced mGluR5 signaling may contribute to sensory impairments seen in *Fmr1* KO mice as mGluR5 signaling is down-regulated during normal maturation and synaptic stabilization in the postnatal brain (Dudek & Bear, 1989). Indeed, using genetic approach, Dölen *et al.* have shown the importance of mGluR5, as well as FMRP, in the regulation of ocular dominance plasticity during the development of visual cortex (Dölen et al., 2007). A 50% reduction in mGluR5 expression prevents ocular dominance plasticity induced by a 3-day monocular deprivation, suggesting that this receptor normally serves to enable plasticity in the visual cortex. In contrast, in the absence of FMRP, *Fmr1* KO mice show altered ocular dominance plasticity (Dölen et al., 2007). The response to monocular deprivation is characterized by both deprived-eye response depression and open-eye response potentiation, suggesting that FMRP normally serves to restrict plasticity in the visual cortex (Dölen & Bear, 2008). Interestingly, since ocular

dominance plasticity is protein synthesis dependent (Taha & Stryker, 2002), it is a possibility that excessive protein synthesis is responsible for altered plasticity in the visual cortex of *Fmr1* KO mice.

Lastly, by examining the visual cortices in *Fmr1* KO mice as well as those in the individuals with FXS, multiple studies have shown that FMRP is critical to the pruning and maturation of dendritic spines (Churchill et al., 2002; Greenough et al., 2001; Irwin et al., 2001). Neurons lacking FMRP retain characteristically immature dendritic spines within the visual cortex (Kogan, Boutet, et al., 2004). Furthermore, the density of immature spines is elevated in FXS humans compared with normal control brains. Interestingly, this immature spine phenotype is also induced by the activation of Gp1 mGluRs in the visual cortical pyramidal neurons (Vanderklish & Edelman, 2002). Spine density is significantly increased in *Fmr1* KO mice and the phenotype can be rescued by 50% reduction in mGluR5 expression (Dölen et al., 2007). This indicates that the absence of FMRP and the upregulation of mGluR5 may therefore lead to abnormal development of visual circuits and potentially impaired processing of visual stimuli.

Somatosensory processing deficits and tactile defensiveness

Impaired processing of tactile information is seen in individuals with FXS, with hypersensitivity to touch being common (C. J. Cascio, 2010). The *Fmr1* KO mouse model has phenotypes similar to those observed in humans with FXS (van den Ouweland et al., 1994). In mice, tactile information received through deflections of whiskers is processed in the somatosensory barrel cortex (Diamond & Arabzadeh, 2013; Diamond, von Heimendahl, Knutsen, Kleinfeld, & Ahissar, 2008; Feldmeyer et al., 2013). Correct

processing of whisker-mediated touch information requires the formation of receptive fields in the somatosensory cortex (Simons, 1978; Simons & Carvell, 1989). Development of intra-cortical connections plays a key role in the formation of the receptive fields and depends on sensory experience (Allen, Celikel, & Feldman, 2003; Bender, Allen, Bender, & Feldman, 2006). Exposure of juvenile animals to patterned sensory input refined the balance of excitation and inhibition (Dorrn, Yuan, Barker, Schreiner, & Froemke, 2010; Sun et al., 2010), resulting in receptive field and sensory map reorganization and a long-lasting impact on sound perception (Han, Köver, Insanally, Semerdjian, & Bao, 2007). Therefore, the enlarged receptive fields in *Fmr1* KO mice may be a consequence of altered sensory integration during the early postnatal development.

In vivo recordings from barrel cortex revealed that *Fmr1* KO mice show an enlargement in the cortical area activated by whisker deflections, i.e., an expansion of the somatosensory maps in L2/3. Furthermore, the encoding of tactile stimuli at different frequencies was severely impaired in layer 2/3 as well (Juczewski et al., 2016). These findings highlight neuronal mechanisms that could contribute to the different exploratory behavior like “tactile defensiveness” or “tactile sensitivity” (Baranek, Foster, & Berkson, 1997; Baranek et al., 2008; Miller et al., 1999; Reiss & Freund, 1990), which is observed in *Fmr1* KO mice (Arnett, Herman, & McGee, 2014; Santos, Kanellopoulos, & Bagni, 2014). Furthermore, a decrease in the whisker selectivity index (WSI) is evident in *Fmr1* KO mice over a range of stimulation parameters indicating that the specificity with which deflection of a given whisker activates cortex has decreased (Juczewski et al., 2016).

Moreover, there are profound alterations in the neuronal excitability in layer 4 of somatosensory barrel cortex in the *Fmr1* KO mouse at the synaptic, cellular, and network levels. Gibson *et al.*'s work on *Fmr1* KO mice somatosensory cortex has shown that there is a decrease in connectivity frequency and strength resulting in an approximate 50% reduction in excitatory drive onto fast-spiking (FS) inhibitory interneurons. Additionally, excitatory neurons become intrinsically more excitable in the KO mice. These changes can lead to hyperexcitable circuits, a hypothesis which was supported by observed increase in UP state duration in somatosensory cortex of *Fmr1* KO mice (Gibson, Bartley, Hays, & Huber, 2008). Consistent with impaired FS inhibitory circuitry, network synchrony within a single cortical column during the UP state is decreased as well (Gibson et al., 2008). Similar to our findings in the auditory cortex (Wen et al., 2017), there is a significant reduction in PV immunoreactivity in the somatosensory cortex of adult *Fmr1* KO mice (Selby et al., 2007). PV interneurons receive both intracortical and thalamic excitatory inputs, which develop during the cortical critical period (Chittajallu & Isaac, 2010; Daw, Ashby, & Isaac, 2007). A recent study has shown that there is a significant delay in the formation of excitatory contacts onto FS interneurons which likely has a large impact on the integration of feedforward inhibitory circuits in the developing somatosensory cortex of *Fmr1* KO mice (Nomura et al., 2017).

Gonçalves *et al.* showed that *Fmr1* KO mice exhibit abnormally high synchrony of neocortical network activity in mouse somatosensory cortex, especially during development. Neuronal firing rates are significantly higher in *Fmr1* KO mice compared to WT mice during whole-cell recordings manifesting UP/Down states (slow-wave sleep,

quiet wakefulness), probably due to the higher firing probability during UP states. Combined electroencephalography and calcium imaging experiments confirmed that neurons in KO mice have abnormally high firing and synchrony during sleep, leading to the conclusion that cortical networks in FXS are hyperexcitable in a brain state–dependent manner during a critical period for experience-dependent plasticity (Gonçalves et al., 2013). Several studies have also shown both molecular and functional disruption in GABA signaling in FXS (D'Hulst et al., 2006; El Idrissi et al., 2005; Gantois et al., 2006; Paluszkiewicz, Olmos-Serrano, Corbin, & Huntsman, 2011). The timing of the switch from depolarizing to hyperpolarizing GABA is delayed in the somatosensory cortex of *Fmr1* KO mice, and there is a concurrent alteration in the expression of the neuronal chloride cotransporter NKCC1 that promotes the accumulation of intracellular chloride (He, Nomura, Xu, & Contractor, 2014). While the actual mechanisms that control the developmental expression of the NKCC1 are not known, it is significant that NKCC1 is predominantly found in astrocytes. With the discovery of FMRP in astrocytes (Pacey & Doering, 2007), coupled with a role of astrocytes in synaptic function and glutamate metabolism (Ethell & Pasquale, 2005; Paixão & Klein, 2010; Ullian, Christopherson, & Barres, 2004), it is possible that astrocytes contribute, in some capacity, to the abnormal dendritic spine and synapse development, as well as circuit hyperexcitability seen in FXS (Higashimori et al., 2013; Higashimori et al., 2016; Jacobs & Doering, 2010; Jacobs, Nathwani, & Doering, 2010). Abnormal trophic effects of GABA during cortical development may also disrupt the normal trophic function of GABA and contribute to the delayed maturation of glutamatergic synapses in FXS.

Cellular deficits have also been observed in the somatosensory cortex of *Fmr1* KO mice. As in the auditory and visual cortices, an abundance of abnormally long, thin dendritic spines have been reported in pyramidal neurons during early development in the somatosensory cortex (Galvez & Greenough, 2005; Nimchinsky et al., 2001), and abnormal developmental pruning of the layer IV spiny stellate cell dendrites has been described in *Fmr1* KO mice (Galvez et al., 2003). Despite the clear alterations in cellular morphology in *Fmr1* KO mice, it is not known whether the anatomical deficits have an impact on the functional development of excitatory glutamatergic synapses in somatosensory cortex. During perinatal development in rodents, activity-dependent refinement of excitatory thalamocortical synapses in the somatosensory cortex leads to a stereotypical maturation of glutamatergic signaling (Barth & Malenka, 2001; Crair & Malenka, 1995). Thalamocortical synapses exhibit long-term potentiation (LTP) and long-term depression (LTD) throughout the critical plasticity period in layer IV (Crair & Malenka, 1995; Feldman, Nicoll, Malenka, & Isaac, 1998). Activity-dependent maturation of excitatory thalamocortical synapses during the critical period results in rapid changes in the synaptic composition of glutamate receptors (Crair & Malenka, 1995; Daw, Scott, & Isaac, 2007; Kidd & Isaac, 1999). The AMPA receptor contribution increases relative to the NMDA receptors (Crair & Malenka, 1995), and the proportion of NMDA-only silent synapses is reduced (Isaac, Crair, Nicoll, & Malenka, 1997).

Cortical glutamate receptors have been implicated in the development of the barrel cortex maps and the refinement of cortical sensory circuits that underlie sensory processing (Schlaggar, Fox, & O'Leary, 1993). *Harlow et al.* showed that early postnatal

development of excitatory connections from the thalamus to layer IV spiny stellate neurons is critically disrupted during a critical plasticity period in *Fmr1* KO mice (Harlow et al., 2010). Moreover, the progressive development of excitatory ionotropic glutamate receptor signaling, that normally occurs over the first postnatal week, is delayed as well (Harlow et al., 2010; Till et al., 2012). There is also an altered NMDAR to AMPAR ratio observed in the somatosensory cortex of *Fmr1* KO mice manifesting as an increase in the fraction of silent synapses (NMDA-only thalamocortical synapses) at the closure of the critical plasticity period (Harlow et al., 2010). Synaptic plasticity and experience-dependent refinement of sensory circuits are inextricably linked, and NMDA receptors play a central role in both processes. Therefore, alteration in NMDA receptor signaling and the developmental maturation of silent synapses during the critical plasticity period will most likely affect the development of cortical circuits.

Just like in the auditory and visual cortices, FMRP is required for the normal developmental progression of synaptic maturation in the somatosensory cortex. Loss of FMRP impacts the development of cortical synapses and results in dysregulation of glutamatergic maturation in the somatosensory cortex during the early postnatal critical plasticity period. Moreover, increased proportion of silent synapses persists into late postnatal development, which coincides with a temporal delay in the window for synaptic plasticity (Harlow et al., 2010; Till et al., 2012).

Conclusions

Hyperarousal and anxiety in humans with FXS may be linked to strong reactions to sensory stimuli. There is an abundance of evidence describing sensory cortical

dysfunctions in the *Fmr1* KO mice and in humans with FXS (**Table 1.1**). The common underlying phenotype is "sensory hypersensitivity", including hypersensitivity to visual, auditory or tactile stimuli that may lead to behavioral alterations such as poor eye contact, avoidance of noisy places, anxiety and impaired social reciprocity. These alterations in sensory processing appear to be a universal problem in individuals with FXS, as they cause impairment in processing and encoding of many types of sensory information, which may affect more complex social behaviors. Moreover, sensory processing disorders could occur because of dysfunction at multiple levels of each sensory system. The *Fmr1* KO mice also display deficiencies in sensory processing that may help to understand the mechanism of sensory hypersensitivity in FXS (**Figure 1.2**). Mechanisms underlying the sensory hypersensitivity may be relatively more tractable compared to more complex social behaviors typically studied in FXS. Therefore, it is of critical importance to use sensory hypersensitivity as a robust, reliable, and translatable phenotype to integrate pre-clinical and clinical investigations at multiple levels of analysis to facilitate drug discovery in FXS.

References

Abe, M., Furukawa, S., Takayama, S., Michitaka, K., Minami, H., Yamamoto, K., . . . Onji, M. (2003). Drug-induced hepatitis with autoimmune features during minocycline therapy. *Intern Med, 42*(1), 48-52. Retrieved from https://www.ncbi.nlm.nih.gov/pubmed/12583618

Adusei, D. C., Pacey, L. K., Chen, D., & Hampson, D. R. (2010). Early developmental alterations in GABAergic protein expression in fragile X knockout mice. *Neuropharmacology, 59*(3), 167-171. doi:10.1016/j.neuropharm.2010.05.002

Akin, E., Miller, L. C., & Tucker, L. B. (1998). Minocycline-induced lupus in adolescents. *Pediatrics, 101*(5), 926. Retrieved from https://www.ncbi.nlm.nih.gov/pubmed/9565427

Allen, C. B., Celikel, T., & Feldman, D. E. (2003). Long-term depression induced by sensory deprivation during cortical map plasticity in vivo. *Nat Neurosci, 6*(3), 291-299. doi:10.1038/nn1012

Ang, E. R., Zimmerman, J. C., & Malkin, E. (2002). Pseudotumor cerebri secondary to minocycline intake. *J Am Board Fam Pract, 15*(3), 229-233. Retrieved from https://www.ncbi.nlm.nih.gov/pubmed/12038730

Antion, M. D., Hou, L., Wong, H., Hoeffer, C. A., & Klann, E. (2008). mGluR-dependent long-term depression is associated with increased phosphorylation of S6 and synthesis of elongation factor 1A but remains expressed in S6K-deficient mice. *Mol Cell Biol, 28*(9), 2996-3007. doi:10.1128/MCB.00201-08

Arnett, M. T., Herman, D. H., & McGee, A. W. (2014). Deficits in tactile learning in a mouse model of fragile X syndrome. *PLoS One, 9*(10), e109116. doi:10.1371/journal.pone.0109116

Ashley, C. T., Sutcliffe, J. S., Kunst, C. B., Leiner, H. A., Eichler, E. E., Nelson, D. L., & Warren, S. T. (1993). Human and murine FMR-1: alternative splicing and translational initiation downstream of the CGG-repeat. *Nat Genet, 4*(3), 244-251. doi:10.1038/ng0793-244

Ashley, C. T., Wilkinson, K. D., Reines, D., & Warren, S. T. (1993). FMR1 protein: conserved RNP family domains and selective RNA binding. *Science, 262*(5133), 563-566. Retrieved from https://www.ncbi.nlm.nih.gov/pubmed/7692601

Atkinson, J. (2002). The developing visual brain.

Bagni, C., & Greenough, W. T. (2005). From mRNP trafficking to spine dysmorphogenesis: the roots of fragile X syndrome. *Nat Rev Neurosci, 6*(5), 376-387. doi:10.1038/nrn1667

Bakker, C. E., Verheij, C., Willemsen, R., van der Helm, R., Oerlemans, F., Vermey, M., . . . Reyniers, E. (1994). Fmr1 knockout mice: a model to study fragile X mental retardation. *Cell, 78*(1), 23-33.

Balmer, T. S. (2016). Perineuronal Nets Enhance the Excitability of Fast-Spiking Neurons. *eNeuro, 3*(4). doi:10.1523/ENEURO.0112-16.2016

Banko, J. L., Hou, L., Poulin, F., Sonenberg, N., & Klann, E. (2006). Regulation of eukaryotic initiation factor 4E by converging signaling pathways during metabotropic glutamate receptor-dependent long-term depression. *J Neurosci, 26*(8), 2167-2173. doi:10.1523/JNEUROSCI.5196-05.2006

Baranek, G. T., Foster, L. G., & Berkson, G. (1997). Tactile defensiveness and stereotyped behaviors. *Am J Occup Ther, 51*(2), 91-95. Retrieved from https://www.ncbi.nlm.nih.gov/pubmed/9124275

Baranek, G. T., Roberts, J. E., David, F. J., Sideris, J., Mirrett, P. L., Hatton, D. D., & Bailey, D. B. (2008). Developmental trajectories and correlates of sensory processing in young boys with fragile X syndrome. *Phys Occup Ther Pediatr, 28*(1), 79-98. Retrieved from https://www.ncbi.nlm.nih.gov/pubmed/18399048

Barnes, E., Roberts, J., Long, S. H., Martin, G. E., Berni, M. C., Mandulak, K. C., & Sideris, J. (2009). Phonological accuracy and intelligibility in connected speech of boys with fragile X syndrome or Down syndrome. *J Speech Lang Hear Res, 52*(4), 1048-1061. doi:10.1044/1092-4388(2009/08-0001)

Barth, A. L., & Malenka, R. C. (2001). NMDAR EPSC kinetics do not regulate the critical period for LTP at thalamocortical synapses. *Nature neuroscience, 4*(3), 235-236.

Bassell, G. J., & Warren, S. T. (2008). Fragile X syndrome: loss of local mRNA regulation alters synaptic development and function. *Neuron, 60*(2), 201-214. doi:10.1016/j.neuron.2008.10.004

Bear, M. F., Huber, K. M., & Warren, S. T. (2004). The mGluR theory of fragile X mental retardation. *Trends Neurosci, 27*(7), 370-377. doi:10.1016/j.tins.2004.04.009

Bender, K. J., Allen, C. B., Bender, V. A., & Feldman, D. E. (2006). Synaptic basis for whisker deprivation-induced synaptic depression in rat somatosensory cortex. *J Neurosci, 26*(16), 4155-4165. doi:10.1523/JNEUROSCI.0175-06.2006

Berman, R. F., Murray, K. D., Arque, G., Hunsaker, M. R., & Wenzel, H. J. (2012). Abnormal dendrite and spine morphology in primary visual cortex in the CGG knock-in mouse model of the fragile X premutation. *Epilepsia, 53 Suppl 1*, 150-160. doi:10.1111/j.1528-1167.2012.03486.x

Berzhanskaya, J., Phillips, M. A., Gorin, A., Lai, C., Shen, J., & Colonnese, M. T. (2017). Disrupted Cortical State Regulation in a Rat Model of Fragile X Syndrome. *Cereb Cortex, 27*(2), 1386-1400. doi:10.1093/cercor/bhv331

Bilousova, T. V., Dansie, L., Ngo, M., Aye, J., Charles, J. R., Ethell, D. W., & Ethell, I. M. (2009). Minocycline promotes dendritic spine maturation and improves behavioural performance in the fragile X mouse model. *J Med Genet, 46*(2), 94-102. doi:10.1136/jmg.2008.061796

Bolduc, F. V., Bell, K., Cox, H., Broadie, K. S., & Tully, T. (2008). Excess protein synthesis in Drosophila fragile X mutants impairs long-term memory. *Nat Neurosci, 11*(10), 1143-1145. doi:10.1038/nn.2175

Braat, S., & Kooy, R. F. (2015). The GABAA Receptor as a Therapeutic Target for Neurodevelopmental Disorders. *Neuron, 86*(5), 1119-1130. doi:10.1016/j.neuron.2015.03.042

Brennan, F. X., Albeck, D. S., & Paylor, R. (2006). Fmr1 knockout mice are impaired in a leverpress escape/avoidance task. *Genes Brain Behav, 5*(6), 467-471. doi:10.1111/j.1601-183X.2005.00183.x

Brown, M. R., Kronengold, J., Gazula, V. R., Chen, Y., Strumbos, J. G., Sigworth, F. J., . . . Kaczmarek, L. K. (2010). Fragile X mental retardation protein controls gating of the sodium-activated potassium channel Slack. *Nat Neurosci, 13*(7), 819-821. doi:10.1038/nn.2563

Brown, V., Jin, P., Ceman, S., Darnell, J. C., O'Donnell, W. T., Tenenbaum, S. A., . . . Warren, S. T. (2001). Microarray identification of FMRP-associated brain mRNAs and altered mRNA translational profiles in fragile X syndrome. *Cell, 107*(4), 477-487. Retrieved from https://www.ncbi.nlm.nih.gov/pubmed/11719188

Cascio, A., Di Liberto, C., D'Angelo, M., Iaria, C., Scarlata, F., Titone, L., & Campisi, G. (2004). No findings of dental defects in children treated with minocycline. *Antimicrob Agents Chemother, 48*(7), 2739-2741. doi:10.1128/AAC.48.7.2739-2741.2004

Cascio, C. J. (2010). Somatosensory processing in neurodevelopmental disorders. *J Neurodev Disord, 2*(2), 62-69. doi:10.1007/s11689-010-9046-3

Castrén, M., Pääkkönen, A., Tarkka, I. M., Ryynänen, M., & Partanen, J. (2003). Augmentation of auditory N1 in children with fragile X syndrome. *Brain Topogr, 15*(3), 165-171. Retrieved from https://www.ncbi.nlm.nih.gov/pubmed/12705812

Cheever, A., & Ceman, S. (2009). Phosphorylation of FMRP inhibits association with Dicer. *RNA, 15*(3), 362-366. doi:10.1261/rna.1500809

Chen, L., & Toth, M. (2001). Fragile X mice develop sensory hyperreactivity to auditory stimuli. *Neuroscience, 103*(4), 1043-1050. Retrieved from https://www.ncbi.nlm.nih.gov/pubmed/11301211

Chittajallu, R., & Isaac, J. T. (2010). Emergence of cortical inhibition by coordinated sensory-driven plasticity at distinct synaptic loci. *Nat Neurosci, 13*(10), 1240-1248. doi:10.1038/nn.2639

Churchill, J. D., Grossman, A. W., Irwin, S. A., Galvez, R., Klintsova, A. Y., Weiler, I. J., & Greenough, W. T. (2002). A converging-methods approach to fragile X syndrome. *Dev Psychobiol, 40*(3), 323-338. Retrieved from https://www.ncbi.nlm.nih.gov/pubmed/11891642

Cornish, K. M., Munir, F., & Cross, G. (1999). Spatial cognition in males with Fragile-X syndrome: evidence for a neuropsychological phenotype. *Cortex, 35*(2), 263-271. Retrieved from https://www.ncbi.nlm.nih.gov/pubmed/10369098

Crair, M. C., & Malenka, R. C. (1995). A critical period for long-term potentiation at thalamocortical synapses. *Nature, 375*(6529), 325-328. doi:10.1038/375325a0

Crawford, D. C., Acuña, J. M., & Sherman, S. L. (2001). FMR1 and the fragile X syndrome: human genome epidemiology review. *Genet Med, 3*(5), 359-371. doi:10.109700125817-200109000-00006

Crowe, S. F., & Hay, D. A. (1990). Neuropsychological dimensions of the fragile X syndrome: support for a non-dominant hemisphere dysfunction hypothesis. *Neuropsychologia, 28*(1), 9-16. Retrieved from https://www.ncbi.nlm.nih.gov/pubmed/2138257

Curia, G., Papouin, T., Séguéla, P., & Avoli, M. (2009). Downregulation of tonic GABAergic inhibition in a mouse model of fragile X syndrome. *Cereb Cortex, 19*(7), 1515-1520. doi:10.1093/cercor/bhn159

D'Hulst, C., De Geest, N., Reeve, S. P., Van Dam, D., De Deyn, P. P., Hassan, B. A., & Kooy, R. F. (2006). Decreased expression of the GABAA receptor in fragile X syndrome. *Brain Res, 1121*(1), 238-245. doi:10.1016/j.brainres.2006.08.115

D'Hulst, C., Heulens, I., Brouwer, J. R., Willemsen, R., De Geest, N., Reeve, S. P., . . . Kooy, R. F. (2009). Expression of the GABAergic system in animal models for fragile X syndrome and fragile X associated tremor/ataxia syndrome (FXTAS). *Brain Res, 1253*, 176-183. doi:10.1016/j.brainres.2008.11.075

Dahlhaus, R. (2018). Of Men and Mice: Modeling the Fragile X Syndrome. *Front Mol Neurosci, 11*, 41. doi:10.3389/fnmol.2018.00041

Dansie, L. E., Phommahaxay, K., Okusanya, A. G., Uwadia, J., Huang, M., Rotschafer, S. E., . . . Ethell, I. M. (2013). Long-lasting effects of minocycline on behavior in young but not adult Fragile X mice. *Neuroscience, 246*, 186-198. doi:10.1016/j.neuroscience.2013.04.058

Darnell, J. C., Fraser, C. E., Mostovetsky, O., Stefani, G., Jones, T. A., Eddy, S. R., & Darnell, R. B. (2005). Kissing complex RNAs mediate interaction between the Fragile-X mental retardation protein KH2 domain and brain polyribosomes. *Genes Dev, 19*(8), 903-918. doi:10.1101/gad.1276805

Darnell, J. C., & Klann, E. (2013). The translation of translational control by FMRP: therapeutic targets for FXS. *Nat Neurosci, 16*(11), 1530-1536. doi:10.1038/nn.3379

Darnell, J. C., Van Driesche, S. J., Zhang, C., Hung, K. Y., Mele, A., Fraser, C. E., . . . Darnell, R. B. (2011). FMRP stalls ribosomal translocation on mRNAs linked to synaptic function and autism. *Cell, 146*(2), 247-261. doi:10.1016/j.cell.2011.06.013

Daw, M. I., Ashby, M. C., & Isaac, J. T. (2007). Coordinated developmental recruitment of latent fast spiking interneurons in layer IV barrel cortex. *Nat Neurosci, 10*(4), 453-461. doi:10.1038/nn1866

Daw, M. I., Scott, H. L., & Isaac, J. T. (2007). Developmental synaptic plasticity at the thalamocortical input to barrel cortex: mechanisms and roles. *Mol Cell Neurosci, 34*(4), 493-502. doi:10.1016/j.mcn.2007.01.001

den Broeder, M. J., van der Linde, H., Brouwer, J. R., Oostra, B. A., Willemsen, R., & Ketting, R. F. (2009). Generation and characterization of FMR1 knockout zebrafish. *PLoS One, 4*(11), e7910. doi:10.1371/journal.pone.0007910

Deng, P. Y., & Klyachko, V. A. (2016). Genetic upregulation of BK channel activity normalizes multiple synaptic and circuit defects in a mouse model of fragile X syndrome. *J Physiol, 594*(1), 83-97. doi:10.1113/JP271031

Deng, P. Y., Rotman, Z., Blundon, J. A., Cho, Y., Cui, J., Cavalli, V., . . . Klyachko, V. A. (2013). FMRP regulates neurotransmitter release and synaptic information transmission by modulating action potential duration via BK channels. *Neuron, 77*(4), 696-711. doi:10.1016/j.neuron.2012.12.018

Desai, N. S., Casimiro, T. M., Gruber, S. M., & Vanderklish, P. W. (2006). Early postnatal plasticity in neocortex of Fmr1 knockout mice. *J Neurophysiol, 96*(4), 1734-1745. doi:10.1152/jn.00221.2006

Diamond, M. E., & Arabzadeh, E. (2013). Whisker sensory system - from receptor to decision. *Prog Neurobiol, 103*, 28-40. doi:10.1016/j.pneurobio.2012.05.013

Diamond, M. E., von Heimendahl, M., Knutsen, P. M., Kleinfeld, D., & Ahissar, E. (2008). 'Where' and 'what' in the whisker sensorimotor system. *Nat Rev Neurosci, 9*(8), 601-612. doi:10.1038/nrn2411

Dockendorff, T. C., Su, H. S., McBride, S. M., Yang, Z., Choi, C. H., Siwicki, K. K., . . . Jongens, T. A. (2002). Drosophila lacking dfmr1 activity show defects in circadian output and fail to maintain courtship interest. *Neuron, 34*(6), 973-984. Retrieved from https://www.ncbi.nlm.nih.gov/pubmed/12086644

Dölen, G., & Bear, M. F. (2008). Role for metabotropic glutamate receptor 5 (mGluR5) in the pathogenesis of fragile X syndrome. *J Physiol, 586*(6), 1503-1508. doi:10.1113/jphysiol.2008.150722

Dölen, G., Osterweil, E., Rao, B. S., Smith, G. B., Auerbach, B. D., Chattarji, S., & Bear, M. F. (2007). Correction of fragile X syndrome in mice. *Neuron, 56*(6), 955-962. doi:10.1016/j.neuron.2007.12.001

Dorrn, A. L., Yuan, K., Barker, A. J., Schreiner, C. E., & Froemke, R. C. (2010). Developmental sensory experience balances cortical excitation and inhibition. *Nature, 465*(7300), 932-936. doi:10.1038/nature09119

Dudek, S. M., & Bear, M. F. (1989). A biochemical correlate of the critical period for synaptic modification in the visual cortex. *Science, 246*(4930), 673-675. Retrieved from https://www.ncbi.nlm.nih.gov/pubmed/2573152

Dziembowska, M., Pretto, D. I., Janusz, A., Kaczmarek, L., Leigh, M. J., Gabriel, N., . . . Tassone, F. (2013). High MMP-9 activity levels in fragile X syndrome are lowered by minocycline. *Am J Med Genet A, 161A*(8), 1897-1903. doi:10.1002/ajmg.a.36023

Dziembowska, M., & Wlodarczyk, J. (2012). MMP9: a novel function in synaptic plasticity. *Int J Biochem Cell Biol, 44*(5), 709-713. doi:10.1016/j.biocel.2012.01.023

Eadie, B. D., Zhang, W. N., Boehme, F., Gil-Mohapel, J., Kainer, L., Simpson, J. M., & Christie, B. R. (2009). Fmr1 knockout mice show reduced anxiety and alterations in neurogenesis that are specific to the ventral dentate gyrus. *Neurobiol Dis, 36*(2), 361-373. doi:10.1016/j.nbd.2009.08.001

Edbauer, D., Neilson, J. R., Foster, K. A., Wang, C. F., Seeburg, D. P., Batterton, M. N., . . . Sheng, M. (2010). Regulation of synaptic structure and function by FMRP-associated microRNAs miR-125b and miR-132. *Neuron, 65*(3), 373-384. doi:10.1016/j.neuron.2010.01.005

Edition, F. (1994). *Diagnostic and statistical manual of mental disorders*: Am Psychiatric Assoc.

Eisen, D., & Hakim, M. D. (1998). Minocycline-induced pigmentation. Incidence, prevention and management. *Drug Saf, 18*(6), 431-440. Retrieved from https://www.ncbi.nlm.nih.gov/pubmed/9638388

El Idrissi, A., Ding, X. H., Scalia, J., Trenkner, E., Brown, W. T., & Dobkin, C. (2005). Decreased GABA(A) receptor expression in the seizure-prone fragile X mouse. *Neurosci Lett, 377*(3), 141-146. doi:10.1016/j.neulet.2004.11.087

Engineer, C. T., Centanni, T. M., Im, K. W., Rahebi, K. C., Buell, E. P., & Kilgard, M. P. (2014). Degraded speech sound processing in a rat model of fragile X syndrome. *Brain Res, 1564*, 72-84. doi:10.1016/j.brainres.2014.03.049

Enriquez-Barreto, L., & Morales, M. (2016). The PI3K signaling pathway as a pharmacological target in Autism related disorders and Schizophrenia. *Mol Cell Ther, 4*, 2. doi:10.1186/s40591-016-0047-9

Ethell, I. M., & Pasquale, E. B. (2005). Molecular mechanisms of dendritic spine development and remodeling. *Prog Neurobiol, 75*(3), 161-205. doi:10.1016/j.pneurobio.2005.02.003

Ethridge, L. E., White, S. P., Mosconi, M. W., Wang, J., Byerly, M. J., & Sweeney, J. A. (2016). Reduced habituation of auditory evoked potentials indicate cortical hyper-excitability in Fragile X Syndrome. *Transl Psychiatry, 6*, e787. doi:10.1038/tp.2016.48

Ethridge, L. E., White, S. P., Mosconi, M. W., Wang, J., Pedapati, E. V., Erickson, C. A., . . . Sweeney, J. A. (2017). Neural synchronization deficits linked to cortical hyper-excitability and auditory hypersensitivity in fragile X syndrome. *Mol Autism, 8*, 22. doi:10.1186/s13229-017-0140-1

Farzin, F., & Rivera, S. M. (2010). Dynamic Object Representations in Infants with and without Fragile X Syndrome. *Front Hum Neurosci, 4*, 12. doi:10.3389/neuro.09.012.2010

Farzin, F., Rivera, S. M., & Whitney, D. (2011). Resolution of spatial and temporal visual attention in infants with fragile X syndrome. *Brain, 134*(Pt 11), 3355-3368. doi:10.1093/brain/awr249

Farzin, F., Whitney, D., Hagerman, R. J., & Rivera, S. M. (2008). Contrast detection in infants with fragile X syndrome. *Vision Res, 48*(13), 1471-1478. doi:10.1016/j.visres.2008.03.019

Feldman, D. E., Nicoll, R. A., Malenka, R. C., & Isaac, J. T. (1998). Long-term depression at thalamocortical synapses in developing rat somatosensory cortex. *Neuron, 21*(2), 347-357. Retrieved from https://www.ncbi.nlm.nih.gov/pubmed/9728916

Feldmeyer, D., Brecht, M., Helmchen, F., Petersen, C. C., Poulet, J. F., Staiger, J. F., . . . Schwarz, C. (2013). Barrel cortex function. *Prog Neurobiol, 103*, 3-27. doi:10.1016/j.pneurobio.2012.11.002

Ferraguti, F., Baldani-Guerra, B., Corsi, M., Nakanishi, S., & Corti, C. (1999). Activation of the extracellular signal-regulated kinase 2 by metabotropic glutamate receptors. *Eur J Neurosci, 11*(6), 2073-2082. Retrieved from https://www.ncbi.nlm.nih.gov/pubmed/10336676

Ferron, L., Nieto-Rostro, M., Cassidy, J. S., & Dolphin, A. C. (2014). Fragile X mental retardation protein controls synaptic vesicle exocytosis by modulating N-type calcium channel density. *Nat Commun, 5*, 3628. doi:10.1038/ncomms4628

Finestack, L. H., Richmond, E. K., & Abbeduto, L. (2009). Language Development in Individuals with Fragile X Syndrome. *Top Lang Disord, 29*(2), 133-148. Retrieved from https://www.ncbi.nlm.nih.gov/pubmed/20396595

Franco, L. M., Okray, Z., Linneweber, G. A., Hassan, B. A., & Yaksi, E. (2017). Reduced Lateral Inhibition Impairs Olfactory Computations and Behaviors in a Drosophila Model of Fragile X Syndrome. *Curr Biol, 27*(8), 1111-1123. doi:10.1016/j.cub.2017.02.065

Frankland, P. W., Wang, Y., Rosner, B., Shimizu, T., Balleine, B. W., Dykens, E. M., . . . Silva, A. J. (2004). Sensorimotor gating abnormalities in young males with fragile X syndrome and Fmr1-knockout mice. *Mol Psychiatry, 9*(4), 417-425. doi:10.1038/sj.mp.4001432

Freund, L. S., & Reiss, A. L. (1991). Cognitive profiles associated with the fra(X) syndrome in males and females. *Am J Med Genet, 38*(4), 542-547. doi:10.1002/ajmg.1320380409

Gallagher, S. M., Daly, C. A., Bear, M. F., & Huber, K. M. (2004). Extracellular signal-regulated protein kinase activation is required for metabotropic glutamate receptor-dependent long-term depression in hippocampal area CA1. *J Neurosci, 24*(20), 4859-4864. doi:10.1523/JNEUROSCI.5407-03.2004

Galvez, R., Gopal, A. R., & Greenough, W. T. (2003). Somatosensory cortical barrel dendritic abnormalities in a mouse model of the fragile X mental retardation syndrome. *Brain Res, 971*(1), 83-89. Retrieved from https://www.ncbi.nlm.nih.gov/pubmed/12691840

Galvez, R., & Greenough, W. T. (2005). Sequence of abnormal dendritic spine development in primary somatosensory cortex of a mouse model of the fragile X mental retardation syndrome. *Am J Med Genet A, 135*(2), 155-160. doi:10.1002/ajmg.a.30709

Gantois, I., Vandesompele, J., Speleman, F., Reyniers, E., D'Hooge, R., Severijnen, L. A., . . . Kooy, R. F. (2006). Expression profiling suggests underexpression of the GABA(A) receptor subunit delta in the fragile X knockout mouse model. *Neurobiol Dis, 21*(2), 346-357. doi:10.1016/j.nbd.2005.07.017

Garcia-Pino, E., Gessele, N., & Koch, U. (2017). Enhanced Excitatory Connectivity and Disturbed Sound Processing in the Auditory Brainstem of Fragile X Mice. *J Neurosci, 37*(31), 7403-7419. doi:10.1523/JNEUROSCI.2310-16.2017

Gibson, J. R., Bartley, A. F., Hays, S. A., & Huber, K. M. (2008). Imbalance of neocortical excitation and inhibition and altered UP states reflect network hyperexcitability in the mouse model of fragile X syndrome. *J Neurophysiol, 100*(5), 2615-2626. doi:10.1152/jn.90752.2008

Gkogkas, C. G., Khoutorsky, A., Cao, R., Jafarnejad, S. M., Prager-Khoutorsky, M., Giannakas, N., . . . Sonenberg, N. (2014). Pharmacogenetic inhibition of eIF4E-dependent Mmp9 mRNA translation reverses fragile X syndrome-like phenotypes. *Cell Rep, 9*(5), 1742-1755. doi:10.1016/j.celrep.2014.10.064

Gonçalves, J. T., Anstey, J. E., Golshani, P., & Portera-Cailliau, C. (2013). Circuit level defects in the developing neocortex of Fragile X mice. *Nat Neurosci, 16*(7), 903-909. doi:10.1038/nn.3415

Greenough, W. T., Klintsova, A. Y., Irwin, S. A., Galvez, R., Bates, K. E., & Weiler, I. J. (2001). Synaptic regulation of protein synthesis and the fragile X protein. *Proc Natl Acad Sci U S A, 98*(13), 7101-7106. doi:10.1073/pnas.141145998

Hall, S. S., Walter, E., Sherman, E., Hoeft, F., & Reiss, A. L. (2009). The neural basis of auditory temporal discrimination in girls with fragile X syndrome. *J Neurodev Disord, 1*(1), 91-99. doi:10.1007/s11689-009-9007-x

Hamilton, S. M., Green, J. R., Veeraragavan, S., Yuva, L., McCoy, A., Wu, Y., . . . Paylor, R. (2014). Fmr1 and Nlgn3 knockout rats: novel tools for investigating autism spectrum disorders. *Behav Neurosci, 128*(2), 103-109. doi:10.1037/a0035988

Han, Y. K., Köver, H., Insanally, M. N., Semerdjian, J. H., & Bao, S. (2007). Early experience impairs perceptual discrimination. *Nature neuroscience, 10*(9), 1191.

Happel, M. F., & Frischknecht, R. (2016). Neuronal Plasticity in the Juvenile and Adult Brain Regulated by the Extracellular Matrix. In *Composition and Function of the Extracellular Matrix in the Human Body*: InTech.

Harlow, E. G., Till, S. M., Russell, T. A., Wijetunge, L. S., Kind, P., & Contractor, A. (2010). Critical period plasticity is disrupted in the barrel cortex of FMR1 knockout mice. *Neuron, 65*(3), 385-398. doi:10.1016/j.neuron.2010.01.024

Hayashi, M. L., Rao, B. S., Seo, J. S., Choi, H. S., Dolan, B. M., Choi, S. Y., . . . Tonegawa, S. (2007). Inhibition of p21-activated kinase rescues symptoms of fragile X syndrome in mice. *Proc Natl Acad Sci U S A, 104*(27), 11489-11494. doi:10.1073/pnas.0705003104

He, Q., Nomura, T., Xu, J., & Contractor, A. (2014). The developmental switch in GABA polarity is delayed in fragile X mice. *J Neurosci, 34*(2), 446-450. doi:10.1523/JNEUROSCI.4447-13.2014

Hébert, B., Pietropaolo, S., Même, S., Laudier, B., Laugeray, A., Doisne, N., . . . Briault, S. (2014). Rescue of fragile X syndrome phenotypes in Fmr1 KO mice by a BKCa channel opener molecule. *Orphanet J Rare Dis, 9*, 124. doi:10.1186/s13023-014-0124-6

Hensch, T. K. (2005). Critical period plasticity in local cortical circuits. *Nat Rev Neurosci, 6*(11), 877-888. doi:10.1038/nrn1787

Higashimori, H., Morel, L., Huth, J., Lindemann, L., Dulla, C., Taylor, A., . . . Yang, Y. (2013). Astroglial FMRP-dependent translational down-regulation of mGluR5 underlies glutamate transporter GLT1 dysregulation in the fragile X mouse. *Hum Mol Genet, 22*(10), 2041-2054. doi:10.1093/hmg/ddt055

Higashimori, H., Schin, C. S., Chiang, M. S., Morel, L., Shoneye, T. A., Nelson, D. L., & Yang, Y. (2016). Selective Deletion of Astroglial FMRP Dysregulates Glutamate Transporter GLT1 and Contributes to Fragile X Syndrome Phenotypes In Vivo. *J Neurosci, 36*(27), 7079-7094. doi:10.1523/JNEUROSCI.1069-16.2016

Hinton, V. J., Brown, W. T., Wisniewski, K., & Rudelli, R. D. (1991). Analysis of neocortex in three males with the fragile X syndrome. *Am J Med Genet, 41*(3), 289-294. doi:10.1002/ajmg.1320410306

Hou, L., Antion, M. D., Hu, D., Spencer, C. M., Paylor, R., & Klann, E. (2006). Dynamic translational and proteasomal regulation of fragile X mental retardation protein controls mGluR-dependent long-term depression. *Neuron, 51*(4), 441-454. doi:10.1016/j.neuron.2006.07.005

Hou, L., & Klann, E. (2004). Activation of the phosphoinositide 3-kinase-Akt-mammalian target of rapamycin signaling pathway is required for metabotropic glutamate receptor-dependent long-term depression. *J Neurosci, 24*(28), 6352-6361. doi:10.1523/JNEUROSCI.0995-04.2004

Hu, H., Qin, Y., Bochorishvili, G., Zhu, Y., van Aelst, L., & Zhu, J. J. (2008). Ras signaling mechanisms underlying impaired GluR1-dependent plasticity associated with fragile X syndrome. *J Neurosci, 28*(31), 7847-7862. doi:10.1523/JNEUROSCI.1496-08.2008

Huber, K. M., Gallagher, S. M., Warren, S. T., & Bear, M. F. (2002). Altered synaptic plasticity in a mouse model of fragile X mental retardation. *Proc Natl Acad Sci U S A, 99*(11), 7746-7750. doi:10.1073/pnas.122205699

Huber, K. M., Kayser, M. S., & Bear, M. F. (2000). Role for rapid dendritic protein synthesis in hippocampal mGluR-dependent long-term depression. *Science, 288*(5469), 1254-1257. Retrieved from https://www.ncbi.nlm.nih.gov/pubmed/10818003

Inoue, S., Shimoda, M., Nishinokubi, I., Siomi, M. C., Okamura, M., Nakamura, A., . . . Siomi, H. (2002). A role for the Drosophila fragile X-related gene in circadian output. *Curr Biol, 12*(15), 1331-1335. Retrieved from https://www.ncbi.nlm.nih.gov/pubmed/12176363

Irwin, S. A., Patel, B., Idupulapati, M., Harris, J. B., Crisostomo, R. A., Larsen, B. P., . . . Greenough, W. T. (2001). Abnormal dendritic spine characteristics in the temporal and visual cortices of patients with fragile-X syndrome: a quantitative examination. *Am J Med Genet, 98*(2), 161-167. Retrieved from https://www.ncbi.nlm.nih.gov/pubmed/11223852

Isaac, J. T., Crair, M. C., Nicoll, R. A., & Malenka, R. C. (1997). Silent synapses during development of thalamocortical inputs. *Neuron, 18*(2), 269-280. Retrieved from https://www.ncbi.nlm.nih.gov/pubmed/9052797

Jackson, A. (2017). Cellular and synaptic pathophysiology in a rat model of Fragile X syndrome.

Jacobs, S., & Doering, L. C. (2010). Astrocytes prevent abnormal neuronal development in the fragile x mouse. *J Neurosci, 30*(12), 4508-4514. doi:10.1523/JNEUROSCI.5027-09.2010

Jacobs, S., Nathwani, M., & Doering, L. C. (2010). Fragile X astrocytes induce developmental delays in dendrite maturation and synaptic protein expression. *BMC Neurosci, 11*, 132. doi:10.1186/1471-2202-11-132

Janusz, A., Milek, J., Perycz, M., Pacini, L., Bagni, C., Kaczmarek, L., & Dziembowska, M. (2013). The Fragile X mental retardation protein regulates matrix metalloproteinase 9 mRNA at synapses. *J Neurosci, 33*(46), 18234-18241. doi:10.1523/JNEUROSCI.2207-13.2013

Jeevakumar, V., & Kroener, S. (2016). Ketamine Administration During the Second Postnatal Week Alters Synaptic Properties of Fast-Spiking Interneurons in the Medial Prefrontal Cortex of Adult Mice. *Cereb Cortex, 26*(3), 1117-1129. doi:10.1093/cercor/bhu293

Juczewski, K., von Richthofen, H., Bagni, C., Celikel, T., Fisone, G., & Krieger, P. (2016). Somatosensory map expansion and altered processing of tactile inputs in a mouse model of fragile X syndrome. *Neurobiol Dis, 96*, 201-215. doi:10.1016/j.nbd.2016.09.007

Kaufmann, W. E., & Moser, H. W. (2000). Dendritic anomalies in disorders associated with mental retardation. *Cereb Cortex, 10*(10), 981-991. Retrieved from https://www.ncbi.nlm.nih.gov/pubmed/11007549

Kidd, F. L., & Isaac, J. T. (1999). Developmental and activity-dependent regulation of kainate receptors at thalamocortical synapses. *Nature, 400*(6744), 569-573. doi:10.1038/23040

Kim, H., Gibboni, R., Kirkhart, C., & Bao, S. (2013). Impaired critical period plasticity in primary auditory cortex of fragile X model mice. *J Neurosci, 33*(40), 15686-15692. doi:10.1523/JNEUROSCI.3246-12.2013

Klann, E., & Dever, T. E. (2004). Biochemical mechanisms for translational regulation in synaptic plasticity. *Nat Rev Neurosci, 5*(12), 931-942. doi:10.1038/nrn1557

Kogan, C. S., Bertone, A., Cornish, K., Boutet, I., Der Kaloustian, V. M., Andermann, E., . . . Chaudhuri, A. (2004). Integrative cortical dysfunction and pervasive motion perception deficit in fragile X syndrome. *Neurology, 63*(9), 1634-1639. Retrieved from https://www.ncbi.nlm.nih.gov/pubmed/15534248

Kogan, C. S., Boutet, I., Cornish, K., Zangenehpour, S., Mullen, K. T., Holden, J. J., . . . Chaudhuri, A. (2004). Differential impact of the FMR1 gene on visual processing in fragile X syndrome. *Brain, 127*(Pt 3), 591-601. doi:10.1093/brain/awh069

Laggerbauer, B., Ostareck, D., Keidel, E. M., Ostareck-Lederer, A., & Fischer, U. (2001). Evidence that fragile X mental retardation protein is a negative regulator of translation. *Hum Mol Genet, 10*(4), 329-338. Retrieved from https://www.ncbi.nlm.nih.gov/pubmed/11157796

LaPorta, V. N., Nikitakis, N. G., Sindler, A. J., & Reynolds, M. A. (2005). Minocycline-associated intra-oral soft-tissue pigmentation: clinicopathologic correlations and review. *Journal of clinical periodontology, 32*(2), 119-122.

Larson, J., Jessen, R. E., Kim, D., Fine, A. K., & du Hoffmann, J. (2005). Age-dependent and selective impairment of long-term potentiation in the anterior piriform cortex of mice lacking the fragile X mental retardation protein. *J Neurosci, 25*(41), 9460-9469. doi:10.1523/JNEUROSCI.2638-05.2005

Lawson, T. M., Amos, N., Bulgen, D., & Williams, B. D. (2001). Minocycline-induced lupus: clinical features and response to rechallenge. *Rheumatology (Oxford), 40*(3), 329-335. Retrieved from https://www.ncbi.nlm.nih.gov/pubmed/11285382

Leigh, M. J., Nguyen, D. V., Mu, Y., Winarni, T. I., Schneider, A., Chechi, T., . . . Hagerman, R. J. (2013). A randomized double-blind, placebo-controlled trial of minocycline in children and adolescents with fragile x syndrome. *J Dev Behav Pediatr, 34*(3), 147-155. doi:10.1097/DBP.0b013e318287cd17

Lensjø, K. K., Lepperød, M. E., Dick, G., Hafting, T., & Fyhn, M. (2017). Removal of Perineuronal Nets Unlocks Juvenile Plasticity Through Network Mechanisms of Decreased Inhibition and Increased Gamma Activity. *J Neurosci, 37*(5), 1269-1283. doi:10.1523/JNEUROSCI.2504-16.2016

Li, J., Pelletier, M. R., Perez Velazquez, J. L., & Carlen, P. L. (2002). Reduced cortical synaptic plasticity and GluR1 expression associated with fragile X mental retardation protein deficiency. *Mol Cell Neurosci, 19*(2), 138-151. doi:10.1006/mcne.2001.1085

Liu, B., Li, L., Chen, J., Wang, Z., Li, Z., & Wan, Q. (2013). Regulation of GABAA receptors by fragile X mental retardation protein. *Int J Physiol Pathophysiol Pharmacol, 5*(3), 169-176. Retrieved from https://www.ncbi.nlm.nih.gov/pubmed/24044036

Lovelace, J. W., Ethell, I. M., Binder, D. K., & Razak, K. A. (2018). Translation-relevant EEG phenotypes in a mouse model of Fragile X Syndrome. *Neurobiology of Disease*.

Lovelace, J. W., Wen, T. H., Reinhard, S., Hsu, M. S., Sidhu, H., Ethell, I. M., . . . Razak, K. A. (2016). Matrix metalloproteinase-9 deletion rescues auditory evoked potential habituation deficit in a mouse model of Fragile X Syndrome. *Neurobiol Dis, 89*, 126-135. doi:10.1016/j.nbd.2016.02.002

Luck, S. J. (2014). *An introduction to the event-related potential technique*: MIT press.

McBride, S. M., Giuliani, G., Choi, C., Krause, P., Correale, D., Watson, K., . . . Siwicki, K. K. (1999). Mushroom body ablation impairs short-term memory and long-term memory of courtship conditioning in Drosophila melanogaster. *Neuron, 24*(4), 967-977. Retrieved from https://www.ncbi.nlm.nih.gov/pubmed/10624959

Miller, L. J., McIntosh, D. N., McGrath, J., Shyu, V., Lampe, M., Taylor, A. K., . . . Hagerman, R. J. (1999). Electrodermal responses to sensory stimuli in individuals with fragile X syndrome: a preliminary report. *Am J Med Genet, 83*(4), 268-279. Retrieved from https://www.ncbi.nlm.nih.gov/pubmed/10208160

Milner, D., & Goodale, M. (2006). *The visual brain in action*: Oxford University Press.

Morales, J., Hiesinger, P. R., Schroeder, A. J., Kume, K., Verstreken, P., Jackson, F. R., . . . Hassan, B. A. (2002). Drosophila fragile X protein, DFXR, regulates neuronal morphology and function in the brain. *Neuron, 34*(6), 961-972. Retrieved from https://www.ncbi.nlm.nih.gov/pubmed/12086643

Muddashetty, R. S., Nalavadi, V. C., Gross, C., Yao, X., Xing, L., Laur, O., . . . Bassell, G. J. (2011). Reversible inhibition of PSD-95 mRNA translation by miR-125a, FMRP phosphorylation, and mGluR signaling. *Mol Cell, 42*(5), 673-688. doi:10.1016/j.molcel.2011.05.006

Murphy, M. M., Mazzocco, M. M., Gerner, G., & Henry, A. E. (2006). Mathematics learning disability in girls with Turner syndrome or fragile X syndrome. *Brain Cogn, 61*(2), 195-210. doi:10.1016/j.bandc.2005.12.014

Musumeci, S. A., Bosco, P., Calabrese, G., Bakker, C., De Sarro, G. B., Elia, M., . . . Oostra, B. A. (2000). Audiogenic seizures susceptibility in transgenic mice with fragile X syndrome. *Epilepsia, 41*(1), 19-23. Retrieved from https://www.ncbi.nlm.nih.gov/pubmed/10643918

Musumeci, S. A., Calabrese, G., Bonaccorso, C. M., D'Antoni, S., Brouwer, J. R., Bakker, C. E., . . . Catania, M. V. (2007). Audiogenic seizure susceptibility is reduced in fragile X knockout mice after introduction of FMR1 transgenes. *Exp Neurol, 203*(1), 233-240. doi:10.1016/j.expneurol.2006.08.007

Myrick, L. K., Deng, P. Y., Hashimoto, H., Oh, Y. M., Cho, Y., Poidevin, M. J., . . . Klyachko, V. A. (2015). Independent role for presynaptic FMRP revealed by an FMR1 missense mutation associated with intellectual disability and seizures. *Proc Natl Acad Sci U S A, 112*(4), 949-956. doi:10.1073/pnas.1423094112

Ng, M. C., Yang, Y. L., & Lu, K. T. (2013). Behavioral and synaptic circuit features in a zebrafish model of fragile X syndrome. *PLoS One, 8*(3), e51456. doi:10.1371/journal.pone.0051456

Nielsen, D. M., Derber, W. J., McClellan, D. A., & Crnic, L. S. (2002). Alterations in the auditory startle response in Fmr1 targeted mutant mouse models of fragile X syndrome. *Brain Res, 927*(1), 8-17. Retrieved from https://www.ncbi.nlm.nih.gov/pubmed/11814427

Nieto Del Rincón, P. L. (2008). Autism: alterations in auditory perception. *Rev Neurosci, 19*(1), 61-78. Retrieved from https://www.ncbi.nlm.nih.gov/pubmed/18561821

Nimchinsky, E. A., Oberlander, A. M., & Svoboda, K. (2001). Abnormal development of dendritic spines in FMR1 knock-out mice. *J Neurosci, 21*(14), 5139-5146. Retrieved from https://www.ncbi.nlm.nih.gov/pubmed/11438589

Nomura, T., Musial, T. F., Marshall, J. J., Zhu, Y., Remmers, C. L., Xu, J., . . . Contractor, A. (2017). Delayed Maturation of Fast-Spiking Interneurons Is Rectified by Activation of the TrkB Receptor in the Mouse Model of Fragile X Syndrome. *J Neurosci, 37*(47), 11298-11310. doi:10.1523/JNEUROSCI.2893-16.2017

Okray, Z., de Esch, C. E., Van Esch, H., Devriendt, K., Claeys, A., Yan, J., . . . Hassan, B. A. (2015). A novel fragile X syndrome mutation reveals a conserved role for the carboxy-terminus in FMRP localization and function. *EMBO Mol Med, 7*(4), 423-437. doi:10.15252/emmm.201404576

Owen, E. R., Baumgartner, H. A., & Rivera, S. M. (2013). Using infrared eye-tracking to explore ordinal numerical processing in toddlers with Fragile X Syndrome. *J Neurodev Disord, 5*(1), 1. doi:10.1186/1866-1955-5-1

Pacey, L. K., & Doering, L. C. (2007). Developmental expression of FMRP in the astrocyte lineage: implications for fragile X syndrome. *Glia, 55*(15), 1601-1609. doi:10.1002/glia.20573

Paixão, S., & Klein, R. (2010). Neuron-astrocyte communication and synaptic plasticity. *Curr Opin Neurobiol, 20*(4), 466-473. doi:10.1016/j.conb.2010.04.008

Paluszkiewicz, S. M., Olmos-Serrano, J. L., Corbin, J. G., & Huntsman, M. M. (2011). Impaired inhibitory control of cortical synchronization in fragile X syndrome. *J Neurophysiol, 106*(5), 2264-2272. doi:10.1152/jn.00421.2011

Pan, L., Woodruff, E., Liang, P., & Broadie, K. (2008). Mechanistic relationships between Drosophila fragile X mental retardation protein and metabotropic glutamate receptor A signaling. *Mol Cell Neurosci, 37*(4), 747-760. doi:10.1016/j.mcn.2008.01.003

Paribello, C., Tao, L., Folino, A., Berry-Kravis, E., Tranfaglia, M., Ethell, I. M., & Ethell, D. W. (2010). Open-label add-on treatment trial of minocycline in fragile X syndrome. *BMC Neurol, 10*, 91. doi:10.1186/1471-2377-10-91

Pascual, A., & Préat, T. (2001). Localization of long-term memory within the Drosophila mushroom body. *Science, 294*(5544), 1115-1117. doi:10.1126/science.1064200

Penagarikano, O., Mulle, J. G., & Warren, S. T. (2007). The pathophysiology of fragile x syndrome. *Annu Rev Genomics Hum Genet, 8*, 109-129. doi:10.1146/annurev.genom.8.080706.092249

Pizzorusso, T., Medini, P., Berardi, N., Chierzi, S., Fawcett, J. W., & Maffei, L. (2002). Reactivation of ocular dominance plasticity in the adult visual cortex. *Science, 298*(5596), 1248-1251. doi:10.1126/science.1072699

Porter, D., & Harrison, A. (2003). Minocycline-induced lupus: a case series. *N Z Med J, 116*(1171), U384. Retrieved from https://www.ncbi.nlm.nih.gov/pubmed/12740634

Reiss, A. L., & Freund, L. (1990). Fragile X syndrome, DSM-III-R, and autism. *J Am Acad Child Adolesc Psychiatry, 29*(6), 885-891. Retrieved from https://www.ncbi.nlm.nih.gov/pubmed/2273015

Rivera, S. M., Menon, V., White, C. D., Glaser, B., & Reiss, A. L. (2002). Functional brain activation during arithmetic processing in females with fragile X Syndrome is

related to FMR1 protein expression. *Hum Brain Mapp, 16*(4), 206-218. doi:10.1002/hbm.10048

Roberts, J. E., Mirrett, P., & Burchinal, M. (2001). Receptive and expressive communication development of young males with fragile X syndrome. *Am J Ment Retard, 106*(3), 216-230. doi:10.1352/0895-8017(2001)1062.0.CO;2

Roberts, T. P., Cannon, K. M., Tavabi, K., Blaskey, L., Khan, S. Y., Monroe, J. F., . . . Edgar, J. C. (2011). Auditory magnetic mismatch field latency: a biomarker for language impairment in autism. *Biol Psychiatry, 70*(3), 263-269. doi:10.1016/j.biopsych.2011.01.015

Rojas, D. C., Benkers, T. L., Rogers, S. J., Teale, P. D., Reite, M. L., & Hagerman, R. J. (2001). Auditory evoked magnetic fields in adults with fragile X syndrome. *Neuroreport, 12*(11), 2573-2576. Retrieved from https://www.ncbi.nlm.nih.gov/pubmed/11496151

Ronesi, J. A., & Huber, K. M. (2008). Homer interactions are necessary for metabotropic glutamate receptor-induced long-term depression and translational activation. *J Neurosci, 28*(2), 543-547. doi:10.1523/JNEUROSCI.5019-07.2008

Rossignol, R., Ranchon-Cole, I., Pâris, A., Herzine, A., Perche, A., Laurenceau, D., . . . Perche, O. (2014). Visual sensorial impairments in neurodevelopmental disorders: evidence for a retinal phenotype in Fragile X Syndrome. *PLoS One, 9*(8), e105996. doi:10.1371/journal.pone.0105996

Rotschafer, S., & Razak, K. (2013). Altered auditory processing in a mouse model of fragile X syndrome. *Brain Res, 1506*, 12-24. doi:10.1016/j.brainres.2013.02.038

Rotschafer, S. E., & Cramer, K. S. (2017). Developmental Emergence of Phenotypes in the Auditory Brainstem Nuclei of Fmr1 Knockout Mice. *eNeuro, 4*(6). doi:10.1523/ENEURO.0264-17.2017

Rotschafer, S. E., Marshak, S., & Cramer, K. S. (2015). Deletion of Fmr1 alters function and synaptic inputs in the auditory brainstem. *PLoS One, 10*(2), e0117266. doi:10.1371/journal.pone.0117266

Rotschafer, S. E., & Razak, K. A. (2014). Auditory processing in fragile x syndrome. *Front Cell Neurosci, 8*, 19. doi:10.3389/fncel.2014.00019

Sánchez, A. R., Rogers, R. S., & Sheridan, P. J. (2004). Tetracycline and other tetracycline-derivative staining of the teeth and oral cavity. *International journal of dermatology, 43*(10), 709-715.

Santoro, M. R., Bray, S. M., & Warren, S. T. (2012). Molecular mechanisms of fragile X syndrome: a twenty-year perspective. *Annu Rev Pathol, 7*, 219-245. doi:10.1146/annurev-pathol-011811-132457

Santos, A. R., Kanellopoulos, A. K., & Bagni, C. (2014). Learning and behavioral deficits associated with the absence of the fragile X mental retardation protein: what a fly and mouse model can teach us. *Learn Mem, 21*(10), 543-555. doi:10.1101/lm.035956.114

Sato, A. (2016). mTOR, a Potential Target to Treat Autism Spectrum Disorder. *CNS Neurol Disord Drug Targets, 15*(5), 533-543. Retrieved from https://www.ncbi.nlm.nih.gov/pubmed/27071790

Scerif, G., Cornish, K., Wilding, J., Driver, J., & Karmiloff-Smith, A. (2007). Delineation of early attentional control difficulties in fragile X syndrome: focus on neurocomputational changes. *Neuropsychologia, 45*(8), 1889-1898. doi:10.1016/j.neuropsychologia.2006.12.005

Schlaggar, B. L., Fox, K., & O'Leary, D. D. (1993). Postsynaptic control of plasticity in developing somatosensory cortex. *Nature, 364*(6438), 623-626. doi:10.1038/364623a0

Schlienger, R. G., Bircher, A. J., & Meier, C. R. (2000). Minocycline-induced lupus. A systematic review. *Dermatology, 200*(3), 223-231. doi:10.1159/000018387

Schneider, A., Leigh, M. J., Adams, P., Nanakul, R., Chechi, T., Olichney, J., . . . Hessl, D. (2013). Electrocortical changes associated with minocycline treatment in fragile X syndrome. *J Psychopharmacol, 27*(10), 956-963. doi:10.1177/0269881113494105

Selby, L., Zhang, C., & Sun, Q. Q. (2007). Major defects in neocortical GABAergic inhibitory circuits in mice lacking the fragile X mental retardation protein. *Neurosci Lett, 412*(3), 227-232. doi:10.1016/j.neulet.2006.11.062

Sharma, A., Hoeffer, C. A., Takayasu, Y., Miyawaki, T., McBride, S. M., Klann, E., & Zukin, R. S. (2010). Dysregulation of mTOR signaling in fragile X syndrome. *J Neurosci, 30*(2), 694-702. doi:10.1523/JNEUROSCI.3696-09.2010

Shepherd, J. (2002). Severe complication of a commonly prescribed drug: minocycline-induced lupus. *J Am Board Fam Pract, 15*(3), 239-241. Retrieved from https://www.ncbi.nlm.nih.gov/pubmed/12038732

Shetty, A. K. (2002). Tetracyclines in pediatrics revisited. *Clin Pediatr (Phila), 41*(4), 203-209. doi:10.1177/000992280204100402

Sidhu, H., Dansie, L. E., Hickmott, P. W., Ethell, D. W., & Ethell, I. M. (2014). Genetic removal of matrix metalloproteinase 9 rescues the symptoms of fragile X syndrome in a mouse model. *J Neurosci, 34*(30), 9867-9879. doi:10.1523/JNEUROSCI.1162-14.2014

Siegel, J. J., Chitwood, R. A., Ding, J. M., Payne, C., Taylor, W., Gray, R., . . . Johnston, D. (2017). Prefrontal Cortex Dysfunction in Fragile X Mice Depends on the Continued Absence of Fragile X Mental Retardation Protein in the Adult Brain. *J Neurosci, 37*(31), 7305-7317. doi:10.1523/JNEUROSCI.0571-17.2017

Simons, D. J. (1978). Response properties of vibrissa units in rat SI somatosensory neocortex. *J Neurophysiol, 41*(3), 798-820. Retrieved from https://www.ncbi.nlm.nih.gov/pubmed/660231

Simons, D. J., & Carvell, G. E. (1989). Thalamocortical response transformation in the rat vibrissa/barrel system. *J Neurophysiol, 61*(2), 311-330. Retrieved from https://www.ncbi.nlm.nih.gov/pubmed/2918357

Sinclair, D., Featherstone, R., Naschek, M., Nam, J., Du, A., Wright, S., . . . Siegel, S. J. (2017). GABA-B Agonist Baclofen Normalizes Auditory-Evoked Neural Oscillations and Behavioral Deficits in the. *eNeuro, 4*(1). doi:10.1523/ENEURO.0380-16.2017

Sinclair, D., Oranje, B., Razak, K. A., Siegel, S. J., & Schmid, S. (2017). Sensory processing in autism spectrum disorders and Fragile X syndrome-From the clinic to animal models. *Neurosci Biobehav Rev, 76*(Pt B), 235-253. doi:10.1016/j.neubiorev.2016.05.029

Smith, K., & Leyden, J. J. (2005). Safety of doxycycline and minocycline: a systematic review. *Clin Ther, 27*(9), 1329-1342. doi:10.1016/j.clinthera.2005.09.005

St Clair, D. M., Blackwood, D. H., Oliver, C. J., & Dickens, P. (1987). P3 abnormality in fragile X syndrome. *Biol Psychiatry, 22*(3), 303-312. Retrieved from https://www.ncbi.nlm.nih.gov/pubmed/2949781

Strumbos, J. G., Brown, M. R., Kronengold, J., Polley, D. B., & Kaczmarek, L. K. (2010). Fragile X mental retardation protein is required for rapid experience-dependent regulation of the potassium channel Kv3.1b. *J Neurosci, 30*(31), 10263-10271. doi:10.1523/JNEUROSCI.1125-10.2010

Sudhakaran, I. P., Hillebrand, J., Dervan, A., Das, S., Holohan, E. E., Hülsmeier, J., . . . Ramaswami, M. (2014). FMRP and Ataxin-2 function together in long-term olfactory habituation and neuronal translational control. *Proc Natl Acad Sci U S A, 111*(1), E99-E108. doi:10.1073/pnas.1309543111

Sun, Y. J., Wu, G. K., Liu, B. H., Li, P., Zhou, M., Xiao, Z., . . . Zhang, L. I. (2010). Fine-tuning of pre-balanced excitation and inhibition during auditory cortical development. *Nature, 465*(7300), 927-931. doi:10.1038/nature09079

Sutcliffe, J. S., Nelson, D. L., Zhang, F., Pieretti, M., Caskey, C. T., Saxe, D., & Warren, S. T. (1992). DNA methylation represses FMR-1 transcription in fragile X syndrome. *Hum Mol Genet, 1*(6), 397-400. Retrieved from https://www.ncbi.nlm.nih.gov/pubmed/1301913

Taha, S., & Stryker, M. P. (2002). Rapid ocular dominance plasticity requires cortical but not geniculate protein synthesis. *Neuron, 34*(3), 425-436

.

Teitelbaum, J. E., Perez-Atayde, A. R., Cohen, M., Bousvaros, A., & Jonas, M. M. (1998). Minocycline-related autoimmune hepatitis: case series and literature review. *Arch Pediatr Adolesc Med, 152*(11), 1132-1136. Retrieved from https://www.ncbi.nlm.nih.gov/pubmed/9811293

Till, S. M., Asiminas, A., Jackson, A. D., Katsanevaki, D., Barnes, S. A., Osterweil, E. K., . . . Kind, P. C. (2015). Conserved hippocampal cellular pathophysiology but distinct behavioural deficits in a new rat model of FXS. *Hum Mol Genet, 24*(21), 5977-5984. doi:10.1093/hmg/ddv299

Till, S. M., Wijetunge, L. S., Seidel, V. G., Harlow, E., Wright, A. K., Bagni, C., . . . Kind, P. C. (2012). Altered maturation of the primary somatosensory cortex in a mouse model of fragile X syndrome. *Hum Mol Genet, 21*(10), 2143-2156. doi:10.1093/hmg/dds030

Tournigand, C., Généreau, T., Prudent, M., Diemert, M. C., Herson, S., & Chosidow, O. (1999). Minocycline-induced clinical and biological lupus-like disease. *Lupus, 8*(9), 773-774. doi:10.1191/096120399678841025

Ullian, E. M., Christopherson, K. S., & Barres, B. A. (2004). Role for glia in synaptogenesis. *Glia, 47*(3), 209-216. doi:10.1002/glia.20082

Ungerleider, L. G. (1982). Two cortical visual systems. *Analysis of visual behavior*, 549-586.

van 't Padje, S., Engels, B., Blonden, L., Severijnen, L. A., Verheijen, F., Oostra, B. A., & Willemsen, R. (2005). Characterisation of Fmrp in zebrafish: evolutionary dynamics of the fmr1 gene. *Dev Genes Evol, 215*(4), 198-206. doi:10.1007/s00427-005-0466-0

van den Ouweland, A. M., de Vries, B. B., Bakker, P. L., Deelen, W. H., de Graaff, E., van Hemel, J. O., . . . Halley, D. J. (1994). DNA diagnosis of the fragile X syndrome in a series of 236 mentally retarded subjects and evidence for a reversal of mutation in the FMR-1 gene. *Am J Med Genet, 51*(4), 482-485. doi:10.1002/ajmg.1320510437

Van der Molen, M. J., Van der Molen, M. W., Ridderinkhof, K. R., Hamel, B. C., Curfs, L. M., & Ramakers, G. J. (2012a). Auditory and visual cortical activity during selective attention in fragile X syndrome: a cascade of processing deficiencies. *Clin Neurophysiol, 123*(4), 720-729. doi:10.1016/j.clinph.2011.08.023

Van der Molen, M. J., Van der Molen, M. W., Ridderinkhof, K. R., Hamel, B. C., Curfs, L. M., & Ramakers, G. J. (2012b). Auditory change detection in fragile X syndrome males: a brain potential study. *Clin Neurophysiol, 123*(7), 1309-1318. doi:10.1016/j.clinph.2011.11.039

Vanderklish, P. W., & Edelman, G. M. (2002). Dendritic spines elongate after stimulation of group 1 metabotropic glutamate receptors in cultured hippocampal neurons. *Proc Natl Acad Sci U S A, 99*(3), 1639-1644. doi:10.1073/pnas.032681099

Verkerk, A. J., Pieretti, M., Sutcliffe, J. S., Fu, Y. H., Kuhl, D. P., Pizzuti, A., . . . Zhang, F. P. (1991). Identification of a gene (FMR-1) containing a CGG repeat coincident with a breakpoint cluster region exhibiting length variation in fragile X syndrome. *Cell, 65*(5), 905-914. Retrieved from https://www.ncbi.nlm.nih.gov/pubmed/1710175

Volk, L. J., Pfeiffer, B. E., Gibson, J. R., & Huber, K. M. (2007). Multiple Gq-coupled receptors converge on a common protein synthesis-dependent long-term depression that is affected in fragile X syndrome mental retardation. *J Neurosci, 27*(43), 11624-11634. doi:10.1523/JNEUROSCI.2266-07.2007

Wan, L., Dockendorff, T. C., Jongens, T. A., & Dreyfuss, G. (2000). Characterization of dFMR1, a Drosophila melanogaster homolog of the fragile X mental retardation protein. *Mol Cell Biol, 20*(22), 8536-8547. Retrieved from https://www.ncbi.nlm.nih.gov/pubmed/11046149

Wang, J., Ethridge, L. E., Mosconi, M. W., White, S. P., Binder, D. K., Pedapati, E. V., . . . Sweeney, J. A. (2017). A resting EEG study of neocortical hyperexcitability and altered functional connectivity in fragile X syndrome. *J Neurodev Disord, 9*, 11. doi:10.1186/s11689-017-9191-z

Wang, Y., Sakano, H., Beebe, K., Brown, M. R., de Laat, R., Bothwell, M., . . . Rubel, E. W. (2014). Intense and specialized dendritic localization of the fragile X mental retardation protein in binaural brainstem neurons: a comparative study in the alligator, chicken, gerbil, and human. *J Comp Neurol, 522*(9), 2107-2128. doi:10.1002/cne.23520

Wen, T. H., Afroz, S., Reinhard, S. M., Palacios, A. R., Tapia, K., Binder, D. K., . . . Ethell, I. M. (2017). Genetic Reduction of Matrix Metalloproteinase-9 Promotes Formation of Perineuronal Nets Around Parvalbumin-Expressing Interneurons and Normalizes Auditory Cortex Responses in Developing Fmr1 Knock-Out Mice. *Cereb Cortex*, 1-14. doi:10.1093/cercor/bhx258

Wilson, B. M., & Cox, C. L. (2007). Absence of metabotropic glutamate receptor-mediated plasticity in the neocortex of fragile X mice. *Proc Natl Acad Sci U S A, 104*(7), 2454-2459. doi:10.1073/pnas.0610875104

Xu, S., Poidevin, M., Han, E., Bi, J., & Jin, P. (2012). Circadian rhythm-dependent alterations of gene expression in Drosophila brain lacking fragile X mental retardation protein. *PLoS One, 7*(5), e37937. doi:10.1371/journal.pone.0037937

Yan, Q. J., Rammal, M., Tranfaglia, M., & Bauchwitz, R. P. (2005). Suppression of two major Fragile X Syndrome mouse model phenotypes by the mGluR5 antagonist MPEP. *Neuropharmacology, 49*(7), 1053-1066. doi:10.1016/j.neuropharm.2005.06.004

Yau, S. Y., Bettio, L., Vetrici, M., Truesdell, A., Chiu, C., Chiu, J., . . . Christie, B. R. (2018). Chronic minocycline treatment improves hippocampal neuronal structure, NMDA receptor function, and memory processing in Fmr1 knockout mice. *Neurobiol Dis, 113*, 11-22. doi:10.1016/j.nbd.2018.01.014

Yun, S. W., Platholi, J., Flaherty, M. S., Fu, W., Kottmann, A. H., & Toth, M. (2006). Fmrp is required for the establishment of the startle response during the critical period of auditory development. *Brain Res, 1110*(1), 159-165. doi:10.1016/j.brainres.2006.06.086

Zalfa, F., Giorgi, M., Primerano, B., Moro, A., Di Penta, A., Reis, S., . . . Bagni, C. (2003). The fragile X syndrome protein FMRP associates with BC1 RNA and regulates the translation of specific mRNAs at synapses. *Cell, 112*(3), 317-327. Retrieved from https://www.ncbi.nlm.nih.gov/pubmed/12581522

Zaman, T., De Oliveira, C., Smoka, M., Narla, C., Poulter, M. O., & Schmid, S. (2017). BK Channels Mediate Synaptic Plasticity Underlying Habituation in Rats. *J Neurosci, 37*(17), 4540-4551. doi:10.1523/JNEUROSCI.3699-16.2017

Zars, T., Fischer, M., Schulz, R., & Heisenberg, M. (2000). Localization of a short-term memory in Drosophila. *Science, 288*(5466), 672-675. Retrieved from https://www.ncbi.nlm.nih.gov/pubmed/10784450

Zhang, J., Fang, Z., Jud, C., Vansteensel, M. J., Kaasik, K., Lee, C. C., . . . Nelson, D. L. (2008). Fragile X-related proteins regulate mammalian circadian behavioral rhythms. *Am J Hum Genet, 83*(1), 43-52. doi:10.1016/j.ajhg.2008.06.003

Zhang, Y., Bonnan, A., Bony, G., Ferezou, I., Pietropaolo, S., Ginger, M., . . . Frick, A. (2014). Dendritic channelopathies contribute to neocortical and sensory hyperexcitability in Fmr1(-/y) mice. *Nat Neurosci, 17*(12), 1701-1709. doi:10.1038/nn.3864

Zhang, Y., Brown, M. R., Hyland, C., Chen, Y., Kronengold, J., Fleming, M. R., . . . Kaczmarek, L. K. (2012). Regulation of neuronal excitability by interaction of fragile X mental retardation protein with slack potassium channels. *J Neurosci, 32*(44), 15318-15327. doi:10.1523/JNEUROSCI.2162-12.2012

Zhang, Y. Q., Bailey, A. M., Matthies, H. J., Renden, R. B., Smith, M. A., Speese, S. D., . . . Broadie, K. (2001). Drosophila fragile X-related gene regulates the MAP1B homolog Futsch to control synaptic structure and function. *Cell, 107*(5), 591-603. Retrieved from https://www.ncbi.nlm.nih.gov/pubmed/11733059

Zhang, Y. Q., Matthies, H. J., Mancuso, J., Andrews, H. K., Woodruff, E., Friedman, D., & Broadie, K. (2004). The Drosophila fragile X-related gene regulates axoneme differentiation during spermatogenesis. *Dev Biol, 270*(2), 290-307. doi:10.1016/j.ydbio.2004.02.010

Zhao, M. G., Toyoda, H., Ko, S. W., Ding, H. K., Wu, L. J., & Zhuo, M. (2005). Deficits in trace fear memory and long-term potentiation in a mouse model for fragile X syndrome. *J Neurosci, 25*(32), 7385-7392. doi:10.1523/JNEUROSCI.1520-05.2005

Zorio, D. A., Jackson, C. M., Liu, Y., Rubel, E. W., & Wang, Y. (2017). Cellular distribution of the fragile X mental retardation protein in the mouse brain. *J Comp Neurol, 525*(4), 818-849. doi:10.1002/cne.24100

Figure 1.1

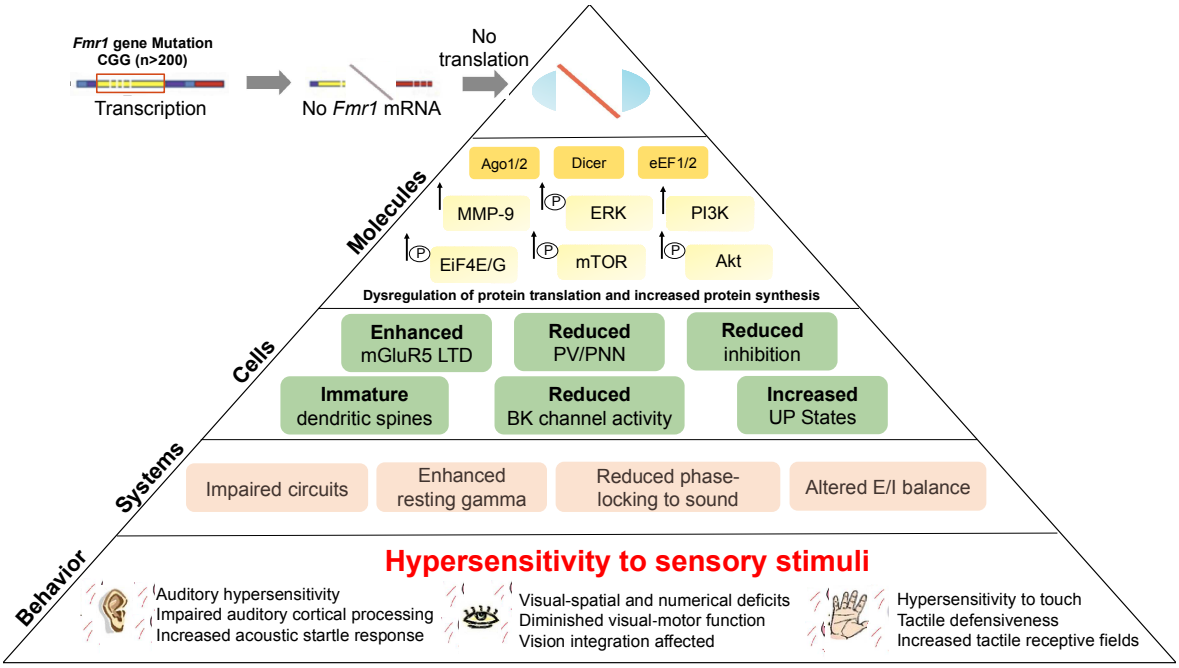

Figure 1.1. Mechanisms of sensory phenotypes associated with FXS.
Fragile X syndrome is associated with an expansion of CGG repeats in 5′ untranslated area of the fragile X mental retardation 1 (*Fmr1*) gene, which leads to silencing *Fmr1* gene and a partial or full loss of the fragile X mental retardation protein (FMRP). FMRP is an RNA-binding protein that regulates translation of mRNAs at synapses, some of which encode proteins involved in protein synthesis and synaptic plasticity. FMRP is known to regulate protein translation through eukaryotic translation elongation factor 1/2 (eEF1/2), argonaute proteins (Ago1/2), eukaryotic translation initiation factor 4 E/G (eIF4E/G), and Dicer. FMRP may also directly regulate phosphatidylinositide-3-kinase (PI3K), Akt, mammalian target of rapamycin (mTOR), and extracellular signal-regulated kinase (ERK) signaling. Lack of FMRP also leads to enhanced metabotropic glutamate receptor 5 (mGluR5)-mediated long-term depression (LTD), reduced voltage and Ca^{2+} activated K^{+} (BK) channel activity, and increased matrix metalloproteinase-9 (MMP-9) activity, which affect cellular responses resulting in reduced inhibition, impaired development of parvalbumin (PV) interneurons and perineuronal nets (PNN), increased UP states, and abnormal dendritic spine development. These molecular and cellular alterations can contribute to system-level changes, such as impaired development of neural circuits, enhanced resting gamma, and altered excitatory/inhibitory (E/I) balance, which may underlie sensory hypersensitivity and altered behaviors observed in FXS.

Figure 1.2

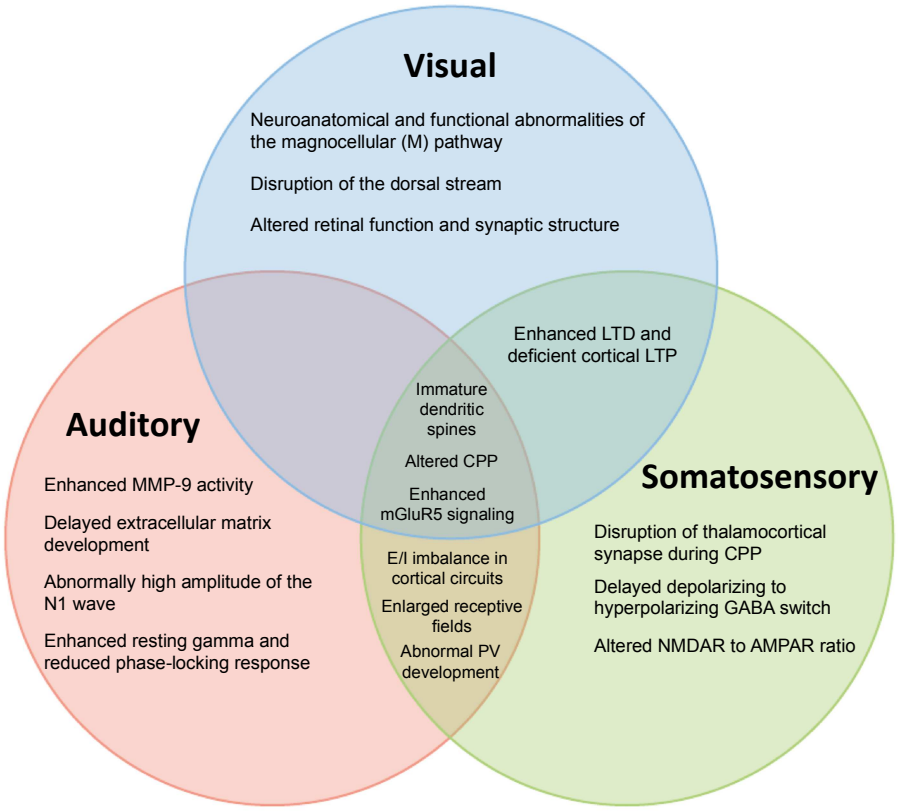

Figure 1.2. Altered auditory, visual, and somatosensory processing phenotypes observed in FXS pathology.

Table 1.1. Impaired Sensory Mechanisms in FXS
***h**= human; **m**=mouse; **r**=rat; **d**=drosophila; **z**=zebrafish

Mechanisms	**Auditory**	**Somato sensory**	**Visual**	**Other systems**
Immature dendritic spine morphology *(Comery et al. 1997, Irwin et al. 2001, Nimchinsky et al. 2001, Kogan et al. 2004b, Galvez & Greenough 2005, Berman et al. 2012, Till et al. 2015)*	m	m	h, m	h*, r
Altered critical period plasticity *(Dölen et al. 2007, Gonçalves et al. 2013, Kim et al. 2013)*	m	m	m	
Enhanced mGluR5 signaling *(Bear et al. 2004, Dölen et al. 2007, Dölen & Bear 2008, Hays et al. 2011, Kim et al. 2013)*	m	m	m	m
Abnormal E/I balance in cortical circuits *(Penagarikano et al. 2007, Gibson et al. 2008, Braat & Kooy 2015, Berzhanskaya et al. 2017)*	m	m	r	
Abnormal PV cell development *(Selby et al. 2007, Nomura et al. 2017, Wen et al. 2017)*	m	m		
Enlarged receptive fields and prolong responses *(Rotschafer & Razak 2013, Juczewski et al. 2016)*	m	m		
Enhanced long-term depression and deficient cortical long-term potentiation *(Li et al. 2002, Zhao et al. 2005, Wilson & Cox 2007, Ng et al. 2013, Jackson 2017)*		m	m	r, z
Enhanced MMP-9 activity *(Bilousova et al. 2009, Gkogkas et al. 2014, Sidhu et al. 2014)*	m			h*
Delayed extracellular matrix and perineuronal net **development** *(Happel & Frischknecht 2016, Wen et al. 2017)*	m			
Abnormally high amplitude of the N1 wave and reduced habituation *(Castrén et al. 2003, Schneider et al. 2013, Ethridge et al. 2016)*	h, m			
Enhanced resting gamma and reduced phase-locking response *(Ethridge et al. 2017, Wang et al. 2017)*	h			

Impaired cortical representation of speech sounds *(Engineer et al. 2014)*	r			
Disruption of thalamocortical synapse during critical period plasticity *(Daw et al. 2007b, Harlow et al. 2010)*		m		
Delayed depolarizing to hyperpolarizing GABA switch *(He et al. 2014)*		m		
Altered NMDAR to AMPAR ratio *(Harlow et al. 2010)*		m		
Abnormal magnocellular pathway *(Kogan et al. 2004b)*			h	
Disruption of the dorsal stream *(Kogan et al. 2004a, Farzin & Rivera 2010)*			h	
Altered retinal function and synaptic structure *(Rossignol et al. 2014)*			m	
Defects in synaptic transmission in the optic lobe *(Zhang et al. 2001)*			d	
Impaired long-term olfactory habituation *(Sudhakaran et al. 2014)*				d
Reduced specificity in odor coding and alterations *(Franco et al. 2017)*				d
Defects in axons and dendrites in the neuromuscular junction and mushroom body *(McBride et al. 1999, Zars et al. 2000, Pascual & Préat 2001, Zhang et al. 2001)*				d
Altered circadian rhythm behaviors *(Dockendorff et al. 2002, Inoue et al. 2002, Morales et al. 2002, Zhang et al. 2008)*				m, d

*post mortem tissue

Chapter 2 – Deletion of *Fmr1* from Forebrain Excitatory Neurons Triggers Abnormal Cellular, Molecular, and Behavioral Phenotypes in the Auditory Cortex of a Mouse Model of Fragile X Syndrome

Abstract

Fragile X Syndrome (FXS) is a leading genetic cause of autism with symptoms that include sensory processing deficits. We previously showed that elevated levels of matrix metalloproteinase-9 (MMP-9) may contribute to these phenotypes by affecting perineuronal nets (PNNs) around parvalbumin (PV) interneurons in the auditory cortex of *Fmr1* KO mice. However, how different cell types within local cortical circuits contribute to these deficits is not known. Here, we examined whether *Fmr1* deletion in forebrain excitatory neurons affects MMP-9 activity and PV/PNN expression in the auditory cortex. We found that cortical MMP-9 gelatinase activity and mTOR/Akt phosphorylation were enhanced in $Cre^{Nex1}/Fmr1^{Flox/y}$ cKO mice, whereas the density of PV/PNN cells was reduced. The $Cre^{Nex1}/Fmr1^{Flox/y}$ cKO mice also show increased locomotor activity, but not the anxiety-like behaviors. These results indicate that FMRP changes in excitatory neurons in the cortex are sufficient to elicit cellular, molecular, and behavioral phenotypes in *Fmr1* KO mice. More broadly, these results indicate that local cortical circuit abnormalities contribute to sensory processing deficits in autism spectrum disorders.

Introduction

Fragile X Syndrome (FXS) is a common monogenic form of autism spectrum disorders (ASD) (Crawford, Acuna, & Sherman, 2001). FXS is usually caused by a CGG repeat expansion in 5'-untranslated region of the *Fragile X mental retardation 1* (*Fmr1) gene* with consequent gene methylation, down-regulation of Fragile X Mental Retardation Protein (FMRP), translational dysregulation, and abnormal protein synthesis (Sutcliffe et al., 1992; Verkerk et al., 1991). Symptoms of FXS include anxiety, intellectual disability, repetitive behaviors, social communication deficits, and abnormal sensory processing (Braat & Kooy, 2015; Penagarikano, Mulle, & Warren, 2007). Abnormal sensory processing in FXS includes debilitating hypersensitivity and reduced habituation to sensory inputs, particularly in the auditory domain (Castrén, Pääkkönen, Tarkka, Ryynänen, & Partanen, 2003; Ethridge et al., 2016; Schneider et al., 2013). These symptoms are seen early in development, and may lead to cognitive deficits and delayed language.

Auditory hypersensitivity and cortical processing deficits are observed in humans with FXS and the mouse model of FXS, the *Fmr1* knockout (KO) mice (Castrén et al., 2003; L. Chen & Toth, 2001; Ethridge et al., 2016; Nielsen, Derber, McClellan, & Crnic, 2002; Rais, Binder, Razak, & Ethell, 2018; Rojas et al., 2001; S. Rotschafer & Razak, 2013; S. E. Rotschafer & Razak, 2014; Sinclair, Oranje, Razak, Siegel, & Schmid, 2017). Our previous studies suggested a novel mechanism for auditory hypersensitivity in FXS. Impaired development of parvalbumin (PV)-expressing inhibitory interneurons may underlie abnormal auditory cortical processing in *Fmr1* KO mice *via* matrix

metalloproteinase-9 (MMP-9)-dependent regulation of perineuronal nets (PNNs) (Wen et al., 2018). FMRP negatively regulates MMP-9 translation in neurons (Dziembowska et al., 2013; Dziembowska & Wlodarczyk, 2012; Janusz et al., 2013), and MMP-9 levels are elevated in the brain of *Fmr1* KO mice and FXS postmortem brain tissues (Bilousova et al., 2009; Gkogkas et al., 2014; Sidhu, Dansie, Hickmott, Ethell, & Ethell, 2014; Wen et al., 2018). MMP-9 is secreted from a number of cell types, including astrocytes and neurons (Szklarczyk, Lapinska, Rylski, McKay, & Kaczmarek, 2002). MMP-9 can also mediate changes in synaptic functions by signaling through the PI3K/Akt/mTOR pathway (Sidhu et al., 2014), potentially through BDNF/trkB signaling by cleaving pro-BDNF (Hwang, Park, Choi, & Koh, 2005; Yang et al., 2009) or activating integrin receptors (L. Y. Chen et al., 2010; Legate, Wickström, & Fässler, 2009). PI3K/Akt/mTOR pathway is implicated in FXS symptoms (Enriquez-Barreto & Morales, 2016; Gross, Yao, Pong, Jeromin, & Bassell, 2011; Hoeffer et al., 2012; Klann & Dever, 2004; Ronesi & Huber, 2008; Sato, 2016; Sharma et al., 2010). Therefore, MMP-9 may contribute to the changes in cortical hyperexcitability of *Fmr1* KO mice by affecting both inhibitory and excitatory neurons. *In vitro* slice recordings showed increased cortical excitability in mouse somatosensory cortex with deletion of *Fmr1* only from excitatory neurons, suggesting that FMRP expression in excitatory cortical neurons is required for normal cortical activity (Hays, Huber, & Gibson, 2011).

One method to begin understanding the cell-type and circuit-specific mechanisms underlying the phenotypes in a genetic disorder is to remove the gene from specific cell types and circuits. Therefore, the main goal of this study was to determine the

neurobehavioral phenotypes following deletion of *Fmr1* from forebrain excitatory neurons. Our data show that removal of FMRP from forebrain excitatory neurons is sufficient to elicit FXS-associated symptoms including enhanced MMP-9 activity and mTOR/Akt signaling, impaired PV/PNN expression and hyperactive behaviors. Together, these data suggest novel mechanisms that lead to sensory hypersensitivity in FXS and potentially other autism spectrum disorders.

Materials and Methods

Mice

C57Bl/6 *Fmr1* KO mice and their congenic controls were obtained from Jackson Laboratories. In order to delete FMRP specifically from forebrain excitatory neurons, we crossed male Cre^{Nex1} with female $Fmr1^{flox/flox}$ mice to produce male $Cre^{Nex1}/Fmr1^{flox/y}$ conditional knock out (cKO) mice and their wild type (WT) littermates, $Fmr1^{flox/y}$ mice. $Fmr1^{flox}$ mice were obtained from Dr. David Nelson (Baylor College of Medicine, Houston, Texas) (Mientjes et al., 2006). *Nex1(NeuroD6)*-Cre mice (Goebbels et al., 2006) were generated in Dr. Klaus Nave's lab (Göttingen, Germany) and breeding pairs were obtained from Dr. Joshua Sanes' lab (Harvard University). Separate groups of mice were used for biochemical analysis and behavior tests. All genotypes were confirmed by PCR analysis of genomic DNA isolated from mouse tails. Mice were maintained in an AAALAC accredited facility under 12 hour light/dark cycle and fed standard mouse chow. All procedures were done according to NIH and Institutional Animal Care and Use

Committee guidelines. All procedures were approved by IACUC. Food and water were provided to the mice *ad libitum*.

Methods Overview

Goebbels et al., (2006) reported that most of the Cre activity in the Nex-Cre mice was in neocortex and hippocampus, and marked pyramidal neurons of the cortex without affecting inhibitory or glial cells. These mice are often used for generating forebrain excitatory neuron specific deletion of specific genes (Ballester-Rosado et al., 2010; Kazdoba et al., 2012; Kerrisk, Greer, & Koleske, 2013). To confirm deletion of FMRP in forebrain excitatory neurons, we examined expression of FMRP in the auditory cortex in P60-70 mice using immunostaining. FMRP is also expressed in auditory thalamus and midbrain of WT mice. To ensure that FMRP is deleted specifically in the forebrain, we quantified expression of FMRP in the medial geniculate body and inferior colliculus, major nuclei of the lemniscal auditory thalamus and midbrain, respectively. We also compared the effects of forebrain excitatory neuron specific *Fmr1* deletion to global *Fmr1* KO mice of the same age on PV/PNN expression in adult auditory cortex. This was necessary because our previous study only examined the developing brain (Wen et al., 2018). This was followed by measurements of the effects of FMRP deletion from forebrain excitatory neurons on gelatinase activity and mTOR/Akt phosphorylation in the adult auditory cortex of both global *Fmr1* KO and $Cre^{Nex1}/Fmr1^{Flox/y}$ cKO mice. Finally, we examined anxiety-like behaviors and hyperactivity in $Cre^{Nex1}/Fmr1^{Flox/y}$ cKO mice to compare with our previous study of these phenotypes in global *Fmr1* KO mice (Dansie et al., 2013).

Immunofluorescence

Age-matched adult (P60-70) male *Fmr1* KO and WT, or $Cre^{Nex1}/Fmr1^{Flox/y}$ cKO and $Fmr1^{Flox/y}$ mice were euthanized with isoflurane and sodium pentobarbital and perfused transcardially first with cold phosphate-buffered saline (PBS, 0.1 M) to clear out the blood and then with 4% paraformaldehyde (PFA) in 0.1M PBS for fixation. Brains were removed and post-fixed for 2–4h in 4% PFA. 40-100μm brain slices were obtained using a vibratome (5100mz Campden Instruments). Auditory cortex was identified using hippocampal and brain atlas landmarks (Paxinos & Franklin, 2004). For each brain, an average of 5–6 brain slices containing auditory cortex, thalamus or inferior colliculus were collected.

Detection of PV/PNN

Immunostaining in 100μm brain slices containing auditory cortex was performed as previously described with minor modifications (Wen et al., 2018). Briefly, brain slices were post-fixed for an additional 2h in 4% PFA in 0.1 M PBS and then washed 3 times in 0.1M PBS for 10 min. Slices were then quenched with 50mM ammonium chloride for 15 min and washed 3 times with PBS for 10 min. Next, brain tissues were permeabilized with 0.1% Triton X-100 in PBS and nonspecific staining was blocked with a 5% Normal Goat Serum (NGS; Sigma, catalog# G9023-10 mL) and 1% Bovine Serum Albumin (BSA; Fisher Scientific, catalog# 9048468) in 0.1M PBS solution. Brain slices were treated overnight with mouse anti-parvalbumin antibody (1:1000; Sigma, catalog# P3088, RRID:AB_477 329) to label parvalbumin-positive (PV) inhibitory interneurons. Wisteria floribunda agglutinin (WFA; 4μg/mL; Vector Laboratories, cat# FL-1351, RRID:AB_2

336875) in 0.1M PBS containing 1% NGS, 0.5% BSA, and 0.1% Tween-20 solution was used to stain for PNNs containing aggrecan, known as WFA+ PNNs. WFA is a lectin, which binds glycosaminoglycan side chains of chondroitin sulfate proteoglycan aggrecan that is found in PNNs (Pizzorusso et al., 2002). After incubation, brain slices were washed 3 times in 0.1M PBS containing 0.5% Tween-20 for 10 min and incubated with secondary antibody, donkey anti-mouse Alexa 594 (4µg/mL; Thermo Fisher Scientific, catalog# A-21203, RRID:AB_2 535789) in 0.1M PBS for 1h. Slices were then washed 3 times with 0.1M PBS containing 0.5% Tween-20 for 10 min, mounted with Vectashield containing DAPI (Vector Labs, catalog# H-1200, RRID: AB_2336790) and Cytoseal (ThermoScientific, catalog# 8310–16).

Detection of FMRP Expression

Immunostaining for FMRP was performed using antigen retrieval methods, as previously described (Christie, Akins, Schwob, & Fallon, 2009; Gabel et al., 2004; Gross et al., 2011), with the following modifications. 40µm brain slices were mounted onto Superfrost Plus Microscope Charged Slides (Fisher Scientific, catalog #22-034-979); washed 3 times with TBS (0.1M Tris Cl pH7.5, 0.15M NaCl) for 10 min; treated with 0.8% Na Borohydride (Sigma S-9125) to reduce background and autofluorescence; and boiled in 0.01M Na Citrate (Citric acid, sodium salt in water pH 6.0, Sigma C-8532) to achieve antigen retrieval. Permeabilization was performed with 0.5% Triton-X 100 for 20 min, and slices were stained overnight with mouse anti-FMRP (1:100; Developmental Studies Hybridoma Bank, catalog #2F5-1-s, RRID: AB_10805421), and rabbit anti-NeuN (1:1000; Abcam, catalog #ab104225, RRID: AB_10711153) in TBS containing 2%

Normal Donkey serum (NDS) and 0.1% Triton-X 100. After incubation with primary antibodies, slices were washed 3 times in TBS for 10 min and incubated with secondary antibodies for 1h. Secondary antibodies used were donkey anti-rabbit Alexa 594 (4µg/mL; Thermo Fisher Scientific, catalog# A-21207, RRID:AB_141637), and donkey anti-mouse Alexa 488 (4µg/mL; Molecular Probes, catalog# A-21202, RRID:AB_141607). Slices were mounted with Vectashield containing DAPI and cytoseal and imaged.

Image Analysis

Slices were imaged using confocal microscopy (Leica SP5) by collecting a series of 20 high-resolution optical sections (1024 × 1024-pixel format) at 1 um step intervals (z-stack) that were captured for each slice using a 10×, 20×, or a 63× water-immersion objective (1.2 numerical aperture), with 1× or 5× zoom. All images were acquired under identical conditions. Each z-stack was collapsed into a single image by projection, converted to a TIFF file, encoded for blind analysis, and analyzed using ImageJ. ImageJ was used to identify and manually count PV-positive cells, WFA-positive PNN cells, PV/PNN co-localization, NeuN-positive cells and FMRP/NeuN co-localization. Cortical layers were identified as previously reported (Anderson, Christianson, & Linden, 2009) and used for layer-specific analysis. Three slices were used per animal and cell counts were obtained in layers 1–4 of both the right and left auditory cortex (cell density was measured per layer). The freehand selection tool and measure function was used to specify layers of the auditory cortex and the point tool was used to label PNNs, PV cells, and NeuN cells added to the ROI manager. Particle Analysis Cell Counter plugin in

Image J was used to count co-localization. Average cell density was calculated for each animal. Because we were comparing different mouse lines, the global *Fmr1* KO and the $Cre^{Nex1}/Fmr1^{Flox/y}$ cKO mice were evaluated against their specific controls (WT and $Fmr1^{Flox/y}$, respectively), and statistical analysis was performed with unpaired t-test using GraphPad Prism 6 software (RRID: SCR_002798). Data represent mean ± standard error of the mean (SEM).

Dye-Quenched (DQ) Gelatin Assay and Analysis

The DQ-Gelatin plate assay was used to assess gelatinase activity. A FITC-quenched gelatin peptide that fluoresces following cleavage by gelatinases MMP-2 and MMP-9 was used to measure gelatinase proteolytic activity. Adult (P60-70) male WT and *Fmr1* KO mice, or $Fmr1^{Flox/y}$ and $Cre^{Nex1}/Fmr1^{Flox/y}$ cKO litter mates (n = 4-6 mice per group) were euthanized with isoflurane and the auditory cortex was dissected based on coordinates (Paxinos & Franklin, 2004) and previous electrophysiological and dye-placement studies (Martin del Campo, Measor, & Razak, 2012). Auditory cortex tissues were re-suspended in lysis buffer (50mM Tris-HCl, pH 7.4, 150mM NaCl, 5mM EDTA, 0.05% Triton X-100, and 1mM PMSF) containing protease inhibitor cocktail (Sigma, cat. # P8340) and phosphatase inhibitor cocktail (Sigma, cat. #P0044). Lysates were measured for total protein concentrations using the protocol for the BCA colorimetric protein assay (Pierce, cat#23235).

Lysates were diluted in reaction buffer and mixed with a fluorescence-labeled gelatin substrate (Molecular Probes, E12055). Samples were incubated in the dark for 3h at room temperature. The fluorescence intensity was analyzed using 495nm excitation

wavelength and 515nm emission wavelength. The signal was measured every 20min during the 3h incubation period using a fluorescence microplate reader equipped with standard fluorescein filters (SoftMax Pro). For each time point, background fluorescence intensity was corrected by subtracting the values derived from reaction buffer control. A standard curve to assess gelatinase activity was generated using recombinant mouse MMP-9 (rmMMP-9, approximately 1,500 pmol/min/μg, R&D Systems, cat. #909-MM-010). A linear regression of rmMMP-9 activity (standard curve) and relative gelatinase activity based on the average fluorescence intensity of five replicates was used to assess gelatinase proteolytic activity in the brain samples. Statistical analysis was performed comparing KO samples to their corresponding WT samples with unpaired t-test using GraphPad Prism 6 software (RRID: SCR_002798). Data represent mean ± standard error of the mean (SEM).

Western Blot Analysis

The auditory cortex was removed from each mouse (n=4 mice per group), cooled in PBS, and homogenized in ice-cold lysis buffer (50mM Tris-HCl, pH 7.4, 150mM NaCl, 5mM EDTA, 0.05% Triton X-100, and 1mM PMSF) containing protease inhibitor cocktail (Sigma, cat. # P8340) and phosphatase inhibitor cocktail (Sigma, cat. #P0044). The samples were rotated at 4°C for at least 1h to allow for complete cell lysis and then cleared by centrifugation at 13,200 rpm for 15 min at 4°C. Supernatants were isolated and boiled in reducing sample buffer (Laemmli 2× concentrate, S3401, Sigma), and separated on 8–16% Tris-Glycine SDS-PAGE precast gels (EC6045BOX, Life Technologies). Proteins were transferred onto Protran BA 85 Nitrocellulose membrane

(GE Healthcare) and blocked for 1h at room temperature in 5% skim milk (catalog #170-6404, Bio-Rad). Primary antibody incubations were performed overnight at 4°C with antibodies diluted in TBS/0.1% Tween-20/5% BSA. The following primary antibodies were used: rabbit anti-mammalian target of rapamycin (mTOR; 7C10; catalog #2983, RRID:AB_2105622); rabbit anti-phospho-mTOR (Ser2481; catalog #2974, RRID:AB_2231885); rabbit anti-Akt (catalog #9272; RRID:AB_10699016); rabbit anti-phospho-Akt (Ser473; catalog #9271, RRID: AB_329825); mouse anti-Aggrecan at 1:200 (Novus, catalog #NB110-6852, RRID: AB_787911); mouse anti-PV (Millipore, catalog #MAB1572, RRID: AB_2174013) and rabbit anti-βactin at 1:2000 (Abcam, catalog #ab8227, RRID: AB_2305186). All primary antibodies were from Cell Signaling Technology and used at a dilution of 1:1000, unless stated otherwise.

Blots were washed 3 × 10 min with TBS/0.1% Tween-20 and incubated with the appropriate HRP-conjugated secondary antibodies for 1h at room temperature in a TBS/0.1% Tween-20/5% BSA solution. The secondary antibodies used were HRP-conjugated donkey anti-mouse IgG (Jackson ImmunoResearch, catalog #715-035-150, RRID: AB_2340770) or HRP-conjugated goat anti-rabbit IgG (Jackson ImmunoResearch, catalog #111-035-003, RRID: AB_2313567). After secondary antibody incubations, blots were washed 3 × 10min in TBS/0.1% Tween-20, incubated in ECL 2 Western Blotting Substrate (Thermo Scientific, catalog #80196) and a signal was collected with CL-XPosure film (Thermo Scientific, catalog #34090). For re-probing, membrane blots were washed in stripping buffer (2% SDS, 100mM β-mercaptoethanol, 50mM Tris-HCl, pH 6.8) for 30min at 55°C, then rinsed repeatedly with TBS/0.1%

Tween-20, finally blocked with 5% skim milk, and then re-probed. Developed films were then scanned, and band density was analyzed by measuring band and background intensity using Adobe Photoshop CS5.1 software (RRID:SCR_014199). Four samples per group (WT vs. *Fmr1* KO or *Fmr1*$^{Flox/y}$ vs. *Cre*^{Nex1}/*Fmr1*$^{Flox/y}$ cKO) were run per blot, and precision/tolerance (P/T) ratios for *Fmr1* KO and *Cre*^{Nex1}/*Fmr1*$^{Flox/y}$ cKO samples were normalized to averaged P/T ratios of WT and *Fmr1*$^{Flox/y}$ samples, respectively. Statistical analysis was performed with unpaired t-test using GraphPad Prism 6 software. Data represent mean ± standard error of the mean (SEM).

Behavioral Assessments

Open-field test

Anxiety was tested in P60 mice (6 mice per group) by quantifying their tendency to travel to the center of an open field and time spent in thigmotaxis (Yan, Asafo-Adjei, Arnold, Brown, & Bauchwitz, 2004; Yan, Rammal, Tranfaglia, & Bauchwitz, 2005). A 72 × 72-cm open-field arena with 50-cm-high walls was constructed from opaque acrylic sheets with a clear acrylic sheet for the bottom The open field arena was placed in a brightly lit room, and one mouse at a time was placed in a corner of the open field and allowed to explore for 10 min while being recorded with digital video from above. The floor was cleaned with 2–3% acetic acid, 70% ethanol, and water between tests to eliminate odor trails. The mice were tested between the hours of 9:00 A.M. and 1:00 P.M., and this test was always performed prior to the elevated plus maze. The arena was subdivided into a 4 × 4 grid of squares with the middle of the grid defined as the center. A line 4 cm from each wall was added to measure thigmotaxis. Locomotor activity was

scored by the analysis of total line crosses and speed as described previously with some modifications (R. E. Brown, Corey, & Moore, 1999; Yan et al., 2005) using TopScan Lite software (Clever Sys., Inc., Reston, VA 20190, USA). A tendency to travel to the center (total number of entries into large and small center squares) and the time in thigmotaxis were used as an indicator of anxiety using TopScan Lite software (CleverSys Inc). The analysis was performed in 5 min intervals for the total 10 min exploration duration. Assessments of the digital recordings were performed blind to the condition. Statistical analysis was performed with unpaired t-test using GraphPad Prism 6 software. Data represent mean ± standard error of the mean (SEM).

Elevated plus maze

The elevated plus maze consisted of four arms in a plus configuration. Two opposing arms had 15-cm tall walls (closed arms), and two arms were without walls (open arms). The entire maze sat on a stand 1 m above the floor. Each arm measured 30 cm long and 10 cm wide. Mice were allowed to explore the maze for 10 min while being recorded by digital video from above. The maze was wiped with 2–3% acetic acid, 70% ethanol and water between each test to eliminate odor trails. This test was always done following the open-field test. TopScan Lite software was used to measure the percent of time spent in open arms and speed. The time spent in open arm was used to evaluate anxiety-like behavior (Carobrez & Bertoglio, 2005). The speed and total arm entries were measured to evaluate overall locomotor activity. The analysis was performed in 5 min intervals for the total 10 min exploration duration. Assessments of the digital recordings were done blind to the condition using TopScan Lite software. Statistical analysis was

performed with unpaired t-test using GraphPad Prism 6 software. Data represent mean ± standard error of the mean (SEM).

Results

In this study we examined (1) whether the deficits in PV and PNN expression observed in developing auditory cortex of global *Fmr1* KO mice are also seen in adulthood; (2) the effects of FMRP deletion from forebrain excitatory neurons on gelatinase activity, PV/PNN expression and mTOR/Akt phosphorylation in the adult auditory cortex of $Cre^{Nex1}/Fmr1^{Flox/y}$ cKO mice; and (3) whether FMRP deletion from forebrain excitatory neurons elicit abnormal FXS-associated behaviors, such as hyperactivity and anxiety.

Reduced PNNs and PV/PNN co-localization were observed in the auditory cortex of adult global *Fmr1* KO mice.

We recently showed evidence for abnormal development of PV neurons and PNNs in the developing auditory cortex of global *Fmr1* KO mice (Wen et al., 2018). Here, we examined whether the deficits were also seen in the adult auditory cortex of *Fmr1* KO mice. For this, we characterized the density of PV+ cells and fluorescently tagged WFA was used to assess the density of WFA+ PNN-containing cells in L1-4 of adult WT and *Fmr1* KO auditory cortex (**Fig. 2.1A-H**). Statistical analysis using unpaired t-test revealed that there was a significant reduction in PV cell density in L4 of *Fmr1* KO auditory cortex compared to WT (n=6, t(10) =2.37, $p = 0.0391$, t-test) (**Table 2.2; Fig. 2.1C**). However, no significant changes were observed in PV cell density in L2/3 of

Fmr1 KO auditory cortex compared to WT (n=6, p = 0.230, t-test) (**Table 2.2; Fig. 2.1F**). We observed a significant reduction in WFA+ PNN cell density in *Fmr1* KO auditory cortex compared to WT in both L4 (n=6, t(10) =5.50, p = 0.0003, t-test) and L2/3 (n=6, t(10) =4.02, p = 0.007, t-test) (**Table 2.2; Fig. 2.1D, G**). We also analyzed the density of PV/PNN double-labeled cells and found that formation of WFA+ PNNs was impaired around PV cells in adult *Fmr1* KO auditory cortex compared to WT in both L4 (n=6, t(10) =3.61, p = 0.0048, t-test) and L2/3 (n=6, t(10) =3.37, p = 0.0151, t-test) (**Table 2.2; Fig. 2.1E, H**). Taken together, these data demonstrate that similar to what we observed in the developing *Fmr1* KO mice, formation of WFA+ PNNs and PV/PNN co-localization remains impaired in the adult auditory cortex of global *Fmr1* KO mice. These deficits may underlie the enhanced sound driven response in adult global *Fmr1* KO auditory cortex (S. Rotschafer & Razak, 2013).

FMRP immunoreactivity was significantly reduced in excitatory neurons of auditory cortex of adult *Cre^{Nex1}/Fmr1$^{Flox/y}$* cKO mice.

To achieve the deletion of FMRP from forebrain excitatory neurons, we crossed male Cre^{Nex1} with female *Fmr1$^{flox/flox}$* KO mice (**Figure 2.2)** and analyzed the expression of FMRP within the regions of the auditory pathway in the *Cre^{Nex1}/Fmr1$^{Flox/y}$* cKO and their littermate controls, *Fmr1*$^{Flox/y}$ mice (**Figure 2.3**, **2.4**). *Fmr1*$^{Flox/y}$ mice showed FMRP expression in NeuN+ cells (**Fig. 2.3A, D**) in the auditory cortex. FMRP immunoreactivity was visibly reduced in the cortex of adult *Cre^{Nex1}/Fmr1$^{Flox/y}$* cKO mice (**Fig. 2.3B, E**). No significant changes were observed in NeuN cell density in the *Fmr1*$^{Flox/y}$ and *Cre^{Nex1}/Fmr1$^{Flox/y}$* cKO mice (n=3, p=0.695, t-test) (**Table 2.1; Fig. 2.3C**).

However, there was a significant decrease in the percentage of NeuN+ neurons with FMRP in the *Cre*^{Nex1}*/Fmr1*$^{Flox/y}$ cKO mice compared to *Fmr1*$^{Flox/y}$ mice (n=3, t(4) =12.6, p=0.0002, t-test) (**Table 2.1; Fig. 2.3F**). The remaining NeuN+ cells with FMRP are presumed to be GABAergic neurons (Tamamaki et al., 2003). These data confirm that FMRP was deleted from forebrain excitatory neurons in the auditory cortex.

Unlike the auditory cortex, no significant changes in FMRP expression were observed in the inferior colliculus and the auditory thalamus (medial geniculate body; **Figure 2.4**). FMRP expression was detected in NeuN+ neurons in the central (**Fig. 2.4A, B**) and external inferior colliculus (**Fig. 2.4D, E**), and medial geniculate body (**Fig. 2.4G, H**) of *Cre*^{Nex1}*/Fmr1*$^{Flox/y}$ cKO mice. No significant changes were observed in the percentage of NeuN+ neurons showing FMRP immunoreactivity in the central (n=3, p=0.0971, t-test; **Table 2.1**; **Fig. 2.4C**) or external inferior colliculus (n=3, p=0.0718, t-test; **Table 2.1**; **Fig. 2.4F**) of *Cre*^{Nex1}*/Fmr1*$^{Flox/y}$ cKO mice compared to *Fmr1*$^{Flox/y}$ mice. In the medial geniculate body as well, no significant changes in the percentage of NeuN+ neurons with FMRP were found between the *Fmr1*$^{Flox/y}$ and *Cre*^{Nex1}*/Fmr1*$^{Flox/y}$ cKO mice (n=3, p=0.697, t-test; **Table 2.1**; **Fig. 2.4I**). These data confirm a significant loss of FMRP from excitatory neurons in the auditory cortex, but not inferior colliculus or medial geniculate body, of *Cre*^{Nex1}*/Fmr1*$^{Flox/y}$ cKO mice.

Deletion of FMRP from excitatory neurons reduces PV, PNN and PV/PNN co-localization in the auditory cortex of adult *Cre*^{Nex1}*/Fmr1*$^{Flox/y}$ cKO mice.

We examined PV+ and WFA+ PNN-containing cell density in auditory cortex of adult *Fmr1*$^{Flox/y}$ and *Cre*^{Nex1}*/Fmr1*$^{Flox/y}$ cKO mice (**Fig. 2.5A-H**). Similar to the adult

Fmr1 KO mice, there was a significant decrease in PV cell density in auditory cortex of $Cre^{Nex1}/Fmr1^{Flox/y}$ cKO mice compared to their littermate controls, $Fmr1^{Flox/y}$ mice in both L4 (n=6, t(10) =2.53, p = 0.0298, t-test) and L2/3 (n=6, t(10) =2.47, p = 0.0483, t-test (**Table 2.2; Fig 2.5C, F**). WFA+ PNN cell density was also significantly reduced in auditory cortex of $Cre^{Nex1}/Fmr1^{Flox/y}$ cKO mice compared to $Fmr1^{Flox/y}$ in both L4 (n=6, t(10) =10.3, p <0.0001, t-test) and L2/3 (n=6, t(10) =7.77, p = 0.0002, t-test) (**Table 2.2; Fig. 2.5D, G**). In addition, PV/PNN co-localization was significantly decreased in auditory cortex of $Cre^{Nex1}/Fmr1^{Flox/y}$ cKO mice compared to $Fmr1^{Flox/y}$ in L4 (n=6, t(10) =5.12, p = 0.0005, t-test) and L2/3 (n=6, t(10) =7.19, p = 0.0004, t-test) (**Table 2.2; Fig. 2.5E, H**). These data indicate that the removal of FMRP from excitatory neurons is sufficient to trigger abnormal development of WFA+ PNNs in the auditory cortex, specifically around inhibitory PV interneurons. Thus, a cell-type specific loss of FMRP may lead to a network-level dysfunction.

Total aggrecan levels are reduced, while cleaved aggrecan levels and gelatinase activity are enhanced in the auditory cortex of adult $Cre^{Nex1}/Fmr1^{Flox/y}$ cKO mice.

As enhanced gelatinase activity may contribute to the loss of PNNs by cleaving extracellular matrix (ECM), we performed a gelatinase activity assay. A significant increase in gelatinase activity was observed in both *Fmr1* KO (n=4, t(6) =4.26, p = 0.0053, t-test) and $Cre^{Nex1}/Fmr1^{Flox/y}$ cKO mice (n=4, t(6) =3.99, p = 0.0072, t-test) as compared to their respective WT counterparts, WT and $Fmr1^{Flox/y}$ mice (**Table 2.3; Fig. 2.6A**). While the gelatinase activity assay measures both MMP-2 and MMP-9 proteolytic activity, our previous study showed that MMP-2 levels were similar in the adult auditory

cortex of WT and *Fmr1* KO mice, while MMP-9 levels were significantly increased in the *Fmr1* KO mice (Lovelace et al., 2016). This suggests that the observed increase in gelatinase activity in adult *Fmr1* KO and $Cre^{Nex1}/Fmr1^{Flox/y}$ cKO mouse auditory cortex could be due to increased MMP-9 levels.

Enhanced gelatinase activity may result in excessive cleavage of aggrecan and a reduction in aggrecan-containing PNNs detected with WFA (Miyata & Kitagawa, 2016; Roughley & Mort, 2014). Therefore, we next analyzed total and cleaved aggrecan levels in the mouse auditory cortex of adult WT, *Fmr1* KO, $Fmr1^{Flox/y}$ and $Cre^{Nex1}/Fmr1^{Flox/y}$ cKO mice (**Fig. 2.6C**). We found that total levels of full-length aggrecan were significantly reduced in both the *Fmr1* KO (n=4, t(6) =5.44, $p = 0.0016$, t-test) and $Cre^{Nex1}/Fmr1^{Flox/y}$ cKO mice (n=4, t(6) =3.32, $p = 0.0159$, t-test) compared to WT and $Fmr1^{Flox/y}$ mice, respectively (**Table 2.3; Fig. 2.6D**). In contrast, cleaved aggrecan levels were significantly increased in both the *Fmr1* KO (n=4, t(6) =6.40, $p = 0.0031$, t-test) and $Cre^{Nex1}/Fmr1^{Flox/y}$ cKO (n=4, t(6) =9.09, $p < 0.0001$, t-test) mice compared to their respective WT counterparts (**Table 2.3; Fig. 2.6E**). As a result, the cleaved aggrecan to total aggrecan ratio was significantly increased in both the *Fmr1* KO (n=4, t(6) =7.25, $p = 0.0003$, t-test) and $Cre^{Nex1}/Fmr1^{Flox/y}$ cKO mice (n=3-4, t(5) =8.66, $p = 0.0001$, t-test) compared to WT and $Fmr1^{Flox/y}$ mice, respectively (**Table 2.3; Fig. 2.6F**). Our data suggest that loss of FMRP in excitatory neurons contributes to the increased gelatinase activity in adult *Fmr1* KO and $Cre^{Nex1}/Fmr1^{Flox/y}$ cKO mouse auditory cortex that may affect formation of WFA+ PNNs around PV interneurons by cleaving aggrecan.

Deletion of FMRP from excitatory neurons triggers a decrease in PV levels, while Akt and mTOR phosphorylation is increased in auditory cortex of adult *$Cre^{Nex1}/Fmr1^{Flox/y}$* cKO mice.

Consistent with the reduced PV cell density in adult *Fmr1* KO and *$Cre^{Nex1}/Fmr1^{Flox/y}$* cKO mice compared to their controls, we observed a significant decrease in PV levels in the cell lysates from auditory cortex of both *Fmr1* KO (n=4, t(6) =32.5, $p < 0.0001$, t-test) and *$Cre^{Nex1}/Fmr1^{Flox/y}$* cKO mice (n=4, t(6) =4.72, $p = 0.0032$, t-test) compared to their WT counterparts (**Table 2.3; Fig. 2.7A, D**). This is consistent with previous findings that show a reduction in PV expression in cortex of mouse models of autism (Filice, Vörckel, Sungur, Wöhr, & Schwaller, 2016).

Enhanced Akt/mTOR signaling may also underlie changes in synaptic functions and hyperexcitability associated with FXS and other autistic spectrum disorders (Enriquez-Barreto & Morales, 2016; Klann & Dever, 2004; Sato, 2016; Sharma et al., 2010). Therefore, we investigated Akt/mTOR activation in adult auditory cortex of global *Fmr1* KO and forebrain excitatory neuron-specific *$Cre^{Nex1}/Fmr1^{Flox/y}$* cKO mice, by examining mTOR and Akt phosphorylation levels (**Table 2.3; Fig. 2.7B, C**). Higher levels of the phosphorylated (i.e., active) forms of both proteins were detected in the adult auditory cortex of *Fmr1* KO mice compared to WT. Specifically, there was a 33% increase in the p-mTOR/mTOR ratio in the *Fmr1* KO mice (n=4, t(6) =6.89, $p = 0.0005$, t-test) compared to WT (**Table 2.3; Fig. 2.7E**). A similar effect was also seen for the p-Akt/Akt ratio, which was 35% higher in the *Fmr1* KO mice (n=4, t(6) =4.30, $p = 0.0051$, t-test) compared to WT mice (**Table 2.3; Fig. 2.7F**). Similar deficits were seen in the

auditory cortex of adult *Cre*^{Nex1}/*Fmr1*$^{Flox/y}$ cKO mice compared to control *Fmr1*$^{Flox/y}$ mice. There was a 30% increase in the p-mTOR/mTOR ratio (n=4, t(6) =3.97, p = 0.0073, t-test) (**Table 2.3; Fig. 2.7E**) and a 40% increase in the p-Akt/Akt ratio in the *Cre*^{Nex1}/*Fmr1*$^{Flox/y}$ cKO mice (n=4, t(6) =7.86, p = 0.0002, t-test) (**Table 2.3; Fig. 2.7F**) compared to *Fmr1*$^{Flox/y}$ mice. These results demonstrate that FMRP deletion from forebrain excitatory neurons is sufficient to trigger enhanced Akt and mTOR phosphorylation in the auditory cortex of adult mice.

Excitatory neuron specific adult *Cre*^{Nex1}/*Fmr1*$^{Flox/y}$ cKO mice display increased locomotor activity, but no anxiety-like behavior.

Adult male *Fmr1*$^{Flox/y}$ (n=6) and *Cre*^{Nex1}/*Fmr1*$^{Flox/y}$ cKO (n=6) mice were tested for locomotor activity and anxiety in an elevated plus maze by measuring total number of entries or speed and time spent in open arms, respectively (**Table 2.4; Fig. 2.8**). *Cre*^{Nex1}/*Fmr1*$^{Flox/y}$ cKO mice demonstrated increased locomotor activity by making significantly more total arm entries than *Fmr1*$^{Flox/y}$ mice (n=6, t(10) =2.61, p = 0.0262, t-test) (**Table 2.4; Fig. 2.8A**), and by showing a significant increase in speed (n=6, t(10) =3.44, p = 0.0063, t-test) (**Table 2.4; Fig. 2.8B**). However, *Cre*^{Nex1}/*Fmr1*$^{Flox/y}$ cKO mice showed no difference in time spent in open arm per entry (n=6, p = 0.273, t-test) or percentage of time in open arms (n=6, p = 0.0521, t-test) compared to *Fmr1*$^{Flox/y}$ mice (**Table 2.4; Fig. 2.8C, D**).

We used an open-field test as another gauge of locomotor activity and anxiety, by determining total number of lines crosses or speed and the tendency of mice to travel through the center of an open field or the time in thigmotaxis, respectively. Similar to the

performance in the elevated plus maze, $Cre^{Nex1}/Fmr1^{Flox/y}$ cKO mice showed increased locomotor activity with significantly more line crosses (n=6, t(10) =4.36, p = 0.0014, t-test) (**Table 2.4; Fig. 2.8E**) and increased speed (n=6, t(10) =3.65, p = 0.0045, t-test) (**Table 2.4; Fig. 2.8F**) than $Fmr1^{Flox/y}$ mice. However, there was no significant difference in time spent in the center per entry (n=6, p = 0.862, t-test) or percentage of time in thigmotaxis (n=6, p = 0.183, t-test) between the two groups (**Table 2.4; Fig. 2.8G, H**). These findings establish that FMRP deletion from forebrain excitatory neurons increases locomotor activity but has no effect on anxiety-like behaviors.

Discussion

Sensory processing deficits commonly co-occur with autism spectrum disorders. The mechanisms of sensory deficits in autism remain poorly understood, and no current therapies are available to alleviate sensory symptoms. The main findings of this study provide novel insights into mechanisms of sensory processing issues in FXS, a leading genetic cause of autism (**Summarized in Fig. 2.9**). We show that cell-type specific deletion of *Fmr1* from forebrain excitatory neurons elicits elevated gelatinase activity, higher mTOR/Akt phosphorylation, and impaired PV/PNN colocalization in the auditory cortex. While both astrocytes and neurons can release gelatinases MMP-2 and MMP-9 (Murase et al., 2016; Szklarczyk et al., 2002; Yong, Krekoski, Forsyth, Bell, & Edwards, 1998), our data suggest that loss of FMRP from excitatory neurons is sufficient to trigger increased gelatinase activity, which may affect the formation of WFA+ PNNs around PV interneurons.

Abnormal density and function of PV+ GABAergic interneurons appears to be a common finding across sensory cortices in FXS model mice, and may be a common mechanism for abnormal sensory processing and sensitivity (Contractor, Klyachko, & Portera-Cailliau, 2015; Goel et al., 2018; Selby, Zhang, & Sun, 2007; Wen et al., 2018). PV expression in inhibitory neurons is activity-dependent (Chang et al., 2010; Patz, Grabert, Gorba, Wirth, & Wahle, 2004). The reduction in PV expression in $Cre^{Nex1}/Fmr1^{Flox/y}$ cKO mouse auditory cortex may occur due to reduced excitatory drive onto these neurons. *In vitro* slice physiology studies of somatosensory cortex in global *Fmr1* KO mice have shown local circuit deficits with reduced excitatory input received by PV interneurons, whereas excitatory and inhibitory drive onto excitatory neurons was normal (Gibson, Bartley, Hays, & Huber, 2008). Consistent with our data, these deficits are seen following removal of FMRP just from excitatory neurons suggesting that a common mechanism across sensory cortices in *Fmr1* KO mice is reduced excitation of PV cells (Contractor et al., 2015; Goel et al., 2018; Selby et al., 2007). A second reason for altered PV cell function might be through the degradation of aggrecan-containing WFA+ PNNs. In the cerebral cortex, PNN loss around PV cells reduces excitability of these cells (Balmer, 2016; Lensjø, Lepperød, Dick, Hafting, & Fyhn, 2017; Wen et al., 2018). Therefore, degradation of PNN is predicted to decrease excitability of PV cells leading to hyperexcitability of cortical networks and abnormal neural oscillations. PNNs protect PV cells from oxidative stress, and the loss of PNNs may lead to PV cell death (Cabungcal et al., 2013).

The decrease in PV cell number and function is predicted to have major implications for processing of auditory input in the cortex and may, at least partially, underlie auditory hypersensitivity. PV+ neurons comprise nearly 50% of all GABAergic cells in the neocortex, and individual PV+ neurons can provide synchronized inhibition on to multiple pyramidal cells contributing to network activity levels and patterns (Packer & Yuste, 2011). PV+ neurons are involved in gain control in the auditory cortex, and shape how neurons respond to increasing sound levels (Moore & Wehr, 2013), suggesting a possible neural correlate of abnormal auditory sensitivity. Reduction of PV expression causes GABA neuron dysfunction and facilitation in response to repetitive stimulation (Lucas et al., 2010). Rapid spiking, putative, PV+ cells are also linked to processing of rapid spectrotemporal changes in acoustic inputs (Atencio & Schreiner, 2008) and may be linked to the reduced selectivity for frequency modulated sweep rates in *Fmr1* KO mouse auditory cortex (S. Rotschafer & Razak, 2013).

Role of enhanced gelatinase activity in $Cre^{Nex1}/Fmr1^{Flox/y}$ cKO mice

PNNs are comprised of hyaluronan, glycoproteins, and chondroitin sulfate proteoglycans (CSPGs), and form a net-like structure on the cell body and proximal dendrites of PV-expressing GABAergic interneurons. Among CSPGs present in PNNs, aggrecan is found almost exclusively in PNNs formed around PV cells (McRae, Baranov, Sarode, Brooks-Kayal, & Porter, 2010; McRae, Rocco, Kelly, Brumberg, & Matthews, 2007; Morawski, Brückner, Arendt, & Matthews, 2012), and excessive proteolytic activity of gelatinases MMP-2 and MMP-9 may affect formation of PNNs and PV functions by cleaving aggrecan (d'Ortho et al., 1997). Indeed in our studies we observed

enhanced gelatinase activity and increased cleavage of aggrecan in the auditory cortex of $Cre^{Nex1}/Fmr1^{Flox/y}$ cKO mice. Consistent with our previous studies in the developing auditory cortex of global *Fmr1* KO mice (Wen et al., 2018), we found that gelatinase activity was also significantly increased in the adult auditory cortex of both *Fmr1* KO and $Cre^{Nex1}/Fmr1^{Flox/y}$ cKO mice, suggesting that the deletion of FMRP from excitatory neurons is sufficient to increase gelatinase activity in the auditory cortex. Our studies suggest that aggrecan cleavage by MMP-9 is likely responsible for impaired formation of WFA+ PNNs around PV interneurons observed in adult auditory cortex of forebrain excitatory neuron-specific $Cre^{Nex1}/Fmr1^{Flox/y}$ cKO mice.

MMP-9 can also regulate mTOR and Akt activation (Sidhu et al., 2014), potentially through integrins or BDNF/TrkB signaling (Hwang et al., 2005; Yang et al., 2009). Enhanced PI3K-Akt-mTOR signaling is implicated in FXS and may contribute to hyperexcitability by regulating protein synthesis through elongation factor 1α (Gross et al., 2011; Hoeffer et al., 2012; Hou & Klann, 2004; Ronesi & Huber, 2008; Sharma et al., 2010). The role of MMP-9 in FXS symptoms is further supported by the fact that the genetic deletion of MMP-9 activity in the brain of *Fmr1* KO mice restored dendritic spine development and mGluR5-dependent LTD in the hippocampus (Sidhu et al., 2014). In addition, MMP-9 reduction in the auditory cortex of *Fmr1* KO mice normalized auditory responses and the formation of WFA+ PNNs around PV cells in the *Fmr1* KO mice to WT levels (Wen et al., 2018). MMP-9 deletion or reduction in the *Fmr1* KO mice also reversed ERP N1 amplitude habituation deficits (Lovelace et al., 2016) and reduced hyperexcitability in the developing auditory cortex (Wen et al., 2018), respectively.

Minocycline, which is known to inhibit MMP-9 activity beside its antibiotic effects, was shown to reduce FXS symptoms in both humans (Schneider et al., 2013) and mice (Dansie et al., 2013; S. E. Rotschafer, Trujillo, Dansie, Ethell, & Razak, 2012), further supporting the therapeutically targeting MMP-9 to alleviate FXS symptoms. While the present study suggests that loss of FMRP expression in excitatory neurons is sufficient to enhance gelatinase activity and affect formation of WFA+ PNNs around PV cells, the effects may be indirect and excitatory neurons may also modulate release of MMP-9 or MMP-2 from astrocytes. Future studies will test the role of astrocytes in regulating MMP-9 activity, PNNs and functional responses in the auditory cortex of the *Fmr1* KO mice.

Increased anxiety and locomotor activity are among the most consistent behavioral symptoms in individuals with FXS (Tranfaglia, 2011). However, our studies show that forebrain excitatory neuron-specific $Cre^{Nex1}/Fmr1^{Flox/y}$ cKO mice only exhibit increased locomotor activity, but no anxiety-like behaviors. The auditory brainstem expresses high FMRP levels (Wang et al., 2014), and abnormal sensory processing at the level of the auditory brainstem may underlie the enhanced susceptibility to audiogenic seizures (L. Chen & Toth, 2001). FMRP may regulate neuronal excitability through the direct interactions with several ion channels, such as sodium-activated potassium channel Slack, presynaptic N-type voltage-gated calcium channels, and calcium-activated potassium BK channels (M. R. Brown et al., 2010; Deng et al., 2013; Ferron, Nieto-Rostro, Cassidy, & Dolphin, 2014; Hébert et al., 2014; Myrick et al., 2015; Zhang et al., 2012). The enhanced excitability is associated with behavioral symptoms observed in

FXS, such as hyperactivity, anxiety, and seizures (Braat & Kooy, 2015; Penagarikano et al., 2007). Brainstem noradrenergic and serotoninergic systems may also contribute to anxiety phenotypes in FXS, which may be unaffected in the forebrain specific deletion model. Taken together, our results suggest the role of subcortical areas in regulating anxiety-like behaviors in global *Fmr1* KO mice as forebrain excitatory neuron specific deletion of FMRP is not sufficient to trigger this abnormal behavior. On the other hand, abnormal locomotor activity may depend on cortex-specific functions of FMRP.

FMRP loss from excitatory neurons in hippocampus and frontal cortex may also contribute to abnormal behaviors observed in *Fmr1* KO mice, such as hyperactivity, obsessive-compulsive behaviors, and learning and memory deficits (Dansie et al., 2013; Santos, Kanellopoulos, & Bagni, 2014; Yau et al., 2018). Indeed FMRP loss is known to affect dendritic spine development in the excitatory neurons in the hippocampus (Sidhu et al., 2014) and mGluR5-dependent LTD in the CA1 hippocampal neurons (Huber, Gallagher, Warren, & Bear, 2002). Future studies of changes in electrocortical activity in different areas of the brain using multi-electrode array EEGs and the analysis of mouse behaviors following cell- or brain area-specific deletion of FMRP would help us better understand the circuit level mechanisms.

Conclusions

Sensory processing issues are frequently associated with autism, but very little is known about underlying mechanisms. Humans with FXS show consistent and debilitating auditory hypersensitivity. Here we found that PV+ inhibitory neurons and the extracellular matrix structures that cover these cells are affected by *Fmr1* gene deletion in

forebrain excitatory neurons, which is likely linked to reduced inhibition and hyperactive behaviors. Increased activity of extracellular matrix modifying enzyme (MMP-9) may contribute to these deficits by cleaving aggrecan-containing WFA+ PNNs or signaling through cell surface receptors to mTOR/Akt pathway. Together, these findings show that local cortical deficits contribute to many, but not all, phenotypes in the *Fmr1* KO mice and suggest cell-type and circuit specific contributions of the genetic mutation to various symptoms in FXS. The utility of identifying the relationships between cell type/circuit specificity and phenotypes in neurodevelopmental disorders is that therapeutic approaches can be potentially targeted to impact specific cell types, circuits and symptoms.

References

Anderson, L. A., Christianson, G. B., & Linden, J. F. (2009). Mouse auditory cortex differs from visual and somatosensory cortices in the laminar distribution of cytochrome oxidase and acetylcholinesterase. *Brain Res, 1252*, 130-142. doi:10.1016/j.brainres.2008.11.037

Atencio, C. A., & Schreiner, C. E. (2008). Spectrotemporal processing differences between auditory cortical fast-spiking and regular-spiking neurons. *J Neurosci, 28*(15), 3897-3910. doi:10.1523/JNEUROSCI.5366-07.2008

Ballester-Rosado, C. J., Albright, M. J., Wu, C. S., Liao, C. C., Zhu, J., Xu, J., . . . Lu, H. C. (2010). mGluR5 in cortical excitatory neurons exerts both cell-autonomous and -nonautonomous influences on cortical somatosensory circuit formation. *J Neurosci, 30*(50), 16896-16909. doi:10.1523/JNEUROSCI.2462-10.2010

Balmer, T. S. (2016). Perineuronal Nets Enhance the Excitability of Fast-Spiking Neurons. *eNeuro, 3*(4). doi:10.1523/ENEURO.0112-16.2016

Bilousova, T. V., Dansie, L., Ngo, M., Aye, J., Charles, J. R., Ethell, D. W., & Ethell, I. M. (2009). Minocycline promotes dendritic spine maturation and improves behavioural performance in the fragile X mouse model. *J Med Genet, 46*(2), 94-102. doi:10.1136/jmg.2008.061796

Braat, S., & Kooy, R. F. (2015). The GABAA Receptor as a Therapeutic Target for Neurodevelopmental Disorders. *Neuron, 86*(5), 1119-1130. doi:10.1016/j.neuron.2015.03.042

Brown, M. R., Kronengold, J., Gazula, V. R., Chen, Y., Strumbos, J. G., Sigworth, F. J., . . . Kaczmarek, L. K. (2010). Fragile X mental retardation protein controls gating of the sodium-activated potassium channel Slack. *Nat Neurosci, 13*(7), 819-821. doi:10.1038/nn.2563

Brown, R. E., Corey, S. C., & Moore, A. K. (1999). Differences in measures of exploration and fear in MHC-congenic C57BL/6J and B6-H-2K mice. *Behavior genetics, 29*(4), 263-271.

Cabungcal, J. H., Steullet, P., Morishita, H., Kraftsik, R., Cuenod, M., Hensch, T. K., & Do, K. Q. (2013). Perineuronal nets protect fast-spiking interneurons against oxidative stress. *Proc Natl Acad Sci U S A, 110*(22), 9130-9135. doi:10.1073/pnas.1300454110

Carobrez, A. P., & Bertoglio, L. J. (2005). Ethological and temporal analyses of anxiety-like behavior: the elevated plus-maze model 20 years on. *Neurosci Biobehav Rev, 29*(8), 1193-1205. doi:10.1016/j.neubiorev.2005.04.017

Castrén, M., Pääkkönen, A., Tarkka, I. M., Ryynänen, M., & Partanen, J. (2003). Augmentation of auditory N1 in children with fragile X syndrome. *Brain Topogr, 15*(3), 165-171. Retrieved from https://www.ncbi.nlm.nih.gov/pubmed/12705812

Chang, M. C., Park, J. M., Pelkey, K. A., Grabenstatter, H. L., Xu, D., Linden, D. J., . . . Worley, P. F. (2010). Narp regulates homeostatic scaling of excitatory synapses on parvalbumin-expressing interneurons. *Nat Neurosci, 13*(9), 1090-1097. doi:10.1038/nn.2621

Chen, L., & Toth, M. (2001). Fragile X mice develop sensory hyperreactivity to auditory stimuli. *Neuroscience, 103*(4), 1043-1050. Retrieved from https://www.ncbi.nlm.nih.gov/pubmed/11301211

Chen, L. Y., Rex, C. S., Babayan, A. H., Kramár, E. A., Lynch, G., Gall, C. M., & Lauterborn, J. C. (2010). Physiological activation of synaptic Rac>PAK (p-21 activated kinase) signaling is defective in a mouse model of fragile X syndrome. *J Neurosci, 30*(33), 10977-10984. doi:10.1523/JNEUROSCI.1077-10.2010

Christie, S. B., Akins, M. R., Schwob, J. E., & Fallon, J. R. (2009). The FXG: a presynaptic fragile X granule expressed in a subset of developing brain circuits. *J Neurosci, 29*(5), 1514-1524. doi:10.1523/JNEUROSCI.3937-08.2009

Contractor, A., Klyachko, V. A., & Portera-Cailliau, C. (2015). Altered Neuronal and Circuit Excitability in Fragile X Syndrome. *Neuron, 87*(4), 699-715. doi:10.1016/j.neuron.2015.06.017

Crawford, D. C., Acuna, J. M., & Sherman, S. L. (2001). FMR1 and the fragile X syndrome: human genome epidemiology review. *Genet Med, 3*(5), 359-371. doi:10.1097/00125817-200109000-00006

d'Ortho, M. P., Will, H., Atkinson, S., Butler, G., Messent, A., Gavrilovic, J., . . . Murphy, G. (1997). Membrane-type matrix metalloproteinases 1 and 2 exhibit broad-spectrum proteolytic capacities comparable to many matrix metalloproteinases. *Eur J Biochem, 250*(3), 751-757. Retrieved from https://www.ncbi.nlm.nih.gov/pubmed/9461298

Dansie, L. E., Phommahaxay, K., Okusanya, A. G., Uwadia, J., Huang, M., Rotschafer, S. E., . . . Ethell, I. M. (2013). Long-lasting effects of minocycline on behavior in young but not adult Fragile X mice. *Neuroscience, 246*, 186-198. doi:10.1016/j.neuroscience.2013.04.058

Deng, P. Y., Rotman, Z., Blundon, J. A., Cho, Y., Cui, J., Cavalli, V., . . . Klyachko, V. A. (2013). FMRP regulates neurotransmitter release and synaptic information transmission by modulating action potential duration via BK channels. *Neuron, 77*(4), 696-711. doi:10.1016/j.neuron.2012.12.018

Dziembowska, M., Pretto, D. I., Janusz, A., Kaczmarek, L., Leigh, M. J., Gabriel, N., . . . Tassone, F. (2013). High MMP-9 activity levels in fragile X syndrome are lowered by minocycline. *Am J Med Genet A, 161A*(8), 1897-1903. doi:10.1002/ajmg.a.36023

Dziembowska, M., & Wlodarczyk, J. (2012). MMP9: a novel function in synaptic plasticity. *Int J Biochem Cell Biol, 44*(5), 709-713. doi:10.1016/j.biocel.2012.01.023

Enriquez-Barreto, L., & Morales, M. (2016). The PI3K signaling pathway as a pharmacological target in Autism related disorders and Schizophrenia. *Mol Cell Ther, 4*, 2. doi:10.1186/s40591-016-0047-9

Ethridge, L. E., White, S. P., Mosconi, M. W., Wang, J., Byerly, M. J., & Sweeney, J. A. (2016). Reduced habituation of auditory evoked potentials indicate cortical hyper-excitability in Fragile X Syndrome. *Transl Psychiatry, 6*, e787. doi:10.1038/tp.2016.48

Ferron, L., Nieto-Rostro, M., Cassidy, J. S., & Dolphin, A. C. (2014). Fragile X mental retardation protein controls synaptic vesicle exocytosis by modulating N-type calcium channel density. *Nat Commun, 5*, 3628. doi:10.1038/ncomms4628

Filice, F., Vörckel, K. J., Sungur, A., Wöhr, M., & Schwaller, B. (2016). Reduction in parvalbumin expression not loss of the parvalbumin-expressing GABA interneuron subpopulation in genetic parvalbumin and shank mouse models of autism. *Mol Brain, 9*, 10. doi:10.1186/s13041-016-0192-8

Gabel, L. A., Won, S., Kawai, H., McKinney, M., Tartakoff, A. M., & Fallon, J. R. (2004). Visual experience regulates transient expression and dendritic localization of fragile X mental retardation protein. *J Neurosci, 24*(47), 10579-10583. doi:10.1523/JNEUROSCI.2185-04.2004

Gibson, J. R., Bartley, A. F., Hays, S. A., & Huber, K. M. (2008). Imbalance of neocortical excitation and inhibition and altered UP states reflect network hyperexcitability in the mouse model of fragile X syndrome. *J Neurophysiol, 100*(5), 2615-2626. doi:10.1152/jn.90752.2008

Gkogkas, C. G., Khoutorsky, A., Cao, R., Jafarnejad, S. M., Prager-Khoutorsky, M., Giannakas, N., . . . Sonenberg, N. (2014). Pharmacogenetic inhibition of eIF4E-dependent Mmp9 mRNA translation reverses fragile X syndrome-like phenotypes. *Cell Rep, 9*(5), 1742-1755. doi:10.1016/j.celrep.2014.10.064

Goebbels, S., Bormuth, I., Bode, U., Hermanson, O., Schwab, M. H., & Nave, K. A. (2006). Genetic targeting of principal neurons in neocortex and hippocampus of NEX-Cre mice. *Genesis, 44*(12), 611-621. doi:10.1002/dvg.20256

Goel, A., Cantu, D. A., Guilfoyle, J., Chaudhari, G. R., Newadkar, A., Todisco, B., . . . Portera-Cailliau, C. (2018). Impaired perceptual learning in a mouse model of Fragile X syndrome is mediated by parvalbumin neuron dysfunction and is reversible. *Nat Neurosci, 21*(10), 1404-1411. doi:10.1038/s41593-018-0231-0

Gross, C., Yao, X., Pong, D. L., Jeromin, A., & Bassell, G. J. (2011). Fragile X mental retardation protein regulates protein expression and mRNA translation of the potassium channel Kv4.2. *J Neurosci, 31*(15), 5693-5698. doi:10.1523/JNEUROSCI.6661-10.2011

Hays, S. A., Huber, K. M., & Gibson, J. R. (2011). Altered neocortical rhythmic activity states in Fmr1 KO mice are due to enhanced mGluR5 signaling and involve changes in excitatory circuitry. *J Neurosci, 31*(40), 14223-14234. doi:10.1523/JNEUROSCI.3157-11.2011

Hébert, B., Pietropaolo, S., Même, S., Laudier, B., Laugeray, A., Doisne, N., . . . Briault, S. (2014). Rescue of fragile X syndrome phenotypes in Fmr1 KO mice by a BKCa channel opener molecule. *Orphanet J Rare Dis, 9*, 124. doi:10.1186/s13023-014-0124-6

Hoeffer, C. A., Sanchez, E., Hagerman, R. J., Mu, Y., Nguyen, D. V., Wong, H., . . . Tassone, F. (2012). Altered mTOR signaling and enhanced CYFIP2 expression levels in subjects with fragile X syndrome. *Genes Brain Behav, 11*(3), 332-341. doi:10.1111/j.1601-183X.2012.00768.x

Hou, L., & Klann, E. (2004). Activation of the phosphoinositide 3-kinase-Akt-mammalian target of rapamycin signaling pathway is required for metabotropic glutamate

receptor-dependent long-term depression. *J Neurosci, 24*(28), 6352-6361. doi:10.1523/JNEUROSCI.0995-04.2004

Huber, K. M., Gallagher, S. M., Warren, S. T., & Bear, M. F. (2002). Altered synaptic plasticity in a mouse model of fragile X mental retardation. *Proc Natl Acad Sci U S A, 99*(11), 7746-7750. doi:10.1073/pnas.122205699

Hwang, J. J., Park, M. H., Choi, S. Y., & Koh, J. Y. (2005). Activation of the Trk signaling pathway by extracellular zinc. Role of metalloproteinases. *J Biol Chem, 280*(12), 11995-12001. doi:10.1074/jbc.M403172200

Janusz, A., Milek, J., Perycz, M., Pacini, L., Bagni, C., Kaczmarek, L., & Dziembowska, M. (2013). The Fragile X mental retardation protein regulates matrix metalloproteinase 9 mRNA at synapses. *J Neurosci, 33*(46), 18234-18241. doi:10.1523/JNEUROSCI.2207-13.2013

Kazdoba, T. M., Sunnen, C. N., Crowell, B., Lee, G. H., Anderson, A. E., & D'Arcangelo, G. (2012). Development and characterization of NEX- Pten, a novel forebrain excitatory neuron-specific knockout mouse. *Dev Neurosci, 34*(2-3), 198-209. doi:10.1159/000337229

Kerrisk, M. E., Greer, C. A., & Koleske, A. J. (2013). Integrin α3 is required for late postnatal stability of dendrite arbors, dendritic spines and synapses, and mouse behavior. *J Neurosci, 33*(16), 6742-6752. doi:10.1523/JNEUROSCI.0528-13.2013

Klann, E., & Dever, T. E. (2004). Biochemical mechanisms for translational regulation in synaptic plasticity. *Nat Rev Neurosci, 5*(12), 931-942. doi:10.1038/nrn1557

Legate, K. R., Wickström, S. A., & Fässler, R. (2009). Genetic and cell biological analysis of integrin outside-in signaling. *Genes Dev, 23*(4), 397-418. doi:10.1101/gad.1758709

Lensjø, K. K., Lepperød, M. E., Dick, G., Hafting, T., & Fyhn, M. (2017). Removal of Perineuronal Nets Unlocks Juvenile Plasticity Through Network Mechanisms of Decreased Inhibition and Increased Gamma Activity. *J Neurosci, 37*(5), 1269-1283. doi:10.1523/JNEUROSCI.2504-16.2016

Lovelace, J. W., Wen, T. H., Reinhard, S., Hsu, M. S., Sidhu, H., Ethell, I. M., . . . Razak, K. A. (2016). Matrix metalloproteinase-9 deletion rescues auditory evoked potential habituation deficit in a mouse model of Fragile X Syndrome. *Neurobiol Dis, 89*, 126-135. doi:10.1016/j.nbd.2016.02.002

Lucas, E. K., Markwardt, S. J., Gupta, S., Meador-Woodruff, J. H., Lin, J. D., Overstreet-Wadiche, L., & Cowell, R. M. (2010). Parvalbumin deficiency and GABAergic dysfunction in mice lacking PGC-1alpha. *J Neurosci, 30*(21), 7227-7235. doi:10.1523/JNEUROSCI.0698-10.2010

Martin del Campo, H. N., Measor, K. R., & Razak, K. A. (2012). Parvalbumin immunoreactivity in the auditory cortex of a mouse model of presbycusis. *Hear Res, 294*(1-2), 31-39. doi:10.1016/j.heares.2012.08.017

McRae, P. A., Baranov, E., Sarode, S., Brooks-Kayal, A. R., & Porter, B. E. (2010). Aggrecan expression, a component of the inhibitory interneuron perineuronal net, is altered following an early-life seizure. *Neurobiol Dis, 39*(3), 439-448. doi:10.1016/j.nbd.2010.05.015

McRae, P. A., Rocco, M. M., Kelly, G., Brumberg, J. C., & Matthews, R. T. (2007). Sensory deprivation alters aggrecan and perineuronal net expression in the mouse barrel cortex. *J Neurosci, 27*(20), 5405-5413. doi:10.1523/JNEUROSCI.5425-06.2007

Mientjes, E. J., Nieuwenhuizen, I., Kirkpatrick, L., Zu, T., Hoogeveen-Westerveld, M., Severijnen, L., . . . Oostra, B. A. (2006). The generation of a conditional Fmr1 knock out mouse model to study Fmrp function in vivo. *Neurobiol Dis, 21*(3), 549-555. doi:10.1016/j.nbd.2005.08.019

Miyata, S., & Kitagawa, H. (2016). Chondroitin 6-Sulfation Regulates Perineuronal Net Formation by Controlling the Stability of Aggrecan. *Neural Plast, 2016*, 1305801. doi:10.1155/2016/1305801

Moore, A. K., & Wehr, M. (2013). Parvalbumin-expressing inhibitory interneurons in auditory cortex are well-tuned for frequency. *J Neurosci, 33*(34), 13713-13723. doi:10.1523/JNEUROSCI.0663-13.2013

Morawski, M., Brückner, G., Arendt, T., & Matthews, R. T. (2012). Aggrecan: Beyond cartilage and into the brain. *Int J Biochem Cell Biol, 44*(5), 690-693. doi:10.1016/j.biocel.2012.01.010

Murase, S., Lantz, C. L., Kim, E., Gupta, N., Higgins, R., Stopfer, M., . . . Quinlan, E. M. (2016). Matrix Metalloproteinase-9 Regulates Neuronal Circuit Development and Excitability. *Mol Neurobiol, 53*(5), 3477-3493. doi:10.1007/s12035-015-9295-y

Myrick, L. K., Deng, P. Y., Hashimoto, H., Oh, Y. M., Cho, Y., Poidevin, M. J., . . . Klyachko, V. A. (2015). Independent role for presynaptic FMRP revealed by an FMR1

missense mutation associated with intellectual disability and seizures. *Proc Natl Acad Sci U S A, 112*(4), 949-956. doi:10.1073/pnas.1423094112

Nielsen, D. M., Derber, W. J., McClellan, D. A., & Crnic, L. S. (2002). Alterations in the auditory startle response in Fmr1 targeted mutant mouse models of fragile X syndrome. *Brain Res, 927*(1), 8-17. Retrieved from https://www.ncbi.nlm.nih.gov/pubmed/11814427

Packer, A. M., & Yuste, R. (2011). Dense, unspecific connectivity of neocortical parvalbumin-positive interneurons: a canonical microcircuit for inhibition? *J Neurosci, 31*(37), 13260-13271. doi:10.1523/JNEUROSCI.3131-11.2011

Patz, S., Grabert, J., Gorba, T., Wirth, M. J., & Wahle, P. (2004). Parvalbumin expression in visual cortical interneurons depends on neuronal activity and TrkB ligands during an Early period of postnatal development. *Cereb Cortex, 14*(3), 342-351. Retrieved from https://www.ncbi.nlm.nih.gov/pubmed/14754872

Paxinos, G., & Franklin, K. B. (2004). *The mouse brain in stereotaxic coordinates*: Gulf professional publishing.

Penagarikano, O., Mulle, J. G., & Warren, S. T. (2007). The pathophysiology of fragile x syndrome. *Annu Rev Genomics Hum Genet, 8*, 109-129. doi:10.1146/annurev.genom.8.080706.092249

Pizzorusso, T., Medini, P., Berardi, N., Chierzi, S., Fawcett, J. W., & Maffei, L. (2002). Reactivation of ocular dominance plasticity in the adult visual cortex. *Science, 298*(5596), 1248-1251. doi:10.1126/science.1072699

Rais, M., Binder, D. K., Razak, K. A., & Ethell, I. M. (2018). Sensory Processing Phenotypes in Fragile X Syndrome. *ASN Neuro, 10*, 1759091418801092. doi:10.1177/1759091418801092

Rojas, D. C., Benkers, T. L., Rogers, S. J., Teale, P. D., Reite, M. L., & Hagerman, R. J. (2001). Auditory evoked magnetic fields in adults with fragile X syndrome. *Neuroreport, 12*(11), 2573-2576. Retrieved from https://www.ncbi.nlm.nih.gov/pubmed/11496151

Ronesi, J. A., & Huber, K. M. (2008). Homer interactions are necessary for metabotropic glutamate receptor-induced long-term depression and translational activation. *J Neurosci, 28*(2), 543-547. doi:10.1523/JNEUROSCI.5019-07.2008

Rotschafer, S., & Razak, K. (2013). Altered auditory processing in a mouse model of fragile X syndrome. *Brain Res, 1506*, 12-24. doi:10.1016/j.brainres.2013.02.038

Rotschafer, S. E., & Razak, K. A. (2014). Auditory processing in fragile x syndrome. *Front Cell Neurosci, 8*, 19. doi:10.3389/fncel.2014.00019

Rotschafer, S. E., Trujillo, M. S., Dansie, L. E., Ethell, I. M., & Razak, K. A. (2012). Minocycline treatment reverses ultrasonic vocalization production deficit in a mouse model of Fragile X Syndrome. *Brain Res, 1439*, 7-14. doi:10.1016/j.brainres.2011.12.041

Roughley, P. J., & Mort, J. S. (2014). The role of aggrecan in normal and osteoarthritic cartilage. *J Exp Orthop, 1*(1), 8. doi:10.1186/s40634-014-0008-7

Santos, A. R., Kanellopoulos, A. K., & Bagni, C. (2014). Learning and behavioral deficits associated with the absence of the fragile X mental retardation protein: what a fly and mouse model can teach us. *Learn Mem, 21*(10), 543-555. doi:10.1101/lm.035956.114

Sato, A. (2016). mTOR, a Potential Target to Treat Autism Spectrum Disorder. *CNS Neurol Disord Drug Targets, 15*(5), 533-543. Retrieved from https://www.ncbi.nlm.nih.gov/pubmed/27071790

Schneider, A., Leigh, M. J., Adams, P., Nanakul, R., Chechi, T., Olichney, J., . . . Hessl, D. (2013). Electrocortical changes associated with minocycline treatment in fragile X syndrome. *J Psychopharmacol, 27*(10), 956-963. doi:10.1177/0269881113494105

Selby, L., Zhang, C., & Sun, Q. Q. (2007). Major defects in neocortical GABAergic inhibitory circuits in mice lacking the fragile X mental retardation protein. *Neurosci Lett, 412*(3), 227-232. doi:10.1016/j.neulet.2006.11.062

Sharma, A., Hoeffer, C. A., Takayasu, Y., Miyawaki, T., McBride, S. M., Klann, E., & Zukin, R. S. (2010). Dysregulation of mTOR signaling in fragile X syndrome. *J Neurosci, 30*(2), 694-702. doi:10.1523/JNEUROSCI.3696-09.2010

Sidhu, H., Dansie, L. E., Hickmott, P. W., Ethell, D. W., & Ethell, I. M. (2014). Genetic removal of matrix metalloproteinase 9 rescues the symptoms of fragile X syndrome in a mouse model. *J Neurosci, 34*(30), 9867-9879. doi:10.1523/JNEUROSCI.1162-14.2014

Sinclair, D., Oranje, B., Razak, K., Siegel, S., & Schmid, S. (2017). Sensory processing in autism spectrum disorders and Fragile X syndrome—From the clinic to animal models. *Neuroscience & Biobehavioral Reviews, 76*, 235-253.

Sutcliffe, J. S., Nelson, D. L., Zhang, F., Pieretti, M., Caskey, C. T., Saxe, D., & Warren, S. T. (1992). DNA methylation represses FMR-1 transcription in fragile X syndrome. *Hum Mol Genet, 1*(6), 397-400. Retrieved from https://www.ncbi.nlm.nih.gov/pubmed/1301913

Szklarczyk, A., Lapinska, J., Rylski, M., McKay, R. D., & Kaczmarek, L. (2002). Matrix metalloproteinase-9 undergoes expression and activation during dendritic remodeling in adult hippocampus. *J Neurosci, 22*(3), 920-930. Retrieved from https://www.ncbi.nlm.nih.gov/pubmed/11826121

Tamamaki, N., Yanagawa, Y., Tomioka, R., Miyazaki, J., Obata, K., & Kaneko, T. (2003). Green fluorescent protein expression and colocalization with calretinin, parvalbumin, and somatostatin in the GAD67-GFP knock-in mouse. *J Comp Neurol, 467*(1), 60-79. doi:10.1002/cne.10905

Tranfaglia, M. R. (2011). The psychiatric presentation of fragile x: evolution of the diagnosis and treatment of the psychiatric comorbidities of fragile X syndrome. *Dev Neurosci, 33*(5), 337-348. doi:10.1159/000329421

Verkerk, A. J., Pieretti, M., Sutcliffe, J. S., Fu, Y. H., Kuhl, D. P., Pizzuti, A., . . . Zhang, F. P. (1991). Identification of a gene (FMR-1) containing a CGG repeat coincident with a breakpoint cluster region exhibiting length variation in fragile X syndrome. *Cell, 65*(5), 905-914. Retrieved from https://www.ncbi.nlm.nih.gov/pubmed/1710175

Wang, Y., Sakano, H., Beebe, K., Brown, M. R., de Laat, R., Bothwell, M., . . . Rubel, E. W. (2014). Intense and specialized dendritic localization of the fragile X mental retardation protein in binaural brainstem neurons: a comparative study in the alligator, chicken, gerbil, and human. *J Comp Neurol, 522*(9), 2107-2128. doi:10.1002/cne.23520

Wen, T. H., Afroz, S., Reinhard, S. M., Palacios, A. R., Tapia, K., Binder, D. K., . . . Ethell, I. M. (2018). Genetic Reduction of Matrix Metalloproteinase-9 Promotes Formation of Perineuronal Nets Around Parvalbumin-Expressing Interneurons and Normalizes Auditory Cortex Responses in Developing Fmr1 Knock-Out Mice. *Cereb Cortex, 28*(11), 3951-3964. doi:10.1093/cercor/bhx258

Yan, Q. J., Asafo-Adjei, P. K., Arnold, H. M., Brown, R. E., & Bauchwitz, R. P. (2004). A phenotypic and molecular characterization of the fmr1-tm1Cgr fragile X mouse. *Genes Brain Behav, 3*(6), 337-359. doi:10.1111/j.1601-183X.2004.00087.x

Yan, Q. J., Rammal, M., Tranfaglia, M., & Bauchwitz, R. P. (2005). Suppression of two major Fragile X Syndrome mouse model phenotypes by the mGluR5 antagonist MPEP. *Neuropharmacology, 49*(7), 1053-1066. doi:10.1016/j.neuropharm.2005.06.004

Yang, F., Je, H. S., Ji, Y., Nagappan, G., Hempstead, B., & Lu, B. (2009). Pro-BDNF-induced synaptic depression and retraction at developing neuromuscular synapses. *J Cell Biol, 185*(4), 727-741. doi:10.1083/jcb.200811147

Yau, S. Y., Bettio, L., Vetrici, M., Truesdell, A., Chiu, C., Chiu, J., . . . Christie, B. R. (2018). Chronic minocycline treatment improves hippocampal neuronal structure, NMDA receptor function, and memory processing in Fmr1 knockout mice. *Neurobiol Dis, 113*, 11-22. doi:10.1016/j.nbd.2018.01.014

Yong, V. W., Krekoski, C. A., Forsyth, P. A., Bell, R., & Edwards, D. R. (1998). Matrix metalloproteinases and diseases of the CNS. *Trends Neurosci, 21*(2), 75-80. Retrieved from https://www.ncbi.nlm.nih.gov/pubmed/9498303

Zhang, Y., Brown, M. R., Hyland, C., Chen, Y., Kronengold, J., Fleming, M. R., . . . Kaczmarek, L. K. (2012). Regulation of neuronal excitability by interaction of fragile X mental retardation protein with slack potassium channels. *J Neurosci, 32*(44), 15318-15327. doi:10.1523/JNEUROSCI.2162-12.2012

Figure 2.1

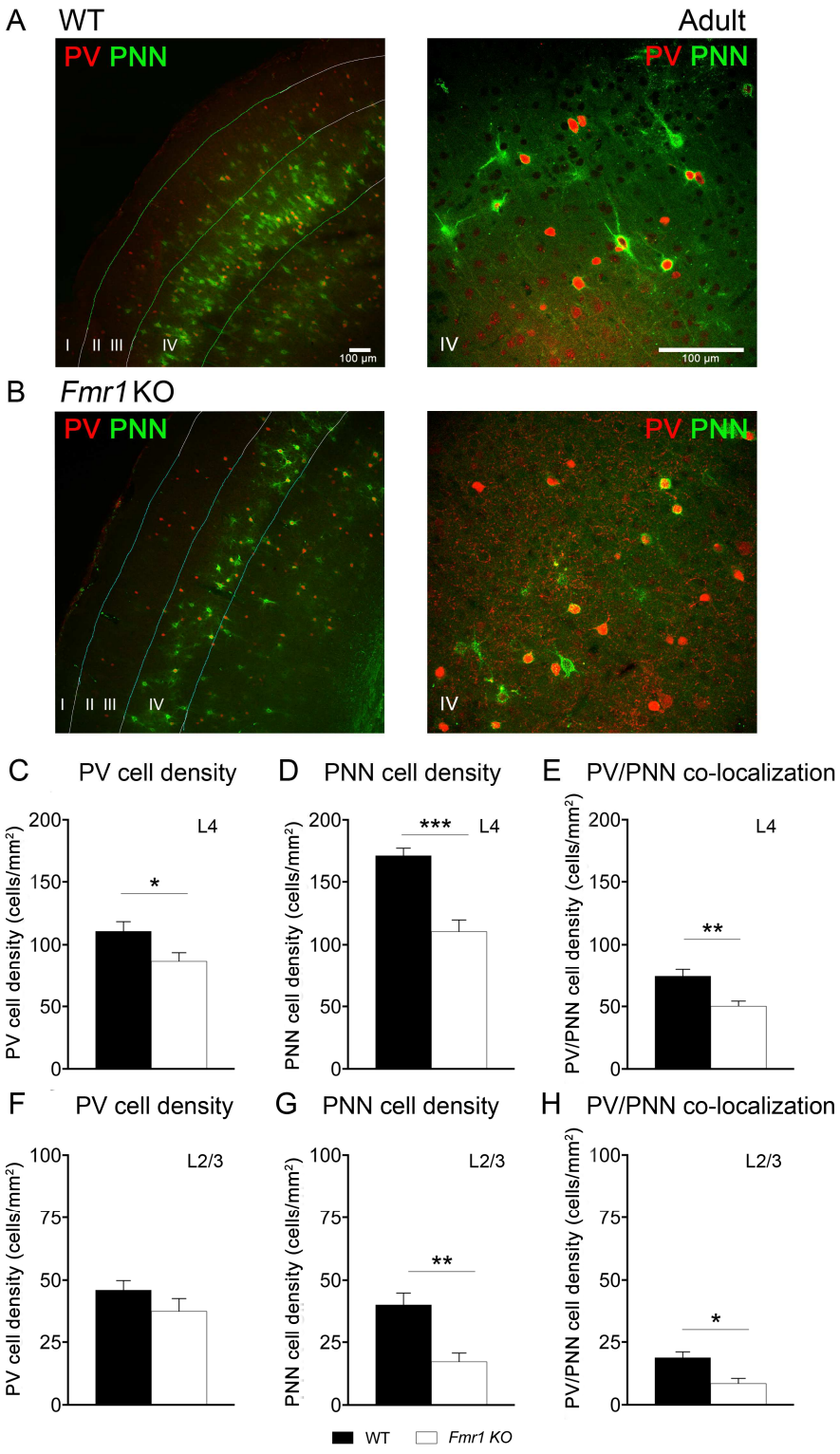
A WT
Adult
PV PNN
I II III IV
100 µm
B Fmr1 KO
C PV cell density
D PNN cell density
E PV/PNN co-localization
L4
L2/3
PV cell density (cells/mm²)
PNN cell density (cells/mm²)
PV/PNN cell density (cells/mm²)
*
**
***
WT
Fmr1 KO

Figure 2.1. Impaired WFA+ PNNs and PV/PNN co-localization are detected in the auditory cortex of adult *Fmr1* KO mice.
(A-B) Confocal images showing PV immunoreactivity (red) and WFA-positive PNN labeling (green) in the auditory cortex of adult WT (A) and *Fmr1* KO mice (B). (C-H) Quantitative analysis of the density of PV, PNN, or PV/PNN positive cells. Graphs show mean ± SEM (n=6/group, *p<0.05; **p<0.01; ***p<0.001, t-test). PV cell density was significantly reduced in L4 auditory cortex of *Fmr1* KO mice compared to WT. (C) No significant changes were observed in PV cell density in L2-3 between the WT and *Fmr1* KO mice (F). PNN cell density was significantly reduced in L4 (D) and L2-3 (G) auditory cortex of *Fmr1* KO mice compared to WT mice (note that only WFA+ cells were counted to measure PNN density). PV/PNN co-localization was also significantly reduced in L4 (E) and L2-3 (H) auditory cortex of *Fmr1* KO mice.

Figure 2.2

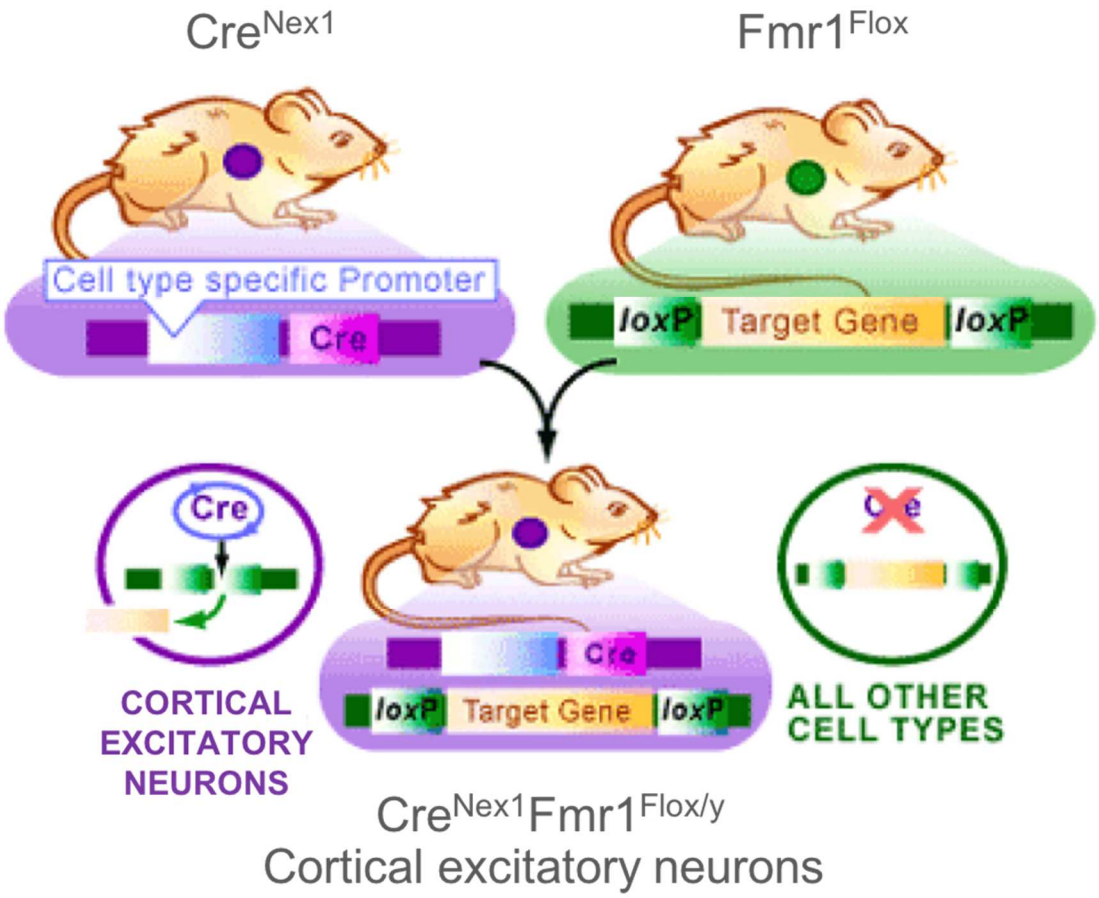

Figure 2.2. Schematic of Cre-mediated deletion of floxed *Fmr1* gene in excitatory neurons using the NeuroD/Nex1 promoter.
Mice were developed to remove FMRP specifically from the cortical excitatory neurons. This was achieved through Cre-mediated deletion of Floxed *Fmr1* gene in excitatory neurons using NeuroD (Cre^{Nex1}) promoter. Male Cre^{Nex1} were crossed with female $Fmr1^{flox/flox}$ mice to produce male $Cre^{Nex1}/Fmr1^{flox/y}$ conditional knock out (cKO) mice and their wild type (WT) littermates, $Fmr1^{flox/y}$ mice.

Figure 2.3

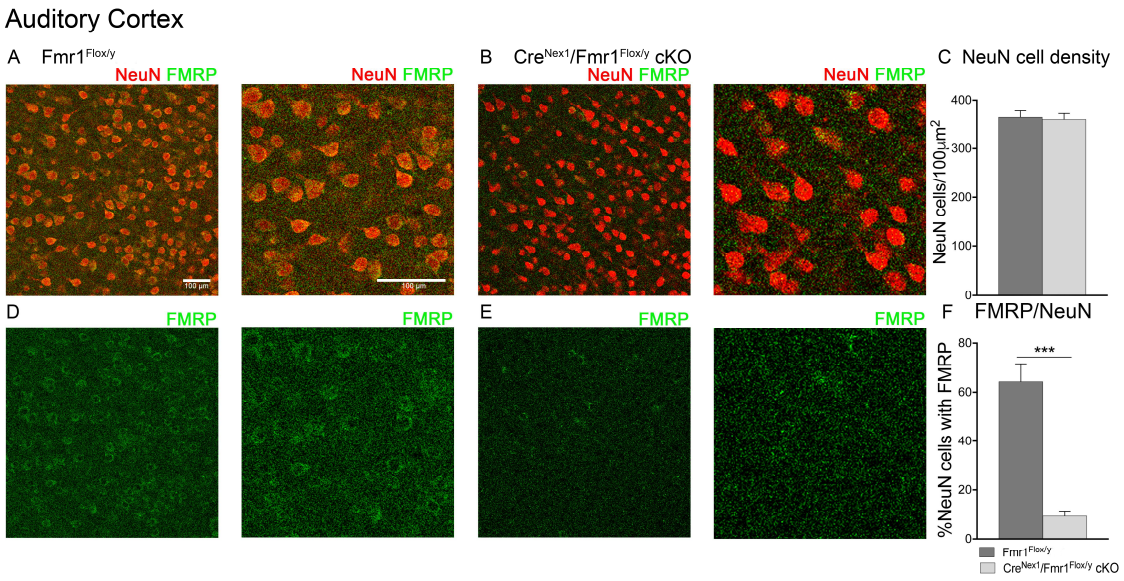

Figure 2.3. Excitatory specific FMRP loss was observed in the auditory cortex of adult *Cre^{Nex1}/Fmr1$^{Flox/y}$* cKO mice.
(A-B) Confocal images showing NeuN (red) and FMRP (green) immunoreactivity in the auditory cortex of adult *Fmr1*$^{Flox/y}$ and *Cre^{Nex1}/Fmr1$^{Flox/y}$* cKO mice. (C) Quantitative analysis of the density of NeuN-positive cells. Graphs show mean ± SEM. No significant changes were observed in NeuN cell density in the *Fmr1*$^{Flox/y}$ and *Cre^{Nex1}/Fmr1$^{Flox/y}$* cKO mice. (D-E) Confocal images showing FMRP (green) immunoreactivity in the auditory cortex of adult *Fmr1*$^{Flox/y}$ and *Cre^{Nex1}/Fmr1$^{Flox/y}$* cKO mice. (F) Quantitative analysis of the percentage of FMRP-positive NeuN cells. Graphs show mean ± SEM (n= 3/group, ***p<0.001, t-test). There is a significant decrease in the percentage of NeuN+ neurons with FMRP in the *Cre^{Nex1}/Fmr1$^{Flox/y}$* cKO mice compared to *Fmr1*$^{Flox/y}$ mice.

Figure 2.4

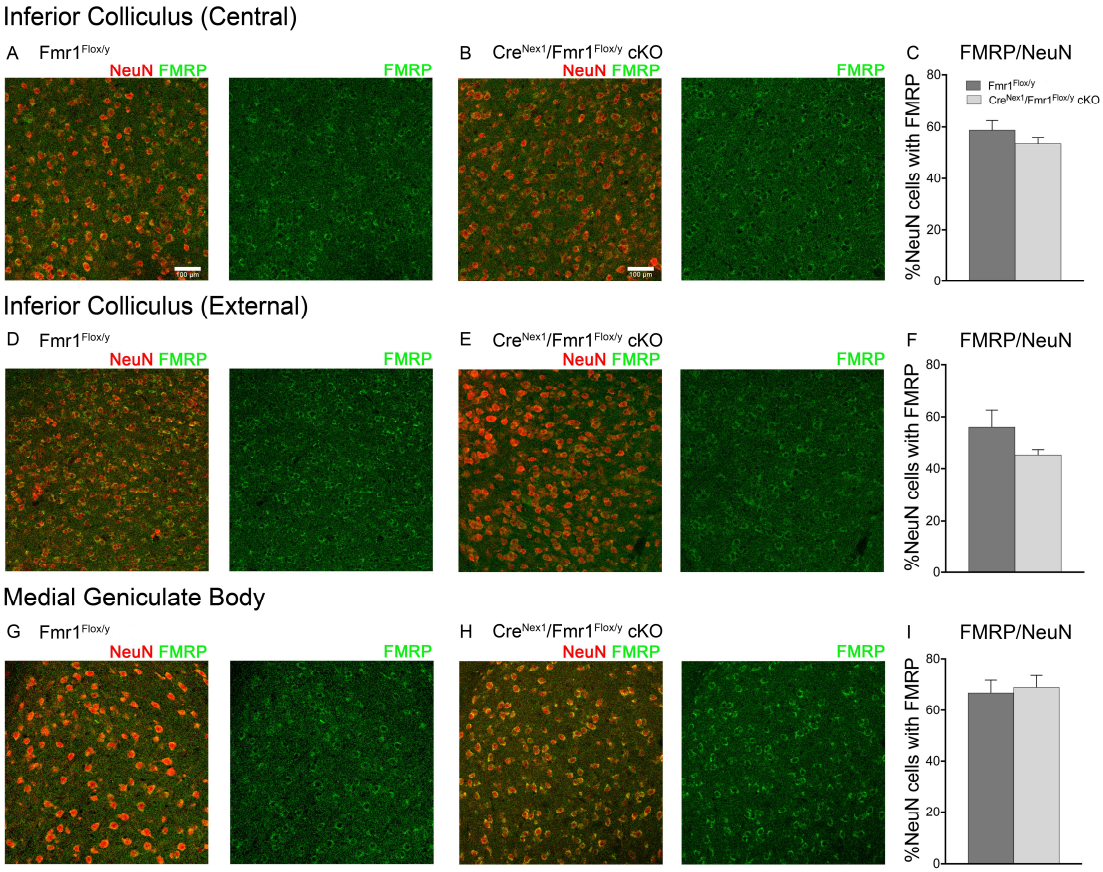

Figure 2.4. FMRP expression remained unchanged in the inferior colliculus and auditory thalamus of adult *Cre^{Nex1}/Fmr1$^{Flox/y}$* cKO mice.
(A-B) Confocal images showing NeuN (red) and FMRP (green) immunoreactivity in the central inferior colliculus of adult *Fmr1*$^{Flox/y}$ and *Cre^{Nex1}/Fmr1$^{Flox/y}$* cKO mice. (C) Quantitative analysis of the density of FMRP-positive cells. Graphs show mean ± SEM (n= 3/group, p>0.05, t-test). No significant changes were observed in the percentage of NeuN+ neurons with FMRP in the *Fmr1*$^{Flox/y}$ and *Cre^{Nex1}/Fmr1$^{Flox/y}$* cKO mice in the central inferior colliculus. (D-E) Confocal images showing NeuN and FMRP immunoreactivity in the external inferior colliculus of adult *Fmr1*$^{Flox/y}$ and *Cre^{Nex1}/Fmr1$^{Flox/y}$* cKO mice. (F) Analysis of the density of FMRP-positive cells. Graphs show mean ± SEM (n= 3/group, p>0.05, t-test). No significant changes were observed in the percentage of NeuN neurons with FMRP in the *Fmr1*$^{Flox/y}$ and *Cre^{Nex1}/Fmr1$^{Flox/y}$* cKO mice in the external inferior colliculus. (G-H) Confocal images showing NeuN and FMRP immunoreactivity in the medial geniculate body of adult *Fmr1*$^{Flox/y}$ and *Cre^{Nex1}/Fmr1$^{Flox/y}$* cKO mice. (I) Analysis of the density of FMRP-positive cells. Graphs show mean ± SEM (n= 3/group, p>0.05, t-test). No significant changes were observed in the percentage of NeuN+ neurons with FMRP in the *Fmr1*$^{Flox/y}$ and *Cre^{Nex1}/Fmr1$^{Flox/y}$* cKO mice in the medial geniculate body of the thalamus.

Figure 2.5

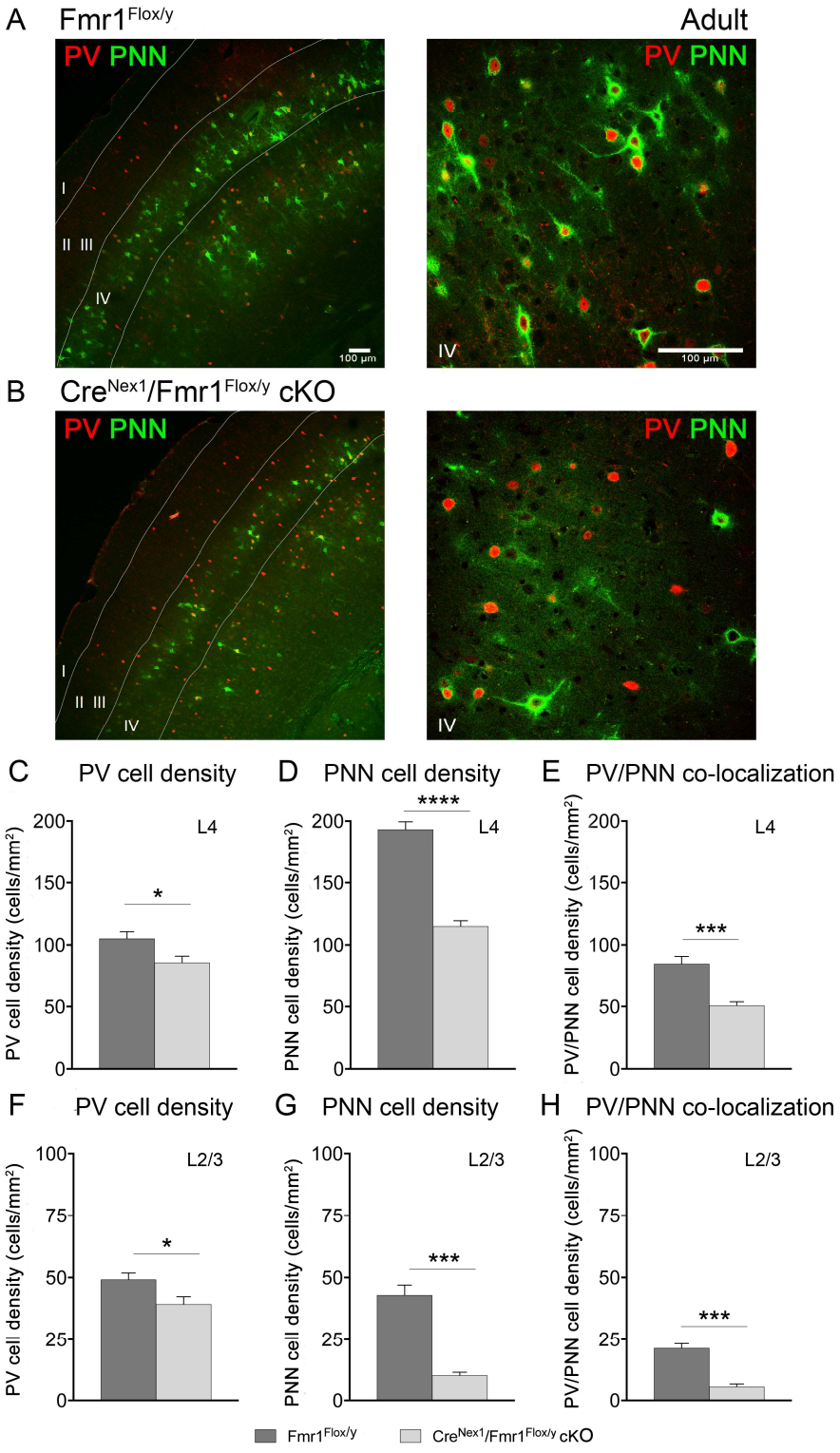
A
Fmr1Flox/y
Adult
PV PNN
I
II III
IV
100 µm
B
CreNex1/Fmr1Flox/y cKO
C
PV cell density
D
PNN cell density
E
PV/PNN co-localization
L4
PV cell density (cells/mm²)
PNN cell density (cells/mm²)
PV/PNN cell density (cells/mm²)
F
G
H
L2/3
Fmr1Flox/y
CreNex1/Fmr1Flox/y cKO

Figure 2.5. Deletion of *Fmr1* from excitatory neurons affected development of WFA+ PNNs and PV/PNN co-localization in the adult mouse auditory cortex. (A-B) Confocal images showing PV immunoreactivity (red) and WFA-positive PNN labeling (green) in the auditory cortex of adult *Fmr1*$^{Flox/y}$ (A) and *Cre*^{Nex1}/*Fmr1*$^{Flox/y}$ cKO (B) mice. (C-H) Quantitative analysis of the density of PV, PNN, or PV/PNN positive cells. Graphs show mean ± SEM (n= 6/group, *p<0.05; ***p<0.001; ****p<0.0001, t-test). PV cell density was significantly reduced in L4 (C) and L2-3 (F) auditory cortex of *Cre*^{Nex1}/*Fmr1*$^{Flox/y}$ cKO mice compared to *Fmr1*$^{Flox/y}$. PNN cell density was significantly reduced in L4 (D) and L2-3 (G) auditory cortex of *Cre*^{Nex1}/*Fmr1*$^{Flox/y}$ cKO mice compared to *Fmr1*$^{Flox/y}$ (note that only WFA-positive cells were counted to measure PNN density). PV/PNN co-localization was also significantly reduced in L4 (E) and L2-3 (H) auditory cortex of *Cre*^{Nex1}/*Fmr1*$^{Flox/y}$ cKO mice compared to *Fmr1*$^{Flox/y}$.

Figure 2.6

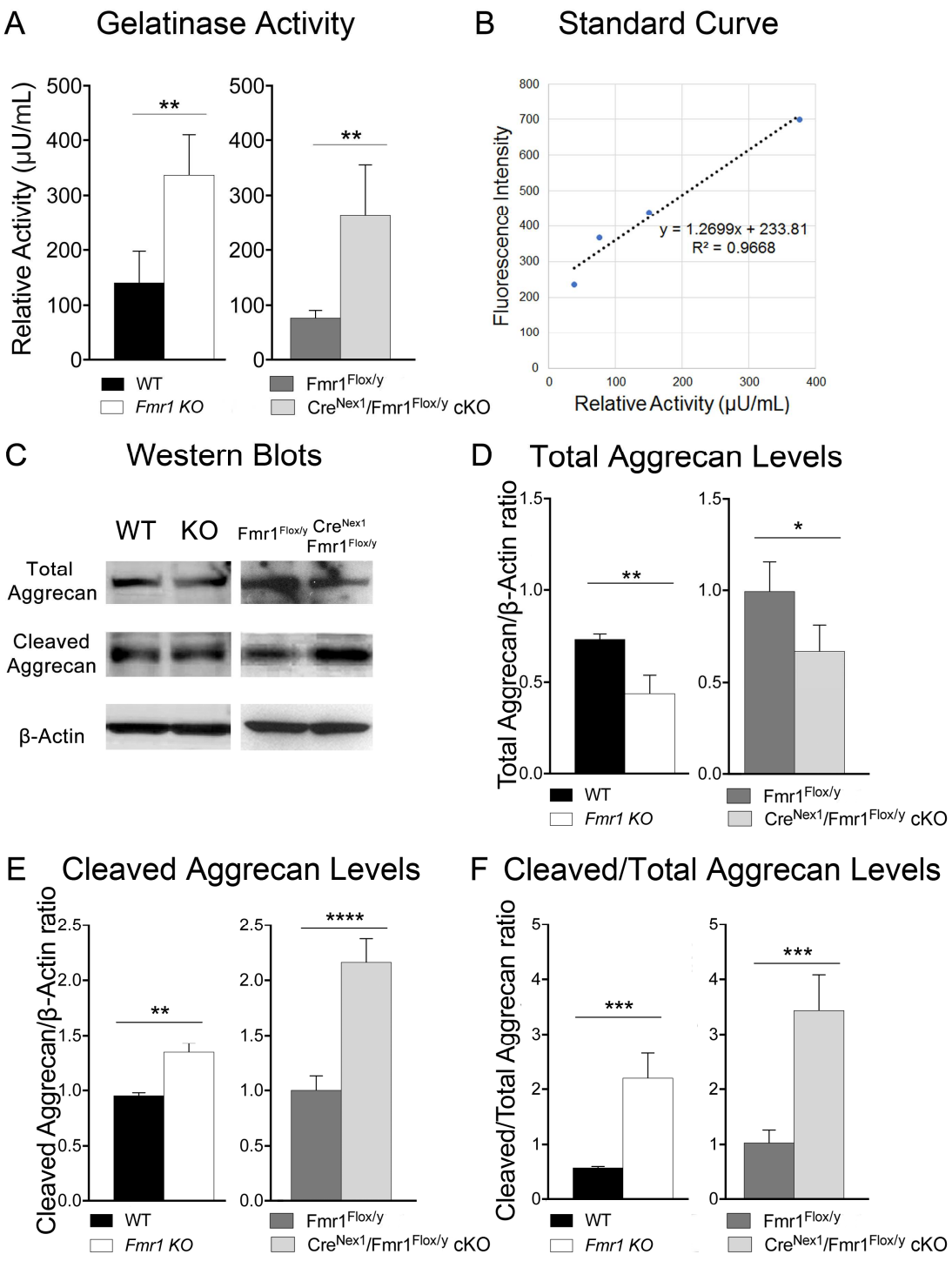
A Gelatinase Activity
Relative Activity (µU/mL)
500
400
300
200
100
0
**
**
WT
Fmr1 KO
Fmr1Flox/y
CreNex1/Fmr1Flox/y cKO
B Standard Curve
Fluorescence Intensity
800
700
600
500
400
300
200
100
0
y = 1.2699x + 233.81
R² = 0.9668
0
100
200
300
400
Relative Activity (µU/mL)
C Western Blots
WT
KO
Fmr1Flox/y
CreNex1
Fmr1Flox/y
Total Aggrecan
Cleaved Aggrecan
β-Actin
D Total Aggrecan Levels
Total Aggrecan/β-Actin ratio
1.5
1.0
0.5
0.0
**
*
WT
Fmr1 KO
Fmr1Flox/y
CreNex1/Fmr1Flox/y cKO
E Cleaved Aggrecan Levels
Cleaved Aggrecan/β-Actin ratio
2.5
2.0
1.5
1.0
0.5
0.0
**
****
WT
Fmr1 KO
Fmr1Flox/y
CreNex1/Fmr1Flox/y cKO
F Cleaved/Total Aggrecan Levels
Cleaved/Total Aggrecan ratio
5
4
3
2
1
0
***
***
WT
Fmr1 KO
Fmr1Flox/y
CreNex1/Fmr1Flox/y cKO

Figure 2.6. Total aggrecan levels are reduced whereas cleaved aggrecan levels and gelatinase activity are elevated in the auditory cortex of adult excitatory neuron specific *Cre^{Nex1}/Fmr1$^{Flox/y}$* cKO mice.
(A) Relative gelatinase activity in adult auditory cortex of WT, *Fmr1* KO, *Fmr1*$^{Flox/y}$ and *Cre^{Nex1}/Fmr1$^{Flox/y}$* cKO mice. Graph shows mean ± SEM (n=4/group, **p<0.01, t-test). Gelatinase activity is elevated in *Fmr1* KO and *Cre^{Nex1}/Fmr1$^{Flox/y}$* cKO mice as compared to WT and *Fmr1*$^{Flox/y}$ mice, respectively. (B) Standard curve showing gelatinase activity of recombinant MMP-9. Linear regression graph represents mean ± SEM (n=5). (C) Western blots showing total and cleaved forms of aggrecan. (D-F) Graphs show mean ± SEM (n=4/group, *p<0.05; **p<0.01; ***p<0.001; ****p<0.0001, t-test). Total aggrecan levels were significantly reduced in both the *Fmr1* KO and *Cre^{Nex1}/Fmr1$^{Flox/y}$* cKO mice compared to WT and *Fmr1*$^{Flox/y}$ mice (D). In contrast, cleaved aggrecan levels were significantly increased in the auditory cortex of both *Fmr1* KO and *Cre^{Nex1}/Fmr1$^{Flox/y}$* cKO mice compared to their WT counterparts (E). Cleaved aggrecan to total aggrecan ratio was significantly increased in both the *Fmr1* KO and *Cre^{Nex1}/Fmr1$^{Flox/y}$* cKO mice compared to WT and *Fmr1*$^{Flox/y}$ mice, respectively (F).

Figure 2.7

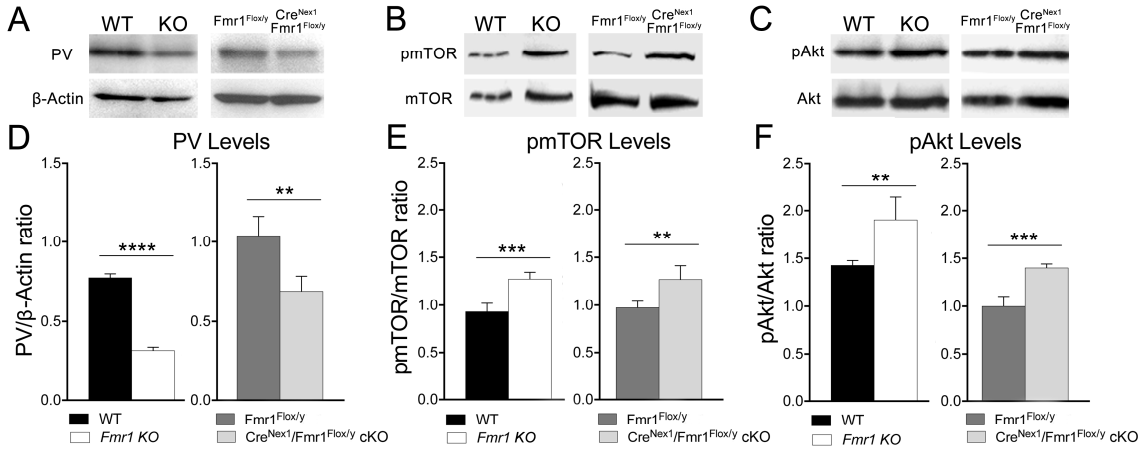

Figure 2.7. FMRP deletion from forebrain excitatory neurons is sufficient to decrease PV levels and trigger enhanced Akt and mTOR phosphorylation in the auditory cortex of adult mice.

(A-C) Western blot showing PV (A), p-mTOR, mTOR (B), p-Akt and Akt (C) levels in lysates from adult auditory cortex of WT, *Fmr1* KO, *Fmr1*$^{Flox/y}$ and *Cre*^{Nex1}*/Fmr1*$^{Flox/y}$ cKO mice. (D) Quantitative analysis of PV levels. Graphs show mean ± SEM (n=4/group, **p<0.01; ****p<0.0001, t-test). PV levels are significantly reduced in adult auditory cortex of both *Fmr1* KO and *Cre*^{Nex1}*/Fmr1*$^{Flox/y}$ cKO mice compared to their WT counterparts. (E-F) Quantitative analysis of p-mTOR/mTOR (E) and p-Akt/Akt ratios. Graphs show mean ± SEM (n=4/group, **p<0.01; ***p<0.001, t-test). There is a significant increase in the p-mTOR/mTOR ratio in the *Fmr1* KO mice compared to WT (E). There is also a significant increase in the p-Akt/Akt ratio in the *Fmr1* KO mice compared to WT mice (F). Similarly, there is a significant increase in the p-mTOR/mTOR ratio (E) and p-Akt/Akt ratio (F) in the adult auditory cortex of *Cre*^{Nex1}*/Fmr1*$^{Flox/y}$ cKO mice compared to *Fmr1*$^{Flox/y}$ mice.

Figure 2.8

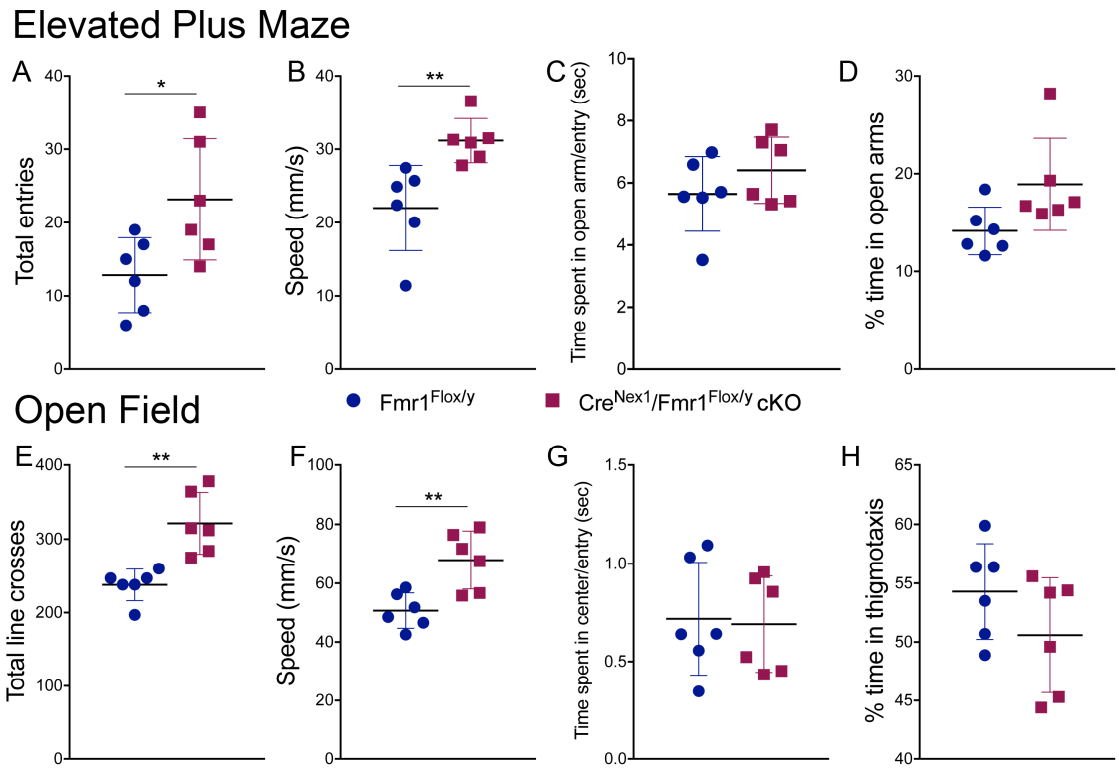

Figure 2.8. Adult excitatory neuron specific *Cre^{Nex1}/Fmr1$^{Flox/y}$* cKO mice display increased locomotor activity, but no anxiety-like behavior.
(A–D) Graphs demonstrate the performance of *Cre^{Nex1}/Fmr1$^{Flox/y}$* cKO mice in the elevated plus maze as measured by the total number of arm entries (A), speed (B), the total amount of time spent in the open arm per entry (C), and the percent of time spent in the open arms (D). Graphs show mean ± SEM (n=8/group, *p<0.05; **p<0.01, t-test). (E–H) Graphs demonstrate the performance of *Cre^{Nex1}/Fmr1$^{Flox/y}$* cKO mice in the open field as measured by the total number of line crosses (E), speed (F), the amount of time spent in the center per entry (G), and the percent time spent in thigmotaxis (H). Graphs show mean ± SEM (n=8/group, **p<0.01, t-test).

Figure 2.9

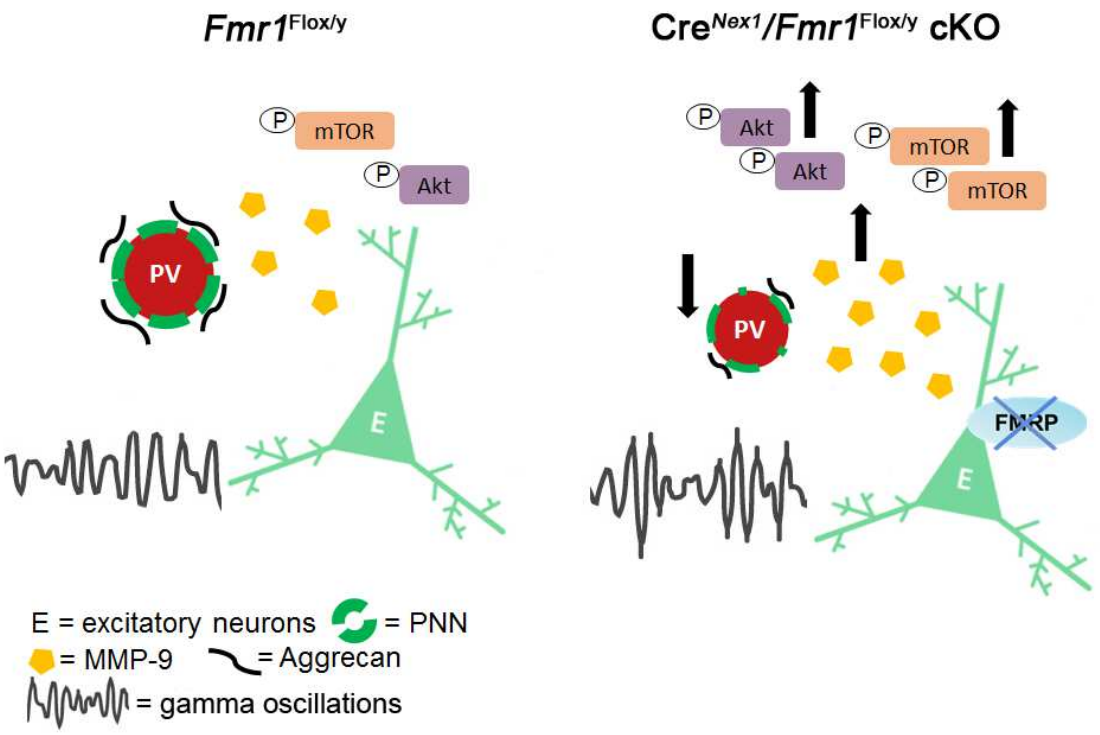

Figure 2.9. Schematic of cellular and EEG phenotypes in the auditory cortex of adult *Cre^{Nex1}/Fmr1$^{Flox/y}$* cKO compared to *Fmr1*$^{Flox/y}$ mice.
Left panel depicts normal cellular and EEG phenotypes in the auditory cortex of *Fmr1*$^{Flox/y}$ mice. Right panel depicts reduced PV levels, impaired formation of WFA+ PNNs around PV cells, increased gelatinase activity and mTOR/Akt phosphorylation, and abnormal neural oscillations in auditory cortex of excitatory neuron-specific *Cre^{Nex1}/Fmr1$^{Flox/y}$* cKO mice.

Table 2.1. Summary table showing percentage of NeuN+ neurons with FMRP expression in different regions of the auditory pathway in the *Fmr1*$^{Flox/y}$ and *Cre*^{Nex1}/*Fmr1*$^{Flox/y}$ cKO mice (mean ± SEM). Statistical analysis of differences between Cre^{Nex1}/*Fmr1*$^{Flox/y}$ cKO and its WT counterpart was performed using t-test (unpaired, two-tailed): ***p<0.001.

	Fmr1$^{Flox/y}$	Cre^{Nex1}/*Fmr1*$^{Flox/y}$ cKO
Auditory cortex	64.33 ± 4.19	9.33 ± 1.19*** P=0.0002
Central inferior colliculus	58.84 ± 2.09	53.30 ± 1.48
External inferior colliculus	53.93 ± 3.88	49.89 ± 2.79
Medial Geniculate Body	66.80 ± 3.40	68.90 ± 3.19

Table 2.2. Summary table showing density of PV cells, WFA+ PNNs, and PV/PNN co-localization in the auditory cortex of adult WT, *Fmr1* KO, *Fmr1*$^{Flox/y}$, and *Cre*^{Nex1}/*Fmr1*$^{Flox/y}$ cKO mice (mean ± SEM). Statistical analysis of differences between *Fmr1* KO and Cre^{Nex1}/*Fmr1*$^{Flox/y}$ cKO with their respective WT counterparts was performed using t-test (unpaired, two-tailed): *p<0.05, **p<0.01, ***p<0.001, ****p<0.0001.

	WT		*Fmr1* KO		*Fmr1*$^{Flox/y}$		Cre^{Nex1}/*Fmr1*$^{Flox/y}$ cKO	
	L4	L2/3	L4	L2/3	L4	L2/3	L4	L2/3
PV+ cell density	110.90 ± 7.53	46.06 ± 3.75	87.05 ± 6.65* P=0.0391	37.71 ± 5.01	105.00 ± 5.61	49.20 ± 2.62	85.91 ± 5.06* P=0.0298	39.32 ± 3.03* P=0.0483
PNN+ cell density	170.80 ± 5.94	40.27 ± 4.64	110.60 ± 9.21*** P=0.0003	17.35 ± 3.33** P=0.007	193.20 ± 6.19	42.92 ± 4.02	115.10 ± 4.41**** P<0.0001	10.27 ± 1.22*** P=0.0002
PV+/PNN+ co-localization	74.31± 5.42	18.81 ± 2.28	50.50 ± 3.77** P=0.0048	8.56 ± 2.02* P=0.0151	84.87 ± 5.92	21.37 ± 1.89	50.80 ± 3.05*** P=0.0005	5.63 ± 1.10*** P=0.0004

Table 2.3. Summary table showing gelatinase activity and protein levels in the auditory cortex of adult WT, *Fmr1* KO, *Fmr1*$^{Flox/y}$, and *Cre*^{Nex1}/*Fmr1*$^{Flox/y}$ cKO mice (mean ± SEM). Statistical analysis of differences between *Fmr1* KO and Cre^{Nex1}/*Fmr1*$^{Flox/y}$ cKO with their respective WT counterparts was performed using t-test (unpaired, two-tailed): *p<0.05, **p<0.01, ***p<0.001, ****p<0.0001.

	WT	*Fmr1* KO	*Fmr1*$^{Flox/y}$	Cre^{Nex1}/*Fmr1*$^{Flox/y}$ cKO
Gelatinase Activity	140.90 ± 28.49	337.40 ± 36.24** P=0.0053	77.24 ± 6.71	263.10 ± 46.13** P=0.0072
Full-length Aggrecan Levels	0.73 ± 0.01	0.44 ± 0.05** P=0.0016	0.99 ± 0.07	0.67 ± 0.07* P=0.0159
Cleaved Aggrecan Levels	0.96 ± 0.02	1.35 ± 0.04** P=0.0031	1.01 ± 0.07	2.14 ± 0.08**** P< 0.0001
Cleaved/Total Aggrecan ratio	0.57 ± 0.01	2.21 ± 0.23*** P=0.0003	0.99 ± 0.10	3.52 ± 0.27*** P=0.0001
PV Levels	0.78 ± 0.01	0.32 ± 0.01**** P<0.0001	1.02 ± 0.05	0.69 ± 0.05** P=0.0032
p-mTOR/mTOR ratio	0.93 ± 0.04	1.28 ± 0.03*** P=0.0005	0.96 ± 0.03	1.27 ± 0.07** P=0.0073
p-Akt/Akt ratio	1.36 ± 0.04	1.91 ± 0.12** P=0.0051	0.97 ± 0.05	1.40 ± 0.02*** P=0.0002

Table 2.4. Summary table showing locomotor activity and *anxiety* measures of *Fmr1*$^{Flox/y}$ and *Cre*^{Nex1}/*Fmr1*$^{Flox/y}$ cKO mice using elevated plus maze (EP) and open-field (OF) behavior tests (mean ± SEM). Statistical analysis of differences between Cre^{Nex1}/*Fmr1*$^{Flox/y}$ cKO and its WT counterpart was performed using t-test (unpaired, two-tailed): *p<0.05, **p<0.01.

	Fmr1$^{Flox/y}$	Cre^{Nex1}/*Fmr1*$^{Flox/y}$ cKO
Total entries (EP)	12.83 ± 2.09	23.17 ± 3.37* P=0.0262
Speed (EP)	21.99 ± 2.37	31.18 ± 1.23** P=0.0063
Time spent in open arm/entry (EP)	5.65 ± 0.49	6.41 ± 0.43
% Time in open arms (EP)	14.15 ± 0.99	18.92 ± 1.92
Total line crosses (OF)	237.80 ± 8.81	321.30 ± 17.03** P=0.0014
Speed (OF)	50.72 ± 2.46	67.90 ± 4.02** P=0.0045
Time spent in center/entry (OF)	0.72 ± 0.12	0.69 ± 0.10
% Time in thigmotaxis (OF)	54.30 ± 1.66	50.58 ± 1.99

Chapter 3 – Postnatal Interventions in Excitatory Neurons to Shape Cortical Circuits in Fragile X Syndrome

Abstract

Fragile X syndrome (FXS) is a leading genetic cause of autism-like symptoms that include sensory processing deficits and cortical hyperexcitability. While gene reactivation shows promise as a treatment strategy for FXS, it is unclear what time window, brain area and cells should be targeted. Growing human and mouse studies suggest that loss and hypofunction of parvalbumin (PV) cells underlie the pathogenesis of autism and FXS, potentially due to impaired ability of PV cells to establish functional connections with excitatory neurons. The goal of this study was to examine whether conditional deletion (cOFF) or re-expression (cON) of *Fmr1* in excitatory neurons during the critical postnatal day (P)14-P21 period of cortical circuit development is sufficient to trigger or prevent abnormal phenotypes in mouse auditory cortex (AuC). We targeted excitatory neurons through Cre-mediated *Fmr1* deletion or re-expression using CaMKIIα promoter. We found that similar to global *Fmr1* KO mice, the density of PV cells with perineuronal nets (PNNs) and sound-evoked gamma synchronization were impaired in $Cre^{CaMKII\alpha}/Fmr1^{Flox/y}$ cOFF mice, whereas cortical MMP-9 gelatinase activity and baseline EEG gamma power were enhanced. In addition, mTOR/Akt signaling and TrkB phosphorylation were altered in cOFF mice, which also showed increased locomotor activity and anxiety-like behaviors. Remarkably, when FMRP levels were restored in excitatory neurons during the P14-P21 period, cortical MMP-9 gelatinase activity,

mTOR/Akt signaling, and baseline EEG gamma power were reduced in $Cre^{CaMKII\alpha}/Fmr1^{FloxNeo/y}$ cON mice. cON mice also showed increased density of PV cell and PNNs, as well as improved sound-evoked gamma synchronization and behaviors. These results indicate that postnatal deletion or re-expression of FMRP in excitatory neurons is sufficient to elicit or ameliorate structural and functional cortical deficits as well as abnormal behavioral phenotypes in mice, informing future gene re-expression studies about appropriate treatment window and providing an insight into the mechanism of cortical circuit disfunctions in FXS.

Introduction

Fragile X Syndrome (FXS) is a common monogenic form of autism spectrum disorders (ASD) (Crawford, Acuna, & Sherman, 2001). FXS is usually caused by a CGG repeat expansion in 5'-untranslated region of the Fragile X mental retardation 1 (*Fmr1*) gene with a consequent gene methylation, down-regulation of Fragile X Mental Retardation Protein (FMRP), translational dysregulation, and abnormal protein synthesis (Okray et al., 2015; Sutcliffe et al., 1992; Verkerk et al., 1991). Prominent symptoms of FXS include increased anxiety, intellectual disability, repetitive behaviors, social communication deficits, and abnormal sensory processing (Braat & Kooy, 2015; Penagarikano, Mulle, & Warren, 2007). Abnormal sensory processing in FXS includes debilitating hypersensitivity and reduced habituation to sensory inputs, particularly in the auditory domain (Castrén, Pääkkönen, Tarkka, Ryynänen, & Partanen, 2003; Ethridge et al., 2016; Schneider et al., 2013). These symptoms affect multiple sensory systems, are

seen early in development, and may contribute to cognitive deficits and delayed language.

Cortical hyperexcitability may cause auditory hypersensitivity in FXS, which is also observed in the mouse model of FXS (Castrén et al., 2003; Chen & Toth, 2001; Ethridge et al., 2016; Frankland et al., 2004; Nielsen, Derber, McClellan, & Crnic, 2002; Rais, Binder, Razak, & Ethell, 2018; Rojas et al., 2001; S. Rotschafer & Razak, 2013; S. E. Rotschafer & Razak, 2014; Sinclair, Oranje, Razak, Siegel, & Schmid, 2017). The *Fmr1* knockout (KO) mouse is an established FXS model that is well suited to study cortical deficits because it shows functional alterations that are similar to humans and suggest abnormal excitatory/inhibitory (E/I) balance (Sinclair et al., 2017). Parvalbumin (PV) interneurons are fast-spiking inhibitory cells that provide temporal precision to excitatory responses and their loss and hypofunction may contribute to cortical hyperexcitability in both in individuals with autism (Ferguson & Gao, 2018; Filice, Janickova, Henzi, Bilella, & Schwaller, 2020; Hashemi, Ariza, Rogers, Noctor, & Martinez-Cerdeno, 2017; Lunden, Durens, Phillips, & Nestor, 2019; Marin, 2012; Rossignol, 2011) and mouse models of autism, including FXS (Goel et al., 2018). Our previous studies suggest that impaired development of PV inhibitory interneurons during postnatal day (P)14-P21 period may underlie abnormal auditory cortical responses in *Fmr1* KO mice via matrix metalloproteinase-9 (MMP-9)-dependent regulation of perineuronal nets (PNNs) (Wen, Afroz, et al., 2018).

FMRP loss affects the communication between excitatory neurons (Ex) and inhibitory interneurons (Gibson, Bartley, Hays, & Huber, 2008; Hays, Huber, & Gibson,

2011) and embryonic deletion of *Fmr1* in cortical Ex is sufficient to affect PV expression, recapitulating some abnormal electrophysiological, and behavioral phenotypes that are seen in global *Fmr1* KO mice (Lovelace et al., 2020). However, it is still not clear whether the FMRP deletion affects PV cell neurogenesis, migration or maturation. Therefore, the main goal of this study was to examine whether deletion or re-expression of *Fmr1* during the critical developmental period of PV cell maturation (P14-P21) is sufficient to trigger or prevent the development of abnormal phenotypes in the auditory cortex (AuC) of *Fmr1* KO mice. Our studies also provide a critical insight into whether cortical defects, in particular PV cell deficits, can be corrected by re-expressing FMRP only in Ex through Cre-mediated recombination using the CaMKIIα promoter. Thus, the purpose of the present study is to gain valuable insights into the relationships between spatiotemporal aspects of FMRP expression and cortical hyperexcitability in FXS. These results will have broad implications in terms of prospects for gene reactivation studies by targeting specific cells and identifying optimal treatment windows.

Materials and Methods

Ethics Statement

All experiments and animal care/use protocols were approved by the Institutional Animal Care and Use Committee at the University of California, Riverside, and were carried out in accordance with NIH Guide for the Care and Use of Laboratory Animals.

Mice

Fmr1^{Flox} and *Fmr1*^{FloxNeo} mice were generated in the laboratory of Dr. David Nelson (Baylor College of Medicine, Houston, Texas) (Mientjes et al., 2006). Cre$^{CaMKII\alpha}$ mice (RRID:IMSR_JAX: 005359) were obtained from Jackson Laboratories. In order to re-express FMRP specifically in excitatory neurons during early postnatal development we crossed male Cre$^{CaMKII\alpha}$ with female *Fmr1*$^{FloxNeo/FloxNeo}$ mice to produce male Cre$^{CaMKII\alpha}$*Fmr1*$^{FloxNeo/y}$ conditional re-expression (cON) mice and their knockout (Ctrl KO) littermates *Fmr1*$^{FloxNeo/y}$ mice. All genotypes were confirmed by PCR analysis of genomic DNA isolated from mouse tails. Mice were maintained in an AAALAC accredited facility under 12h light/dark cycle and fed standard mouse chow, food and water was available *ad libitum*. All procedures were done according to NIH and Institutional Animal Care and Use Committee guidelines. All procedures were approved by IACUC. Food and water were provided to the mice *ad libitum*.

Methods Overview

The CaMKIIα promoter was used to generate conditional deletion (cOFF) and re-expression (cON) mouse lines because CaMKIIα expression is localized to excitatory neuronal populations, and there is a developmental up-regulation of CaMKIIα expression in pyramidal neurons during second and third postnatal weeks (Burgin et al., 1990). To confirm deletion and re-expression of FMRP in cortical Ex during early postnatal development, we examined expression of FMRP in AuC at P14, P21, and P60 using immunostaining. All other analysis was done in adult P60-P70 mice. We analyzed the effects of Ex specific *Fmr1* deletion and re-expression on PV/PNN levels in adult AuC

using immunohistochemistry. EEG recordings were performed in awake, freely moving adult male mice to determine the effects of FMRP deletion and re-expression in Ex on neural oscillations in AuC at baseline and in response to sound (Lovelace, Ethell, Binder, & Razak, 2018). Furthermore, we analyzed the activation of PV cells with cFos immunoreactivity. Biochemical measurements of gelatinase activity, mTOR/Akt signaling and TrkB phosphorylation were also done in AuC of both cOFF and cON adult male mice. Finally, we examined anxiety-like behaviors, hyperactivity, and socialization in cOFF and cON adult male mice.

Immunofluorescence

Age-matched P14, P21, and P60-70 male Ctrl WT and cOFF, or Ctrl KO and cON mice were euthanized with isoflurane and sodium pentobarbital and perfused transcardially first with cold phosphate-buffered saline (PBS, 0.1 M) to clear out the blood and then with 4% paraformaldehyde (PFA) in 0.1M PBS for fixation. Brains were removed and post-fixed for 2–4h in 4% PFA. 40-100μm brain slices were obtained using a vibratome (5100mz Campden Instruments). Auditory cortex was identified using hippocampal landmarks and the Franklin and Paxinos mouse brain atlas (Paxinos & Franklin, 2004). For each brain, an average of 5–6 brain slices containing auditory cortex were collected.

Detection of PV/PNN

Immunostaining in 100μm brain slices containing auditory cortex was performed as previously described with minor modifications (Lovelace et al., 2020). Briefly, brain slices were post-fixed for an additional 2h in 4% PFA in 0.1 M PBS and then washed 3

times in 0.1M PBS for 10 min. Slices were then quenched with 50mM ammonium chloride for 15 min and washed 3 times with PBS for 10 min. Next, brain tissues were permeabilized with 0.1% Triton X-100 in PBS and nonspecific staining was blocked with a 5% Normal Goat Serum (NGS; Sigma, catalog# G9023-10 mL) and 1% Bovine Serum Albumin (BSA; Fisher Scientific, catalog# 9048468) in 0.1M PBS solution. Brain slices were treated overnight with mouse anti-parvalbumin antibody (1:1000; Sigma, catalog# P3088, RRID: AB_477 329) to label parvalbumin-positive (PV) inhibitory interneurons. Wisteria floribunda agglutinin (WFA; 4μg/mL; Vector Laboratories, cat# FL-1351, RRID: AB_2 336875) in 0.1M PBS containing 1% NGS, 0.5% BSA, and 0.1% Tween-20 solution was used to stain for PNNs containing aggrecan, known as WFA+ PNNs. WFA is a lectin, which binds glycosaminoglycan side chains of chondroitin sulfate proteoglycan aggrecan that is found in PNNs (Pizzorusso et al., 2002). After incubation, brain slices were washed 3 times in 0.1M PBS containing 0.5% Tween-20 for 10 min and incubated with secondary antibody, donkey anti-mouse Alexa 594 (4μg/mL; Thermo Fisher Scientific, catalog# A-21203, RRID: AB_2 535789) in 0.1M PBS for 1h. Slices were then washed 3 times with 0.1M PBS containing 0.5% Tween-20 for 10 min, mounted with Vectashield containing DAPI (Vector Labs, catalog# H-1200, RRID: AB_2336790) and Cytoseal (ThermoScientific, catalog# 8310–16).

Detection of FMRP Expression

Immunostaining for FMRP was performed using antigen retrieval methods, as previously described (Lovelace et al., 2020). Briefly, 40μm brain slices were mounted onto Superfrost Plus Microscope Charged Slides (Fisher Scientific, catalog #22-034-

979); washed 3 times with TBS (0.1M Tris Cl pH7.5, 0.15M NaCl) for 10 min; treated with 0.8% Na Borohydride (Sigma S-9125) to reduce background and autofluorescence; and boiled in 0.01M Na Citrate (Citric acid, sodium salt in water pH 6.0, Sigma C-8532) to achieve antigen retrieval. Permeabilization was performed with 0.5% Triton-X 100 for 20 min, and slices were stained overnight with mouse anti-FMRP (1:100; Developmental Studies Hybridoma Bank, catalog #2F5-1-s, RRID: AB_10805421), and rabbit anti-NeuN (1:1000; Abcam, catalog #ab104225, RRID: AB_10711153) in TBS containing 2% Normal Donkey serum (NDS) and 0.1% Triton-X 100. After incubation with primary antibodies, slices were washed 3 times in TBS for 10 min and incubated with secondary antibodies for 1h. Secondary antibodies used were donkey anti-rabbit Alexa 594 (4μg/mL; Thermo Fisher Scientific, catalog# A-21207, RRID: AB_141637), and donkey anti-mouse Alexa 488 (4μg/mL; Molecular Probes, catalog# A-21202, RRID: AB_141607). Slices were mounted with Vectashield containing DAPI and Cytoseal.

Image Analysis

Slices were imaged using confocal microscopy (Leica SP5) by collecting a series of 20 high-resolution optical sections (1024 × 1024-pixel format) at 1 μm step intervals (z-stack) that were captured for each slice using a 10×, 20×, or a 63× water-immersion objective (1.2 numerical aperture), with 1× or 5× zoom. All images were acquired under identical conditions. Each z-stack was collapsed into a single image by projection, converted to a TIFF file, encoded for blind analysis, and analyzed using ImageJ. ImageJ was used to identify and manually count PV-positive cells, WFA-positive PNN cells, PV/PNN co-localization, NeuN-positive cells and FMRP/NeuN co-localization. Cortical

layers were identified as previously reported (Anderson, Christianson, & Linden, 2009) and used for layer-specific analysis. Three slices were used per animal and cell counts were obtained in layers 1–4 of both the right and left auditory cortex (cell density was measured per layer). The freehand selection tool and measure function was used to specify layers of the auditory cortex and the point tool was used to label PNNs, PV cells, and NeuN cells added to the ROI manager. Particle Analysis Cell Counter plugin in Image J was used to count co-localization. Average cell density was calculated for each animal. Because we were comparing different mouse lines, the cOFF and the cON mice were evaluated against their specific controls (Ctrl WT and Ctrl KO, respectively), and statistical analysis was performed with unpaired t-test using GraphPad Prism 6 software (RRID: SCR_002798). Data represent mean ± standard error of the mean (SEM).

Surgery for *in vivo* EEG recordings

Age-matched adult P60-70 male cOFF (*n*=10) and their littermate controls (Ctrl WT; *n*=10), or adult P60-70 cON (*n*=13) and their littermate controls (Ctrl KO; *n*=13) were used for the EEG studies as previously described with modifications (Lovelace et al., 2018; Lovelace et al., 2020). Mice were anesthetized with isoflurane inhalation (0.2-0.5%) and an injection of ketamine and xylazine (K/X) (i.p. 80/10 mg/kg), and then secured in a bite bar, and placed in a stereotaxic apparatus (model 930; Kopf, CA). Artificial tear gel was applied to the eyes to prevent drying. Toe pinch reflex was used to measure anesthetic state every 10min throughout the surgery, and supplemental doses of K/X were administered as needed. Once the mouse was anesthetized, a midline sagittal incision was made along the scalp to expose the skull. A Foredom dental drill was used to

drill 1mm diameter holes in the skull overlying the right auditory cortex (-1.6mm, +4.8mm), left frontal lobe (+3.0mm, -1.6mm), and left occipital (-4.2mm, -5.1mm) (coordinate relative to Bregma: anterior/posterior, medial/lateral). Three channel electrode posts from Plastics One (MS333-2-A-SPC) were attached to 1mm stainless steel screws from Plastics One (8L003905201F) and screws were advanced into drilled holes until secure. Special care was taken not to advance the screws beyond the point of contact with the Dura. Dental cement was applied around the screws, on the base of the post, and exposed skull. Triple antibiotic was applied along the edges of the dental cement followed by an injection of subcutaneous Buprenorphine (0.1mg/kg). Mice were placed on a heating pad to aid recovery from anesthesia. A second Buprenorphine injection was administered between 6 and 10 hours after surgery. Mice were then individually housed, returned to the vivarium and monitored daily until the day of EEG recordings. The separation between the last post-surgical Buprenorphine injection and EEG recordings was between 3 and 5 days.

Electrophysiology

Baseline and auditory event-related potential (ERP) recordings were obtained using the BioPac system (BIOPAC Systems, Inc.) from awake and freely moving mice as published previously (Lovelace et al., 2018). Mice were allowed to habituate to the recording chamber for 15 min prior to being connected to the BioPac system. A three-channel tether was connected to the electrode post (implanted during surgery) under brief isoflurane anesthesia. The mouse was then placed inside a grounded Faraday cage after recovery from isoflurane. This tether was then connected to a commutator located

directly above the cage. Mice were then allowed to habituate while being connected to the tether for an additional 20 min before EEG recordings were obtained.

The BioPac MP150 acquisition system was connected to two EEG 100C amplifier units (one for each channel) to which the commutator was attached. The lead to the occipital cortex was used as reference for both frontal and auditory cortex screw electrodes. The acquisition hardware was set to high-pass (>0.5Hz) and low-pass (<100Hz) filters. Normal EEG output data were collected with gain maintained the same (10,000x) between all recordings. Data were sampled at a rate of either 2.5 or 5 kHz using Acqknowledge software and down sampled to 1024Hz post hoc using Analyzer 2.1 (Brain Vision Inc.). Sound delivery was synchronized with EEG recording using a TTL pulse to mark the onset of each sound in a train. Baseline EEGs were recorded for 5 min (no auditory stimuli were presented), followed by recordings in response to auditory stimulation. After these experiments were completed, mice were returned to the colony and euthanized on a later date.

Acoustic Stimulation

All experiments were conducted in a sound-attenuated chamber lined with anechoic foam (Gretch-Ken Industries, OR) as previously described with modifications (Lovelace et al., 2018; Lovelace et al., 2020). Acoustic stimuli were generated using RVPDX software and RZ6 hardware (Tucker-Davis Technologies, FL) and presented through a free-field speaker (MF1 Multi-Field Magnetic Speaker; Tucker-Davis Technologies, FL) located 12 inches directly above the cage. Sound pressure level (SPL) was modified using programmable attenuators in the RZ6 system. The speaker output

was ~65-70dB SPL at the floor of the recording chamber with fluctuation of +/- 3 dB for frequencies between 5 and 35 kHz as measured with a ¼ inch Bruel & Kjaer microphone.

We used acoustic stimulation paradigms that have been previously established in *Fmr1* KO mice (Lovelace et al., 2018), which is analogous to work in humans with FXS (Ethridge et al., 2017). A chirp-modulated signal (henceforth, 'chirp') to induce synchronized oscillations in EEG recordings was used. The chirp is a 2s broadband noise stimulus with amplitude modulated (100% modulation depth) by a sinusoid whose frequencies increase (Up-chirp) or decrease (Down-chirp) linearly in the 1-100 Hz range (Artieda et al., 2004; Pérez-Alcázar et al., 2008; Purcell, John, Schneider, & Picton, 2004). The chirp facilitates a rapid measurement of transient oscillatory response (delta to gamma frequency range) to auditory stimuli of varying frequencies and can be used to compare oscillatory responses in different groups in clinical and pre-clinical settings (Purcell et al., 2004). Inter-trial coherence analysis (Tallon-Baudry, Bertrand, Delpuech, & Pernier, 1996) can then be used to determine the ability of the neural generator to synchronize oscillations to the frequencies present in the stimulus.

To avoid onset responses contaminating phase locking to the amplitude modulation of the chirp, the stimulus was ramped in sound level from 0-100% over 1s (rise time), which then smoothly transitioned into chirp modulation of the noise. Up and Down chirp trains were presented 300 times each (for a total of 600 trains). Both directions of modulation were tested to ensure any frequency specific effects were not due to the frequency transition history within the stimulus. Up- and Down- chirp trains

were presented in an alternating sequence. The interval between each train was randomly varied between 1 and 1.5s.

To study evoked response amplitudes and habituation, trains of 100ms broadband noise were presented at two repetition rates, 0.25Hz (a non-habituating rate) and 4Hz (a strongly habituating rate) (Lovelace et al., 2016). Each train consisted of 10 noise bursts and the inter-train interval used was 8 seconds. Each repetition rate was presented 100 times in an alternating pattern (Lovelace et al., 2016). The onset of trains and individual noise bursts were tracked with separate TTL pulses that were used to quantify latency of response.

EEG Data Analysis

Data were extracted from Acqknowledge and files saved in a file format (EDF) compatible with BrainVision Analyzer 2.1 software as previously described with modifications (Lovelace et al., 2018; Lovelace et al., 2020). All data were notch filtered at 60Hz to remove residual line frequency power from recordings. EEG artifacts were removed using a semi-automatic procedure in Analyzer 2.1 for all recordings. Less than 20% of data were rejected due to artifacts from any single mouse. Baseline EEG data were divided into 2s segments and Fast Fourier Transforms (FFT) were calculated on each segment using 0.5Hz bins and then average power ($\mu V^2/Hz$) was calculated for each mouse from 1-100Hz. Power was then binned into standard frequency bands: Delta (1-4Hz), Theta (4-10Hz), Alpha (10-13Hz), Beta (13-30Hz), Low Gamma (30-55Hz), and High Gamma (65-100Hz). Responses to chirp trains were analyzed using Morlet wavelet analysis. Chirp trains were segmented into windows of 500ms before chirp onset to

500ms after the end of the chirp sound (total of 3s because each chirp was 2s in duration). EEG traces were processed with Morlet wavelets from 1-100Hz using complex number output (voltage density, μV/Hz) for ITPC calculations, and power density (μV^2/Hz) for non-phase locked single trial power (STP) calculations and baseline corrected non-phase locked single trial power (induced power). Wavelets were run with a Morlet parameter of 10 as this gave the best frequency/power discrimination. This parameter was chosen since studies in humans found most robust difference around 40Hz, where this parameter is centered (Ethridge et al., 2017). To measure phase synchronization at each frequency across trials Inter Trial Phase Coherence (ITPC) was calculated. The equation used to calculate ITPC is:

$$ITPC(f,t) = \frac{1}{n}\sum_{k=1}^{n}\frac{F_k(f,t)}{|F_k(f,t)|}$$

where *f* is the frequency, *t* is the time point, and *k* is trial number. Thus, $F_k(f,t)$ refers to the complex wavelet coefficient at a given frequency and time for the *k*th trial. There were no less than 275 trials (out of 300) for any given mouse after segments containing artifacts were rejected.

Statistical analysis and definition of movement states

Statistical group comparisons of chirp responses (ITPC and STP) and broadband noise trains (ITPC and induced power) were quantified by wavelet analysis. Analysis was conducted by binning time into 256 parts and frequency into 100 parts, resulting in a 100x256 matrix. Non-parametric cluster analysis was used to determine contiguous regions in the matrix that were significantly different from a distribution of 1000

randomized Monte Carlo permutations based on previously published methods (Maris & Oostenveld, 2007). Briefly, if the cluster sizes of the real genotype assignments (both positive and negative direction, resulting in a two-tailed alpha of $p = 0.025$) were larger than 97.25% of the random group assignments, those clusters were considered significantly different between genotypes. This method avoids statistical assumptions about the data and corrects for multiple comparisons.

Because movement can alter cortical gain (Fu, Kaneko, Tang, Alvarez-Buylla, & Stryker, 2015; Niell & Stryker, 2010), and *Fmr1* KO mice show hyperactivity, a piezoelectric transducer was placed underneath the recording cage to detect when the mouse was moving. The term 'baseline' is used to indicate EEGs recorded in these mice without any specific auditory stimuli. The term 'still' is used to describe baseline EEG when the mouse was stationary. The term 'moving' is used to describe baseline EEG when the mouse was moving based on a threshold criterion for the piezoelectric signal that was confirmed by analyzing the video recording (under IR light) that was taken throughout the EEG recording procedure. In all cases where genotype means are reported, SEM was used. The genotype differences in baseline power were analyzed on 6 dependent variables using one-way Multivariate analysis of co-variance (MANCOVA) with one covariate (movement), Independent Variables (IV): Genotype (Ctrl WT, cOFF, Ctrl KO, and cON mice), dependent variables (DV): 6 frequency bins (delta to high gamma). The proportion of time spent moving during the 5-minute recording session was used as a covariate to isolate effects of genotype and control for the effect movement has on cortical gain. When multiple comparisons for MANCOVA were made, genotype

comparisons were corrected using Bonferroni adjustments. The divisor for Bonferroni correction for multiple comparisons (for 6 frequency bands) on MANCOVA was set to 6, $\alpha = 0.05/6 = 0.0083$. Data are often expressed and plotted as ratio of control group values to gauge relative differences in various factors using the same scale.

cFos Analysis

Neuronal activation marker, cFos, was used to examine activation of PV-expressing cells and other neurons under quiet condition without any specific auditory stimuli (quiet) and after exposure to sound (sound). Age-matched adult (P60-70) male Ctrl WT and cOFF, or Ctrl KO and cON mice (n=4 per group) were habituated in a sound attenuated chamber (Gretch-Ken, OR) for 3h after which they were exposed to either 15 min of silence (quiet) or broadband noise at 65-70 dB SPL (sound). Following exposure, the mice were kept in the sound attenuated chamber for another 45 min after which they were euthanized with isoflurane and sodium pentobarbital and perfused transcardially. Brains were removed and post-fixed for 2h in 4% PFA. 100µm brain slices were obtained and immunostaining was performed as described above. Brain slices were treated overnight with mouse anti-parvalbumin antibody (1:500; Sigma, catalog #P3088, RRID: AB_477 329), and rabbit anti-cFos antibody (1:500; Cell Signaling Technology, catalog #2250, RRID: AB_2247211). After primary antibody, brain slices were incubated with secondary antibody, donkey anti-rabbit Alexa 594 (4µg/mL; Thermo Fisher Scientific, catalog# A-21207, RRID: AB_141637), and donkey anti-mouse Alexa 488 (4µg/mL; Molecular Probes, catalog# A-21202, RRID: AB_141607) for 1h. Slices mounted with Vectashield containing DAPI (Vector Labs, catalog# H-1200, RRID: AB_2336790) and

Cytoseal (ThermoScientific, catalog# 8310–16). Slices were imaged using confocal microscopy (Leica SP5) as described above. All images were acquired under identical conditions. Image analysis was performed using ImageJ macro plugin PIPSQUEAK (https://labs.wsu.edu/sorg/research-resources/). Slaker, Barnes, et al. (2016), Slaker, Blacktop, et al. (2016), and Slaker, Harkness, et al. (2016) introduced a standardized methodology for analyzing cell density and intensity called PIPSQUEAK. For image analysis, 10 images in the Z-stack (1.194 pixels/μm) were compiled into a single image using ImageJ macro plugin PIPSQUEAK, scaled, and converted into 32-bit, grayscale, TIFF files. PIPSQUEAK was run in "semi-automatic mode" to select ROIs to identify individual PV-positive and cFos-positive cells, as well as PV/cFos co-localization, which were then verified by a trained experimenter who was blinded to the experimental conditions. The plug-in compiles this analysis to identify single-(M. Slaker, Barnes, Sorg, & Grimm, 2016; M. Slaker, Blacktop, & Sorg, 2016; M. L. Slaker, Harkness, & Sorg, 2016), double-(Reinhard et al., 2019), and triple-labeled neurons (Harkness et al., 2019) (https://ai.RewireNeuro.com). Distributions of densities and intensities were compared between experimental groups, to assess differences in cell densities and intensities between Ctrl WT and cOFF, or Crtl KO and cON mice under both conditions (quiet and sound). Statistical analysis was performed with two-way ANOVA followed by Bonferroni multiple comparison post-test using GraphPad Prism 6 software (RRID: SCR_002798). Data represent mean ± standard error of the mean (SEM).

Dye-Quenched (DQ) Gelatin Assay and Analysis

The DQ-Gelatin plate assay was used to assess gelatinase activity as described previously (Lovelace et al., 2020; Pirbhoy et al., 2020). A FITC-quenched gelatin peptide that fluoresces following cleavage by gelatinases MMP-2 and MMP-9 was used to measure gelatinase proteolytic activity. Adult (P60-70) male Ctrl WT and cOFF mice, or Ctrl KO and cON littermates (n = 4-6 mice per group) were euthanized with isoflurane and the auditory cortex was dissected based on coordinates (Paxinos & Franklin, 2004) and previous electrophysiological and dye-placement studies (Martin del Campo, Measor, & Razak, 2012). Auditory cortical tissues were re-suspended in lysis buffer (50mM Tris-HCl, pH 7.4, 150mM NaCl, 5mM EDTA, 0.05% Triton X-100, and 1mM PMSF) containing protease inhibitor cocktail (Sigma, cat. # P8340) and phosphatase inhibitor cocktail (Sigma, cat. #P0044). Lysates were measured for total protein concentrations using the protocol for the BCA colorimetric protein assay (Pierce, cat#23235).

Lysates were diluted in reaction buffer and mixed with a fluorescence-labeled gelatin substrate (Molecular Probes, E12055). Samples were incubated in the dark for 3h at room temperature. The fluorescence intensity was analyzed using 495nm excitation wavelength and 515nm emission wavelength. The signal was measured every 20min during the 3h incubation period using a fluorescence microplate reader equipped with standard fluorescein filters (SoftMax Pro). For each time point, background fluorescence intensity was corrected by subtracting the values derived from reaction buffer control. A standard curve to assess gelatinase activity was generated using recombinant mouse

MMP-9 (rmMMP-9, approximately 1,500 pmol/min/µg, R&D Systems, cat. #909-MM-010). A linear regression of rmMMP-9 activity (standard curve) and relative gelatinase activity based on the average fluorescence intensity of five replicates was used to assess gelatinase proteolytic activity in the brain samples. Statistical analysis was performed comparing cOFF and cON samples to their corresponding Ctrl WT and Ctrl KO samples with unpaired t-test using GraphPad Prism 6 software (RRID: SCR_002798). Data represent mean ± standard error of the mean (SEM).

Western Blot Analysis

The auditory cortex was removed from each mouse (*n*=4 mice per group), cooled in PBS, and homogenized in ice-cold lysis buffer (50mM Tris-HCl, pH 7.4, 150mM NaCl, 5mM EDTA, 0.05% Triton X-100, and 1mM PMSF) containing protease inhibitor cocktail (Sigma, cat. #P8340) and phosphatase inhibitor cocktail (Sigma, cat. #P0044). The samples were processed as previously described with modifications (Lovelace et al., 2020). The samples were rotated at 4°C for at least 1h to allow for complete cell lysis and then cleared by centrifugation at 13,200 rpm for 15 min at 4°C. Supernatants were isolated and boiled in reducing sample buffer (Laemmli 2× concentrate, S3401, Sigma), and separated on 8–16% Tris-Glycine SDS-PAGE precast gels (EC6045BOX, Life Technologies). Proteins were transferred onto Protran BA 85 Nitrocellulose membrane (GE Healthcare) and blocked for 1h at room temperature in 5% skim milk (catalog #170-6404, Bio-Rad). Primary antibody incubations were performed overnight at 4°C with antibodies diluted in TBS/0.1% Tween-20/5% BSA. The following primary antibodies were used: rabbit anti-mammalian target of rapamycin (mTOR; 7C10; Cell Signaling

catalog #2983, RRID:AB_2105622); rabbit anti-phospho-mTOR (Ser2481; Cell Signaling catalog #2974, RRID:AB_2231885); rabbit anti-Akt (Cell Signaling catalog #9272; RRID:AB_10699016); rabbit anti-phospho-Akt (Ser473; Cell Signaling catalog #9271, RRID: AB_329825); mouse anti-PV (Millipore, catalog #MAB1572, RRID: AB_2174013); rabbit anti-βactin at 1:2000 (1:2000; Abcam, catalog #ab8227, RRID: AB_2305186); mouse anti-total TrkB (1:2000; BD Transduction Laboratories, catalog #610101, RRID:AB_397507); rabbit anti-phospho-TrkB (Tyr816) (1:2000; Millipore, catalog #ABN1381, RRID:AB_2721199); and rabbit anti-phospho-TrkB (Tyr515) (Bioworld, catalog #AP0236). For primary antibodies from Cell Signaling Technology a dilution of 1:1000 was used, unless stated otherwise.

Blots were washed 3 × 10 min with TBS/0.1% Tween-20 and incubated with the appropriate HRP-conjugated secondary antibodies for 1h at room temperature in a TBS/0.1% Tween-20/5% BSA solution. The secondary antibodies used were HRP-conjugated donkey anti-mouse IgG (Jackson ImmunoResearch, catalog #715-035-150, RRID: AB_2340770) or HRP-conjugated goat anti-rabbit IgG (Jackson ImmunoResearch, catalog #111-035-003, RRID: AB_2313567). After secondary antibody incubations, blots were washed 3 × 10min in TBS/0.1% Tween-20, incubated in ECL 2 Western Blotting Substrate (Thermo Scientific, catalog #80196) and a signal was collected with CL-XPosure film (Thermo Scientific, catalog #34090). For re-probing, membrane blots were washed in stripping buffer (2% SDS, 100mM β-mercaptoethanol, 50mM Tris-HCl, pH 6.8) for 30min at 55°C, then rinsed repeatedly with TBS/0.1% Tween-20, finally blocked with 5% skim milk, and then re-probed. Developed films were

then scanned, and band density was analyzed by measuring band and background intensity using Adobe Photoshop CS5.1 software (RRID:SCR_014199). Four samples per group (Ctrl WT vs. cOFF or Ctrl KO vs. cON) were run per blot, and precision/tolerance (P/T) ratios for cOFF and cON samples were normalized to P/T ratios of Ctrl WT and Ctrl KO samples, respectively. Statistical analysis was performed with unpaired t-test using GraphPad Prism 6 software. Data represent mean ± standard error of the mean (SEM).

Behavioral Assessments

Social Novelty Test

Sociability and social memory were studied in cOFF mice and their littermate controls (Ctrl WT), and cON mice and their littermate controls (Ctrl KO) (*n*=6-8 per group) using a three-chamber test as described previously with minor modifications (Nguyen et al., 2020). Briefly, a rectangular box contained three adjacent chambers 19 × 45 cm each, with 30-cm-high walls and a bottom constructed from clear Plexiglas. The three chambers were separated by dividing walls, which were made from clear Plexiglas with openings between the middle chamber and each side chamber. Removable doors over these openings permitted chamber isolation or free access to all chambers. All testing was done in a brightly lit room (650 lux), between 9:00 A.M. and 2:00 P.M. Before testing, mice were housed in a room with a 12 h light/dark cycle with *ad libitum* access to food and water. The cages were transferred to the behavioral room 30 min before the first trial began for habituation. The test mouse was placed in the central chamber with no access to the left and right chambers and allowed to habituate to the test

chamber for 5 min before testing began. Session 1 measured sociability; in Session 1, another mouse (Stranger 1) was placed in a wire cup-like container in one of the side chambers. The opposite side had an empty cup of the same design. The doors between the chambers were removed, and the test mouse was allowed to explore all three chambers freely for 10 min, while being digitally recorded from above. The following parameters were monitored: the duration of direct contact between the test mouse and either the stranger mouse or empty cup and the duration of time spent in each chamber. Session 2 measured social memory; in Session 2, a new mouse (Stranger 2) was placed in the empty wire cup in the second side chamber. Stranger 1, a now familiar mouse, remained in the first side chamber. The test mouse was allowed to freely explore all three chambers for another 10 min, while being recorded, and the same parameters were monitored. Placement of Stranger 1 in the left or right side of the chamber was randomly altered between trials. The floor of the chamber was cleaned with 2%-3% acetic acid, 70% ethanol, and water between tests to eliminate odor trails. Assessments of the digital recordings were done using TopScan Lite software (Clever Sys., Inc., VA). To measure changes in sociability and social memory, percent time spent in each chamber was calculated in each test. Further, a sociability index $\left(\frac{time\ in\ S1\ chamber}{time\ in\ S1\ chamber\ +\ time\ in\ empty\ chamber}\right)$ and social novelty preference index $\left(\frac{time\ in\ S2\ chamber}{time\ in\ S2\ chamber\ +\ time\ in\ S1\ chamber}\right)$ were calculated as described previously (Nguyen et al., 2020; Nygaard, Maloney, & Dougherty, 2019). For sociability index, values <0.5 indicate more time spent in the

empty chamber, >0.5 indicate more time spent in the chamber containing Stranger 1, and 0.5 indicates equal amount of time in both chambers. For social novelty preference index, values <0.5 indicate more time spent in the chamber containing Stranger 1 or now familiar mouse, >0.5 indicate more time spent in the chamber containing Stranger 2 or new stranger mouse, and 0.5 indicates equal amount of time in both chambers. Statistical analysis for time spent in each chamber was performed using two-way ANOVA followed by Bonferroni multiple comparison post-test, while statistical analysis for sociability index and social novelty preference index was performed with unpaired t-test using GraphPad Prism 6 software (RRID: SCR_002798). Data represent mean ± standard error of the mean (SEM).

Open-field test

Anxiety-like behaviors and locomotor activity were tested in P60 Ctrl WT and cOFF, or Ctrl KO and cON littermate mice (6-8 mice per group) as described previously (Lovelace et al., 2020). A 72 × 72-cm open-field arena with 50-cm-high walls was constructed from opaque acrylic sheets with a clear acrylic sheet for the bottom. The open field arena was placed in a brightly lit room, and one mouse at a time was placed in a corner of the open field and allowed to explore for 10 min while being recorded with digital video from above. The floor was cleaned with 2–3% acetic acid, 70% ethanol, and water between tests to eliminate odor trails. The mice were tested between the hours of 9:00 A.M. and 1:00 P.M., and this test was always performed prior to the elevated plus maze. The arena was subdivided into a 4 × 4 grid of squares with the middle of the grid defined as the center. A line 4 cm from each wall was added to measure thigmotaxis.

Locomotor activity was scored by the analysis of total line crosses and speed using TopScan Lite software (Clever Sys., Inc., VA). A tendency to travel to the center (total number of entries into large and small center squares) and the time in thigmotaxis were used as an indicator of anxiety. The analysis was performed in 5 min intervals for the total 10 min exploration duration. Assessments of the digital recordings were performed blind to the condition. Statistical analysis was performed with unpaired t-test using GraphPad Prism 6 software. Data represent mean ± standard error of the mean (SEM).

Elevated plus maze

The elevated plus maze consisted of four arms in a plus configuration. Two opposing arms had 15-cm tall walls (closed arms), and two arms were without walls (open arms). The entire maze sat on a stand 1 m above the floor. Each arm measured 30 cm long and 10 cm wide. Mice were allowed to explore the maze for 10 min while being recorded by digital video from above. The maze was wiped with 2–3% acetic acid, 70% ethanol and water between each test to eliminate odor trails. This test was always done following the open-field test. TopScan Lite software was used to measure the percent of time spent in open arms and speed. The time spent in open arm was used to evaluate anxiety-like behavior while speed and total arm entries were measured to evaluate overall locomotor activity (Lovelace et al., 2020). The analysis was performed in 5 min intervals for the total 10 min exploration duration. Assessments of the digital recordings were done blind to the condition using TopScan Lite software. Statistical analysis was performed with unpaired t-test using GraphPad Prism 6 software. Data represent mean ± standard error of the mean (SEM).

Results

In this study we examined (1) whether removal of *Fmr1* from excitatory neurons starting from the early postnatal development is sufficient to elicit cortical deficits in the adult cOFF mice; and (2) whether re-expression of *Fmr1* in excitatory neurons during the early postnatal development will normalize cortical development and improve responses in the adult cON mice. This study will delineate the developmental role of *Fmr1* in shaping cortical responses and reinforce the idea that FMRP expression in excitatory neurons during early postnatal development is not only required but is sufficient to restore normal cortical responses and PV cell development.

Deletion and re-expression of *Fmr1* in Ex during the P14-P21 developmental period.

To achieve the deletion of FMRP from Ex during early postnatal development, we crossed male $Cre^{CaMKII\alpha}$ with female $Fmr1^{Flox/Flox}$ mice and analyzed the expression of FMRP at P14 and P21 in $Cre^{CaMKII\alpha}$ */Fmr1*$^{Flox/y}$ (cOFF) and their littermate controls, $Fmr1^{Flox/y}$ (Ctrl WT) mice (**Figure 3.1**). Ctrl WT mice showed FMRP expression in NeuN+ cells in AuC at P14 (**Fig. 3.1A, E**) and P21 (**Fig. 3.1C, E**). FMRP expression was also detected in NeuN+ cells in AuC of cOFF mice at P14 (**Fig. 3.1B, E**). However, FMRP immunoreactivity was visibly reduced in AuC of cOFF mice by P21 (**Fig. 3.1D**). There was a significant decrease in the percentage of NeuN+ neurons with FMRP in the cOFF mice compared to Ctrl WT mice (**Fig. 3.1E; Table 3.1**). The remaining NeuN+ cells with FMRP are presumed to be GABAergic neurons (Tamamaki et al., 2003). These data confirm that FMRP was deleted from cortical Ex in AuC during the P14-P21 developmental window.

To achieve the re-expression of FMRP in cortical Ex during early postnatal development, we crossed male $Cre^{CaMKII\alpha}$ with female *Fmr1*$^{FloxNeo/FloxNeo}$ mice and analyzed the expression of FMRP at P14 and P21 in $Cre^{CaMKII\alpha}$ */Fmr1*$^{FloxNeo/y}$ (cON) and their littermate controls, *Fmr1*$^{FloxNeo/y}$ (Ctrl KO) mice (**Figure 3.1**). Ctrl KO mice showed no FMRP expression in NeuN+ cells at P14 (**Fig. 3.1F, J**) and P21 (**Fig. 3.1H, J**). FMRP expression was also not detected in NeuN+ cells of cON mice at P14 (**Fig. 3.1G, J**). However, FMRP immunoreactivity was observed in AuC of cON mice by P21 (**Fig. 3.1I**). There was a significant increase in the percentage of NeuN+ neurons with FMRP in the cON mice compared to Ctrl WT mice (**Fig. 3.1J; Table 3.1**). These data confirm that FMRP was re-expressed in cortical Ex during the P14-P21 developmental window in AuC and FMRP expression was also maintained in adult P60 cON mice (**Table 3.1**).

Deletion and re-expression of *Fmr1* in Ex during early postnatal development affect PV and PNN levels.

We examined PV and WFA+ PNN-containing cell density in AuC of adult Ctrl WT and cOFF, or Ctrl KO and cON mice (**Fig. 3.2A-D**). Similar to what we had previously seen in the adult *Fmr1* KO mice (Lovelace et al., 2020), there was a significant decrease in PV cell density in cOFF mice compared to their littermate Ctrl WT mice in L4, however no changes were observed in L2/3 (**Fig 3.2E, H; Table 3.2**). In addition, WFA+ PNN cell density and PV/PNN co-localization were significantly reduced in cOFF mice in both L4 and L2/3 (**Fig. 3.2F, I, G, J; Table 3.2**). Conversely, there was a significant increase in PV cell density, WFA+ PNN cell density and PV/PNN

co-localization in AuC of cON mice compared to their littermate Ctrl KO mice in both L4 and L2/3 (**Fig. 3.2E, H, F, I, G, J; Table 3.2**). These data indicate that postnatal deletion of FMRP from Ex is sufficient to trigger abnormal development of inhibitory PV interneurons, whereas the re-expression of FMRP in Ex during the same period is able to prevent the abnormal phenotypes. Thus, expression of FMRP in Ex before critical postnatal period might not be required for normal network development, in particular PV cells.

Baseline EEG gamma power is significantly altered following postnatal deletion and re-expression of *Fmr1* in Ex.

If impaired PNN and PV expression in AuC underlie abnormal neural oscillations observed in the global *Fmr1* KO mice, then we should see similar deficits in Ex-specific cOFF mice, and a reversal of those abnormal phenotypes in cON mice. To test this hypothesis, we measured electrocortical activity in cOFF and cON mice using EEG recordings. Baseline (no sound simulation) EEG power spectral density was calculated in AuC and frontal cortex (FC) of Ctrl WT (n=10) and cOFF (n=10) mice, or Ctrl KO (n=13) and cON (n=13) mice from EEGs recorded during five min period. Examples of 1s segments of baseline EEG for each genotype, as well as genotype averages (+/- SEM) of power spectra are depicted in **Figure 3.3**. Even in the raw traces (**Fig. 3.3A**), enhanced high frequency oscillations are apparent in AuC of cOFF mice compared to Ctrl WT, while high frequency oscillations appear to be reduced in AuC of cON mice compared to Ctrl KO. The group average power spectral densities are shown in **Fig. 3.3B**, wherein genotype differences (Ctrl WT vs. cOFF and Ctrl KO vs. cON) in AuC can

be seen at frequencies ~40Hz (**Fig. 3.3B**). No changes were observed in FC (data not shown).

Statistical analysis was performed using a one-way MANCOVA approach with percentage time spent moving as a covariate. We compared genotype mean differences on 6 bands per region: Delta (1-4Hz), Theta (4-10Hz), Alpha (10-13Hz), Beta (13-30Hz), Low gamma (30-55Hz), and High Gamma (65-100Hz). The gamma band (30-100 Hz) was divided because low (30-60 Hz) versus high frequency (>60 Hz) bands in gamma range may arise from different mechanisms (Balakrishnan & Pearce, 2014; Dvorak & Fenton, 2014; Ray & Maunsell, 2011). We confirmed assumptions of equality of covariance using Box's M, $p = 0.080$ (for Ctrl WT vs. cOFF) and $p = 0.153$ (for Ctrl KO vs. cON). For Ctrl WT vs. cOFF mice, Levene's test of equality of error variance showed only difference between genotypes in the delta band of the cOFF group ($p = 0.003$), therefore further analysis of delta was not carried out. We report an effect of genotype (Ctrl WT vs. cOFF: Pillai's Trace = 0.709, $p = 0.010$; Ctrl KO vs. cON: Pillai's Trace = 0.513, $p = 0.027$) across all 6 of the combined frequency variables, which include movement as a covariate. We then determined that the only individual frequency band difference between genotypes in AuC of cOFF and cON mice was in the low-gamma band (**Fig. 3.3C-F**). Low-gamma power was significantly different between genotypes after correction for multiple comparisons (Ctrl WT and cOFF: AC low-gamma, $F(1,17) = 9.042$, $p = 0.0079$, $\eta^2 = 0.35$; Ctrl KO vs. cON: AC low-gamma, $F(1,23) = 14.992$, $p = 0.001$, $\eta 2 = 0.395$).

These data suggest that enhanced baseline low-gamma oscillations observed in AuC of global *Fmr1* KO mice likely arise later in development and can be reversed with the re-expression of *Fmr1* in the mouse brain after the 2nd postnatal week. In addition, beneficial effects of re-expression of FMRP only in Ex suggest that these cells play a critical role in controlling low-gamma oscillations, most likely by influencing the development of PV interneurons.

Postnatal deletion and re-expression of *Fmr1* in Ex affect synchronization to dynamic acoustic stimuli.

We hypothesized that the increased baseline gamma in cOFF mouse AuC would lead to a deficit in mounting consistent phase locking in gamma frequencies across sound presentation trials, but it would be normalized in cON mice. Because the differences to modulation frequencies were not affected by the direction of frequency change in the sound when up or down chirps were tested, results are presented only for up chirp. After repeated chirp presentation (300 trials for up, 300 for down), the inter-trial phase coherence (ITPC) was calculated across trials in the time X frequency domain using Morlet Wavelet analysis, similar to our previously published results (Lovelace et al., 2018; Lovelace et al., 2020). After grand average ITPC was calculated for each group, means for Ctrl WT mice (*n*=10) were subtracted from the means for cOFF mice (*n*=10), and means for Ctrl KO mice (*n*=13) were subtracted from the means for cON mice (*n*=13) (**Fig. 3.4A, B; Fig. 3.5A, B**, only 'up' chirp data are shown). For statistical comparisons, non-parametric cluster analysis was used to determine contiguous regions in the time X frequency domain that were statistically different between genotypes (**Fig.**

3.5A, B). We observed significant decrease in low-gamma band ITPC in AuC of cOFF mice centered ~55Hz (**Fig. 3.5A**). Conversely, we observed a significant increase in low-gamma band ITPC in AuC of cON mice in ~ 40-55Hz range (**Fig. 3.5B**). Similar patterns and statistics of ITPC were observed for both up and down chirps (down chirp data not shown). No changes in ITPC were observed in FC (data not shown).

These data indicate that postnatal deletion of FMRP is sufficient to trigger the gamma synchronization deficits similar to what is observed in AuC of germline *Fmr1* KO mice. Importantly, the phenotype was reversed by postnatal re-expression of FMRP only in Ex, suggesting that changes in communications between excitatory and inhibitory neurons contribute to the impaired sound-evoked gamma synchronization in AuC of *Fmr1* KO mice.

Postnatal deletion and re-expression of *Fmr1* in Ex affect background gamma power in mouse AuC during chirp stimulation.

We investigated non-phase locked single trial power (STP) during the chirp stimulation period (**Fig. 3.4C, D; Fig. 3.5C, D**) because any increase in gamma power during the duration of acoustic stimulation is predicted to decrease the ability of the neural generators to produce temporally consistent responses to the dynamic chirp stimulus. In addition, an increased in STP is seen in the global *Fmr1* KO mouse (Lovelace et al., 2018) and in humans with FXS (Ethridge et al., 2017). Using the same statistical cluster analysis as for the chirp ITPC, the cOFF mice showed a significant increase in background gamma power in AuC and only in the low-gamma band (**Fig. 3.4C; Fig. 3.5C**). In contrast, the cON mice showed a significant decrease in background

gamma power in AuC in the low-gamma band (**Fig. 3.4D; Fig. 3.5D**). These data suggest that Ex control background gamma power in AuC, most likely through their interactions with fast-spiking inhibitory interneurons, as deletion or re-expression of FMRP only in Ex can induce or reduce background gamma power during sound presentation.

Induced power and ITPC to sound onset are differentially regulated in AuC of cOFF and cON mice.

We compared evoked responses to trains of brief (100 ms) broadband noise stimuli (10 noise stimuli per train, 65-70 dB SPL, 100 repetitions of each train). We tested both a habituating rate of sound presentation (4Hz repetition rate) and a non-habituating repetition rate (0.25Hz) (Lovelace et al., 2020; Lovelace et al., 2016). Example traces are shown for the first stimulus in the 0.25Hz train for Ctrl WT and cOFF (**Fig. 3.7A**) or Ctrl KO and cON (**Fig. 3.7G**) and the first 4 stimuli in the 4Hz train for Ctrl WT and cOFF (**Fig. 3.7D**) or Ctrl KO and cON (**Fig. 3.7J**). We measured both ITPC and induced power (baseline corrected) for each repetition rate. In cOFF mice, the ITPC for 0.25Hz rate showed a significant increase in phase locking in the beta to low-gamma range (~20-40Hz) during sound onset (**Fig. 3.6A; Fig. 3.7B**). This suggests that cOFF mice show elevated synchrony compared to Ctrl WT mice at those specific frequencies. When analyzing phase locking to sound for cON mice compared to Ctrl KO mice, we observed no changes in beta (20-30Hz) range but a significant increase in gamma (30-80Hz) range consistent with improved phase locking in the gamma band observed with the chirp stimuli (**Fig 3.6E; Fig. 3.7H**). In addition, while cOFF mice displayed a significant increase in induced power during the sound onset (0-100ms) from the beta to

low-gamma range (~20-40Hz) (**Fig 3.6B; Fig. 3.7C**), cON mice showed a decrease in induced power during sound onset with significant changes in gamma 30-100Hz range (**Fig. 3.6F; Fig. 3.7I**). These results show increased power during sound onset in cOFF mice and a decrease in cON mice, with no significant difference in long latency or "on-going" activity after the initial sound onset (S. Rotschafer & Razak, 2013).

Analysis of the first 4 responses to a 4Hz train of sounds reveals the same ITPC increase to the first sound in the train in the beta/low-gamma (~25-35Hz) range (**Fig. 3.6C; Fig. 3.7E**) in cOFF mice compared to Ctrl WT, with an additional increase in ITPC to the second sound in the train centered ~80Hz (**Fig. 3.6C; Fig. 3.7E**). We observed an increase in phase locking to the first sound in cON mice compared to Ctrl KO within gamma 30-80Hz range with no significant changes in the beta range (**Fig. 3.6G; Fig. 3.7K**). The increase in power also centered ~30Hz during first sound onset (0-100ms) in cOFF mice (**Fig. 3.6D; Fig. 3.7F**), but the power around 30Hz was significantly downregulated during first and second sound onset in cON mice (**Fig. 3.6H; Fig. 3.7L**). Interestingly, global KO mice (Ctrl KO) showed high on-going non-phase power after sound onset, which was not observed in cOFF mice (**Fig. 3.6B-D** and **3.6F-H**). There was a trend for suppression of the on-going power following FMRP re-expression in cON mice (**Fig. 3.6F-H; Fig. 3.7I, L**). The suppression of on-going oscillation power is visually apparent in the example traces shown in **Figure 3.7J**, where the cON mouse shows lower amplitude oscillations throughout the sound train, compared to Ctrl KO mice.

These results indicate elevated synchrony of sound evoked responses in the beta frequency range when FMRP is deleted from Ex during early postnatal development, but elevated gamma band synchrony in the evoked response when FMRP expression was restored during the same period. In addition, induced power was higher during sound onset in cOFF mice, while re-expression of FMRP suppressed the power of both onset and on-going responses following sound presentation.

Deletion and re-expression of *Fmr1* in Ex during postnatal development affect activation of PV cells.

Impaired PNN development can lead to reduced excitability of cortical PV cells resulting in increased excitation of the network. It is possible that altered gamma oscillations in FXS may arise from dysfunction of PV interneurons and awakening of PV cells is responsible for enhanced sound evoked gamma synchronization in cON mice. To test this hypothesis, we examined overall levels of cFos immunoreactivity and cFos expression in PV cells in AuC of Ctrl WT and cOFF mice, as well as Ctrl KO and cON mice under quiet condition (quiet) (**Fig. 3.8A-D**). cFos levels were also measured in the same four groups 45 min following the exposure to broadband noise at 65-70dB (sound) (**Fig. 3.8A-D**).

In cOFF mice under quiet condition, the density of cFos-positive cells and cFos levels (intensity of cFos immunoreactivity) were significantly higher in L1-4 AuC of cOFF mice compared to Ctrl WT (**Fig. 3.8E, F; Table 3.3**). However, after exposure to sound, overall density of cFos-positive cells and cFos levels were similar between genotypes. This is most likely a result of significant increase in cFos cell density and

intensity in sound-exposed Ctrl WT but not cOFF mice compared to respective quiet condition groups. When cFos levels were analyzed in PV cells, under quiet condition the percentage of cFos-positive PV cell and cFos levels in PV cells were significantly lower in L1-4 AuC of cOFF mice compared to Ctrl WT (**Fig. 3.8G, H; Table 3.3**). After exposure to sound, percentage of cFos-positive PV cell and cFos levels in PV cells remain lower in cOFF mice compared to Ctrl WT (**Fig. 3.8G, H; Table 3.3**). There was a significant increase in the percentage of cFos-positive PV cell and cFos levels in PV cells in both sound-exposed Ctrl WT and cOFF mice when compared to respective quiet condition groups.

In cON mice under quiet condition, the density of cFos-positive cells and cFos levels were lower in cON mice compared to their littermate Ctrl KO mice (**Fig. 3.8E, F; Table 3.3**). However, after exposure to sound there was no significant difference in cFos cell density and intensity between cON mice and their littermate Ctrl KO mice. Statistical analysis showed a significant increase in cFos cell density and cFos intensity in sound-exposed cON, but not Ctrl KO mice, when compared to respective quiet condition groups. When cFos levels were analyzed in PV cells, in quiet condition there was a significant increase in percentage of PV-positive cFos cells and cFos intensity in PV cells in cON mice compared to their littermate Ctrl KO mice (**Fig. 3.8G, H; Table 3.3**). After exposure to sound, percentage of PV-positive cFos cells and cFos intensity in PV cells (**Fig. 3.8G, H; Table 3.3**) remained higher in cON mice compared to their littermate Ctrl KO mice. There was also a significant increase in percentage of PV-positive cFos cells

and cFos intensity in PV cells in both sound-exposed Ctrl KO and cON mice when compared to corresponding quiet condition groups.

These data indicate that reduced PV cell activation may underlie the alterations in auditory processing in cOFF mice, and that postnatal re-expression of FMRP only in Ex might be sufficient to promote PV cell activation and restore EEG responses in cON mice.

Postnatal deletion and re-expression of *Fmr1* in Ex affect gelatinase activity, Akt/mTOR signaling, PV levels and TrkB phosphorylation.

As enhanced MMP-9 activity may contribute to the loss of PNNs by cleaving extracellular matrix (ECM), we performed a gelatinase activity assay. A significant increase in gelatinase activity was observed in AuC of cOFF mice as compared to their Ctrl WT counterparts (**Fig. 3.9A**). Conversely, a significant decrease in gelatinase activity was observed in cON mice as compared to Ctrl KO mice (**Fig. 3.9A**). As enhanced Akt/mTOR signaling may also underlie changes in hyperexcitability associated with FXS and other autistic spectrum disorders (Enriquez-Barreto & Morales, 2016; Klann & Dever, 2004; Sato, 2016; Sharma et al., 2010), we investigated Akt/mTOR activation in adult AuC of cOFF and cON mice. mTOR and Akt phosphorylation levels were higher in cOFF mice and lower in cON mice compared to their controls (**Fig. 3.9C, D; Table 3.4**). Consistent with the changes in PV cell density, PV levels were significantly decreased in cOFF and increased in cON mice compared to their respective controls (**Fig. 3.9E; Table 3.4**). As TrkB signaling is implicated in PV cell development and survival, we evaluated total TrkB (tTrkB) levels but found no changes in AuC of

cOFF or cON mice compared to Ctrl WT or Ctrl KO, respectively (**Fig. 3.9F; Table 3.4**). However, lower levels of phosphorylated (i.e., active) forms of TrkB (Y515 and Y816) were detected in AuC of cOFF mice compared to Ctrl WT (**Fig. 3.9G, H; Table 3.4**). In contrast, higher levels of both phosphorylated forms of TrkB were detected in AuC of cON mice compared to Ctrl KO (**Fig. 3.9G, H; Table 3.4**).

Together, our results indicate that postnatal deletion of FMRP from Ex is sufficient to enhance gelatinase activity and mTOR/Akt phosphorylation but reduces PV levels and TrkB phosphorylation, while postnatal re-expression of FMRP in only Ex reverses the deficits in adult AuC of *Fmr1* KO mice.

Postnatal deletion and re-expression of *Fmr1* in Ex affect anxiety-like behaviors, locomotor activity and socialization.

Cortical hyperexcitability as a result of aberrant PV cell development is also observed in several ASD mouse models (Lee, Lee, & Kim, 2017) and may underlie ASD-like behaviors, such as impaired social behaviors, as well as enhanced anxiety and hyperactivity. It is possible that the changes we see in AuC may not be exclusive to this area of the brain. Therefore, adult male Ctrl WT and cOFF mice (n=6 per group), or Ctrl KO and cON mice (n=8 per group) were tested for hyperactivity and anxiety-like behaviors in an elevated plus maze or open field test (**Figure 3.10; Table 3.5**). cOFF mice exhibited increased anxiety-like behaviors by spending significantly less total time in open arms and time per entry in an elevated plus maze (**Fig. 3.10A; Table 3.5**); and a significantly higher percentage of time in thigmotaxis and less time in the center per entry in open field than Ctrl WT mice (**Fig. 3.10C; Table 3.5**). cOFF mice also demonstrated

increased locomotor activity by making significantly more total arm entries and line crosses, and showed higher speed than Ctrl WT mice (**Fig. 3.10B, D; Table 3.5**). In contrast, cON mice exhibited decreased anxiety-like behaviors by spending significantly more total time in open arms and time per entry, lower percentage of time in thigmotaxis and more time in the center per entry than Ctrl KO mice (**Fig. 3.10A, C; Table 3.5**). cON mice also demonstrated decreased locomotor activity by making significantly less total arm entries, less line crosses and decreased speed than Ctrl KO mice (**Fig. 3.10B, D; Table 3.5**).

Social novelty and social preference were assessed using a three-chamber test on adult male cOFF or cON mice and their respective controls. cOFF mice had a significantly lower sociability index and spent less time in the chamber with a stranger mouse (**Fig 3.10E; Table 3.6**). The social novelty preference index was also significantly lower in cOFF mice that spent less time with a novel mouse (**Fig 3.10F; Table 3.6**). Conversely, both sociability and social novelty preference were higher in cON mice (**Fig 3.10E, F; Table 3.6**). Our findings establish that postnatal deletion of FMRP from Ex is sufficient to increase anxiety-like behaviors and locomotor activity and decrease socialization, while FMRP re-expression only in Ex is sufficient to reduce anxiety-like behaviors and locomotor activity, and increase socialization.

Discussion

Cortical hyperexcitability may underlie sensory hypersensitivity that is frequently observed in individuals with FXS and other ASDs and is recapitulated in mouse models

of the disorders. The main findings of this study provide novel insights into (1) how postnatal developmental changes contribute to cortical deficits observed in *Fmr1* KO mice; (2) the role of Ex in regulating inhibitory PV interneurons during this postnatal development in *Fmr1* KO mice; and (3) whether re-expression of FMRP in only Ex during the same period is sufficient to ameliorate deficits. We show that *Fmr1* deletion in Ex during the P14-21 critical developmental window recapitulates most of the deficits observed in germline *Fmr1* KO mice, including enhanced mTOR and Akt activity, but reduced PV expression and activity of PV cells, impaired responses to sound, and behavior deficits. The increased gelatinase activity may be further contributing to these deficits by cleaving PNNs and affecting communications between Ex and PV cells during critical period of development of cortical circuits. Importantly, our data show that restoration of *Fmr1* expression in cortical Ex during the same developmental period, prevents the development of these abnormal cellular, electrophysiological and behavioral phenotypes (**Figure 3.12**).

The major results of the present study point to the sufficiency of expressing *Fmr1* during P14-P21, and only in Ex, to reverse structural, functional and behavioral deficits in the *Fmr1* KO mice. As gene reactivation to treat FXS is receiving increasing attention (Hampson, Hooper, & Niibori, 2019; Shitik, Velmiskina, Dolskiy, & Yudkin, 2020; Tabolacci, Palumbo, Nobile, & Neri, 2016; Vershkov et al., 2019), our results suggest that postnatal expression of FMRP may provide benefits in terms of improving anxiety-like behaviors and sensory hypersensitivity. The cortical hyperexcitability commonly seen in global *Fmr1* KO mice and individuals with FXS may arise from dysfunction

across multiple brain regions expressing FMRP and spanning the brainstem to forebrain. The present results with Ex-specific removal or re-expression of FMRP using CaMKIIα promoter mostly target cortical pyramidal neurons indicating that cell-targeted reactivation may produce benefits in terms of physiological responses and behaviors (Gatto & Broadie, 2008; Siegel et al., 2017). As activation of CaMKIIα promoter using reporter mice is primarily observed in L2/3 of AuC with a little expression in L4 (Wang, Zhang, Szabo, & Sun, 2013) (**Figure 3.11**), L2/3 Ex may influence development and maturation of PV and PNN expression in L4. However, our study doesn't rule out the involvements of the midbrain as Ex in the rostral or caudal portion of the external Inferior Colliculus are also shown to express GFP under CaMKIIα promoter (Wang et al., 2013), suggesting a possible role of subcortical structures in deficits observed in AuC of cOFF mice.

Altered auditory processing in individuals with FXS and *Fmr1* KO animals suggests that development and plasticity in the auditory system may be affected in FXS (Chen & Toth, 2001; Miller et al., 1999; Nielsen et al., 2002). Multiple studies support the notion that impaired development during the critical postnatal period may be responsible for abnormal sensory responses in FXS, which could then lead to impaired development of higher cognitive functions, such as language learning (Kim, Gibboni, Kirkhart, & Bao, 2013; LeBlanc & Fagiolini, 2011). The development of acoustic representations in primary AuC is profoundly influenced by early experience (de Villers-Sidani, Chang, Bao, & Merzenich, 2007; Insanally, Kover, Kim, & Bao, 2009; Popescu & Polley, 2010; Zhang, Bao, & Merzenich, 2001). Exposure of young animals to sensory

input refines the balance of excitation and inhibition (Dorrn, Yuan, Barker, Schreiner, & Froemke, 2010; Kulinich et al., 2020; Sun et al., 2010), resulting in receptive field and sensory map reorganization and a long-lasting impact on sound perception (Han, Köver, Insanally, Semerdjian, & Bao, 2007). Cortical inhibition and excitation become correlated in mouse AuC by the third postnatal week, with the frequency tuning of the inhibitory component of the receptive fields becoming narrower during P14-P21 period in a sensory experience dependent manner (Dorrn et al., 2010). Experience dependent developmental plasticity is impaired in AuC of global *Fmr1* KO mice (Kim et al., 2013), and may correlate with the development of hyperexcitability seen during P14-P21 period in these mice (Wen, Afroz, et al., 2018). Our results show that manipulation of FMRP, only in Ex, during this developmental window (P14-P21), can either disrupt or restore AuC function and indicate that embryonic or early postnatal (P0-P14) re-expression may not be required to normalize sensory hypersensitivity in FXS. Future studies will examine whether the re-expression of FMRP in adulthood will provide the same benefits.

Converging evidence suggests that the loss or dysfunction of PV inhibitory interneurons may contribute to these deficits (Gibson et al., 2008; Goel et al., 2018; Nomura et al., 2017; Selby, Zhang, & Sun, 2007; Wen, Afroz, et al., 2018). However, the mechanism is still not clear. It is imperative to identify the sources of PV cell dysfunction and which developmental stage to target, such as neurogenesis, migration or maturation. Our findings provide novel insight into cellular mechanism underlying the normalization of cortical function following re-expression of FMRP and emphasize the role of the handshake between Ex and inhibitory PV neurons during the developmental refinements

of cortical networks. Abnormal density and function of PV GABAergic interneurons may be a common mechanism for abnormal sensory sensitivity and cortical hyperexcitability (Contractor, Klyachko, & Portera-Cailliau, 2015; Goel et al., 2018; Selby et al., 2007; Wen, Binder, Ethell, & Razak, 2018). Many symptoms of FXS can be linked to a reduced GABAergic inhibition, which has been suggested to lead to an increased ratio of excitation to inhibition (E/I) (Hussman, 2001), another probable cause for impaired cortical maturation (Rubenstein & Merzenich, 2003). Parvalbumin interneurons receive both intracortical and thalamic excitatory inputs, which develop during the cortical critical period (Chittajallu & Isaac, 2010; Daw, Ashby, & Isaac, 2007). There is a significant delay in the formation of Ex contacts onto fast-spiking interneurons, which likely has a large impact on the integration of feedforward inhibitory circuits in the developing somatosensory cortex of *Fmr1* KO mice (Nomura et al., 2017). Previous studies also suggest that FMRP expression in Ex is required for normal cortical activity (Hays et al., 2011) and show that embryonic FMRP loss in cortical Ex is sufficient to affect the development of PV inhibitory interneurons (Lovelace et al., 2020). The reduction in PV expression in cOFF mice may occur due to reduced Ex drive onto these neurons (Gibson et al., 2008). Our current study indicate that these deficits are seen following removal of FMRP just from Ex during P14-P21 period when connections are established between Ex and inhibitory neurons. Moreover, we observed a reduced cFos immunoreactivity in PV cells of cOFF mice, suggesting that a common mechanism across sensory cortices in *Fmr1* KO mice is reduced excitation/activation of PV cells. Strikingly, the increase in PV expression and cFos immunoreactivity in PV cells in cON

mice AuC further reinforces the idea that expression of FMRP in Ex during postnatal period might be required for normal network development, in particular PV cells.

Enhanced MMP-9 activity observed in cOFF mice may also disrupt the communications between Ex and PV cells through the degradation of aggrecan-containing WFA+ PNNs. In the cerebral cortex, PNN loss around PV cells reduces excitability of these cells (Balmer, 2016; Lensjø, Lepperød, Dick, Hafting, & Fyhn, 2017; Wen, Afroz, et al., 2018). PNNs protect PV cells from oxidative stress, and the loss of PNNs may lead to PV cell death (Cabungcal et al., 2013). Therefore, degradation of PNN is predicted to decrease excitability of PV cells leading to hyperexcitability of cortical networks and abnormal neural oscillations. Conversely, the increase of PNNs and reduction in gelatinase activity observed in cON mice following FMRP re-expression coincided with increased density of PV cells, enhanced PV cell activity and improved responses to sound assessed with EEG.

Our findings show EEG phenotypes in cOFF mice that are similar to germline *Fmr1* KO mice and significant improvements in EEG measures in cON mice. EEG studies in individuals with FXS report altered network synchrony including excessive baseline state gamma power and reduced alpha power. Of interest is the gamma band power as it is thought to associate with changes in the activity of fast-spiking inhibitory interneurons. Reduction of PV expression causes GABAergic dysfunction, particularly at gamma frequencies (Lucas et al., 2010) and cortical gamma oscillations are linked to the function of PV interneurons (Cardin et al., 2009; Carlén et al., 2012; Gonzalez-Burgos & Lewis, 2008; Keeley, Fenton, & Rinzel, 2017; Sohal, Zhang, Yizhar, & Deisseroth, 2009;

Volman, Behrens, & Sejnowski, 2011). Ray and Maunsell (2011) suggested that the low-gamma band reflects true oscillations that arise through PV neuron firing and synchronization of pyramidal cell activity. Similar to germline *Fmr1* KO mice (Lensjø et al., 2017; Sidhu, Dansie, Hickmott, Ethell, & Ethell, 2014), cOFF mice show reduced gamma synchronization to the chirp stimulus, while the re-expression of FMRP in Ex during postnatal period enhanced chirp-elicited phase-locking to 40-55Hz oscillations and consistently elicited fast gamma range (30-80Hz) sound-evoked oscillations. Our previous study showed that embryonic deletion of *Fmr1* from forebrain Ex did not elicit changes in phase locking to the chirp stimuli (Lovelace et al., 2020). This could indicate that *Fmr1* expression in subcortical Ex might be needed for normal phase locking response to auditory stimuli. Furthermore, our previous study in forebrain Ex specific *Fmr1* KO mice also showed that there was a reduction in ITPC in the ~ 20–30 Hz range immediately after sound presentation (Lovelace et al., 2020), which was not present in the cOFF mice when *Fmr1* was deleted from Ex during postnatal development. Because the auditory system consists of a number of feed-forward and feedback loops, potential for nonlinear interactions in terms of cortical deficits influencing sub-cortical processing cannot be discounted. Re-expression of FMRP suppressed the power of both onset and on-going sound evoked responses indicating the future potential of spatiotemporally targeted reactivation strategies. Gamma band activity is involved in a broad array of sensory and cognitive processes, several of which are affected in FXS. The deficits in gamma phase–locking to sound may cause sensory discrimination deficits (Cardin et al., 2009; Sohal et al., 2009) that may lead to delayed language and cognitive development in

FXS. Together, our data suggest that alterations in the development of PV cells, specifically impaired communications between Ex and PV cells, contribute to changes in physiological responses observed in AuC of *Fmr1* KO mice.

FMRP negatively regulates mTOR/Akt signaling (Sharma et al., 2010), and we also see upregulation in mTOR/Akt phosphorylation in cOFF mice and a down-regulation in cON mice. Although it is not clear whether the increase is attributed to changes in Ex or PV cells, increased mTOR/Akt signaling was suggested to negatively affect PV cell functions (Vogt, Cho, Lee, Sohal, & Rubenstein, 2015). Consistent with the role of BDNF-TrkB signaling in the development and function of GABAergic neurons (Berghuis et al., 2006; Nakahara, Zhang, & Merzenich, 2004), we observed significant changes in TrkB phosphorylation which positively correlated with PV expression, suggesting a role of TrkB signaling in regulating PV cells in AuC. TrkB signaling supports PV cells and influences gamma-band synchronization in hippocampus (Lucas, Jegarl, & Clem, 2014; Zheng et al., 2011). In the cortex, TrkB deletion from PV interneurons resulted in dysregulation of patterned high-frequency cortical activity and disinhibition of local Ex (Xenos et al., 2018). In *Fmr1* KO mice, BDNF-TrkB signaling was also implicated in FXS-associated alterations (Castren & Castren, 2014) and delayed development of fast spiking interneurons in somatosensory cortex (Nomura et al., 2017). Interestingly, hyperactivity and deficits in startle responses were ameliorated in BDNF(+/−)/*Fmr1* KO mice, suggesting a possible role of BDNF/TrkB signaling in these behaviors (Uutela et al., 2012).

Increased anxiety and locomotor activity and reduced socialization are among the most consistent behavioral symptoms in individuals with FXS (Tranfaglia, 2011). Our studies show that cOFF mice exhibit increased anxiety-like behaviors and locomotor activity, and reduced socialization. Conversely, cON mice display reduced anxiety-like behaviors and locomotor activity, and increased socialization. Since we didn't see any changes in anxiety-like behaviors when *Fmr1* was embryonically deleted only from forebrain Ex (Lovelace et al., 2020), this could indicate that the anxiety-like behaviors observed in the cOFF mice is not driven by the absence of *Fmr1* in forebrain. As several brain areas are involved in these behaviors, including brainstem and basal ganglia, impairments in PV cell development following FMRP deletion from Ex in subcortical areas may contribute to these abnormal behaviors observed in cOFF mice. Most importantly, re-expression of FMRP in Ex during postnatal development is sufficient to ameliorate behavior deficits in cON mice, suggesting potential time window for re-activation studies to improve social behaviors.

In conclusion, these findings show that (1) Ex contribute to many phenotypes in the *Fmr1* KO mice and suggest cell-type, time period, and circuit specific contributions to various FXS-associated phenotypes; and (2) postnatal *Fmr1* re-expression in Ex is sufficient for the development of normal cortical responses and anxiety-like/social behaviors. Our understanding of how Ex contribute to the cortical deficits observed in FXS and the time period during which these deficits manifest may allow for the development of therapeutic approaches that can potentially be targeted to impact specific cell types, circuits and symptoms.

References

Anderson, L. A., Christianson, G. B., & Linden, J. F. (2009). Mouse auditory cortex differs from visual and somatosensory cortices in the laminar distribution of cytochrome oxidase and acetylcholinesterase. *Brain Res, 1252*, 130-142. doi:10.1016/j.brainres.2008.11.037

Artieda, J., Valencia, M., Alegre, M., Olaziregi, O., Urrestarazu, E., & Iriarte, J. (2004). Potentials evoked by chirp-modulated tones: a new technique to evaluate oscillatory activity in the auditory pathway. *Clin Neurophysiol, 115*(3), 699-709. doi:10.1016/j.clinph.2003.10.021

Balakrishnan, S., & Pearce, R. A. (2014). Spatiotemporal characteristics and pharmacological modulation of multiple gamma oscillations in the CA1 region of the hippocampus. *Front Neural Circuits, 8*, 150. doi:10.3389/fncir.2014.00150

Balmer, T. S. (2016). Perineuronal Nets Enhance the Excitability of Fast-Spiking Neurons. *eNeuro, 3*(4). doi:10.1523/ENEURO.0112-16.2016

Berghuis, P., Agerman, K., Dobszay, M. B., Minichiello, L., Harkany, T., & Ernfors, P. (2006). Brain-derived neurotrophic factor selectively regulates dendritogenesis of parvalbumin-containing interneurons in the main olfactory bulb through the PLCgamma pathway. *J Neurobiol, 66*(13), 1437-1451. doi:10.1002/neu.20319

Braat, S., & Kooy, R. F. (2015). The GABAA Receptor as a Therapeutic Target for Neurodevelopmental Disorders. *Neuron, 86*(5), 1119-1130. doi:10.1016/j.neuron.2015.03.042

Burgin, K. E., Waxham, M. N., Rickling, S., Westgate, S. A., Mobley, W. C., & Kelly, P. T. (1990). In situ hybridization histochemistry of Ca2+/calmodulin-dependent protein kinase in developing rat brain. *J Neurosci, 10*(6), 1788-1798. Retrieved from https://www.ncbi.nlm.nih.gov/pubmed/2162385

Cabungcal, J. H., Steullet, P., Morishita, H., Kraftsik, R., Cuenod, M., Hensch, T. K., & Do, K. Q. (2013). Perineuronal nets protect fast-spiking interneurons against oxidative stress. *Proc Natl Acad Sci U S A, 110*(22), 9130-9135. doi:10.1073/pnas.1300454110

Cardin, J. A., Carlén, M., Meletis, K., Knoblich, U., Zhang, F., Deisseroth, K., . . . Moore, C. I. (2009). Driving fast-spiking cells induces gamma rhythm and controls sensory responses. *Nature, 459*(7247), 663-667. doi:10.1038/nature08002

Carlén, M., Meletis, K., Siegle, J. H., Cardin, J. A., Futai, K., Vierling-Claassen, D., . . . Tsai, L. H. (2012). A critical role for NMDA receptors in parvalbumin interneurons for gamma rhythm induction and behavior. *Mol Psychiatry, 17*(5), 537-548. doi:10.1038/mp.2011.31

Castrén, M., Pääkkönen, A., Tarkka, I. M., Ryynänen, M., & Partanen, J. (2003). Augmentation of auditory N1 in children with fragile X syndrome. *Brain Topogr, 15*(3), 165-171. Retrieved from https://www.ncbi.nlm.nih.gov/pubmed/12705812

Castren, M. L., & Castren, E. (2014). BDNF in fragile X syndrome. *Neuropharmacology, 76 Pt C*, 729-736. doi:10.1016/j.neuropharm.2013.05.018

Chen, L., & Toth, M. (2001). Fragile X mice develop sensory hyperreactivity to auditory stimuli. *Neuroscience, 103*(4), 1043-1050. Retrieved from https://www.ncbi.nlm.nih.gov/pubmed/11301211

Chittajallu, R., & Isaac, J. T. (2010). Emergence of cortical inhibition by coordinated sensory-driven plasticity at distinct synaptic loci. *Nat Neurosci, 13*(10), 1240-1248. doi:10.1038/nn.2639

Contractor, A., Klyachko, V. A., & Portera-Cailliau, C. (2015). Altered Neuronal and Circuit Excitability in Fragile X Syndrome. *Neuron, 87*(4), 699-715. doi:10.1016/j.neuron.2015.06.017

Crawford, D. C., Acuna, J. M., & Sherman, S. L. (2001). FMR1 and the fragile X syndrome: human genome epidemiology review. *Genet Med, 3*(5), 359-371. doi:10.1097/00125817-200109000-00006

Daw, M. I., Ashby, M. C., & Isaac, J. T. (2007). Coordinated developmental recruitment of latent fast spiking interneurons in layer IV barrel cortex. *Nat Neurosci, 10*(4), 453-461. doi:10.1038/nn1866

de Villers-Sidani, E., Chang, E. F., Bao, S., & Merzenich, M. M. (2007). Critical period window for spectral tuning defined in the primary auditory cortex (A1) in the rat. *J Neurosci, 27*(1), 180-189. doi:10.1523/JNEUROSCI.3227-06.2007

Dorrn, A. L., Yuan, K., Barker, A. J., Schreiner, C. E., & Froemke, R. C. (2010). Developmental sensory experience balances cortical excitation and inhibition. *Nature, 465*(7300), 932-936. doi:10.1038/nature09119

Dvorak, D., & Fenton, A. A. (2014). Toward a proper estimation of phase-amplitude coupling in neural oscillations. *J Neurosci Methods, 225*, 42-56. doi:10.1016/j.jneumeth.2014.01.002

Enriquez-Barreto, L., & Morales, M. (2016). The PI3K signaling pathway as a pharmacological target in Autism related disorders and Schizophrenia. *Mol Cell Ther, 4*, 2. doi:10.1186/s40591-016-0047-9

Ethridge, L. E., White, S. P., Mosconi, M. W., Wang, J., Byerly, M. J., & Sweeney, J. A. (2016). Reduced habituation of auditory evoked potentials indicate cortical hyper-excitability in Fragile X Syndrome. *Transl Psychiatry, 6*, e787. doi:10.1038/tp.2016.48

Ethridge, L. E., White, S. P., Mosconi, M. W., Wang, J., Pedapati, E. V., Erickson, C. A., . . . Sweeney, J. A. (2017). Neural synchronization deficits linked to cortical hyper-excitability and auditory hypersensitivity in fragile X syndrome. *Mol Autism, 8*, 22. doi:10.1186/s13229-017-0140-1

Ferguson, B. R., & Gao, W. J. (2018). PV Interneurons: Critical Regulators of E/I Balance for Prefrontal Cortex-Dependent Behavior and Psychiatric Disorders. *Front Neural Circuits, 12*, 37. doi:10.3389/fncir.2018.00037

Filice, F., Janickova, L., Henzi, T., Bilella, A., & Schwaller, B. (2020). The Parvalbumin Hypothesis of Autism Spectrum Disorder. *Front Cell Neurosci, 14*, 577525. doi:10.3389/fncel.2020.577525

Frankland, P. W., Wang, Y., Rosner, B., Shimizu, T., Balleine, B. W., Dykens, E. M., . . . Silva, A. J. (2004). Sensorimotor gating abnormalities in young males with fragile X syndrome and Fmr1-knockout mice. *Mol Psychiatry, 9*(4), 417-425. doi:10.1038/sj.mp.4001432

Fu, Y., Kaneko, M., Tang, Y., Alvarez-Buylla, A., & Stryker, M. P. (2015). A cortical disinhibitory circuit for enhancing adult plasticity. *Elife, 4*, e05558. doi:10.7554/eLife.05558

Gatto, C. L., & Broadie, K. (2008). Temporal requirements of the fragile X mental retardation protein in the regulation of synaptic structure. *Development, 135*(15), 2637-2648. doi:10.1242/dev.022244

Gibson, J. R., Bartley, A. F., Hays, S. A., & Huber, K. M. (2008). Imbalance of neocortical excitation and inhibition and altered UP states reflect network hyperexcitability in the mouse model of fragile X syndrome. *J Neurophysiol, 100*(5), 2615-2626. doi:10.1152/jn.90752.2008

Goel, A., Cantu, D. A., Guilfoyle, J., Chaudhari, G. R., Newadkar, A., Todisco, B., . . . Portera-Cailliau, C. (2018). Impaired perceptual learning in a mouse model of Fragile X syndrome is mediated by parvalbumin neuron dysfunction and is reversible. *Nat Neurosci, 21*(10), 1404-1411. doi:10.1038/s41593-018-0231-0

Gonzalez-Burgos, G., & Lewis, D. A. (2008). GABA neurons and the mechanisms of network oscillations: implications for understanding cortical dysfunction in schizophrenia. *Schizophr Bull, 34*(5), 944-961. doi:10.1093/schbul/sbn070

Hampson, D. R., Hooper, A. W. M., & Niibori, Y. (2019). The Application of Adeno-Associated Viral Vector Gene Therapy to the Treatment of Fragile X Syndrome. *Brain Sci, 9*(2). doi:10.3390/brainsci9020032

Han, Y. K., Köver, H., Insanally, M. N., Semerdjian, J. H., & Bao, S. (2007). Early experience impairs perceptual discrimination. *Nature neuroscience, 10*(9), 1191.

Harkness, J. H., Bushana, P. N., Todd, R. P., Clegern, W. C., Sorg, B. A., & Wisor, J. P. (2019). Sleep disruption elevates oxidative stress in parvalbumin-positive cells of the rat cerebral cortex. *Sleep, 42*(1). doi:10.1093/sleep/zsy201

Hashemi, E., Ariza, J., Rogers, H., Noctor, S. C., & Martinez-Cerdeno, V. (2017). The Number of Parvalbumin-Expressing Interneurons Is Decreased in the Prefrontal Cortex in Autism. *Cereb Cortex, 27*(3), 1931-1943. doi:10.1093/cercor/bhw021

Hays, S. A., Huber, K. M., & Gibson, J. R. (2011). Altered neocortical rhythmic activity states in Fmr1 KO mice are due to enhanced mGluR5 signaling and involve changes in excitatory circuitry. *J Neurosci, 31*(40), 14223-14234. doi:10.1523/JNEUROSCI.3157-11.2011

Hussman, J. P. (2001). Suppressed GABAergic inhibition as a common factor in suspected etiologies of autism. *J Autism Dev Disord, 31*(2), 247-248. doi:10.1023/a:1010715619091

Insanally, M. N., Kover, H., Kim, H., & Bao, S. (2009). Feature-dependent sensitive periods in the development of complex sound representation. *J Neurosci, 29*(17), 5456-5462. doi:10.1523/JNEUROSCI.5311-08.2009

Keeley, S., Fenton, A. A., & Rinzel, J. (2017). Modeling fast and slow gamma oscillations with interneurons of different subtype. *J Neurophysiol, 117*(3), 950-965. doi:10.1152/jn.00490.2016

Kim, H., Gibboni, R., Kirkhart, C., & Bao, S. (2013). Impaired critical period plasticity in primary auditory cortex of fragile X model mice. *J Neurosci, 33*(40), 15686-15692. doi:10.1523/JNEUROSCI.3246-12.2013

Klann, E., & Dever, T. E. (2004). Biochemical mechanisms for translational regulation in synaptic plasticity. *Nat Rev Neurosci, 5*(12), 931-942. doi:10.1038/nrn1557

Kulinich, A. O., Reinhard, S. M., Rais, M., Lovelace, J. W., Scott, V., Binder, D. K., . . . Ethell, I. M. (2020). Beneficial effects of sound exposure on auditory cortex development in a mouse model of Fragile X Syndrome. *Neurobiol Dis, 134*, 104622. doi:10.1016/j.nbd.2019.104622

LeBlanc, J. J., & Fagiolini, M. (2011). Autism: a "critical period" disorder? *Neural Plast, 2011*, 921680. doi:10.1155/2011/921680

Lee, E., Lee, J., & Kim, E. (2017). Excitation/Inhibition Imbalance in Animal Models of Autism Spectrum Disorders. *Biol Psychiatry, 81*(10), 838-847. doi:10.1016/j.biopsych.2016.05.011

Lensjø, K. K., Lepperød, M. E., Dick, G., Hafting, T., & Fyhn, M. (2017). Removal of Perineuronal Nets Unlocks Juvenile Plasticity Through Network Mechanisms of Decreased Inhibition and Increased Gamma Activity. *J Neurosci, 37*(5), 1269-1283. doi:10.1523/JNEUROSCI.2504-16.2016

Lovelace, J. W., Ethell, I. M., Binder, D. K., & Razak, K. A. (2018). Translation-relevant EEG phenotypes in a mouse model of Fragile X Syndrome. *Neurobiol Dis*. doi:10.1016/j.nbd.2018.03.012

Lovelace, J. W., Rais, M., Palacios, A. R., Shuai, X. S., Bishay, S., Popa, O., . . . Razak, K. A. (2020). Deletion of Fmr1 from Forebrain Excitatory Neurons Triggers Abnormal Cellular, EEG, and Behavioral Phenotypes in the Auditory Cortex of a Mouse Model of Fragile X Syndrome. *Cereb Cortex, 30*(3), 969-988. doi:10.1093/cercor/bhz141

Lovelace, J. W., Wen, T. H., Reinhard, S., Hsu, M. S., Sidhu, H., Ethell, I. M., . . . Razak, K. A. (2016). Matrix metalloproteinase-9 deletion rescues auditory evoked potential habituation deficit in a mouse model of Fragile X Syndrome. *Neurobiol Dis, 89*, 126-135. doi:10.1016/j.nbd.2016.02.002

Lucas, E. K., Jegarl, A., & Clem, R. L. (2014). Mice lacking TrkB in parvalbumin-positive cells exhibit sexually dimorphic behavioral phenotypes. *Behav Brain Res, 274*, 219-225. doi:10.1016/j.bbr.2014.08.011

Lucas, E. K., Markwardt, S. J., Gupta, S., Meador-Woodruff, J. H., Lin, J. D., Overstreet-Wadiche, L., & Cowell, R. M. (2010). Parvalbumin deficiency and GABAergic dysfunction in mice lacking PGC-1alpha. *J Neurosci, 30*(21), 7227-7235. doi:10.1523/JNEUROSCI.0698-10.2010

Lunden, J. W., Durens, M., Phillips, A. W., & Nestor, M. W. (2019). Cortical interneuron function in autism spectrum condition. *Pediatr Res, 85*(2), 146-154. doi:10.1038/s41390-018-0214-6

Marin, O. (2012). Interneuron dysfunction in psychiatric disorders. *Nat Rev Neurosci, 13*(2), 107-120. doi:10.1038/nrn3155

Maris, E., & Oostenveld, R. (2007). Nonparametric statistical testing of EEG- and MEG-data. *J Neurosci Methods, 164*(1), 177-190. doi:10.1016/j.jneumeth.2007.03.024

Martin del Campo, H. N., Measor, K. R., & Razak, K. A. (2012). Parvalbumin immunoreactivity in the auditory cortex of a mouse model of presbycusis. *Hear Res, 294*(1-2), 31-39. doi:10.1016/j.heares.2012.08.017

Mientjes, E. J., Nieuwenhuizen, I., Kirkpatrick, L., Zu, T., Hoogeveen-Westerveld, M., Severijnen, L., . . . Oostra, B. A. (2006). The generation of a conditional Fmr1 knock out mouse model to study Fmrp function in vivo. *Neurobiol Dis, 21*(3), 549-555. doi:10.1016/j.nbd.2005.08.019

Miller, L. J., McIntosh, D. N., McGrath, J., Shyu, V., Lampe, M., Taylor, A. K., . . . Hagerman, R. J. (1999). Electrodermal responses to sensory stimuli in individuals with fragile X syndrome: a preliminary report. *Am J Med Genet, 83*(4), 268-279. Retrieved from https://www.ncbi.nlm.nih.gov/pubmed/10208160

Nakahara, H., Zhang, L. I., & Merzenich, M. M. (2004). Specialization of primary auditory cortex processing by sound exposure in the "critical period". *Proc Natl Acad Sci U S A, 101*(18), 7170-7174. doi:10.1073/pnas.0401196101

Nguyen, A. Q., Sutley, S., Koeppen, J., Mina, K., Woodruff, S., Hanna, S., . . . Ethell, I. M. (2020). Astrocytic Ephrin-B1 Controls Excitatory-Inhibitory Balance in Developing Hippocampus. *J Neurosci, 40*(36), 6854-6871. doi:10.1523/JNEUROSCI.0413-20.2020

Niell, C. M., & Stryker, M. P. (2010). Modulation of visual responses by behavioral state in mouse visual cortex. *Neuron, 65*(4), 472-479. doi:10.1016/j.neuron.2010.01.033

Nielsen, D. M., Derber, W. J., McClellan, D. A., & Crnic, L. S. (2002). Alterations in the auditory startle response in Fmr1 targeted mutant mouse models of fragile X syndrome. *Brain Res, 927*(1), 8-17. Retrieved from https://www.ncbi.nlm.nih.gov/pubmed/11814427

Nomura, T., Musial, T. F., Marshall, J. J., Zhu, Y., Remmers, C. L., Xu, J., . . . Contractor, A. (2017). Delayed Maturation of Fast-Spiking Interneurons Is Rectified by Activation of the TrkB Receptor in the Mouse Model of Fragile X Syndrome. *J Neurosci, 37*(47), 11298-11310. doi:10.1523/JNEUROSCI.2893-16.2017

Nygaard, K. R., Maloney, S. E., & Dougherty, J. D. (2019). Erroneous inference based on a lack of preference within one group: Autism, mice, and the social approach task. *Autism Res, 12*(8), 1171-1183. doi:10.1002/aur.2154

Okray, Z., de Esch, C. E., Van Esch, H., Devriendt, K., Claeys, A., Yan, J., . . . Hassan, B. A. (2015). A novel fragile X syndrome mutation reveals a conserved role for the carboxy-terminus in FMRP localization and function. *EMBO Mol Med, 7*(4), 423-437. doi:10.15252/emmm.201404576

Paxinos, G., & Franklin, K. B. (2004). *The mouse brain in stereotaxic coordinates*: Gulf professional publishing.

Penagarikano, O., Mulle, J. G., & Warren, S. T. (2007). The pathophysiology of fragile x syndrome. *Annu Rev Genomics Hum Genet, 8*, 109-129. doi:10.1146/annurev.genom.8.080706.092249

Pérez-Alcázar, M., Nicolás, M. J., Valencia, M., Alegre, M., Iriarte, J., & Artieda, J. (2008). Chirp-evoked potentials in the awake and anesthetized rat. A procedure to assess changes in cortical oscillatory activity. *Exp Neurol, 210*(1), 144-153. doi:10.1016/j.expneurol.2007.10.017

Pirbhoy, P. S., Rais, M., Lovelace, J. W., Woodard, W., Razak, K. A., Binder, D. K., & Ethell, I. M. (2020). Acute pharmacological inhibition of matrix metalloproteinase-9 activity during development restores perineuronal net formation and normalizes auditory processing in Fmr1 KO mice. *J Neurochem, 155*(5), 538-558. doi:10.1111/jnc.15037

Pizzorusso, T., Medini, P., Berardi, N., Chierzi, S., Fawcett, J. W., & Maffei, L. (2002). Reactivation of ocular dominance plasticity in the adult visual cortex. *Science, 298*(5596), 1248-1251. doi:10.1126/science.1072699

Popescu, M. V., & Polley, D. B. (2010). Monaural deprivation disrupts development of binaural selectivity in auditory midbrain and cortex. *Neuron, 65*(5), 718-731. doi:10.1016/j.neuron.2010.02.019

Purcell, D. W., John, S. M., Schneider, B. A., & Picton, T. W. (2004). Human temporal auditory acuity as assessed by envelope following responses. *J Acoust Soc Am, 116*(6), 3581-3593. Retrieved from https://www.ncbi.nlm.nih.gov/pubmed/15658709

Rais, M., Binder, D. K., Razak, K. A., & Ethell, I. M. (2018). Sensory Processing Phenotypes in Fragile X Syndrome. *ASN Neuro, 10*, 1759091418801092. doi:10.1177/1759091418801092

Ray, S., & Maunsell, J. H. (2011). Different origins of gamma rhythm and high-gamma activity in macaque visual cortex. *PLoS Biol, 9*(4), e1000610. doi:10.1371/journal.pbio.1000610

Reinhard, S. M., Rais, M., Afroz, S., Hanania, Y., Pendi, K., Espinoza, K., . . . Razak, K. A. (2019). Reduced perineuronal net expression in Fmr1 KO mice auditory cortex and amygdala is linked to impaired fear-associated memory. *Neurobiol Learn Mem, 164*, 107042. doi:10.1016/j.nlm.2019.107042

Rojas, D. C., Benkers, T. L., Rogers, S. J., Teale, P. D., Reite, M. L., & Hagerman, R. J. (2001). Auditory evoked magnetic fields in adults with fragile X syndrome. *Neuroreport, 12*(11), 2573-2576. Retrieved from https://www.ncbi.nlm.nih.gov/pubmed/11496151

Rossignol, E. (2011). Genetics and function of neocortical GABAergic interneurons in neurodevelopmental disorders. *Neural Plast, 2011*, 649325. doi:10.1155/2011/649325

Rotschafer, S., & Razak, K. (2013). Altered auditory processing in a mouse model of fragile X syndrome. *Brain Res, 1506*, 12-24. doi:10.1016/j.brainres.2013.02.038

Rotschafer, S. E., & Razak, K. A. (2014). Auditory processing in fragile x syndrome. *Front Cell Neurosci, 8*, 19. doi:10.3389/fncel.2014.00019

Rubenstein, J. L., & Merzenich, M. M. (2003). Model of autism: increased ratio of excitation/inhibition in key neural systems. *Genes Brain Behav, 2*(5), 255-267. Retrieved from https://www.ncbi.nlm.nih.gov/pubmed/14606691

Sato, A. (2016). mTOR, a Potential Target to Treat Autism Spectrum Disorder. *CNS Neurol Disord Drug Targets, 15*(5), 533-543. Retrieved from https://www.ncbi.nlm.nih.gov/pubmed/27071790

Schneider, A., Leigh, M. J., Adams, P., Nanakul, R., Chechi, T., Olichney, J., . . . Hessl, D. (2013). Electrocortical changes associated with minocycline treatment in fragile X syndrome. *J Psychopharmacol, 27*(10), 956-963. doi:10.1177/0269881113494105

Selby, L., Zhang, C., & Sun, Q. Q. (2007). Major defects in neocortical GABAergic inhibitory circuits in mice lacking the fragile X mental retardation protein. *Neurosci Lett, 412*(3), 227-232. doi:10.1016/j.neulet.2006.11.062

Sharma, A., Hoeffer, C. A., Takayasu, Y., Miyawaki, T., McBride, S. M., Klann, E., & Zukin, R. S. (2010). Dysregulation of mTOR signaling in fragile X syndrome. *J Neurosci, 30*(2), 694-702. doi:10.1523/JNEUROSCI.3696-09.2010

Shitik, E. M., Velmiskina, A. A., Dolskiy, A. A., & Yudkin, D. V. (2020). Reactivation of FMR1 gene expression is a promising strategy for fragile X syndrome therapy. *Gene Ther, 27*(6), 247-253. doi:10.1038/s41434-020-0141-0

Sidhu, H., Dansie, L. E., Hickmott, P. W., Ethell, D. W., & Ethell, I. M. (2014). Genetic removal of matrix metalloproteinase 9 rescues the symptoms of fragile X syndrome in a mouse model. *J Neurosci, 34*(30), 9867-9879. doi:10.1523/JNEUROSCI.1162-14.2014

Siegel, J. J., Chitwood, R. A., Ding, J. M., Payne, C., Taylor, W., Gray, R., . . . Johnston, D. (2017). Prefrontal Cortex Dysfunction in Fragile X Mice Depends on the Continued Absence of Fragile X Mental Retardation Protein in the Adult Brain. *J Neurosci, 37*(31), 7305-7317. doi:10.1523/JNEUROSCI.0571-17.2017

Sinclair, D., Oranje, B., Razak, K. A., Siegel, S. J., & Schmid, S. (2017). Sensory processing in autism spectrum disorders and Fragile X syndrome-From the clinic to animal models. *Neurosci Biobehav Rev, 76*(Pt B), 235-253. doi:10.1016/j.neubiorev.2016.05.029

Slaker, M., Barnes, J., Sorg, B. A., & Grimm, J. W. (2016). Impact of Environmental Enrichment on Perineuronal Nets in the Prefrontal Cortex following Early and Late Abstinence from Sucrose Self-Administration in Rats. *PLoS One, 11*(12), e0168256. doi:10.1371/journal.pone.0168256

Slaker, M., Blacktop, J. M., & Sorg, B. A. (2016). Caught in the Net: Perineuronal Nets and Addiction. *Neural Plast, 2016*, 7538208. doi:10.1155/2016/7538208

Slaker, M. L., Harkness, J. H., & Sorg, B. A. (2016). A standardized and automated method of perineuronal net analysis using. *IBRO Rep, 1*, 54-60. doi:10.1016/j.ibror.2016.10.001

Sohal, V. S., Zhang, F., Yizhar, O., & Deisseroth, K. (2009). Parvalbumin neurons and gamma rhythms enhance cortical circuit performance. *Nature, 459*(7247), 698-702. doi:10.1038/nature07991

Sun, Y. J., Wu, G. K., Liu, B. H., Li, P., Zhou, M., Xiao, Z., . . . Zhang, L. I. (2010). Fine-tuning of pre-balanced excitation and inhibition during auditory cortical development. *Nature, 465*(7300), 927-931. doi:10.1038/nature09079

Sutcliffe, J. S., Nelson, D. L., Zhang, F., Pieretti, M., Caskey, C. T., Saxe, D., & Warren, S. T. (1992). DNA methylation represses FMR-1 transcription in fragile X syndrome. *Hum Mol Genet, 1*(6), 397-400. Retrieved from https://www.ncbi.nlm.nih.gov/pubmed/1301913

Tabolacci, E., Palumbo, F., Nobile, V., & Neri, G. (2016). Transcriptional Reactivation of the FMR1 Gene. A Possible Approach to the Treatment of the Fragile X Syndrome. *Genes (Basel), 7*(8). doi:10.3390/genes7080049

Tallon-Baudry, C., Bertrand, O., Delpuech, C., & Pernier, J. (1996). Stimulus specificity of phase-locked and non-phase-locked 40 Hz visual responses in human. *J Neurosci, 16*(13), 4240-4249. Retrieved from https://www.ncbi.nlm.nih.gov/pubmed/8753885

Tamamaki, N., Yanagawa, Y., Tomioka, R., Miyazaki, J., Obata, K., & Kaneko, T. (2003). Green fluorescent protein expression and colocalization with calretinin,

parvalbumin, and somatostatin in the GAD67-GFP knock-in mouse. *J Comp Neurol, 467*(1), 60-79. doi:10.1002/cne.10905

Tranfaglia, M. R. (2011). The psychiatric presentation of fragile x: evolution of the diagnosis and treatment of the psychiatric comorbidities of fragile X syndrome. *Dev Neurosci, 33*(5), 337-348. doi:10.1159/000329421

Uutela, M., Lindholm, J., Louhivuori, V., Wei, H., Louhivuori, L. M., Pertovaara, A., . . . Castrén, M. L. (2012). Reduction of BDNF expression in Fmr1 knockout mice worsens cognitive deficits but improves hyperactivity and sensorimotor deficits. *Genes Brain Behav, 11*(5), 513-523. doi:10.1111/j.1601-183X.2012.00784.x

Verkerk, A. J., Pieretti, M., Sutcliffe, J. S., Fu, Y. H., Kuhl, D. P., Pizzuti, A., . . . Zhang, F. P. (1991). Identification of a gene (FMR-1) containing a CGG repeat coincident with a breakpoint cluster region exhibiting length variation in fragile X syndrome. *Cell, 65*(5), 905-914. Retrieved from https://www.ncbi.nlm.nih.gov/pubmed/1710175

Vershkov, D., Fainstein, N., Suissa, S., Golan-Lev, T., Ben-Hur, T., & Benvenisty, N. (2019). FMR1 Reactivating Treatments in Fragile X iPSC-Derived Neural Progenitors In Vitro and In Vivo. *Cell Rep, 26*(10), 2531-2539 e2534. doi:10.1016/j.celrep.2019.02.026

Vogt, D., Cho, K. K. A., Lee, A. T., Sohal, V. S., & Rubenstein, J. L. R. (2015). The parvalbumin/somatostatin ratio is increased in Pten mutant mice and by human PTEN ASD alleles. *Cell Rep, 11*(6), 944-956. doi:10.1016/j.celrep.2015.04.019

Volman, V., Behrens, M. M., & Sejnowski, T. J. (2011). Downregulation of parvalbumin at cortical GABA synapses reduces network gamma oscillatory activity. *J Neurosci, 31*(49), 18137-18148. doi:10.1523/JNEUROSCI.3041-11.2011

Wang, X., Zhang, C., Szabo, G., & Sun, Q. Q. (2013). Distribution of CaMKIIalpha expression in the brain in vivo, studied by CaMKIIalpha-GFP mice. *Brain Res, 1518*, 9-25. doi:10.1016/j.brainres.2013.04.042

Wen, T. H., Afroz, S., Reinhard, S. M., Palacios, A. R., Tapia, K., Binder, D. K., . . . Ethell, I. M. (2018). Genetic Reduction of Matrix Metalloproteinase-9 Promotes Formation of Perineuronal Nets Around Parvalbumin-Expressing Interneurons and Normalizes Auditory Cortex Responses in Developing Fmr1 Knock-Out Mice. *Cereb Cortex, 28*(11), 3951-3964. doi:10.1093/cercor/bhx258

Wen, T. H., Binder, D. K., Ethell, I. M., & Razak, K. A. (2018). The Perineuronal 'Safety' Net? Perineuronal Net Abnormalities in Neurological Disorders. *Front Mol Neurosci, 11*, 270. doi:10.3389/fnmol.2018.00270

Xenos, D., Kamceva, M., Tomasi, S., Cardin, J. A., Schwartz, M. L., & Vaccarino, F. M. (2018). Loss of TrkB Signaling in Parvalbumin-Expressing Basket Cells Results in Network Activity Disruption and Abnormal Behavior. *Cereb Cortex, 28*(10), 3399-3413. doi:10.1093/cercor/bhx173

Zhang, L. I., Bao, S., & Merzenich, M. M. (2001). Persistent and specific influences of early acoustic environments on primary auditory cortex. *Nat Neurosci, 4*(11), 1123-1130. doi:10.1038/nn745

Zheng, K., An, J. J., Yang, F., Xu, W., Xu, Z. Q., Wu, J., . . . Lu, B. (2011). TrkB signaling in parvalbumin-positive interneurons is critical for gamma-band network synchronization in hippocampus. *Proc Natl Acad Sci U S A, 108*(41), 17201-17206. doi:10.1073/pnas.1114241108

Figure 3.1

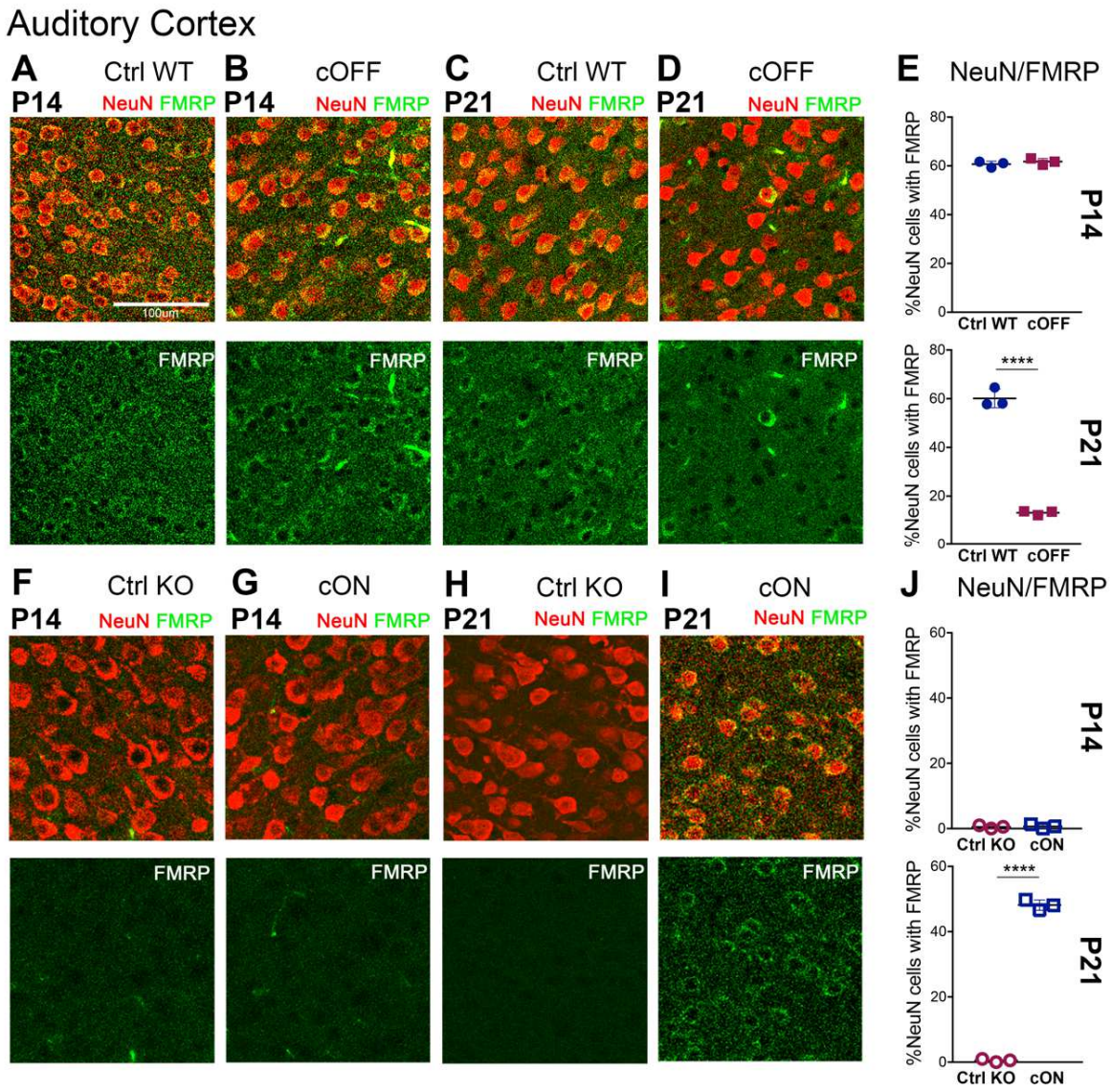
Auditory Cortex
A
P14
Ctrl WT
NeuN FMRP
100um
B
P14
cOFF
NeuN FMRP
C
P21
Ctrl WT
NeuN FMRP
D
P21
cOFF
NeuN FMRP
FMRP
E
NeuN/FMRP
%NeuN cells with FMRP
P14
Ctrl WT cOFF
****
P21
F
P14
Ctrl KO
NeuN FMRP
G
P14
cON
NeuN FMRP
H
P21
Ctrl KO
NeuN FMRP
I
P21
cON
NeuN FMRP
J
NeuN/FMRP
Ctrl KO cON

Figure 3.1. Deletion and re-expression of *Fmr1* in Ex occurs between the P14-P21 developmental period.
(A-D) Confocal images showing NeuN (red) and FMRP (green) immunoreactivity in AuC of Ctrl WT and cOFF mice at P14 and P21. (E) Quantitative analysis of the percentage of FMRP-positive NeuN cells. Graphs show mean ± SEM (*n*= 3 mice/group, ****$p<0.0001$, t-test). No significant differences were observed in the percentage of NeuN+ neurons with FMRP in Ctrl WT and cOFF mice at P14. However, there is a significant decrease in the percentage of NeuN+ neurons with FMRP in cOFF mice compared to Ctrl WT mice at P21. (F-I) Confocal images showing NeuN (red) and FMRP (green) immunoreactivity in AuC of Ctrl KO and cON mice at P14 and P21. (J) Quantitative analysis of the percentage of FMRP-positive NeuN cells. Graphs show mean ± SEM (*n*= 3 mice/group, ****$p<0.0001$, t-test). No significant differences were observed in the percentage of NeuN+ neurons with FMRP in Ctrl KO and cON mice at P14. However, there is a significant increase in the percentage of NeuN+ neurons with FMRP in cON mice compared to Ctrl KO mice at P21.

Figure 3.2

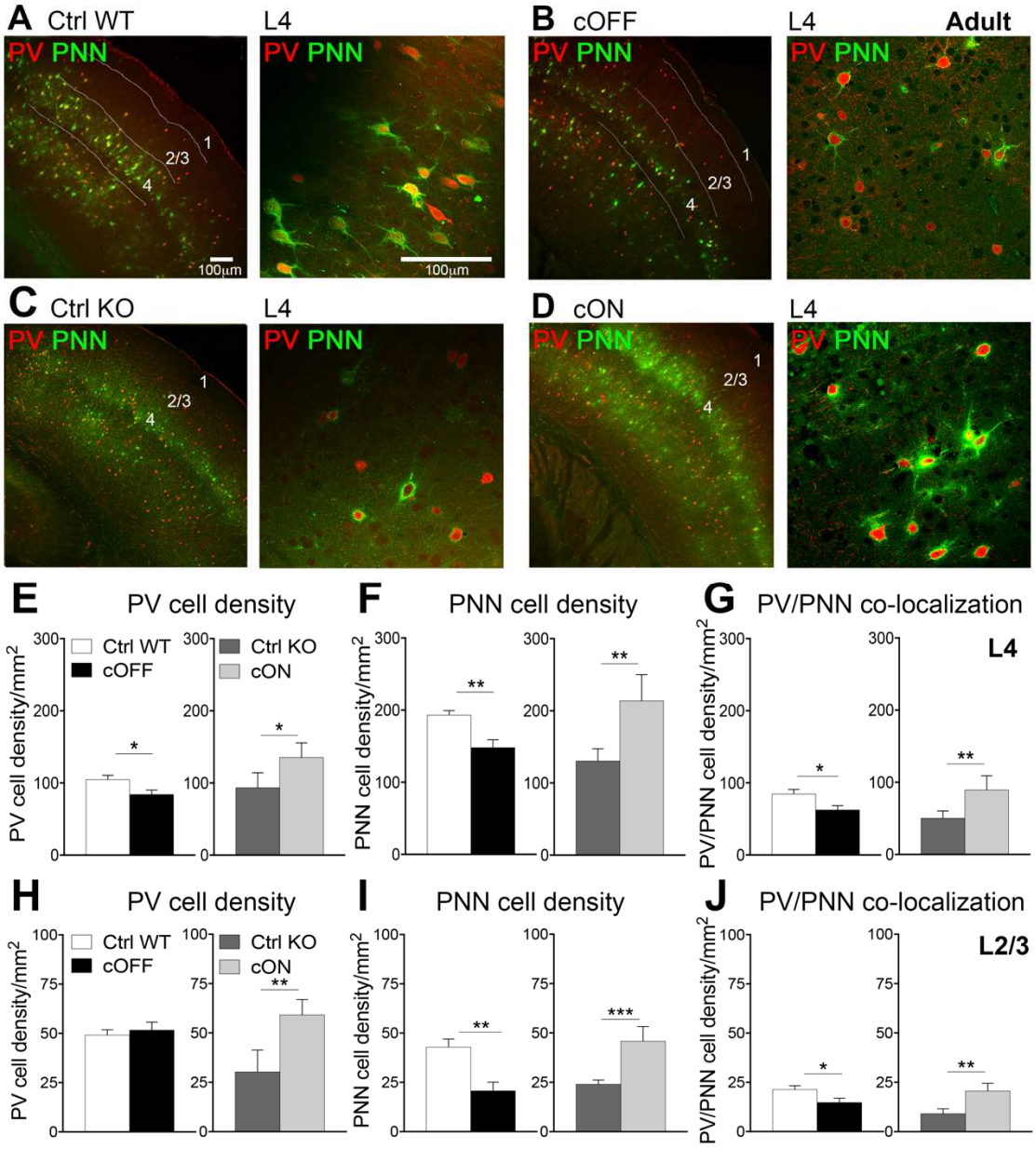
A Ctrl WT
L4
PV PNN
1
2/3
4
100μm
B cOFF
L4
Adult
C Ctrl KO
D cON
E PV cell density
F PNN cell density
G PV/PNN co-localization
L4
PV cell density/mm2
PNN cell density/mm2
PV/PNN cell density/mm2
Ctrl WT
cOFF
Ctrl KO
cON
H PV cell density
I PNN cell density
J PV/PNN co-localization
L2/3

Figure 3.2. Postnatal deletion or re-expression of *Fmr1* from Ex affected development of PV cells, WFA+ PNNs, and PV/PNN co-localization in the adult mouse AuC.
(A-D) Confocal images showing PV immunoreactivity (red) and WFA+ PNN labeling (green) in AuC of adult Ctrl WT (A), cOFF (B), Ctrl KO (C), and cON (D) mice. (E-J) Quantitative analysis of the density of PV, PNN, or PV/PNN positive cells. Graphs show mean ± SEM (n= 6 mice/group, *p<0.05; **p<0.01; ***p<0.001, t-test). PV cell density was significantly reduced in L4 (E) but not L2-3 (H) AuC of cOFF mice compared to Ctrl WT. PNN cell density was significantly reduced in both L4 (F) and L2-3 (I) AuC of cOFF mice compared to Ctrl WT (note that only WFA+ cells were counted to measure PNN density). PV/PNN co-localization was also significantly reduced in L4 (G) and L2-3 (J) AuC of cOFF mice compared to Ctrl WT. Conversely, PV cell density was significantly increased in L4 (E) and L2-3 (H) AuC of cON mice compared to Ctrl KO. PNN cell density was significantly increased in L4 (F) and L2-3 (I) AuC of cON mice compared to Ctrl KO. PV/PNN co-localization was also significantly increased in L4 (G) and L2-3 (J) AuC of cON mice compared to Ctrl KO.

Figure 3.3

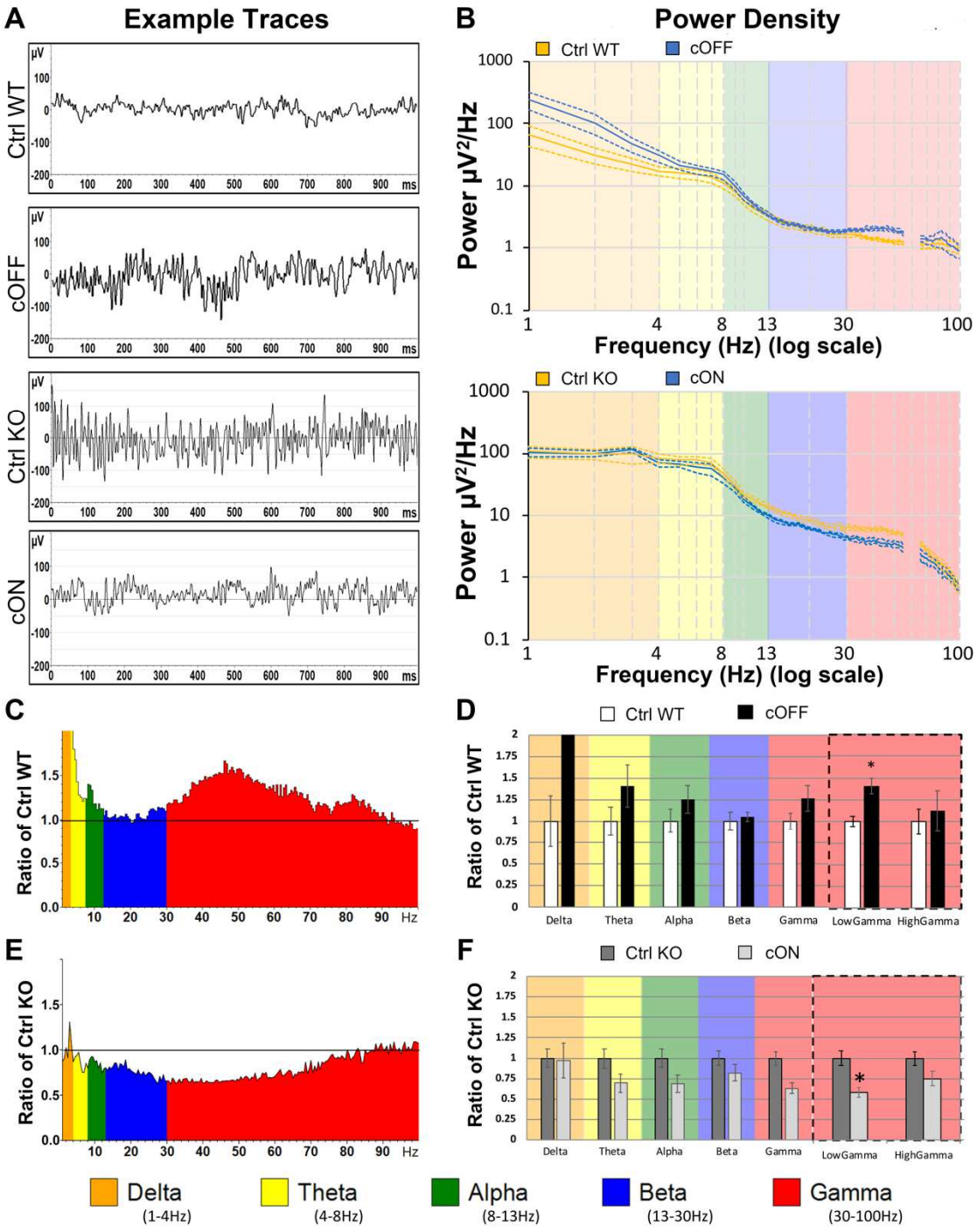
A
Example Traces
Ctrl WT
cOFF
Ctrl KO
cON
μV
ms
B
Power Density
Ctrl WT
cOFF
Ctrl KO
cON
Power μV²/Hz
Frequency (Hz) (log scale)
C
Ratio of Ctrl WT
Hz
D
Ratio of Ctrl WT
Delta
Theta
Alpha
Beta
Gamma
LowGamma
HighGamma
E
Ratio of Ctrl KO
F
Ratio of Ctrl KO
Delta (1-4Hz)
Theta (4-8Hz)
Alpha (8-13Hz)
Beta (13-30Hz)
Gamma (30-100Hz)

Figure 3.3. Characterization of baseline EEG power in AuC of cOFF and cON mice. Five min of baseline EEG data (in the absence of auditory stimulation) from electrodes implanted in the auditory cortex of Ctrl WT (*n*=10) and cOFF (*n*=10), and Ctrl KO (*n*=13) and cON (*n*=13) mice was recorded and FFT analysis was done to determine spectral power.
(A) Examples of 1s segments of raw baseline EEG from control Ctrl WT and cOFF or Ctrl KO and cON mouse AuC. The enhanced high frequency oscillations can be qualitatively observed in the cOFF and control KO mice, compared to the control WT and cON mice. (B) Power density ($\mu V^2/Hz$) was calculated for each artifact-free segment using Fast Fourier Transform, followed by averaging of all segments for a given mouse. These individual averages then contributed to the genotype grand average for each genotype (*n*=10-13 per genotype). Significant differences between genotypes are observed in AuC at low-gamma Frequencies (30-55Hz). Frequencies from 55-65Hz were excluded in *all* analysis, as a 60Hz notch filter was utilized to eliminate line noise.
(C, E) Average power in the cOFF and cON mouse AuC is expressed as the ratio of control levels (Ctrl WT and Ctrl KO, respectively). A value of 1 (horizontal black line) indicates no mean difference in power at that frequency between genotypes while values above the black line indicate cOFF>Ctrl WT or cON>Ctrl KO, and below the black line indicates cOFF<Ctrl WT or cON<Ctrl KO. The elevated low-gamma power in the cOFF mice relative to control WT and the reduced low-gamma power in the cON relative to control KO can be visualized in these plots.
(D, F) Quantification of spectral power differences across genotype pairs shown in C, E. AuC values were divided into canonical frequency bands. MANCOVA analysis controlling for the effect of movement, revealed differences in the low-gamma range of AuC after Bonferroni correction for multiple comparisons. **p*<0.05.

Figure 3.4

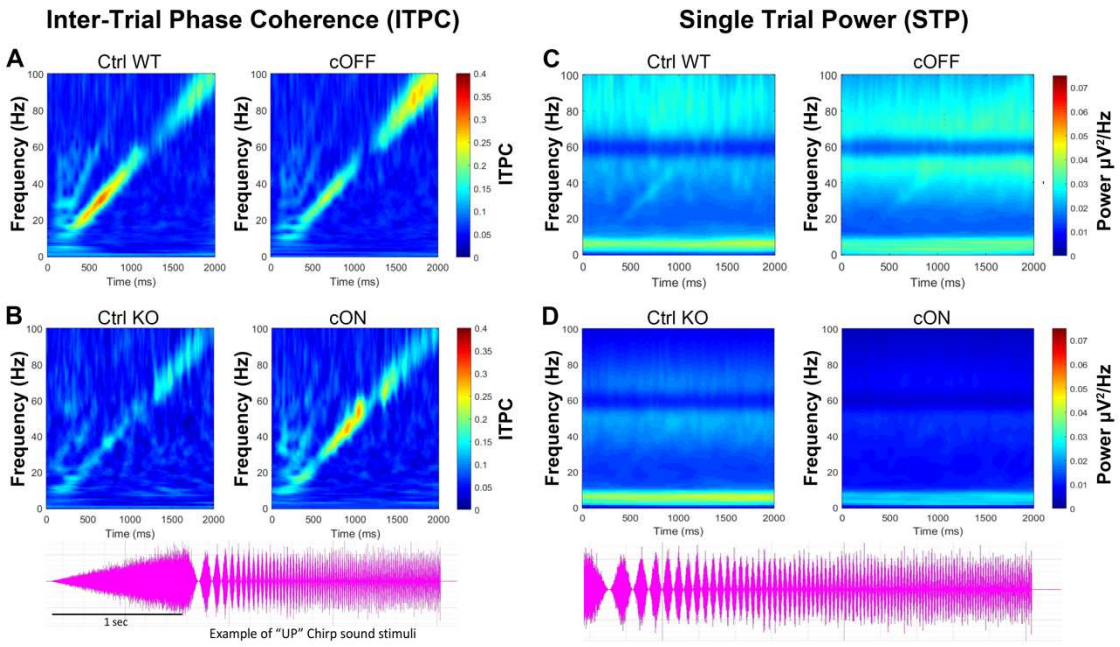

Figure 3.4. Phase locking to auditory "Up Chirp" stimuli.
The chirp stimulus (oscillogram shown at the bottom of this figure) is a 1s broadband noise whose amplitude is modulated linearly by a frequency sweep with frequencies increasing from 1 to 100 Hz. To reduce stimulus onset from overwhelming the early response, the chirp is preceded by a 1s slow ramp of broadband noise. The ability of AuC neural generators of EEG to follow this temporally dynamic stimulus is quantified by measuring the inter-trial phase coherence (ITPC, also known as phase locking factor). Trains of chirp stimuli were presented to each mouse 300 times. (A, B) For each mouse, ITPC was measured to determine the degree of phase locking across trials. Grand average of Ctrl WT and cOFF Phase Locking Factor (PLF) to upward chirp in auditory cortex (A). Auditory cortex grand average PLF to up chirp in Ctrl KO and cON mice (B). (C, D) For each mouse, single-trial power (STP) was measured to determine the average total non-phase locked power during chirp train presentation. Grand average matrices were calculated for each genotype. Grand average Ctrl WT and cOFF STP to up chirp in auditory cortex. This is on-going 'background' power during auditory stimulation (C). Auditory cortex grand average Ctrl KO and cON STP to up chirp (D).

Figure 3.5

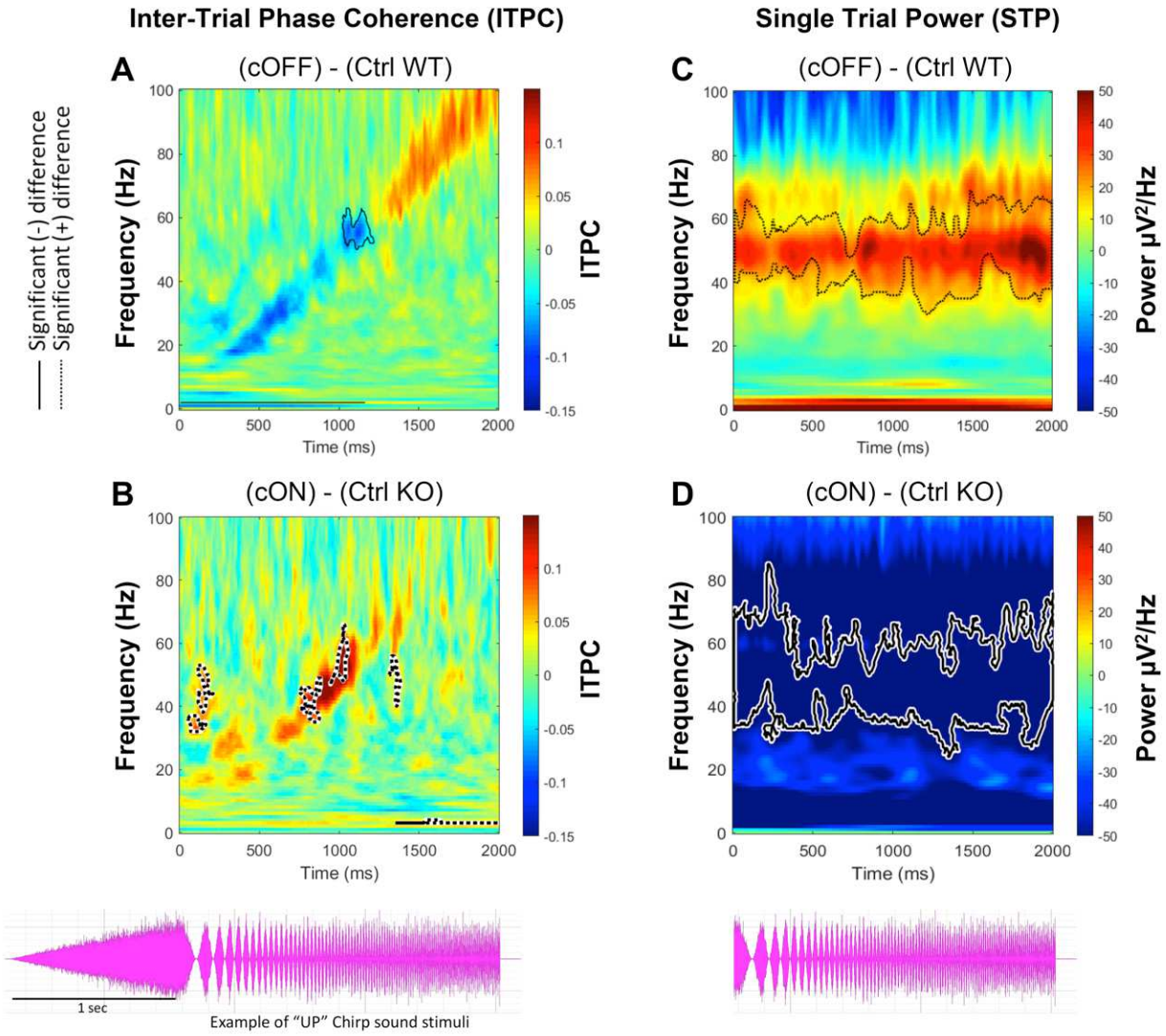
Inter-Trial Phase Coherence (ITPC)
Single Trial Power (STP)
A
(cOFF) - (Ctrl WT)
B
(cON) - (Ctrl KO)
C
(cOFF) - (Ctrl WT)
D
(cON) - (Ctrl KO)
Significant (-) difference
Significant (+) difference
Frequency (Hz)
Time (ms)
ITPC
Power µV²/Hz
1 sec
Example of "UP" Chirp sound stimuli

Figure 3.5. Postnatal deletion or re-expression of *Fmr1* from Ex affect phase locking to time varying auditory stimuli (chirps), as well as non-phase locked single trial power.
(A, B) Ctrl WT (*n*=10) and Ctrl KO (*n*=13) ITPC values were subtracted from cOFF (*n*=10) and cON (*n*=13) values, respectively. Blue areas indicating cOFF<Ctrl WT, green areas no difference, and red cON>Ctrl KO. Statistical cluster analysis reveals contiguous time x frequency regions that are significantly different between genotypes. Black solid contours (mean negative difference) and black dashed contours (mean positive difference) indicate clusters with significant differences. After subtraction and cluster analysis in AuC, cOFF mice express statistically significant decrease in ITPC at low-gamma frequencies (50-60 Hz, blue) (A). Conversely, cON mice express statistically significant increase in ITPC at low-gamma frequencies (~40-60 Hz, red) (B).
(C, D) Ctrl WT (*n*=10) and Ctrl KO (*n*=13) STP values were subtracted from cOFF (*n*=10) and cON (*n*=13) values, respectively. Statistical cluster analysis reveals contiguous time x frequency regions that are significantly different between genotypes. Black dashed contour indicates these significant clusters. Consistent with the low-gamma power changes in baseline EEGs, cOFF mice express statistically significant increase in STP throughout the sound presentation in the low-gamma range (~40-60Hz, red) (C), while cON mice express statistically significant decrease in STP throughout the sound presentation in the low-gamma range (~40-60Hz, blue) (D).

Figure 3.6

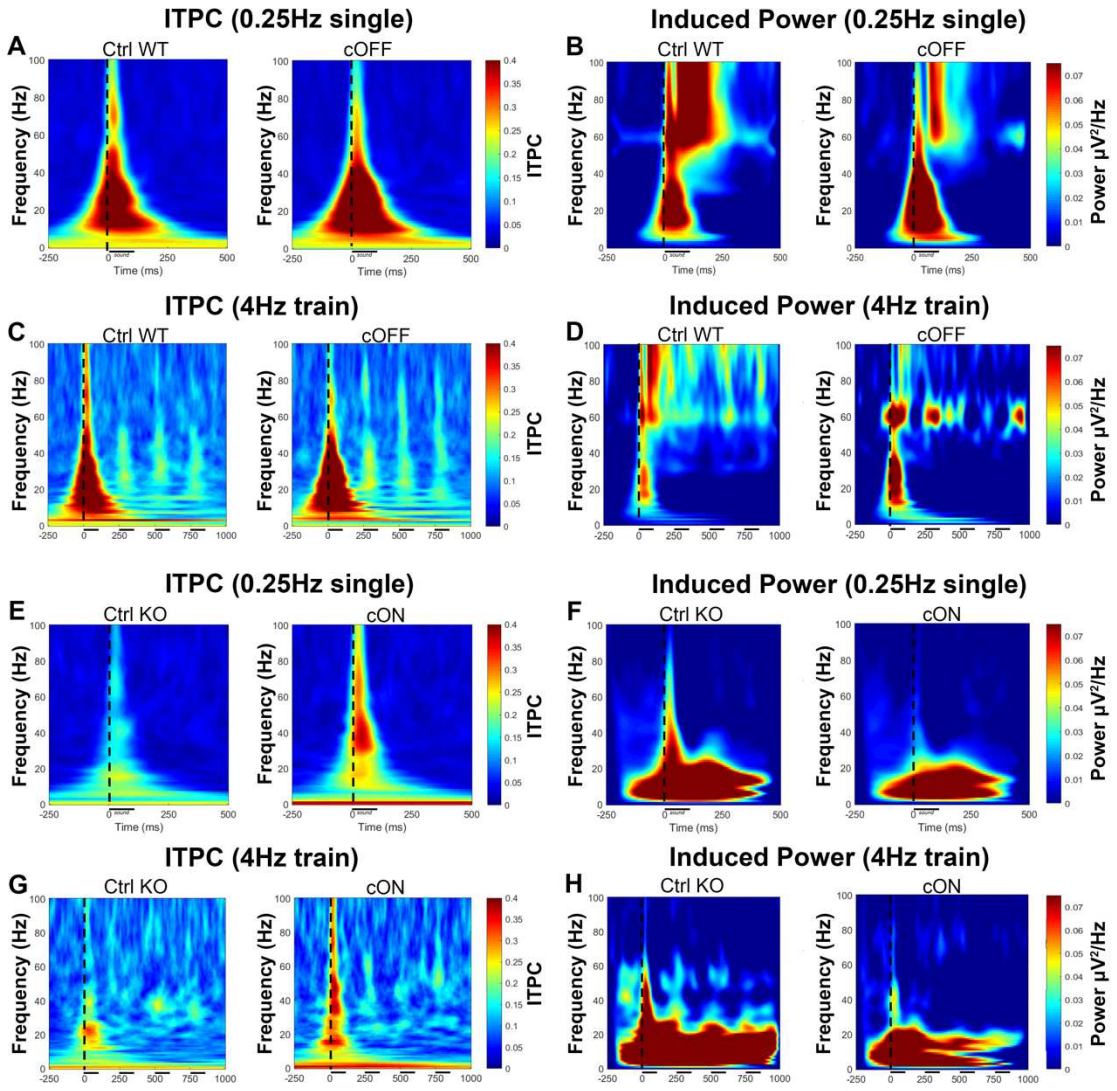

Figure 3.6. ITPC and induced (non–phase-locked) power in response to single sound presentations at 0.25Hz and 4Hz sound train.
(A) Ctrl WT and cOFF grand average of ITPC and (B) induced power during single-sound presentations at 0.25 Hz in auditory cortex. Black dashed line indicates onset of sound; black solid line indicates duration of 100ms broadband noise. (C) Ctrl WT and cOFF grand average of ITPC and (D) induced power during 4Hz sound train in auditory cortex. Only the first four noise bursts of each train were analyzed. (E) Ctrl KO and cON grand average of ITPC and (F) induced power during single-sound presentations at 0.25Hz. (G) Ctrl KO and cON grand average of ITPC and (H) induced power during 4Hz sound train.

Figure 3.7

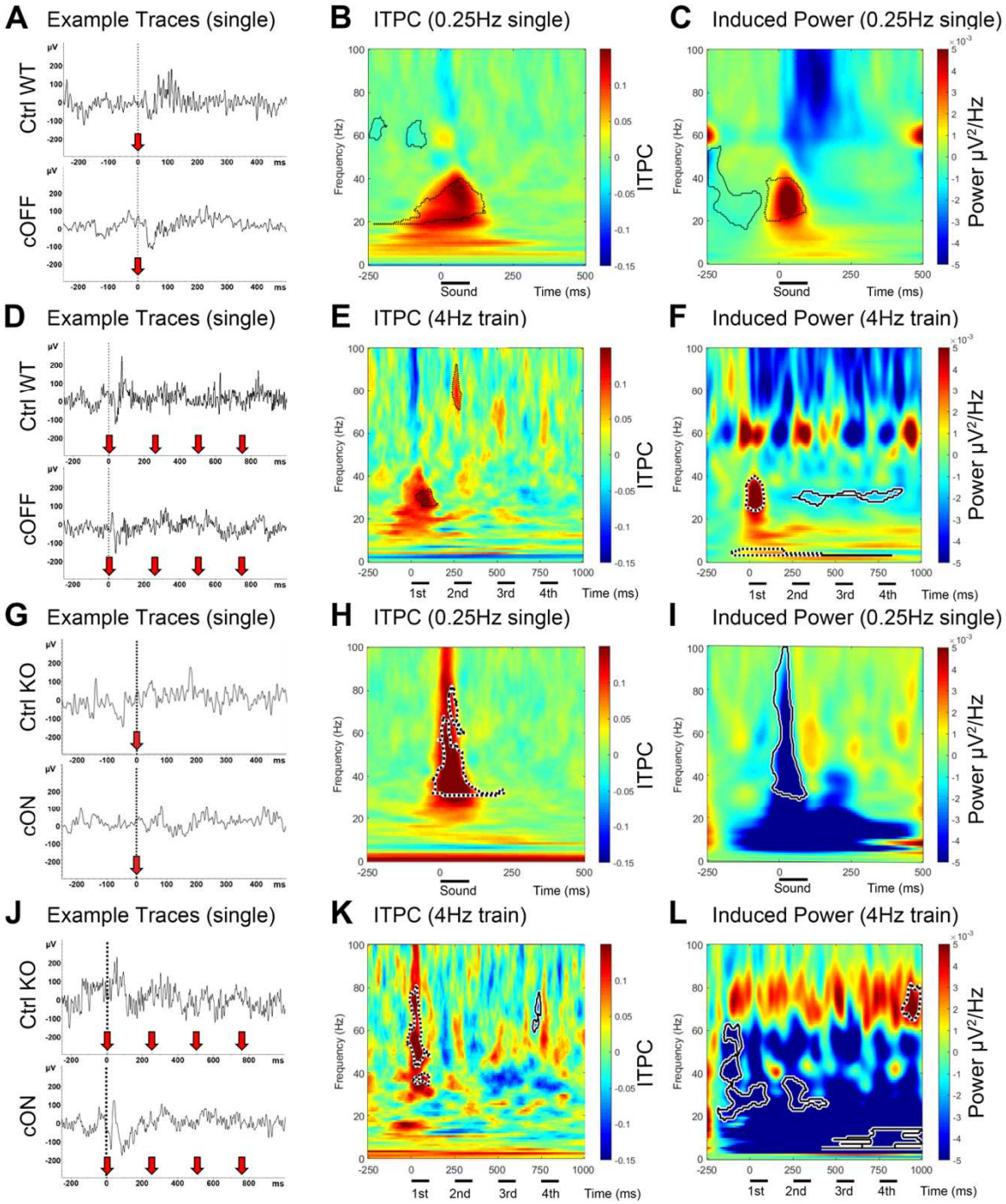
A Example Traces (single)
Ctrl WT
cOFF
B ITPC (0.25Hz single)
C Induced Power (0.25Hz single)
D Example Traces (single)
E ITPC (4Hz train)
F Induced Power (4Hz train)
G Example Traces (single)
Ctrl KO
cON
H ITPC (0.25Hz single)
I Induced Power (0.25Hz single)
J Example Traces (single)
K ITPC (4Hz train)
L Induced Power (4Hz train)
Frequency (Hz)
ITPC
Power μV²/Hz
Sound
Time (ms)
1st
2nd
3rd
4th

Figure 3.7. Postnatal deletion or re-expression of *Fmr1* from Ex affects ITPC and induced (baseline corrected) power in AuC at onset of sound.
(A) Example traces in response to sound presentations at 0.25Hz for Ctrl WT and cOFF mice. Red arrow indicates onset of 100ms broadband noise. (B) Grand average difference plot of inter trial phase coherence (ITPC) during sound presentations between genotypes (cOFF – Ctrl WT). For average plots of each genotype see Figure 3.6. Black solid line indicates duration of 100ms broadband noise. There is an increase in ITPC in the cOFF mice ~20-40Hz during sound presentation. (C) Baseline corrected sound-induced power was calculated for each genotype and difference plot is shown. Increased induced power is observed in response to the sound, indicating increased onset activity, but no differences at longer latencies after sound presentation. (D) Example traces of responses to broadband noise train presented at 4 Hz for Ctrl WT and cOFF mice. (E) ITPC differences were observed for the first sound in the train in the same range as seen in B. (F) Increased induced power is observed during the onset of the ERP response in 20-40Hz range. (G) Example traces in response to single sound presentations at 0.25Hz for Ctrl KO and cON mice. (H) Grand average difference plot of ITPC during sound presentations between genotypes (cON – Ctrl KO). There is an increase in ITPC in the cON mice ~30-80Hz immediately after sound presentation. (I) Baseline corrected sound-induced power was calculated for each genotype and difference plot is shown. Decreased induced power is observed during the onset of the ERP response, indicating decreased onset activity. (J) Examples traces of 4Hz sound presentation for Ctrl KO and cON mice. (K) ITPC differences were observed for the first sound in the train in the same range as seen in the single response in H. (L) Decreased induced power ~20-40Hz was observed after the first and second sound presentations, decreased induced power ~4-20Hz was observed after the third and fourth sound presentations.

Figure 3.8

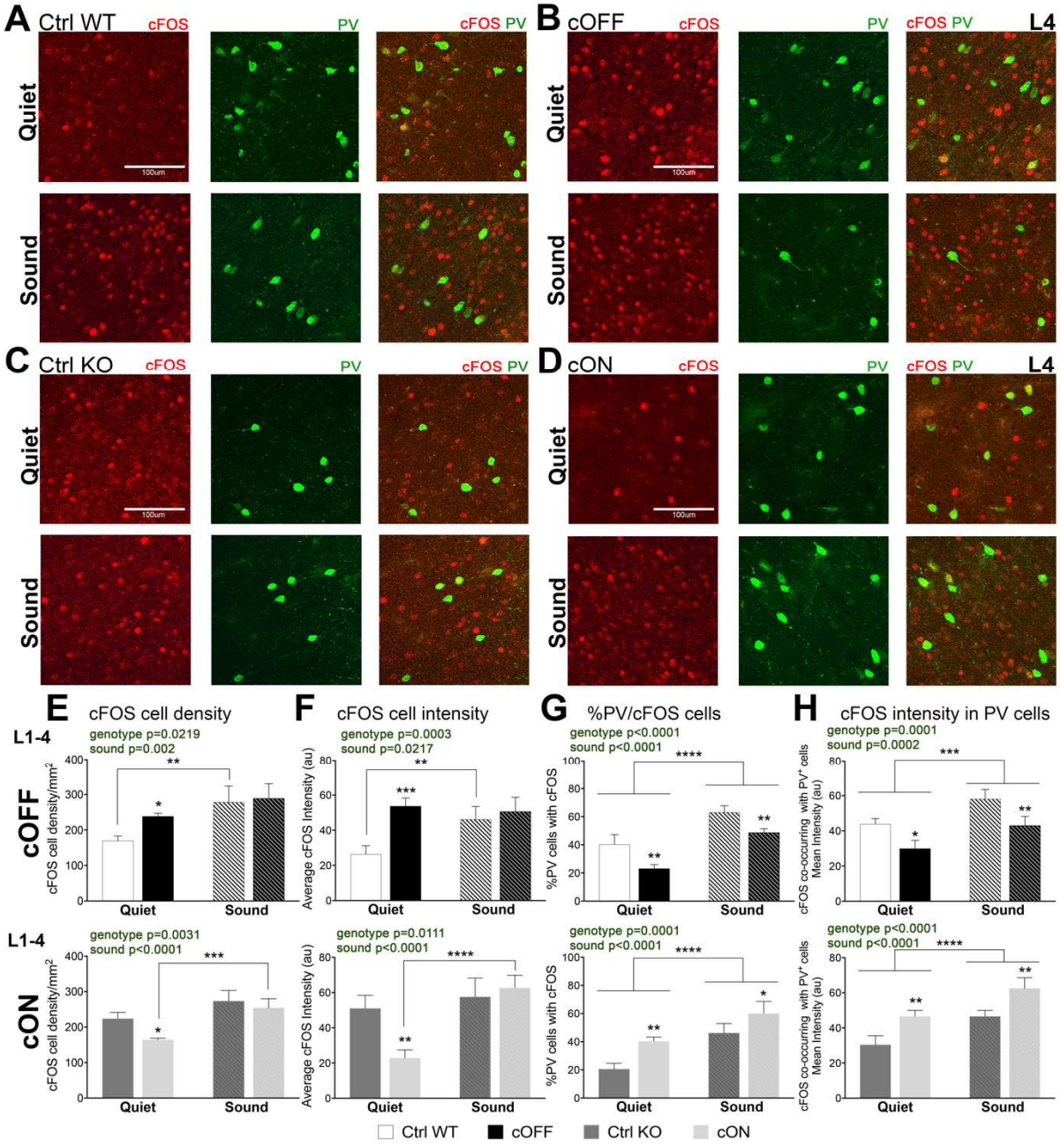
A Ctrl WT
cFOS
PV
cFOS PV
Quiet
Sound
100um
B cOFF
L4
C Ctrl KO
D cON
E cFOS cell density
genotype p=0.0219
sound p=0.002
cFOS cell density/mm2
F cFOS cell intensity
genotype p=0.0003
sound p=0.0217
Average cFOS Intensity (au)
G %PV/cFOS cells
genotype p<0.0001
sound p<0.0001
%PV cells with cFOS
H cFOS intensity in PV cells
genotype p=0.0001
sound p=0.0002
cFOS co-occurring with PV+ cells Mean Intensity (au)
L1-4
cOFF
genotype p=0.0031
sound p<0.0001
cON
genotype p=0.0111
sound p<0.0001
genotype p=0.0001
sound p<0.0001
genotype p<0.0001
sound p<0.0001
Quiet
Sound
Ctrl WT
cOFF
Ctrl KO
cON

Figure 3.8. Postnatal deletion or re-expression of *Fmr1* in Ex differentially altered neuronal activity and PV cell activation.
(A-D) Confocal images showing PV (green) and cFOS (red) expression in L4 AuC of adult Ctrl WT (A), cOFF (B), Ctrl KO (C), and cON (D) mice after being exposed to either silence (quiet) or broadband noise at 65-70dB (sound) for 15min.
(E, F) Quantitative analysis of cFOS+ cell density and cFOS intensity in L1-4 AuC. Under quiet condition, cFOS+ cell density (E) and cFOS intensity (F) were significantly increased in cOFF mice compared to Ctrl WT but reduced in cON compared to Ctrl KO. Following sound exposure, cFOS+ cell density and cFOS intensity were significantly increased in sound-exposed Ctrl WT mice and cON mice, but not in sound-exposed cOFF and Ctrl KO mice compared to their corresponding quiet groups. However, no significant changes were observed in cFOS cell density and c-FOS intensity between sound-exposed Ctrl WT and cOFF or sound-exposed Ctrl KO and cON mice.
(G, H) Quantitative analysis of %PV cells with cFOS, and cFOS intensity in PV cells in L1-4 AuC. %PV cells with cFOS (G) and cFOS intensity in PV cells (H) were significantly reduced in cOFF mice compared to Ctrl WT and increased in cON mice compared to Ctrl KO mice in both quiet condition and after sound exposure. %PV cells with cFOS and cFOS intensity in PV cells were significantly increased in sound-exposed mice compared to quiet groups for all genotypes. Graphs show mean ± SEM (n= 4/group, *p<0.05; **p<0.01; ***p<0.001; ****p<0.0001, two-way ANOVA followed by Bonferroni multiple comparison post-test).

Figure 3.9

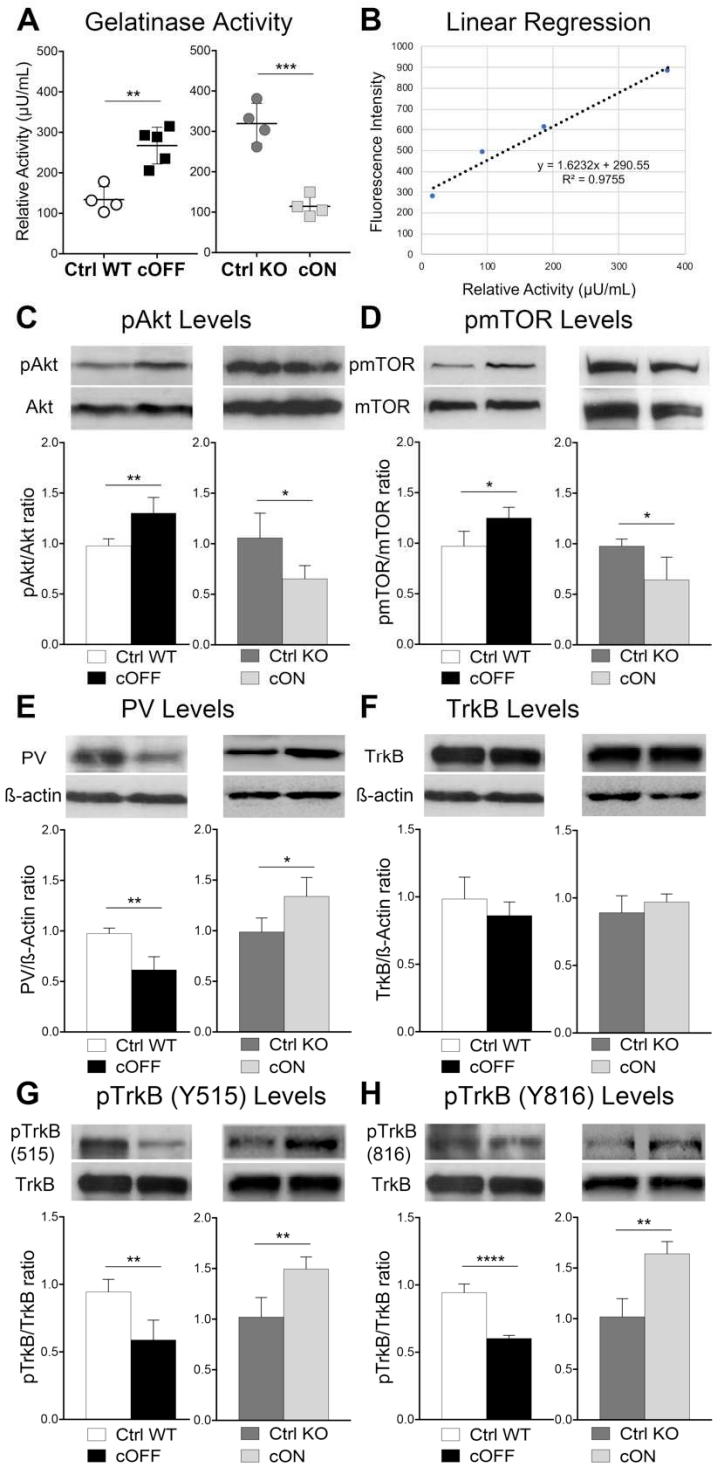
A
Gelatinase Activity
Relative Activity (µU/mL)
Ctrl WT cOFF
Ctrl KO cON
B
Linear Regression
Fluorescence Intensity
y = 1.6232x + 290.55
R² = 0.9755
Relative Activity (µU/mL)
C
pAkt Levels
pAkt
Akt
pAkt/Akt ratio
D
pmTOR Levels
pmTOR
mTOR
pmTOR/mTOR ratio
E
PV Levels
PV
ß-actin
PV/ß-Actin ratio
F
TrkB Levels
TrkB
ß-actin
TrkB/ß-Actin ratio
G
pTrkB (Y515) Levels
pTrkB (515)
TrkB
pTrkB/TrkB ratio
H
pTrkB (Y816) Levels
pTrkB (816)
TrkB
pTrkB/TrkB ratio
Ctrl WT
cOFF
Ctrl KO
cON

Figure 3.9. Gelatinase activity, Akt/mTOR activation, PV levels and TrkB phosphorylation are altered in AuC of adult cOFF and cON mice compared to their control counterparts.
(A) Relative gelatinase activity in AuC of adult Ctrl WT, cOFF, Ctrl KO, and cON mice. Graph shows mean ± SEM (n=4-5 mice/group, **p<0.01; ***p<0.001, t-test). Gelatinase activity is elevated in AuC of cOFF mice compared to Ctrl WT and is lower in cON mice than in Ctrl KO. (B) Standard curve showing gelatinase activity of recombinant MMP-9. (C, D) Western blots showing total and phosphorylated levels of Akt and mTOR. Quantitative analysis of p-Akt/Akt (C) and p-mTOR/mTOR (D) ratios. Graphs show mean ± SEM (n=4/group, *p<0.05; **p<0.01, t-test). p-Akt/Akt ratio is increased in the cOFF mice and decreased in cON mice compared to their control counterparts (C). p-mTOR/mTOR ratio also shows a significant increase in the cOFF mice and a decrease in cON mice compared to their control counterparts (D).
(E-H) Western blot showing PV (E), TrkB (F), p-TrkB(Y515) (G), and p-TrkB(Y816) (H) levels in lysates from adult AuC of Ctrl WT, cOFF, Ctrl KO, and cON mice. (E) Quantitative analysis of PV levels. Graphs show mean ± SEM (n=4/group, *p<0.05; **p<0.01, t-test). PV levels are significantly reduced in adult AuC of cOFF mice and increased in cON mice compared their control counterparts (F) Quantitative analysis of total TrkB levels. No significant changes were observed in total TrkB levels in AuC of both cOFF and cON mice compared to their respective controls. (G, H) Quantitative analysis of p-TrkB(Y515)/TrkB (G) and p-TrkB(Y816)/TrkB (H) ratios. Graphs show mean ± SEM (n=4/group, **p<0.01; ****p<0.0001, t-test). p-TrkB(Y515)/TrkB ratio (G) and the p-TrkB(Y816)/TrkB ratio (H) are significantly decreased in AuC of cOFF mice, and up-regulated in cON mice compared to their control counterparts.

Figure 3.10

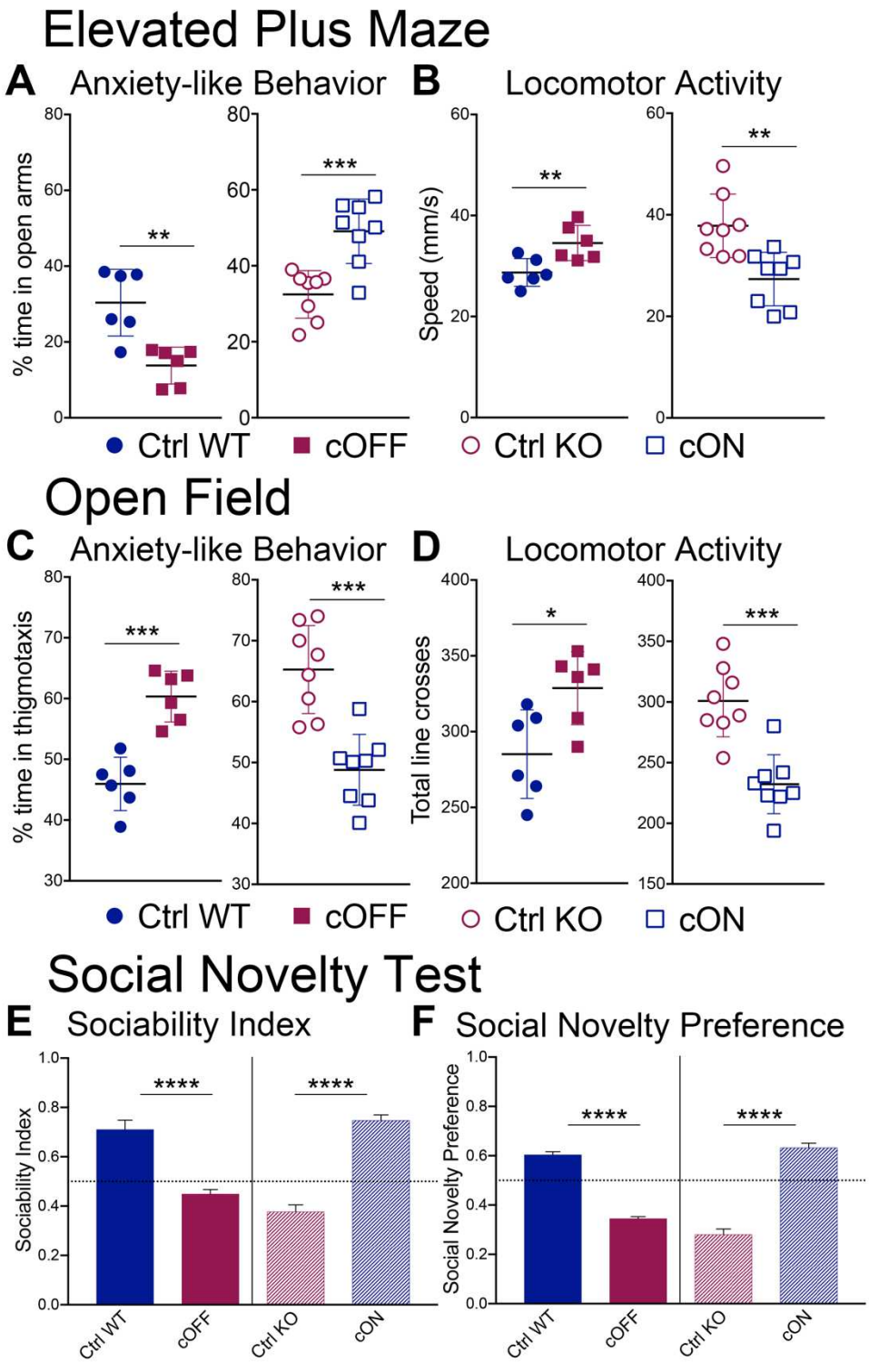
Elevated Plus Maze
A Anxiety-like Behavior
B Locomotor Activity
% time in open arms
Speed (mm/s)
Ctrl WT
cOFF
Ctrl KO
cON
Open Field
C Anxiety-like Behavior
D Locomotor Activity
% time in thigmotaxis
Total line crosses
Social Novelty Test
E Sociability Index
F Social Novelty Preference
Sociability Index
Social Novelty Preference

Figure 3.10. Postnatal deletion of re-expression of *Fmr1* in Ex affect behavioral responses in cOFF and cON mice.
(A, B) Graphs demonstrate the performance of cOFF and cON mice in the elevated plus maze as measured by the percent time in open arms (A) and speed (B). Graphs show mean ± SEM (n=6-8 mice/group, **p<0.01; ***p<0.001, t-test).
(C, D) Graphs demonstrate the performance of cOFF and cON mice in the open field as measured by the percent time in thigmotaxis (C) and total number of line crosses (D). Graphs show mean ± SEM (n=6-8 mice/group, *p<0.05; ***p<0.001, t-test).
(E, F) Graphs demonstrate the sociability index (E) and social novelty preference index (F) of cOFF and cON mice in the social novelty test. For sociability index, values <0.5 indicate more time spent in the empty chamber, >0.5 indicate more time spent in the chamber containing Stranger 1, and 0.5 indicates equal amount of time in both chambers. For social novelty preference index, values <0.5 indicate more time spent in the chamber containing Stranger 1 or now familiar mouse, >0.5 indicate more time spent in the chamber containing Stranger 2 or new stranger mouse, and 0.5 indicates equal amount of time in both chambers (n=6-8 mice/group, ****p<0.001, t-test).

Figure 3.11

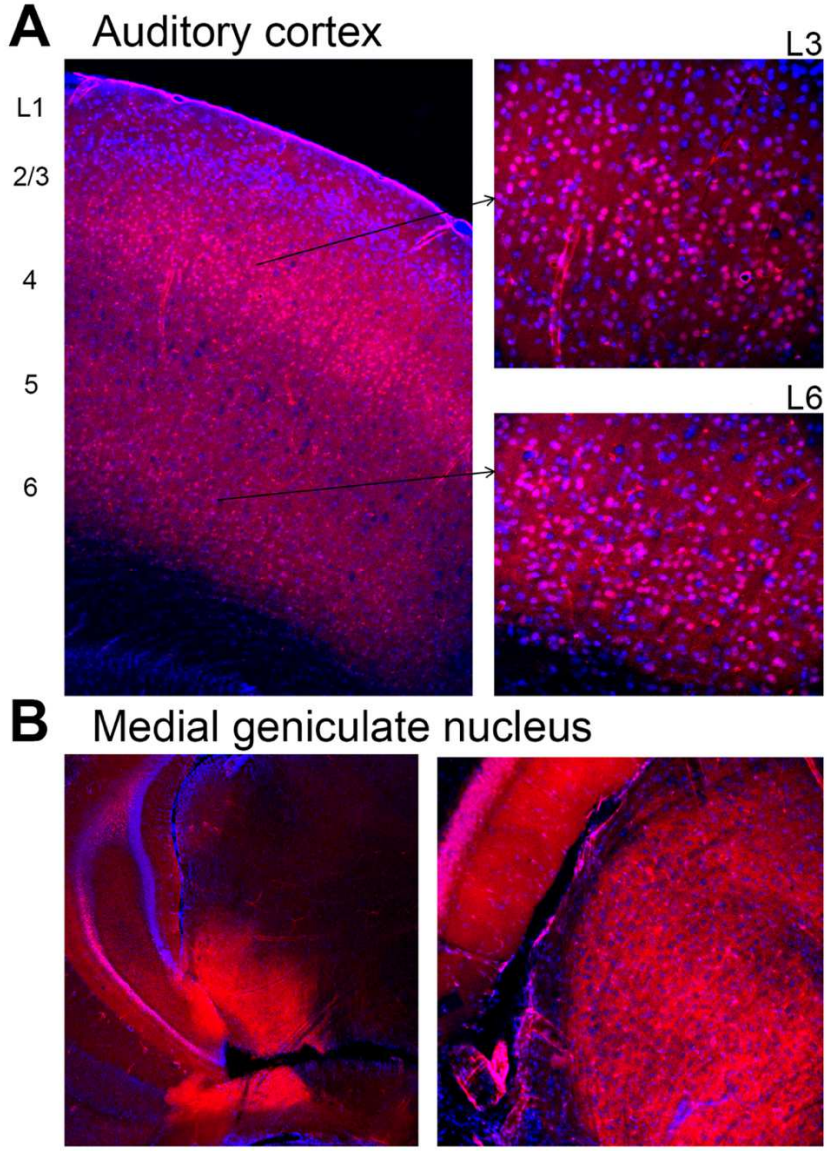

Figure 3.11. Expression of tdTomato under the CaMK2a promoter in different regions of the brain.
(A) tdTomato expression in the auditory cortex of *Fmr1*^{Flox}-Cre^{CaMK2a}-*STOP*-tdTomato adult mice. (B) tdTomato expression in the hippocampal neurons and afferent fibers in medial geniculate nucleus (MGN) of *Fmr1*^{Flox}-Cre^{CaMK2a}*STOP*-tdTomato adult mice.

Figure 3.12

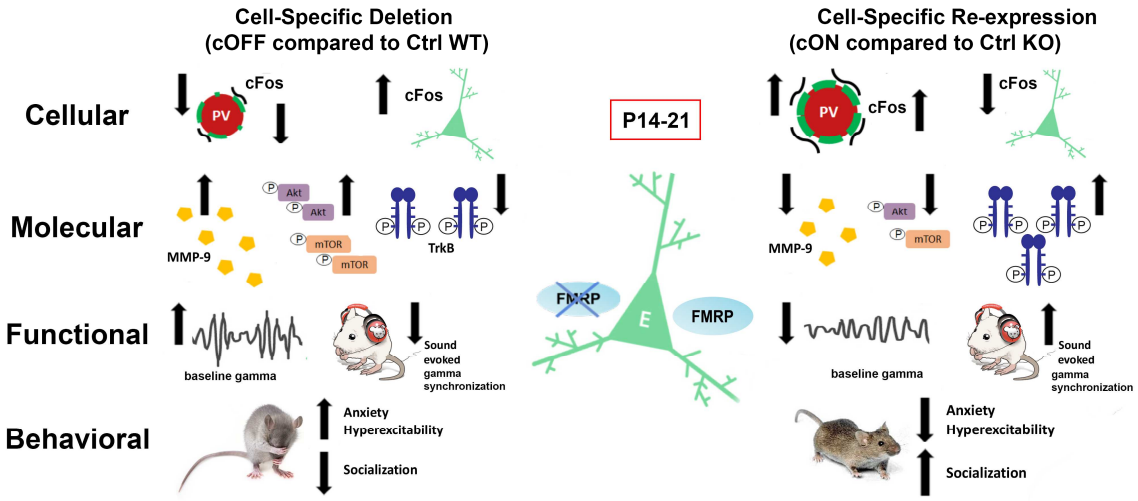

Figure 3.12. Schematic of phenotypes observed following deletion or re-expression of *Fmr1* in excitatory neurons during early postnatal development.
Left panel depicts cellular, molecular, functional and behavioral phenotypes caused by the cell-specific deletion of *Fmr1* from excitatory neurons during critical postnatal development. cOFF mice exhibit reduced PV and TrkB phosphorylation levels, impaired formation of WFA+ PNNs around PV cells, upregulated overall cFOS immunoreactivity but lower levels of cFOS in PV cells, increased gelatinase activity, higher mTOR/Akt phosphorylation, enhanced baseline gamma power, abnormal phase locking to time varying stimuli, and behavioral deficits compared to Ctrl WT mice.
Right panel depicts cellular, molecular, functional and behavioral phenotypes caused by the cell specific re-expression of *Fmr1* in cortical excitatory neurons during early postnatal development. cON mice exhibit increased PV and TrkB phosphorylation levels, increased WFA+ PNNs around PV cells, reduced overall cFOS immunoreactivity but higher levels of cFOS in PV cells, decreased gelatinase activity, reduced mTOR/Akt phosphorylation, normalized neural oscillations, and corrected behavioral deficits compared to Ctrl KO mice.

Table 3.1. Summary table showing percentage of NeuN+ neurons with FMRP expression in the auditory cortex of Ctrl WT and cOFF, or Ctrl KO and cON mice at P14, P21, and P60 (mean ± SEM). Statistical analysis of differences between cOFF or cON mice and their respective Ctrl WT or Ctrl KO counterparts was performed using t-test (unpaired, two-tailed): ***p<0.001, ****p<0.0001.

	Ctrl WT n=3	cOFF n=3	Ctrl KO n=3	cON n=3
P14	61 ± 0.7%	62 ± 0.8%	0.4 ± 0.1%	0.6 ± 0.3%
P21	60 ± 2.0%	13 ± 0.5% t(4) =20.50 ****(p<0.0001)	0.5 ± 0.2%	48 ± 1.0% t(4) =49.89 ****(p<0.0001)
P60	64 ± 4.2%	8.4 ± 1.4% t(4) =12.68 ***(p=0.0002)	0.6 ± 0.3%	47 ± 1.4% t(4) =33.91 ****(p<0.0001)

Table 3.2. Summary table showing density of PV cells, WFA+ PNNs, and PV/PNN co-localization in the auditory cortex of adult Ctrl WT and cOFF, or Ctrl KO and cON mice (mean ± SEM). Statistical analysis of differences between cOFF or cON mice and their respective Ctrl WT or Ctrl KO counterparts was performed using t-test (unpaired, two-tailed): **p*<0.05, ***p*<0.01, ****p*<0.001.

	Ctrl WT *n*=3		cOFF *n*=6		Ctrl KO *n*=4		cON *n*=5	
	L4	L2/3	L4	L2/3	L4	L2/3	L4	L2/3
PV+ cell density	105 ± 5	49 ± 2	84 ± 6* t(10)=2.59 (*p*=0.0270)	51 ± 4	94 ± 10	30 ± 5	136 ± 9* t(7) =3.11 (*p*=0.0172)	59 ± 3** t(7) =4.67 (*p*=0.0023)
PNN+ cell density	193 ± 6	43 ± 4	148 ± 10** t(10)=3.65 (*p*=0.0045)	21 ± 4** t(10)=3.76 (*p*=0.0037)	131 ± 8	24 ± 1	214 ± 16** t(7) =4.21 (*p*=0.0040)	46 ± 3*** t(7) =5.70 (*p*=0.0007)
PV+/PNN+ co-localization	85 ± 6	21 ± 2	62 ± 5* t(10)=2.68 (*p*=0.0231)	14 ± 2* t(10)=2.28 (*p*=0.0456)	50 ± 5	9 ± 1	90 ± 9** t(7) =3.62 (*p*=0.0085)	21 ± 2** t(7) =5.21 (*p*=0.0012)

Table 3.3. Summary table showing overall cFos+ cells density and intensity, % cFos+ PV cells, and cFos intensity in PV cells in L1-4 auditory cortex of adult Ctrl WT and cOFF, or Ctrl KO and cON mice under quiet condition vs. after exposure to sound (mean ± SEM). Statistical analysis of differences between cOFF or cON mice and their respective Ctrl WT or Ctrl KO counterparts under both conditions was performed using two-way ANOVA followed by Bonferroni multiple comparison post-test: *p<0.05, **p<0.01, ***p<0.001, ****p<0.0001 for genotype comparison; $^{\#}p$<0.05, $^{\#\#}p$<0.01, $^{\#\#\#}p$<0.001, $^{\#\#\#\#}p$<0.0001 for sound exposure comparison.

	Ctrl WT n=4		cOFF n=4		Ctrl KO n=4		cON n=4	
	Quiet	**Sound**	*Quiet*	**Sound**	*Quiet*	**Sound**	*Quiet*	**Sound**
cFos+ cell density	167 ± 5	278 ± 22 $^{\#\#}p$=0.0018	239 ± 4 *p=0.0429	289 ± 20	224 ± 9	274 ± 14	164 ± 2 *p=0.0114	255 ± 12 $^{\#\#\#}p$=0.0004
cFos intensity	26 ± 2	46 ± 3 $^{\#\#}p$=0.0052	54 ± 2 ***p=0.0003	51 ± 4	51 ± 3	57 ± 5	23 ± 2 **p=0.0014	63 ± 3 $^{\#\#\#\#}p$<0.0001
%PV/cFos cells	40 ± 3	63 ± 2 $^{\#\#\#\#}p$<0.0001	23 ± 1 **p=0.0011	49 ± 1 **p=0.0052 $^{\#\#\#\#}p$<0.0001	21 ± 2	46 ± 3 $^{\#\#\#}p$<0.0003	40 ± 1 **p=0.0031	60 ± 4 *p=0.0377 $^{\#\#}p$<0.0030
cFos intensity in PV cells	44 ± 2	58 ± 3 $^{\#}p$<0.0152	30 ± 2 *p=0.0179	43 ± 3 **p=0.0061 $^{\#}p$<0.0157	31 ± 3	46 ± 2 $^{\#\#}p$<0.0013	47 ± 1 **p=0.0012	62 ± 3 **p=0.0016 $^{\#\#}p$<0.0018

Table 3.4. Summary table showing gelatinase activity and protein levels in the auditory cortex of adult Ctrl WT, cOFF, Ctrl KO, and cON mice (mean ± SEM). Statistical analysis of differences between cOFF or cON mice and their respective Ctrl WT or Ctrl KO counterparts was performed was performed using t-test (unpaired, two-tailed): **p*<0.05, ***p*<0.01, ****p*<0.001, *****p*<0.0001.

	Ctrl WT *n*=4	cOFF *n*=4	Ctrl KO *n*=4	cON *n*=4
Gelatinase Activity	133.8 ± 16.02	267.4 ± 20.27 t(7) =4.96 ***p*=0.0016	319.5 ± 25.04	114.5 ± 12.65 t(6) =7.31 ****p*=0.0003
p-Akt/Akt ratio	0.98 ± 0.03	1.30 ± 0.07 t(6) =3.82 ***p*=0.0088	1.05 ± 0.12	0.66 ± 0.06 t(6) =2.93 **p*=0.0263
p-mTOR/mTOR ratio	0.97 ± 0.07	1.25 ± 0.05 t(6) =3.11 **p*=0.0209	0.98 ± 0.03	0.64 ± 0.11 t(6) =2.86 **p*=0.0289
PV Levels	0.98 ± 0.03	0.62 ± 0.06 t(6) =5.129 ***p*=0.0022	0.99 ± 0.07	1.34 ± 0.09 t(6) =3.056 **p*=0.0224
tTrkB Levels	0.98 ± 0.08	0.86 ± 0.05	0.89 ± 0.06	0.97 ± 0.03
p-TrkB(515)/ tTrkB ratio	0.95 ± 0.04	0.59 ± 0.07 t(6) =4.14 ***p*=0.0061	1.02 ± 0.09	1.49 ± 0.05 t(6) =4.24 ***p*=0.0054
p-TrkB(816)/ tTrkB ratio	0.94 ± 0.03	0.60 ± 0.01 t(6) =10.19 *****p*<0.0001	1.01 ± 0.09	1.64 ± 0.06 t(6) =5.79 ***p*=0.0012

Table 3.5. Summary table showing locomotor activity and anxiety-like behaviors of adult Ctrl WT, cOFF, Ctrl KO, and cON mice using elevated plus maze (EP) and open-field (OF) behavior tests (mean ± SEM). Statistical analysis of differences between cOFF or cON mice and their respective Ctrl WT and Ctrl KO counterparts was performed was performed using t-test (unpaired, two-tailed): *p<0.05, **p<0.01, ***p<0.001, ****p<0.0001.

	Ctrl WT n=6	cOFF n=6	Ctrl KO n=8	cON n=8
Total entries (EP)	20 ± 1.7	28 ± 1.5 t(10) =3.34 *p=0.0075	44 ± 2.4	31 ± 1.7 t(14) =4.67 ***p=0.0004
Speed (EP)	29 ± 1.1	35 ± 1.4 t(10) =3.22 **p=0.0091	38 ± 2.2	27 ± 1.8 t(14) =3.63 **p=0.0027
Time spent in open arm/entry (EP)	5.9 ± 0.6	1.6 ± 0.5 t(10) =5.36 ***p=0.0003	2.1 ± 0.4	6.5 ± 0.5 t(14) =7.03 ****p<0.0001
% Time in open arms (EP)	30 ± 3.6	14 ± 1.9 t(10) =4.05 **p=0.0023	32 ± 2.2	49 ± 2.9 t(14) =4.47 ***p=0.0005
Total line crosses (OF)	285 ± 12	329 ± 9.8 t(10) =2.82 *p=0.0182	301 ± 10	232 ± 8.6 t(14) =5.08 ***p=0.0002
Speed (OF)	58 ± 1.5	66 ± 1.8 t(10) =3.74 **p=0.0039	70 ± 2.9	50 ± 2.6 t(14) =5.15 ***p=0.0001
Time spent in center/entry (OF)	0.84 ± 0.11	0.58 ± 0.02 t(10) =2.45 *p=0.0340	0.52 ± 0.04	0.93 ± 0.12 t(14) =3.17 **p=0.0068
% Time in thigmotaxis (OF)	46 ± 1.8	60 ± 1.7 t(10) =5.82 ***p=0.0002	65 ± 2.5	49 ± 2.1 t(14) =5.02 ***p=0.0002

Table 3.6. Summary table showing sociability (Session 1) and social novelty preference (Session 2) of adult Ctrl WT, cOFF, Ctrl KO, and cON mice using the social novelty behavior test (mean ± SEM). Statistical analysis of differences between cOFF or cON mice and their respective Ctrl WT and Ctrl KO counterparts was performed using two-way ANOVA followed by Bonferroni multiple comparison post-test for "time spent in chamber" comparisons; and using t-test (unpaired, two-tailed) for sociability and social novelty preference index comparisons: *p<0.05, **p<0.01, ***p<0.001, ****p< 0.0001 for genotype comparison; $^{\#}p$<0.05, $^{\#\#}p$<0.01, $^{\#\#\#}p$<0.001, $^{\#\#\#\#}p$<0.0001 for chamber comparison.

	Ctrl WT n=6	cOFF n=6	Ctrl KO n=8	cON n=8
Time spent in empty chamber	25 ± 4.4	29 ± 2.6	49 ± 3.7	24 ± 1.4 *p=0.0264
Time spent with stranger mouse (S1)	59 ± 4.3 $^{\#\#}p$=0.0033	23 ± 0.8 **p=0.0027	30 ± 3.6	74 ± 4.2 ***p=0.0009 $^{\#\#\#}p$=0.0004
Sociability index	0.71 ± 0.04	0.45 ± 0.02 t(10) = 6.31 ****p<0.0001	0.37 ± 0.03	0.75 ± 0.02 t(14) = 10.62 ****p<0.0001
Time spent with novel mouse (S2)	73 ± 0.9	23 ± 1.4 ****p<0.0001	31 ± 2.5	112 ± 6.6 ****p<0.0001
Time spent with familiar mouse (S1)	48 ± 2.7 $^{\#\#\#\#}p$<0.0001	44 ± 1.8 $^{\#\#\#}p$=0.0002	66 ± 3.4 $^{\#\#}p$<0.0024	65 ± 4.2 $^{\#\#\#}p$=0.0004
Social novelty preference index	0.60 ± 0.01	0.35 ± 0.01 t(10) = 18.08 ****p<0.0001	0.28 ± 0.02	0.63 ± 0.02 t(14) = 12.30 ****p<0.0001

Chapter 4 – Astrocytes Regulate Inhibition in Fragile X Syndrome

Abstract

Fragile X syndrome (FXS) is a leading genetic cause of autism-like symptoms that include sensory hypersensitivity and cortical hyperexcitability. Recent studies in *Fmr1* knockout (KO) animal models of FXS suggest abnormal GABAergic signaling. Although most studies focused on neuron-centered mechanisms, astrocytes' contribution to the deficits is largely unknown. Here we propose a non-neuronal mechanism of abnormal inhibitory circuit development in FXS. Astrocyte-specific deletion of *Fmr1* during postnatal period leads to increased astrocytic GABA levels, but negatively impacts synaptic $GABA_A$ receptors and genes involved in parvalbumin (PV) cell development. Developmental deletion of *Fmr1* from astrocytes also affects communications between excitatory neurons and PV cells, impairs sound-evoked gamma synchronization in the cortex, while enhancing baseline and on-going sound-evoked EEG power, leading to increased locomotor activity and altered social behaviors in adult mice. These results demonstrate a profound role of astrocytic FMRP in the development of inhibitory circuits and shaping normal inhibitory responses.

Introduction

Fragile X Syndrome (FXS) is the most common genetic form of autism spectrum disorders (ASD) (Crawford, Acuña, & Sherman, 2001). FXS is usually caused by a CGG repeat expansion in 5'-untranslated region of the Fragile X mental retardation 1 (*Fmr1*)

gene followed by gene methylation, loss of Fragile X Mental Retardation Protein (FMRP), translational dysregulation, and abnormal protein synthesis (Sutcliffe et al., 1992; Verkerk et al., 1991). Prominent symptoms of FXS include intellectual disability, repetitive behaviors, social communication deficits, and sensory hypersensitivity (Penagarikano, Mulle, & Warren, 2007; Rais, Binder, Razak, & Ethell, 2018), particularly in the auditory domain (Castrén, Pääkkönen, Tarkka, Ryynänen, & Partanen, 2003; Ethridge et al., 2016; Schneider et al., 2013). Although FMRP is involved in the regulation of neuronal communications in the brain and synaptic functions (Darnell et al., 2011; Edbauer et al., 2010; Y. Q. Zhang et al., 2001), little is known how different cell types that express FMRP in the brain may contribute to the deficits.

Cortical hyperexcitability is proposed to underlie sensory hypersensitivity that is common in both humans with FXS and the mouse models of FXS (Castrén et al., 2003; Ethridge et al., 2016; Frankland et al., 2004; Rais et al., 2018; Rotschafer & Razak, 2013; D. Sinclair, B. Oranje, K. A. Razak, S. J. Siegel, & S. Schmid, 2017). The *Fmr1* knockout (KO) mouse is an established FXS model that is well suited to study cortical hyperexcitability. FMRP loss increases network-level hyperexcitability in the rodent cortex through impaired inhibition and altered excitatory/inhibitory (E/I) balance (Antoine, Langberg, Schnepel, & Feldman, 2019) that most likely affect neural synchrony (Gonçalves, Anstey, Golshani, & Portera-Cailliau, 2013; Y. Zhang et al., 2014). The *Fmr1* KO mouse shows decreased density and function of parvalbumin (PV)-expressing inhibitory interneurons (Gibson, Bartley, Hays, & Huber, 2008; Goel et al., 2018; Lovelace et al., 2020; T. H. Wen et al., 2018), reduced gamma-aminobutyric acid

(GABA) receptor levels, decreased GABA synthesis, increased GABA catabolism, and overall decreased GABAergic input in several areas of the brain (Adusei, Pacey, Chen, & Hampson, 2010; Braat & Kooy, 2015; Curia, Papouin, Séguéla, & Avoli, 2009; D'Hulst et al., 2006). FMRP is also shown to regulate neuronal excitability through the direct interactions with sodium-activated potassium channel Slack, presynaptic N-type voltage-gated calcium channels, and calcium-activated potassium BK channels (Brown et al., 2010; Deng et al., 2013; Ferron, Nieto-Rostro, Cassidy, & Dolphin, 2014; Myrick et al., 2015). The enhanced excitability is also linked to reduced levels of glutamate transporter on FMRP-deficient astrocytes and reduced glutamate uptake by the astrocytes (Higashimori et al., 2016) that may contribute to increased hyperactivity and reduced sociability in these mice (Jin et al., 2021). Although there is some disagreement in terms of the mechanisms underlying cortical hyperexcitability, studies to date suggest that FMRP loss affects the communications between excitatory pyramidal neurons and inhibitory interneurons (Gibson et al., 2008; Hays, Huber, & Gibson, 2011) resulting in overall reduced E/I balance (Contractor, Klyachko, & Portera-Cailliau, 2015). Astrocytes are well positioned to control the neuronal communications and are known not only to regulate glutamate metabolism (Ullian, Christopherson, & Barres, 2004), but also to uptake and synthesize GABA controlling GABAergic transmission as well (Ishibashi, Egawa, & Fukuda, 2019). With the discovery of FMRP expression in developing astrocytes (Pacey & Doering, 2007), it is plausible that astrocytes contribute, in some capacity, to the abnormal PV cell development and circuit hyperexcitability by altering GABAergic signaling in FXS.

Therefore, the main goal of this study was to determine whether cell specific deletion of *Fmr1* from astrocytes during critical developmental period would alter GABAergic signaling and PV cell development leading to cortical hyperexcitability and behavioral alterations. In the present study, we used a multidisciplinary approach including transcriptional, cellular, molecular, electrophysiological, and behavioral methods to delineate the astrocyte-mediated mechanisms of cortical hyperexcitability. We also utilized the analysis of translationally relevant electroencephalogram (EEG) phenotypes, that are remarkably similar between mouse model of FXS and human condition, across different brain areas implicated in FXS-associated behaviors. Our findings provide a novel insight into the role of astrocytic FMRP in the development of cortical circuits and suggest non-neuronal mechanism of abnormal inhibitory circuit development in FXS with potential for translating the results of the mouse study into successful clinical trials.

Materials and Methods

Ethics Statement

All mouse studies were done according to National Institutes of Health and Institutional Animal Care and Use Committee at the University of California Riverside (approval AUP20190015 and AUP20190029) guidelines. All procedures were approved by IACUC; animal welfare assurance #A3439-01 is on file with the Office of Laboratory Animal Welfare. Mice were maintained in an AAALAC accredited facility under 12h

light/dark cycle and fed standard mouse chow. Food and water were provided to the mice *ad libitum*.

Mice

To achieve specific *Fmr1* deletion in astrocytes, three different mouse lines were generated. In Group 1, Ctrl WT ERT2-Cre^{GFAP} (B6.Cg-Tg(*GFAP*-cre/ERT2)505Fmv/J RRID:IMSR_JAX:012849) male mice were crossed with *Fmr1*$^{flox/flox}$ female mice (generated in and obtained from the laboratory of Dr. David Nelson (Baylor College of Medicine, Houston, Texas) (Mientjes et al., 2006)) to obtain ERT2-Cre^{GFAP}*Fmr1*$^{flox/y}$ condition KO (cKO) male mice. In Group 2, ERT2-Cre^{GFAP} mice and ERT2-Cre^{GFAP}*Fmr1*$^{flox/flox}$ mice were crossed with Rosa-CAG-LSL-tdTomato reporter mice (CAG-tdTomato; RRID:IMSR_JAX:007909) to generate tdTomatoERT2-Cre^{GFAP} Ctrl WT and tdTomatoERT2-Cre^{GFAP}*Fmr1*$^{flox/y}$ cKO mice, respectively, allowing for tdTomato expression in astrocytes and analysis of *Fmr1* levels. In Group 3, ERT2-Cre^{GFAP} mice and ERT2-Cre^{GFAP}*Fmr1*$^{flox/flox}$ mice were crossed with Pvalb-tdTomato mice (Tg(Pvalb-tdTomato)15Gfng/J, RRID:IMSR_JAX:027395) to obtain Pvalb-tdTomato-ERT2-Cre^{GFAP} Ctrl WT and Pvalb-tdvTomato-ERT2-Cre^{GFAP}*Fmr1*$^{flox/y}$ cKO mice, respectively, allowing for tdTomato expression in parvalbumin (PV) inhibitory interneurons for analysis of inhibitory and excitatory synapses. Real-time PCR-based analysis of genomic DNA isolated from mouse tails was used to confirm genotypes by Transnetyx.

In all groups of mice, Ctrl WT and cKO mice received tamoxifen at P14 intraperitoneally (0.5 mg in 5 mg/ml of 1:9 ethanol/sunflower seed oil solution) once a

day for 5 consecutive days, and analysis was performed at P28 or P60 (see "Experimental Timeline" in Fig. 1a). Group 1 was used for immunohistochemistry, Western blot, ELISA, qRT-PCR, Nanostring, EEG, and behavioral analysis; Group 2 was used for immunohistochemical analysis of *Fmr1* expression levels; and Group 3 was used for immunohistochemical analysis of inhibitory and excitatory synapses.

Methods overview

As *Fmr1* is expressed in astrocytes during postnatal development (Jacobs & Doering, 2010; Pacey & Doering, 2007) and we observed major changes in PV cell development during postnatal day (P)14-P21, we used ERT2-Cre^{GFAP} line to delete *Fmr1* from astrocytes during the same P14-P21 period by administering tamoxifen daily from P14 to P19. To confirm deletion of FMRP in astrocytes, we examined expression of FMRP in the cortex of P28 mice using immunostaining, we also analyzed *Fmr1* mRNA levels in the hippocampus and cortex using qRT-PCR. Once deletion was established, all further analysis was performed in either P28 male mice or in adult P60-P70 male mice.

At P28, we analyzed the effects of astrocyte specific *Fmr1* deletion on gene expression in the hippocampus and cortex using the NanoString "Glial Profiling Panel" and qRT-PCR. Biochemical measurements of GFAP, $GABA_A$ receptors, as well as PV and ErbB4 were done in the hippocampus and cortex of cKO and Ctrl WT mice using Western blot, and an ELISA was performed to determine GABA concentration. Lastly, immunohistochemistry was used (1) to assess GABA levels in astrocytes, and (2) to analyze excitatory and inhibitory synapses by measuring vGlut1/PSD95 and

vGAT/Gephyrin co-localization in the hippocampus and cortex of cKO and Ctrl WT mice.

In adult P60-P70 mice, EEG recordings were performed in awake, freely moving mice to determine the long-term effects of postnatal FMRP deletion in astrocytes on neural oscillations in the adult auditory and frontal cortex at baseline and in response to sound (Lovelace, Ethell, Binder, & Razak, 2018b). Finally, we used established behavioral tests to examine hyperactivity, anxiety-like behaviors, and socialization in cKO mice.

Immunofluorescence

P28 male Ctrl WT and cKO mice were euthanized with isoflurane and sodium pentobarbital and perfused transcardially first with cold phosphate-buffered saline (PBS, 0.1 M) to clear out the blood and then with 4% paraformaldehyde (PFA) in 0.1M PBS for fixation. Brains were removed and post-fixed for 2–4h in 4% PFA. 40-100μm brain slices were obtained using a vibratome (5100mz Campden Instruments). Hippocampus, auditory cortex (AuC), and frontal cortex (FC) were identified using the brain atlas (Paxinos & Franklin, 2004). For each brain, an average of 5–6 brain slices were collected per region.

Immunostaining for FMRP was performed using antigen retrieval methods, as previously described (Lovelace et al., 2020). Briefly, 40μm brain slices obtained from tdTomatoERT2-Cre^{GFAP}*Fmr1*$^{flox/y}$ cKO and tdTomatoERT2-Cre^{GFAP} Ctrl WT male mice were stained overnight with mouse anti-FMRP (1:100; Developmental Studies Hybridoma Bank, catalog #2F5-1-s, RRID: AB_10805421). Secondary antibody was

donkey anti-mouse Alexa 488 (4µg/mL; Molecular Probes, catalog# A-21202, RRID: AB_141607). Slices were mounted on slides with Vectashield mounting medium containing DAPI (Vector Laboratories, catalog # H-1200, RRID:AB_2336790) and Cytoseal.

Immunostaining in 100µm brain slices containing hippocampus, auditory cortex, and frontal cortex was performed as previously described (Lovelace et al., 2020). For slices obtained from ERT2-Cre^{GFAP}*Fmr1*$^{flox/y}$ cKO or ERT2-Cre^{GFAP} Ctrl WT male mice, astrocyte cell bodies were identified by immunolabeling against Glutamine Synthetase using rabbit anti-Glutamine Synthetase antibody (1:500, Sigma-Aldrich Cat# G2781, RRID:AB_259853), and GABA immunoreactivity was detected by immunostaining with guinea pig anti-GABA antibody (1:500, Abcam Cat# ab17413, RRID:AB_443865). For slices obtained from Pvalb-tdvTomato-ERT2-Cre^{GFAP}*Fmr1*$^{flox/y}$ cKO and Pvalb-tdTomato-ERT2-Cre^{GFAP} Ctrl WT male mice, excitatory presynaptic boutons were labeled by immunostaining against vGlut1 using rabbit anti-vGlut1 antibody (0.25 mg/ml, Invitrogen, 482400, RRID:AB_2533843), and excitatory postsynaptic sites were identified with mouse anti-PSD95 antibody (1.65 µg/ml, Invitrogen, MA1-045, RRID:AB_325399). Inhibitory presynaptic sites were detected by immunolabeling against vesicular GABA transporter (vGAT) using rabbit anti-vGAT antibody (1:100, Synaptic Systems, 131002, RRID:AB_887871). Inhibitory postsynaptic sites were detected by immunolabeling against gephyrin using mouse anti-gephyrin antibody (1:500, Synaptic Systems, 147111, RRID:AB_887719). Secondary antibodies used were as follows: AlexaFluor-647-conjugated donkey anti-rabbit IgG (4mg/ml, Invitrogen, A-

31573, RRID:AB_2536183), AlexaFluor-488-conjugated goat anti-guinea pig IgG (4 mg/ml, Invitrogen, A-11073, RRID:AB_2534117), AlexaFluor-488-conjugated goat anti-mouse IgG (4 mg/ml, Invitrogen, A-11001, RRID:AB_2534069), AlexaFluor-488-conjugated donkey anti-rabbit IgG (4 mg/ml, Invitrogen, A-21206, RRID:AB_2535792), and AlexaFluor-647-conjugated donkey anti-mouse IgG (4mg/ml, Invitrogen, A-31571, RRID:AB_162542). Slices were mounted on slides with Vectashield mounting medium containing DAPI (Vector Laboratories, catalog # H-1200, RRID:AB_2336790) and Cytoseal.

Image Analysis

Confocal images of coronal brain slices containing CA1 hippocampus, superficial layers of AuC, and FC were taken with an SP5 confocal laser-scanning microscope (Leica Microsystems) as previously described with modifications (Koeppen et al., 2018; Nguyen et al., 2020). Briefly, high-resolution optical sections (1024 × 1024 pixel format) were captured with a 40× water-immersion and 1× zoom at 1μm step intervals to assess FMRP immunoreactivity. Confocal images of synaptic puncta were taken using a 40× objective (1.2 NA), and 1× zoom at high resolution (1024 × 1024 pixel format) with a 0.5 μm intervals. All images were acquired under identical conditions and processed for analysis as follows: (1) For analysis of overall FMRP immunoreactivity, superficial layers of AuC were analyzed per each brain slice from at least 3 animals per group. Cortical layers were identified as previously reported (Anderson, Christianson, & Linden, 2009) and used for layer-specific analysis. Image analysis was performed using ImageJ macro plugin PIPSQUEAK (https://labs.wsu.edu/sorg/research-resources/). 10

images in the Z-stack (1.194 pixels/μm) were compiled into a single image using ImageJ macro plugin PIPSQUEAK, scaled, and converted into 32-bit, grayscale, TIFF files. PIPSQUEAK was run in "semi-automatic mode" to select ROIs to identify individual FMRP-positive cells, which were then verified by a trained experimenter. Distributions of density and intensity were compared between experimental groups, to assess differences in FMRP cell density and intensity between Ctrl WT and cKO mice. (2) For analysis of FMRP immunoreactivity in astrocytes, astrocytes were visualized with tdTomato. Cell areas were outlined using selection tool, then cell area, integrated fluorescent intensity, and mean intensity were measured for FMRP in each astrocyte. (3) For analysis of GABA immunoreactivity in Glutamine Synthetase (GS) labeled astrocytes, astrocytic cell bodies in CA1 hippocampus, superficial layers of AuC, and FC were selected and outlined using selection tool. These ROIs were saved in the ROI manager and used to measure area and perform analysis of integrated fluorescent intensity and mean intensity of GABA in each astrocyte. (4) For the analysis of vGlut1/PSD95 co-localization onto PV cells, three-dimensional fluorescent images were created by the projection of each z stack containing 40-50 high-resolution optical serial sections (1024 × 1024 pixel format) taken at 0.224 μm intervals in the X-Y plane. td-Tomato labeled PV somas were selected for the analysis, then PSD95 and vGlut1 puncta (within 1 μm distance) onto PV soma were selected. Quantifications of vGlut/PSD95 co-localization on enclosed volume of PV cells (μm^3) were conducted using Neurolucida 360 software (MicroBrightField RRID:SCR_001775). (5) For the analysis of vGAT and Gephyrin, vGAT puncta were co-localized with td-Tomato labeled PV-positive pre-

synaptic boutons (within 0.5 µm distance). PV/vGAT puncta were then co-localized with Gephyrin puncta (within 1 µm distance). Quantification of vGAT/Gephyrin, PV/Gephyrin, and vGAT/PV puncta co-localization was conducted using Neurolucida 360 software (MicroBrightField RRID:SCR_001775). Statistical analysis was performed with unpaired *t* test using GraphPad Prism 7 software (RRID:SCR_002798). Data represent mean ± SEM.

RNA Extraction

Total RNA was extracted from the hippocampus and cortical regions of Ctrl WT and cKO mice (n=4 per group) using the RNeasy kit (Qiagen, Valencia, CA, USA) method (see location of cortical areas 1 and 2 in **Fig. 4.2**). First-strand complementary DNA (cDNA) was generated using iScript™ cDNA Synthesis Kit (Catalog #1708891, Bio-Rad), and reverse transcription of total RNA (500ng) was performed for 26 min at 37°C. All surfaces for tissue collection and processing were sanitized using 70% ethanol and then treated with an RNAse inhibitor (RNAse out, G-Biosciences, St. Louis, MO, USA) to maintain integrity of isolated RNA. cDNA obtained from the hippocampus was used for NanoString analysis, and cDNA from all regions was utilized for qRT-PCR.

NanoString nCounter Gene Expression Assays and Analysis

nCounter gene expression assays (NanoString Technologies) were performed for the Glial Profiling NanoString Panel. Briefly, panel codeset probes were hybridized with 150ng of total RNA per hippocampus sample over 18 hr at 65°C according to NanoString protocol. Hybridized RNA was then diluted in molecular grade water and loaded into nCounter SPRINT cartridge (NanoString), placed into nCounter SPRINT Profiler, and

quantified. RNA-conjugated probes were counted via NanoString Sprint Profiler technology.

nSolver and Advanced Analysis

Results from the panel were normalized in nSolver following best practices, and analyzed using nSolver and Advanced Analysis software according to previously published protocols (Bergersen, Barnes, Worth, David, & Wilson, 2021; Danaher et al., 2017). nSolver-generated heat maps were created using normalized data and agglomerative clustering, a bottom-up form of hierarchical clustering (NanoString User Manual C0019-08). For Advanced Analysis, normalized data was used (NanoString User Manual 10030-03). Differential expression (DE) analysis was performed to identify specific targets that exhibit significantly increased or decreased expression compared to Ctrl WT values. Gene set analysis was run to determine the change in direction of regulation within each pre-defined gene set relative to Ctrl WT. Global significance scores, a summary T-statistic used to measure change (NanoString User Manual 10030-03) were calculated, and the directed global significance scores were expressed via heatmap. Pathway analysis was also conducted to determine overall changes in pathways based on the first principal component of the targets within a pathway as annotated by NanoString (NanoString User Manual 10030-03). Direction of pathway change (up- or downregulated) was determined by cross referencing the pathway score with the corresponding volcano plot for that pathway. Summary pathway score plot colors are based on calculated scores and are represented as downregulation (yellow) to upregulation (blue).

Separate Statistical Analyses

Normalized linear counts for all genes in the panel were used in fold change analysis of cKO genes compared to Ctrl WT. Differentially expressed genes (DEGs) were defined by a p-value < 0.05. Statistical analysis was performed with unpaired Welch's t-test using GraphPad Prism 7 software (RRID:SCR_002798). Data represent mean ± standard error of the mean (SEM). Gene enrichment and functional annotation analyses of DEGs was performed using open source functional enrichment tool DAVID (https://david.ncifcrf.gov/home.jsp). All raw NanoString data is available on: https://www.dropbox.com/sh/19b420pr1nl1zlh/AAAJ_qe0uhyIjeNzFAwVECFsa?dl=0.

Quantitative Real Time PCR Analysis

qRT-PCR was carried out using PrimePCR Sybr Green Assays (Biorad, Hercules, CA, USA) with the following primers for mouse genes: *Fmr1, Gabra1, Gabra3, Gabrg2, Gabra4, Gabra5, Gabrd, Aldh1a1, DAO, GFAP, PV, ErbB4, NRG-3*, and *TrkB* (see **Table 4.10** for sequences of primers used for qRT-PCR). GAPDH was selected as a housekeeping gene and no changes in its expression were found across genotype. Relative quantification using the delta-delta ($2^{-\Delta\Delta Cq}$) method was used to compare changes in gene expression between cKO mice and Ctrl WT mice. Reactions were run in duplicate for each animal. Statistical analysis was performed with unpaired t-test using GraphPad Prism 7 software (RRID:SCR_002798). Data represent mean ± standard error of the mean (SEM).

Western Blot Analysis

The hippocampus and cortical regions (see location of cortical areas 1 and 2 in **Fig. 4.2**) were removed from each mouse (n=4 mice per group), cooled in PBS, and homogenized in ice-cold lysis buffer (50mM Tris-HCl, pH 7.4, 150mM NaCl, 5mM EDTA, 0.05% Triton X-100, and 1mM PMSF) containing protease inhibitor cocktail (Sigma, cat. # P8340) and phosphatase inhibitor cocktail (Sigma, cat. #P0044). The samples were processed as previously described with modifications (Lovelace et al., 2020). The samples were rotated at 4°C for at least 1h to allow for complete cell lysis and then cleared by centrifugation at 13,200 rpm for 15 min at 4°C. Supernatants were isolated and boiled in reducing sample buffer (Laemmli 2× concentrate, S3401, Sigma), and separated on 8–16% Tris-Glycine SDS-PAGE precast gels (EC6045BOX, Life Technologies). Proteins were transferred onto Protran BA 85 Nitrocellulose membrane (GE Healthcare) and blocked for 1h at room temperature in 5% skim milk (Catalog #170-6404, Bio-Rad). Primary antibody incubations were performed overnight at 4°C with antibodies diluted in TBS/0.1% Tween-20/5% BSA. The following primary antibodies were: rabbit anti-GABRG2 (1:1000; ThermoFisher Scientific, Catalog #14104-1-AP, RRID:AB_10693527); rabbit anti-GABRA5 (1:1000; ThermoFisher Scientific, Catalog #PA5-31163, RRID:AB_2548637); rabbit anti-GFAP (1:1000; Cell Signaling, Catalog #12389, RRID:AB_2631098); mouse anti-PV (1:1000; Millipore, Catalog #MAB1572, RRID: AB_2174013); rabbit anti-ErbB4 (1:1000; Cell Signaling, Catalog #4795, RRID:AB_2099883); and rabbit anti-βactin (1:2000; Abcam, Catalog #ab8227, RRID: AB_2305186).

Blots were washed 3 × 10 min with TBS/0.1% Tween-20 and incubated with the appropriate HRP-conjugated secondary antibodies for 1h at room temperature in a TBS/0.1% Tween-20/5% BSA solution. The secondary antibodies used were HRP-conjugated donkey anti-mouse IgG (Jackson ImmunoResearch, catalog #715-035-150, RRID: AB_2340770) or HRP-conjugated goat anti-rabbit IgG (Jackson ImmunoResearch, catalog #111-035-003, RRID: AB_2313567). After secondary antibody incubations, blots were washed 3 × 10min in TBS/0.1% Tween-20, incubated in ECL 2 Western Blotting Substrate (Thermo Scientific, catalog #80196) and a signal was collected with CL-XPosure film (Thermo Scientific, catalog #34090). For re-probing, membrane blots were washed in stripping buffer (2% SDS, 100mM β-mercaptoethanol, 50mM Tris-HCl, pH 6.8) for 30min at 55°C, then rinsed repeatedly with TBS/0.1% Tween-20, finally blocked with 5% skim milk, and then re-probed. The first set of blots were stained for PV, B-actin, and ErbB4. The second set of blots were probed for GABRG2, GABRA5, GFAP, and B-actin. Developed films were then scanned, and band density was analyzed by measuring band and background intensity using Adobe Photoshop CS5.1 software (RRID:SCR_014199). 3-4 samples per group (Ctrl WT vs. cKO) were run per blot, and precision/tolerance (P/T) ratios for individual cKO samples were normalized to P/T ratios of Ctrl WT samples with the similar actin levels. Statistical analysis was performed with unpaired t-test using GraphPad Prism 7 software (RRID:SCR_002798). Data represent mean ± standard error of the mean (SEM).

Enzyme-linked Immunosorbent Assay (ELISA)

GABA concentration in tissue lysates from hippocampus and cortical regions (see location of cortical areas 1 and 2 in **Fig. 4.2**) of Ctrl WT and cKO mice (n=4 per group) was measured using a competitive GABA ELISA Kit (OKEH02564) according to the manufacturer's instructions (AVIVA Systems Biology, San Diego, CA, USA). Briefly, the microtiter 96-well plate was pre-coated with an anti-GABA antibody. Standards or tissue lysate samples were added to the wells along with a fixed quantity of biotinylated GABA and incubated for 1h at 37°C. Excess unbound biotinylated GABA and sample or standard GABA was washed from the plate followed by incubation with avidin-HRP conjugate for 45 min at 37°C. After another wash cycle, TMB substrate was added to the wells allowing the enzymatic reaction to occur which generated a blue color product that changed to yellow after adding the acidic stop solution. The density of yellow coloration was measured by reading the absorbance at 450 nm on a plate reader (BioTek Instruments, Winooski, VT, USA), which is quantitatively proportional to the amount of biotinylated GABA captured in the well and inversely proportional to the amount of GABA which was contained in the sample or standard. A standard curve to assess GABA concentration was generated using the standards. A linear regression of GABA concentration (standard curve) and relative optical density (OD) at 450 nm based on the average fluorescence intensity was used to assess GABA concentration in the brain samples. Statistical analysis was performed comparing cKO samples to their Ctrl WT samples with unpaired t-test using GraphPad Prism 7 software (RRID: SCR_002798). Data represent mean ± standard error of the mean (SEM).

Surgery for *in vivo* EEG recordings

Age-matched adult P60-70 male Ctrl WT (n = 10) and cKO (n = 9) mice were used for the EEG studies as previously described with modifications (Lovelace et al., 2018b; Lovelace et al., 2020). Mice were anesthetized with isoflurane inhalation (0.2-0.5%) and an injection of ketamine and xylazine (K/X) (i.p. 80/10 mg/kg), and then secured in a bite bar, and placed in a stereotaxic apparatus (model 930; Kopf, CA). Artificial tear gel was applied to the eyes to prevent drying. Toe pinch reflex was used to measure anesthetic state every 10min throughout the surgery, and supplemental doses of K/X were administered as needed. Once the mouse was anesthetized, a midline sagittal incision was made along the scalp to expose the skull. A Foredom dental drill was used to drill 1mm diameter holes in the skull overlying the right auditory cortex (-1.6mm, +4.8mm), left frontal lobe (+3.0mm, -1.6mm), and left occipital (-4.2mm, -5.1mm) (coordinate relative to Bregma: anterior/posterior, medial/lateral). Three channel electrode posts from Plastics One (MS333-2-A-SPC) were attached to 1mm stainless steel screws from Plastics One (8L003905201F) and screws were advanced into drilled holes until secure. Special care was taken not to advance the screws beyond the point of contact with the Dura. Dental cement was applied around the screws, on the base of the post, and exposed skull. Triple antibiotic was applied along the edges of the dental cement followed by an injection of subcutaneous Buprenorphine (0.1mg/kg). Mice were placed on a heating pad to aid recovery from anesthesia. A second Buprenorphine injection was administered between 6 and 10 hours after surgery. Mice were then individually housed, returned to the vivarium and monitored daily until the day of EEG

recordings. The separation between the last post-surgical Buprenorphine injection and EEG recordings was between 3 and 5 days.

Electrophysiology

Baseline and auditory event-related potential (ERP) recordings were obtained using the BioPac system (BIOPAC Systems, Inc.) from awake and freely moving mice as published previously with modifications (Lovelace et al., 2018b). Mice were allowed to habituate to the recording chamber for 15 min prior to being connected to the BioPac system. A three-channel tether was connected to the electrode post (implanted during surgery) under brief isoflurane anesthesia. The mouse was then placed inside a grounded Faraday cage after recovery from isoflurane. This tether was then connected to a commutator located directly above the cage. Mice were then allowed to habituate while being connected to the tether for an additional 20 min before EEG recordings were obtained.

The BioPac MP150 acquisition system was connected to two EEG 100C amplifier units (one for each channel) to which the commutator was attached. The lead to the occipital cortex was used as reference for both frontal and auditory cortex screw electrodes. The acquisition hardware was set to high-pass (>0.5Hz) and low-pass (<100Hz) filters. Normal EEG output data were collected with gain maintained the same (10,000x) between all recordings. Data were sampled at a rate of either 2.5 or 5 kHz using Acqknowledge software and down sampled to 1024Hz post hoc using Analyzer 2.1 (Brain Vision Inc.). Sound delivery was synchronized with EEG recording using a TTL pulse to mark the onset of each sound in a train. Baseline EEGs were recorded for 5 min

(no auditory stimuli were presented), followed by recordings in response to auditory stimulation. After these experiments were completed, mice were returned to the colony and euthanized on a later date.

Acoustic Stimulation

All experiments were conducted in a sound-attenuated chamber lined with anechoic foam (Gretch-Ken Industries, OR) as previously described with modifications (Lovelace et al., 2018b; Lovelace et al., 2020). Acoustic stimuli were generated using RVPDX software and RZ6 hardware (Tucker-Davis Technologies, FL) and presented through a free-field speaker (MF1 Multi-Field Magnetic Speaker; Tucker-Davis Technologies, FL) located 12 inches directly above the cage. Sound pressure level (SPL) was modified using programmable attenuators in the RZ6 system. The speaker output was ~65-70dB SPL at the floor of the recording chamber with fluctuation of +/- 3 dB for frequencies between 5 and 35 kHz as measured with a ¼ inch Bruel & Kjaer microphone.

We used acoustic stimulation paradigms that have been previously established in *Fmr1* KO mice (Lovelace et al., 2018b), which is analogous to work in humans with FXS (Ethridge et al., 2017). A chirp-modulated signal (henceforth, 'chirp') to induce synchronized oscillations in EEG recordings was used. The chirp is a 2s broadband noise stimulus with amplitude modulated (100% modulation depth) by a sinusoid whose frequencies increase (Up-chirp) or decrease (Down-chirp) linearly in the 1-100 Hz range (Artieda et al., 2004; Pérez-Alcázar et al., 2008; Purcell, John, Schneider, & Picton, 2004). The chirp facilitates a rapid measurement of transient oscillatory response (delta to gamma frequency range) to auditory stimuli of varying frequencies and can be used to

compare oscillatory responses in different groups in clinical and pre-clinical settings (Purcell et al., 2004). Inter-trial coherence analysis (Tallon-Baudry, Bertrand, Delpuech, & Pernier, 1996) can then be used to determine the ability of the neural generator to synchronize oscillations to the frequencies present in the stimulus.

To avoid onset responses contaminating phase locking to the amplitude modulation of the chirp, the stimulus was ramped in sound level from 0-100% over 1s (rise time), which then smoothly transitioned into chirp modulation of the noise. Up and Down chirp trains were presented 300 times each (for a total of 600 trains). Both directions of modulation were tested to ensure any frequency specific effects were not due to the frequency transition history within the stimulus. Up- and Down- chirp trains were presented in an alternating sequence. The interval between each train was randomly varied between 1 and 1.5s.

To study evoked response amplitudes and habituation, trains of 100ms broadband noise were presented at two repetition rates, 0.25Hz (a non-habituating rate) and 4Hz (a strongly habituating rate) (Lovelace et al., 2016). Each train consisted of 10 noise bursts and the inter-train interval used was 8 seconds. Each repetition rate was presented 100 times in an alternating pattern (Lovelace et al., 2016). The onset of trains and individual noise bursts were tracked with separate TTL pulses that were used to quantify latency of response.

EEG Data Analysis

Data were extracted from Acqknowledge and files saved in a file format (EDF) compatible with BrainVision Analyzer 2.1 software as previously described with

modifications (Lovelace et al., 2018b; Lovelace et al., 2020). All data were notch filtered at 60Hz to remove residual line frequency power from recordings. EEG artifacts were removed using a semi-automatic procedure in Analyzer 2.1 for all recordings. Less than 20% of data were rejected due to artifacts from any single mouse. Baseline EEG data were divided into 2s segments and Fast Fourier Transforms (FFT) were calculated on each segment using 0.5Hz bins and then average power (μV^2/Hz) was calculated for each mouse from 1-100Hz. Power was then binned into standard frequency bands: Delta (1-4Hz), Theta (4-10Hz), Alpha (10-13Hz), Beta (13-30Hz), Low Gamma (30-55Hz), and High Gamma (65-100Hz). Responses to chirp trains were analyzed using Morlet wavelet analysis. Chirp trains were segmented into windows of 500ms before chirp onset to 500ms after the end of the chirp sound (total of 3s because each chirp was 2s in duration). EEG traces were processed with Morlet wavelets from 1-100Hz using complex number output (voltage density, μV/Hz) for ITPC calculations, and power density (μV^2/Hz) for non-phase locked single trial power (STP) calculations and baseline corrected non-phase locked single trial power (induced power). Wavelets were run with a Morlet parameter of 10 as this gave the best frequency/power discrimination. This parameter was chosen since studies in humans found most robust difference around 40Hz, where this parameter is centered (Ethridge et al., 2017). To measure phase synchronization at each frequency across trials Inter Trial Phase Coherence (ITPC) was calculated. The equation used to calculate ITPC is:

$$ITPC(f,t) = \frac{1}{n}\sum_{k=1}^{n}\frac{F_k(f,t)}{|F_k(f,t)|}$$

where *f* is the frequency, *t* is the time point, and *k* is trial number. Thus, $F_k(f,t)$ refers to the complex wavelet coefficient at a given frequency and time for the *k*th trial. There were no less than 275 trials (out of 300) for any given mouse after segments containing artifacts were rejected. All raw EEG data analysis is available on: https://www.dropbox.com/sh/kerg6hj3kcnon81/AABrMHa2BW8Rwckng8e9wZ9ba?dl=0

EEG Statistical Analysis

Statistical group comparisons of chirp responses (ITPC and STP) and broadband noise trains (ITPC and induced power) were quantified by wavelet analysis. Analysis was conducted by binning time into 256 parts and frequency into 100 parts, resulting in a 100x256 matrix. Non-parametric cluster analysis was used to determine contiguous regions in the matrix that were significantly different from a distribution of 1000 randomized Monte Carlo permutations based on previously published methods with modifications (Maris & Oostenveld, 2007). Briefly, if the cluster sizes of the real genotype assignments (both positive and negative direction, resulting in a two-tailed alpha of $p = 0.025$) were larger than 97.25% of the random group assignments, those clusters were considered significantly different between genotypes. This method avoids statistical assumptions about the data and corrects for multiple comparisons.

Because movement can alter cortical gain (Fu, Kaneko, Tang, Alvarez-Buylla, & Stryker, 2015; Niell & Stryker, 2010), and *Fmr1* KO mice show hyperactivity, a piezoelectric transducer was placed underneath the recording cage to detect when the mouse was moving. The term 'baseline' is used to indicate EEGs recorded in these mice

without any specific auditory stimuli. The term 'still' is used to describe baseline EEG when the mouse was stationary. The term 'moving' is used to describe baseline EEG when the mouse was moving based on a threshold criterion for the piezoelectric signal that was confirmed by analyzing the video recording (under IR light) that was taken throughout the EEG recording procedure. In all cases where genotype means are reported, SEM was used. The genotype differences in baseline power were analyzed on 6 dependent variables using one-way Multivariate analysis of co-variance (MANCOVA) with one covariate (movement), Independent Variables (IV): Genotype (Ctrl WT and cKO mice), dependent variables (DV): 6 frequency bins (delta to high gamma). The proportion of time spent moving during the 5-minute recording session was used as a covariate to isolate effects of genotype and control for the effect movement has on cortical gain. When multiple comparisons for MANCOVA were made, genotype comparisons were corrected using Bonferroni adjustments. The divisor for Bonferroni correction for multiple comparisons (for 6 frequency bands) on MANCOVA was set to 6, $\alpha = 0.05/6 = 0.0083$. Data are often expressed and plotted as ratio of control group values to gauge relative differences in various factors using the same scale.

Behavioral Assessments

Social Novelty Test

Sociability and social memory were studied in aged-matched adult Ctrl WT and cKO mice (n=8 per group) using a three-chamber test as described previously with minor modifications(Nguyen et al., 2020). Briefly, a rectangular box contained three adjacent chambers 19 × 45 cm each, with 30-cm-high walls and a bottom constructed from clear

Plexiglas. The three chambers were separated by dividing walls, which were made from clear Plexiglas with openings between the middle chamber and each side chamber. Removable doors over these openings permitted chamber isolation or free access to all chambers. All testing was done in a brightly lit room (650 lux), between 9:00 A.M. and 2:00 P.M. Before testing, mice were housed in a room with a 12 h light/dark cycle with *ad libitum* access to food and water. The cages were transferred to the behavioral room 30 min before the first trial began for habituation. The test mouse was placed in the central chamber with no access to the left and right chambers and allowed to habituate to the test chamber for 5 min before testing began. Session 1 measured sociability. In session 1, another mouse (Stranger 1) was placed in a wire cup-like container in one of the side chambers. The opposite side had an empty cup of the same design. The doors between the chambers were removed, and the test mouse was allowed to explore all three chambers freely for 10 min, while being digitally recorded from above. The following parameters were monitored: the duration of direct contact between the test mouse and either the stranger mouse or empty cup and the duration of time spent in each chamber. Session 2 measured social memory and social novelty preference. In session 2, a new mouse (Stranger 2) was placed in the empty wire cup in the second side chamber. Stranger 1, a now familiar mouse, remained in the first side chamber. The test mouse was allowed to freely explore all three chambers for another 10 min, while being recorded, and the same parameters were monitored. Placement of Stranger 1 in the left or right side of the chamber was randomly altered between trials. The floor of the chamber was cleaned with 2%-3% acetic acid, 70% ethanol, and water between tests to eliminate odor

trails. Assessments of the digital recordings were done using TopScan Lite software (Clever Sys., Inc., VA). To measure changes in sociability and social memory, percent time spent in each chamber was calculated in each test. Further, a sociability index $\left(\frac{time\ in\ S1\ chamber}{time\ in\ S1\ chamber\ +\ time\ in\ empty\ chamber}\right)$ and social novelty preference index $\left(\frac{time\ in\ S2\ chamber}{time\ in\ S2\ chamber\ +\ time\ in\ S1\ chamber}\right)$ were calculated as described previously (Nguyen et al., 2020; Nygaard, Maloney, & Dougherty, 2019). For sociability index, values <0.5 indicate more time spent in the empty chamber, >0.5 indicate more time spent in the chamber containing Stranger 1, and 0.5 indicates equal amount of time in both chambers. For social novelty preference index, values <0.5 indicate more time spent in the chamber containing Stranger 1 or now familiar mouse, >0.5 indicate more time spent in the chamber containing Stranger 2 or new stranger mouse, and 0.5 indicates equal amount of time in both chambers. Statistical analysis for time spent in each chamber was performed using two-way ANOVA followed by Bonferroni multiple comparison post-test, while statistical analysis for sociability index and social novelty preference index was performed with unpaired t-test using GraphPad Prism 7 software (RRID:SCR_002798). Data represent mean ± standard error of the mean (SEM).

Open-field test

Anxiety-like behaviors and locomotor activity were tested in age-matched adult Ctrl WT and cKO mice (n=8 per group) as described previously with modifications (Lovelace et al., 2020). A 72 × 72-cm open-field arena with 50-cm-high walls was

constructed from opaque acrylic sheets with a clear acrylic sheet for the bottom. The open field arena was placed in a brightly lit room, and one mouse at a time was placed in a corner of the open field and allowed to explore for 10 min while being recorded with digital video from above. The floor was cleaned with 2–3% acetic acid, 70% ethanol, and water between tests to eliminate odor trails. The mice were tested between the hours of 9:00 A.M. and 1:00 P.M., and this test was always performed prior to the elevated plus maze. The arena was subdivided into a 4 × 4 grid of squares with the middle of the grid defined as the center. A line 4 cm from each wall was added to measure thigmotaxis. Locomotor activity was scored by the analysis of total line crosses and speed using TopScan Lite software (Clever Sys., Inc., VA). A tendency to travel to the center (total number of entries into large and small center squares) and the time in thigmotaxis were used as an indicator of anxiety. The analysis was performed in 5 min intervals for the total 10 min exploration duration. Assessments of the digital recordings were performed blind to the condition. Statistical analysis was performed with unpaired t-test using GraphPad Prism 7 software (RRID:SCR_002798). Data represent mean ± standard error of the mean (SEM).

Elevated plus maze

The elevated plus maze consisted of four arms in a plus configuration. Two opposing arms had 15-cm tall walls (closed arms), and two arms were without walls (open arms). The entire maze sat on a stand 1 m above the floor. Each arm measured 30 cm long and 10 cm wide. Mice were allowed to explore the maze for 10 min while being recorded by digital video from above. The maze was wiped with 2–3% acetic acid, 70%

ethanol and water between each test to eliminate odor trails. This test was always done following the open-field test. TopScan Lite software was used to measure the percent of time spent in open arms and speed. The time spent in open arm was used to evaluate anxiety-like behavior while speed and total arm entries were measured to evaluate overall locomotor activity (Lovelace et al., 2020). The analysis was performed in 5 min intervals for the total 10 min exploration duration. Assessments of the digital recordings were done blind to the condition using TopScan Lite software. Statistical analysis was performed with unpaired t-test using GraphPad Prism 7 software (RRID:SCR_002798). Data represent mean ± standard error of the mean (SEM).

Results

In the current study we aimed to delineate the role of astrocytes in abnormal inhibition in FXS. We examined whether developmental FMRP deletion from astrocytes during postnatal period of inhibitory circuit refinements affects (1) GABAergic synapses; (2) PV cell development and connectivity in the hippocampus and cortex; (3) maturation of baseline and sound-evoked responses in the adult auditory cortex (AuC) and frontal cortex (FC); and (4) mouse behaviors, such as locomotor activity, anxiety and sociability.

Astrocyte-specific FMRP deletion during postnatal developmental period

To achieve specific *Fmr1* deletion in astrocytes, ERT2-Cre^{GFAP}*Fmr1*$^{flox/y}$ condition KO (cKO) (Group 1) were generated and ERT2-Cre^{GFAP} wild-type (WT) mice were used as controls (Ctrl WT; **Fig. 4.1A**). For analysis of FMRP levels in astrocytes, tdTomato was expressed in astrocytes using Rosa-CAG-LSL-

tdTomato reporter mice to generate tdTomatoERT2-Cre^{GFAP}*Fmr1*$^{flox/y}$ cKO mice and tdTomatoERT2-Cre^{GFAP} Ctrl WT mice (Group 2) (**Fig. 4.1A**). For analysis of connectivity of parvalbumin (PV) inhibitory interneurons tdTomato was expressed under *Pvalb* promoter in *Pvalb*-tdvTomato-ERT2-Cre^{GFAP}*Fmr1*$^{flox/y}$ cKO and *Pvalb*-tdTomato-ERT2-Cre^{GFAP} Ctrl WT mice (Group 3) (**Fig. 4.1A**). In all groups, Ctrl WT and cKO mice received tamoxifen at postnatal day (P)14 intraperitoneally (IP, 0.5 mg in 5 mg/ml of 1:9 ethanol/sunflower seed oil solution) once a day for 5 days, and analysis was performed at P28 or P60 (adult) (**Fig. 4.1A**).

We observed an overall reduction in *Fmr1* (exon 16/17) mRNA levels in the hippocampus and cortex of P28 cKO mice using qRT-PCR (**Fig. 4.1B, Fig. 4.2, Table 4.1)**. To confirm specific ablation of *Fmr1* in astrocytes, FMRP immunoreactivity was analyzed in the cortex of tdTomatoERT2-Cre^{GFAP} Ctrl WT (**Fig. 4.1C**) and tdTomatoERT2-Cre^{GFAP}*Fmr1*$^{flox/y}$ cKO mice at P28 (**Fig. 4.1D**). Although no significant changes were observed in FMRP+ cell density (**Fig. 4.1E)** and FMRP levels in FMRP+ cells (**Fig. 4.1F**) between genotypes, FMRP immunoreactivity was significantly decreased in cortical astrocytes of cKO mice compared to Ctrl WT (**Fig. 4.1G, Table 4.1**). The results confirm successful deletion FMRP specifically from developing astrocytes during the postnatal P14-P28 window, without affecting FMRP levels in neurons.

Postnatal deletion of *Fmr1* from astrocytes alters expression of genes involved in GABAergic transmission.

To determine if postnatal deletion of *Fmr1* from astrocytes affects gene expression, we analyzed mRNA levels of selected glial and neuronal genes in the hippocampus and cortex of P28 Ctrl WT and cKO mice (**Fig. 4.2**). Hippocampal mRNA expression was first analyzed with NanoString "Glial Profiling" panel (**Fig. 4.3A).** Analysis identified 81 differentially expressed genes (DEGs), including 66 downregulated and 15 upregulated DEGs (**Fig. 4.3C**). Using DAVID analysis (**Fig. 4.4**) we found that although some of the 81 DEGs were glial specific (**Fig. 4.5**), most of DEGs were associated with synaptic signaling (**Fig. 4.6**), regulation of synaptic plasticity, GABAergic synaptic transmission and GABA receptor complex **(Fig. 4.4A-C)**. Further Gene Ontology (GO) analysis indicated strongly association of DEGs with the "Synaptic vesicle cycle" and "GABAergic synapse" pathways in the Kyoto Encyclopedia of Genes and Genomes (KEGG) pathway database (**Fig. 4.4D**). As previous studies have indicated that $GABA_A$ receptors ($GABA_AR$), are affected in FXS(Braat & Kooy, 2015; D'Hulst et al., 2006; Gao et al., 2018; Gatto, Pereira, & Broadie, 2014; Sabanov et al., 2017), we further analyzed the specific genes encoding subunits of $GABA_AR$ in the hippocampus followed by qRT-PCR analysis of mRNA expression in the cortex.

NanoString normalized gene expression data indicate that some but not all genes associated with GABAergic transmission were dysregulated (**Fig. 4.7A)**. We found no significant differences in mRNA levels of neuronal GABA synthesizing enzymes Gad1 and Gad2 in the hippocampus between genotypes (**Fig. 4.7B**). However, mRNA

expression of Gabra1, Gabra3 and Gabrg2 genes encoding synaptic $GABA_AR$ subunits was significant decreased in the hippocampus (NanoString) and cortex (qRT-PCR) of cKO mice compared to Ctrl WT (**Fig. 4.7C**, **Table 4.2**). Interestingly, we found no changes in the expression of Gabra4, Gabra5 and Gabrd genes that encode extrasynaptic $GABA_AR$ subunits **(Fig. 4.7D),** as well as Gabrb3 that is associated with both synaptic and extrasynaptic $GABA_AR$ (**Fig. 4.7B**). Consistent with the reduced mRNA levels, we also observed a significant decrease in the protein levels of synaptic $GABA_AR\gamma2$ subunit but not extrasynaptic $GABA_AR\alpha5$ subunit in cKO mice compared to Ctrl WT (**Fig. 4.7E-F, Table 4.2**). Taken together these data indicate that postnatal deletion of *Fmr1* from astrocytes affects the expression of synaptic $GABA_AR$ subunits, while the levels of extrasynaptic $GABA_AR$ subunits remain unchanged.

Astrocytic GABA is significantly increased in the hippocampus and cortex of cKO mice.

Reduced synaptic $GABA_AR$ gene expression may serve to compensate for increased GABA concentration, which we observed in the hippocampus and cortex of cKO mice (**Fig. 4.8A, Table 4.3**). As FRMP is deleted only from astrocytes the changes in the levels of GABA may suggest astrocyte-mediated mechanism. Indeed, we observed a significant increase in mRNA expression levels of GABA-synthesizing enzymes Aldh1a1 (**Fig. 4.8B**) and DAO (**Fig. 4.8C**), which convert putrescine into GABA in astrocytes (**Fig. 4.8B-C, Table 4.3**). Consistent with published study showing that reactive astrocytes with enhanced GFAP immunoreactivity are shown to synthesize more GABA(Lin, Polsky, & Matesic, 1993) through the putrescine-mediated mechanism, we

also observed a significant increase in GFAP mRNA and protein levels in the cortex of cKO mice (**Fig. 4.8D-E, Table 4.3**). Lastly, to demonstrate that *Fmr1* deficient astrocytes were producing higher levels of GABA in the hippocampus and cortex of cKO mice, we analyzed GABA immunoreactivity in glutamate synthetase (GS)-positive astrocytes (**Fig. 4.8F, Table 4.3**). Our data indicate that deletion of *Fmr1* from astrocytes during postnatal development of inhibitory circuits leads to increased GABA levels in astrocytes, which may trigger a compensatory decrease in synaptic $GABA_A$ receptors.

Deletion of *Fmr1* from astrocytes leads to impaired development of PV-expressing inhibitory cells.

It is also possible that a decrease in $GABA_A$ receptor levels is a result of reduced connectivity between PV cells and Pyramidal neurons (Pyr), which was previously observed in global *Fmr1* KO mice (Gibson et al., 2008; Hays et al., 2011). PV-expressing cells are fast-spiking inhibitory interneurons that provide temporal precision to excitatory responses and their loss and hypofunction may contribute to cortical hyperexcitability in individuals with autism (Ferguson & Gao, 2018; Filice, Janickova, Henzi, Bilella, & Schwaller, 2020; Hashemi, Ariza, Rogers, Noctor, & Martinez-Cerdeno, 2017; Lunden, Durens, Phillips, & Nestor, 2019; Marin, 2012; Rossignol, 2011) and mouse models of autism, including FXS (Goel et al., 2018; T. H. Wen et al., 2018). Interestingly, we observed a significant decrease in PV mRNA levels in the developing hippocampus and cortex following FMRP deletion from astrocytes (**Fig. 4.9A**). However, PV protein levels were only reduced in the cortex (**Fig. 4.9E, Table 4.4**). We also found a significant decrease in mRNA levels of ErbB4 (**Fig. 4.9B**) in the hippocampus and cortex, however

ErbB4 protein levels were only reduced in the hippocampus (**Fig. 4.9F, Table 4.4**). ErbB4 is expressed by a majority of PV+ cells (Fazzari et al., 2010; L. Wen et al., 2010) and plays an important role in establishing connections with Pyr excitatory neurons as well as PV cell survival (Sun et al., 2016). Although we did not observe changes in the expression of ErbB4 ligand Neuroregulin 1 (NRG-1) that is expressed by both astrocytes and neurons, there was a significant decrease in mRNA levels of neuronal NRG-3, an ErbB4 receptor ligand that is expressed by excitatory neurons at the synaptic connections between Pyr and PV cells (Exposito-Alonso et al., 2020; Muller et al., 2018) (**Fig. 4.9C, Table 4.4**). In contrast, mRNA level of BDNF receptor TrkB was significantly up-regulated (**Fig. 4.9D, Table 4.4)**, that is also implicated in PV cell development and survival, including mouse model of FXS (Nomura et al., 2017).

Since NRG-3/ErbB4 interactions promote excitatory synapse formation on parvalbumin-positive (PV) interneurons (Exposito-Alonso et al., 2020; Muller et al., 2018), we examined whether reduced expression of the genes affects the number of excitatory synapses on tdTomato-expressing PV inhibitory neurons by analyzing presynaptic vGlut1 and postsynaptic PSD95 puncta in the auditory cortex of Pvalb-tdvTomato-ERT2-Cre^{GFAP}*Fmr1*$^{flox/y}$ cKO and Pvalb-tdTomato-ERT2-Cre^{GFAP} Ctrl WT male mice (**Fig. 4.9G-H**). Our preliminary data indicates that there is a significant decrease in vGlut1/PSD95 puncta colocalization onto PV neurons in superficial layers of AuC of cKO mice compared to Ctrl WT (**Fig. 4.9H, Table 4.5)**. Lastly, to determine whether astrocyte-specific deletion of *Fmr1* affects the PV innervation of Pyr neurons, inhibitory perisomatic synaptic sites were detected with immunostaining against VGAT

and gephyrin in association with PV-positive pre-synaptic boutons that were visualized with tdTomato in *Pvalb*-tdvTomato-ERT2-Cre^{GFAP}*Fmr1*$^{flox/y}$ cKO and Pvalb-tdTomato-ERT2-Cre^{GFAP} Ctrl WT male mice (**Fig. 4.9I)**. We observed a significant decrease in vGAT/Gephyrin, PV/Gephyrin, and vGAT/PV puncta colocalization in superficial layers of AuC of cKO mice compared to Ctrl WT , suggesting reduced PV innervation of Pyr neurons (**Fig. 4.9J-L**, **Table 4.5)**. Taken together, our results suggest that the loss of astrocytic *Fmr1* results in reduced excitatory synapse formation onto PV neurons, possibly to compensate for increased GABA produced by astrocytes. The reduced excitatory drive onto PV inhibitory neurons in the developing cortex may contribute to impaired PV function and lower inhibitory activity, resulting in an overall increased cortical excitability in astrocyte-specific *Fmr1* cKO mice.

Enhanced baseline EEG gamma band power and impaired power coupling across frequencies are observed in the auditory and frontal cortex of adult cKO mice.

If impaired GABAergic signaling, including PV cell loss and reduced $GABA_AR$ levels, underlies abnormal neural oscillations in the cortex of global *Fmr1* KO mice (Lovelace et al., 2018b), then we should see similar deficits in astrocyte-specific cKO mice. To test this hypothesis, we first measured baseline electrocortical activity in adult cKO mice using EEG recordings. Spectral density of baseline (no sound simulation) EEG power was calculated in AuC and FC of Ctrl WT (n=10) and cKO (n=9) mice. Enhanced high frequency gamma oscillations are apparent from the examples of 2s raw traces (**Fig. 4.10A**) and group average power spectral densities from 5-min EEG recordings in both AuC (**Fig. 4.10B, C)** and FC (**Fig. 4.10B, E)** of cKO mice compared to Ctrl WT.

Statistical analysis was performed using a one-way MANCOVA approach with percentage time spent moving as a covariate to compare genotype mean differences on 6 bands per region: Delta (1-4Hz), Theta (4-8Hz), Alpha (8-13Hz), Beta (13-30Hz), Low Gamma (30-55Hz), and High Gamma (65-100Hz) that was further sub-divided into low (30-60 Hz) and high (>60 Hz) gamma frequency bands. We confirmed assumptions of equality of covariance using Box's M, $p = 0.071$ (for Ctrl WT vs. cKO **Auc**) and $p = 0.319$ (for Ctrl WT vs cKO **FC**). Levene's test of equality of error variance showed no difference in variance between genotypes in any of the bands (all $p > 0.05$). A significant effect of genotype (**AuC**: Ctrl WT vs. cKO: Pillai's Trace = 0.748, $p = 0.020$; **FC**: Ctrl WT vs. cKO: Pillai's Trace = 0.707, $p = 0.038$) was observed across all 6 of the combined frequency variables, which included movement as a covariate. Further post-hoc comparisons identified significant differences between genotypes in gamma power, including low and high gamma power, in both AuC (**Fig. 4.10D**) and FC (**Fig. 4.10F**) after correction for multiple comparisons (**Table 4.6**).

Human EEG studies also report power abnormalities in delta, theta and alpha frequencies, as well as impaired coupling between low- and high-frequency oscillations in individuals with FXS and ASD (D. Sinclair, B. Oranje, K. Razak, S. Siegel, & S. Schmid, 2017; Wang et al., 2013). To assess the relationship between power across different frequencies and/or regions, a Pearson's correlation analysis was done using the same approach that was used in a clinical study of FXS (Wang et al., 2013) (**Fig. 4.10G)**. While there was a positive correlation in power coupling of the AuC Delta/AuC Gamma (D1/G1), AuC Theta/AuC Gamma (T1/G1), and AuC Alpha/AuC Gamma (A1/G1) in

Ctrl WT mice, the correlation was lost in astrocyte-specific *Fmr1* cKO mice (**Fig. 4.10G, Table 4.7**). Results also show a positive correlation in power coupling of the Delta/Gamma in the FC of Ctrl WT mice, but not in cKO mice (D2/G2, **Fig. 4.10G, Table 4.7**). Similar results were observed for delta and theta coupling to gamma between AuC and FC (D1/G2, T1/G2 for AuC to FC and D2/G1 for FC to AuC correlations, **Fig. 4.10G, Table 4.7**). Overall, these findings indicate that abnormalities in baseline gamma power and EEG power coupling between low- and high-frequency oscillations in the AuC and across brain areas, suggesting that GABA changes in astrocytes and impaired connectivity between Pyr and PV cells most likely influence neuronal activity, leading to abnormal synchronization in firing of excitatory and inhibitory neurons.

Postnatal deletion of *Fmr1* from astrocytes affects phase locking to sound chirp in the auditory and frontal cortex of adult mice.

Abnormal GABAergic signaling and PV cell development would most likely affect sound-evoked responses. This was examined by analyzing the ability of the cortex to mount a consistent phase locking to frequency-modulating sound (chirp) across sound presentation trials. After repeated chirp presentations (300 trials for up, 300 for down), the inter-trial phase coherence (ITPC) was calculated across trials in the time X frequency domain using Morlet Wavelet analysis as previously described (Lovelace et al., 2018b; Lovelace et al., 2020). Here, the results are presented only for 'up' chirp, because the responses to modulation frequencies were not affected by the direction of frequency change in the sound when 'up' or 'down' chirps were tested. After grand average ITPC was calculated for each group, means for Ctrl WT mice (n=10) were

subtracted from the means for cKO mice (n=9) (AuC, **Fig. 4.11A;** FC, **Fig. 4.11B**). For statistical comparisons, non-parametric cluster analysis was used to determine contiguous regions in the time X frequency domain that were statistically different between genotypes. We observed a significant decrease in ITPC at beta (13-30Hz) and gamma frequencies (30-100Hz) in AuC (**4.11A**) and FC (**Fig. 4.11B**) of cKO mice. These data indicate that postnatal deletion of FMRP from astrocytes can result in the development of gamma synchronization deficits in adult mice as was previously observed global *Fmr1* KO mice (Lovelace, Ethell, Binder, & Razak, 2018a).

Next, we investigated non-phase locked single trial power (STP) during the chirp stimulation period (**Fig. 4.11C-D, Fig. 4.12**) because any increase in gamma power during the duration of acoustic stimulation is predicted to decrease the ability of the neural generators to produce temporally consistent responses to the dynamic chirp stimulus. cKO mice showed a significant increase in non-phase locked background gamma power in AuC (**Fig. 4.11C**) and FC (**Fig. 4.11D**) in the entire gamma band (~30-100Hz), similar to the findings in the global *Fmr1* KO mouse (Lovelace et al., 2018b) and in humans with FXS (Ethridge et al., 2017). These results suggest that astrocytes might indirectly control frequency-modulated responses to sound by enhancing background gamma power, most likely by influencing the activity of fast-spiking inhibitory interneurons via alterations in both synaptic and tonic GABAergic signaling.

Postnatal deletion of *Fmr1* from astrocytes affects alpha and gamma synchronization and amplifies on-going response to broadband noise in the cortex of adult cKO mice.

To compared sound-evoked responses to trains of brief (100 ms) broadband noise stimuli (10 noise stimuli per train, 65-70 dB SPL, 100 repetitions of each train), we tested both a non-habituating repetition rate (0.25Hz) and a habituating rate of sound presentation (4Hz) (Lovelace et al., 2020; Lovelace et al., 2016). Example traces are shown for the first stimulus in the 0.25 Hz train (**Fig. 4.13A**) and the first 4 stimuli in the 4Hz train (**Fig. 4.12B**) in AuC and FC of Ctrl WT and cKO. We measured both ITPC and a magnitude of the onset and on-going responses for each repetition rate. There was a decrease in ITPC at ~30-40Hz (low gamma) and ~60-70Hz (high gamma) during a single 0.25Hz sound presentation in both AuC and FC (**Fig. 4.13C**) with an additional decrease at ~8-13Hz (alpha) in AuC, Analysis of the first 4Hz train of sounds also revealed a decrease in ITPC at ~8-13Hz (alpha) and ~30-40Hz (low gamma) during the first sound in the train in the AuC and FC of cKO mice (**Fig. 4.13D**). In FC we also observed an additional decrease at ~20-30Hz (beta) during the first and fourth sound in the train, but an increase at ~10-13Hz (alpha) during the fourth sound, suggesting reduced habituation (**Fig. 4.13D**). These data suggest that cKO mice show reduced synchrony of sound-evoked responses in alpha and gamma range, which is consistent with decreased phase locking in the gamma band during the chirp stimuli. Interestingly, we also observed some unique differences in FC suggesting changes in the synchronized responses in alpha frequency range during sound habituation.

In contrast to impaired gamma synchronization, we observed enhanced power of the response in gamma range in the AuC but not FC during the onset of single sound presentation at 0.25Hz repletion rate and all four sounds in 4Hz sound train (**Fig. 4.13E-F**). In addition, both the AuC and FC exhibited enhanced "on-going" power across frequencies after sound presentation at 0.25Hz rate, indicating increased on-going activity potentially due to impaired inhibition (Rotschafer & Razak, 2013). Lastly, in both the AuC and FC, increased onset and on-going power is observed at ~10-30Hz frequencies during the presentation of all four sounds in 4Hz sound train (**Fig. 4.13F**). This increase of on-going oscillation power is visually apparent in the example traces shown in **Fig. 4.13B**, where cKO shows higher amplitude oscillations throughout the sound train compared to Ctrl WT group. These results demonstrate high sound-induced power during both sound onset and on-going responses following sound presentation in the alpha, beta and gamma frequency range in adult mice following postnatal FMRP deletion from astrocytes with some differences between AuC and FC.

Postnatal deletion of *Fmr1* in astrocytes leads to increased locomotor activity and decreased socialization in adult cKO mice.

Cortical hyperexcitability as a result of aberrant PV cell development and impaired inhibition is also observed in several ASD mouse models (Lee, Lee, & Kim, 2017) and may underlie ASD-like behaviors, such as impaired social behaviors, as well as enhanced anxiety and hyperactivity. Therefore, we tested adult male Ctrl WT and cKO mice (n=8 per group) for hyperactivity, anxiety-like behaviors, and sociability in elevated plus maze (**Fig. 4.14A-B**), open field (**Fig. 4.14C-D**) and three-chamber (**Fig. 4.14E-F**)

tests. cKO mice demonstrated increased locomotor activity by making significantly more total arm entries (**Fig. 4.14A),** significantly more line crosses (**Fig. 4.14C**) and by showing a significant increase in speed than Ctrl WT mice **(Fig. 4.14A, C**, **Table 4.8**). However, cKO mice showed no changes in anxiety-like behaviors when compared to Ctrl WT mice (**Fig. 4.14B, D**). Assessment of sociability and social novelty preference using a three-chamber test showed impaired sociability of adult male cKO mice in session 1 (**Fig. 4.14E, Table 4.9**), as well as impaired social novelty preference in session 2 (**Fig. 4.14F, Table 4.9**). Our findings establish that postnatal deletion of FMRP from astrocytes leads to increased locomotor activity and impaired socialization in adult mice, while no changes are observed in anxiety-like behaviors.

Discussion

Recent studies in human and mouse models of FXS and other ASDs suggest that impaired inhibition, in particular the development of PV-expressing interneurons, underlies cortical hyperexcitability through yet unknown mechanism. The main findings of this study support a novel non-neuronal mechanism of cortical hyperexcitability and demonstrate that the deletion of *Fmr1* from astrocytes during postnatal developmental period of inhibitory circuit refinements affects (1) GABAergic synapses and GABA levels; (2) PV cell development and connectivity; (3) electrocortical EEG activity and cortical responses to sound; and (4) FXS-associated behaviors including hyperactivity and sociability in adult mice.

First, we found that postnatal *Fmr1* deletion from astrocytes leads to increased astrocytic GABA levels, but decreased expression of synaptic $GABA_AR$ and genes involved in synaptic wiring and survival of PV interneurons. Previous studies have shown reduced expression of astroglial glutamate transporter GLT1 and impaired clearance of extracellular glutamate in astroglial *Fmr1* cKO mice that may contribute to enhanced hyperexcitability (Higashimori et al., 2013; Higashimori et al., 2016; Jin et al., 2021). However, whether astrocytic *Fmr1* affects GABA-mediated signaling remains largely unexplored. FMRP is shown to target the mRNAs encoding eight different $GABA_AR$ subunits (α1, α3, α4, β1, β2, γ1, γ2, and δ) (D'Hulst et al., 2006; Olmos-Serrano et al., 2010; Sabanov et al., 2017; N. Zhang et al., 2017), which are downregulated in the neocortex of *Fmr1* KO mice (Adusei et al., 2010; D'Hulst et al., 2009; Gantois et al., 2006) and humans with FXS (D'Hulst et al., 2015). However, clinical trials using drugs that enhance $GABA_AR$ signaling failed to show clinical benefits (Braat & Kooy, 2015; Erickson et al., 2011). Our findings demonstrate that astrocyte-specific deletion of *Fmr1* also leads to reduced expression of synaptic $GABA_AR$ subunits α1, α3, and γ2, indicating that the reduced $GABA_AR$ levels cannot be explained by direct interaction between FMRP and $GABA_AR$ mRNA in neurons. In contrast, the expression of extrasynaptic $GABA_A$ receptor subunits α5 and δ remained unchanged in astrocyte-specific *Fmr1* cKO mice, which is consistent with a study on FX human neurons derived from three different lines of FXS-hESCs that also showed no changes in extrasynaptic $GABA_AR$ δ subunit (Telias, Segal, & Ben-Yosef, 2016).

Extrasynaptic $GABA_AR$ subunits α5 and δ play important role in tonic inhibition (Caraiscos et al., 2004) and tonic GABA-mediated currents are shown to be reduced in subiculum of global *Fmr1* KO mice (Curia et al., 2009), which is also consistent with reported decrease in GABA levels (Braat & Kooy, 2015; Olmos-Serrano et al., 2010). However, postnatal deletion of *Fmr1* from astrocytes lead to GABA increase, specifically in astrocytes, and showed no changes in the expression of extrasynaptic $GABA_AR$ subunits α5 and δ in both hippocampus and cortex. Increased GABA levels in astrocytes can be explained by increased GABA production from putrescine through the DAO/Adh1a1 (Kwak et al., 2020), GABA-synthesizing enzymes that were upregulated in astrocyte-specific *Fmr1* cKO mice. It is still unclear whether the upregulation of astrocytic GABA affects tonic inhibition or if there is an alteration in the trafficking of the $GABA_AR$ to the membrane surface. In addition, other subunits responsible for tonic $GABA_ARs$ may be downregulated in astrocyte-specific *Fmr1* cKO mice. Although FMRP loss from neurons most likely contributes to the changes in tonic inhibition in FXS, our data suggest that the role of astrocytic GABA should be considered in clinical studies targeting tonic inhibition in FXS as it may differentially affect GABAergic signaling in neurons and astrocytes.

Second, decreased levels of PV, ErbB4 and NRG-3 as well as a reduction in synaptic $GABA_AR$ can be explained by the loss of PV-expressing GABAergic interneurons and impaired connectivity between excitatory neurons and PV cells. ErbB4 signaling is implicated in PV cell survival (Sun et al., 2016), and along with NRG-3 is shown to play an important role in the development of connections between PV cells and

pyramidal excitatory neurons (Exposito-Alonso et al., 2020). Indeed, we observed a reduction in excitatory drive onto PV-expressing neurons, as well as changes in the density of vGAT/PV positive bouton at GABAergic synapses. Abnormal density and function of PV cells is a common finding in FXS and is proposed to underlie cortical hyperexcitability (Contractor et al., 2015; Goel et al., 2018; Selby, Zhang, & Sun, 2007). Although the mechanism of PV cell dysfunction in astrocyte-specific *Fmr1* KO is still unclear, previous studies support the role of *Fmr1*KO astrocytes in synaptic changes in neurons that can be restored by *Fmr1* expression in astrocytes (Jacobs & Doering, 2010).

Third, our findings show that similar to global *Fmr1* KO mice loss of *Fmr1* from astrocytes impaired sound-evoked gamma synchronization in the adult AuC and FC, while baseline gamma power was enhanced. The abnormal sound-evoked gamma synchronization is consistent with the observed reduction in synaptic $GABA_A$Rs and PV-positive inhibitory connections as cortical gamma oscillations are linked to the function of PV interneurons (Cardin et al., 2009; Sohal, Zhang, Yizhar, & Deisseroth, 2009; Volman, Behrens, & Sejnowski, 2011). Our data also show that induced power of alpha and gamma oscillations was higher during sound onset and remained elevated after the sound presentation supporting disfunction in inhibitory control of cortical activity. The deficits in gamma phase–locking to sound and prolonged responses may cause sensory discrimination deficits (Cardin et al., 2009; Sohal et al., 2009) and can lead to delayed language and cognitive impairments in FXS.

Indeed, we observed reduced social interactions and increased locomotor activity in astrocyte-specific *Fmr1* cKO mice. Astrocytes are known to modulate cognitive

functions and complex animal behaviors, such as emotion, motor activity, memory formation, and sensory processing (Oliveira, Sardinha, Guerra-Gomes, Araque, & Sousa, 2015). Our current study presents direct evidence that astrocytic FMRP modulates FXS-related behaviors, especially locomotor activity and social behaviors, most likely through the regulation of PV cell development and functions. Although how astrocytes modulate inhibition remains largely unknown, some progress has been made in defining astrocyte-mediated mechanisms in modulating synaptic connectivity and plasticity in the developing and adult CNS (Clarke & Barres, 2013; Nguyen et al., 2020; Tan, Burrus Lane, & Eroglu, 2021). Indeed, alterations of astroglia-secreted synaptogenic signals have been observed in *Fmr1* KO mice (Wallingford, Scott, Rodrigues, & Doering, 2017). In addition, our analysis of gene expression in the hippocampus and cortex of astrocyte-specific *Fmr1* cKO mice has identified a number of genes that are directly linked to GABAergic synaptic transmission and inhibition.

Together, our findings provide a novel insight into the role of astrocytic FMRP in the development of cortical hyperexcitability, suggest non-neuronal mechanism of abnormal inhibitory circuit development in FXS and call for a better understanding how astrocytes shape inhibitory responses in the healthy and diseased brain with direct consequences for therapeutic interventions in FXS and other ASDs.

References

Adusei, D. C., Pacey, L. K., Chen, D., & Hampson, D. R. (2010). Early developmental alterations in GABAergic protein expression in fragile X knockout mice. *Neuropharmacology, 59*(3), 167-171. doi:10.1016/j.neuropharm.2010.05.002

Anderson, L. A., Christianson, G. B., & Linden, J. F. (2009). Mouse auditory cortex differs from visual and somatosensory cortices in the laminar distribution of cytochrome oxidase and acetylcholinesterase. *Brain Res, 1252*, 130-142. doi:10.1016/j.brainres.2008.11.037

Antoine, M. W., Langberg, T., Schnepel, P., & Feldman, D. E. (2019). Increased Excitation-Inhibition Ratio Stabilizes Synapse and Circuit Excitability in Four Autism Mouse Models. *Neuron*. doi:10.1016/j.neuron.2018.12.026

Artieda, J., Valencia, M., Alegre, M., Olaziregi, O., Urrestarazu, E., & Iriarte, J. (2004). Potentials evoked by chirp-modulated tones: a new technique to evaluate oscillatory activity in the auditory pathway. *Clin Neurophysiol, 115*(3), 699-709. doi:10.1016/j.clinph.2003.10.021

Bergersen, K. V., Barnes, A., Worth, D., David, C., & Wilson, E. H. (2021). Targeted Transcriptomic Analysis of C57BL/6 and BALB/c Mice During Progressive Chronic Toxoplasma gondii Infection Reveals Changes in Host and Parasite Gene Expression Relating to Neuropathology and Resolution. *Front Cell Infect Microbiol, 11*, 645778. doi:10.3389/fcimb.2021.645778

Braat, S., & Kooy, R. F. (2015). The GABAA Receptor as a Therapeutic Target for Neurodevelopmental Disorders. *Neuron, 86*(5), 1119-1130. doi:10.1016/j.neuron.2015.03.042

Brown, M. R., Kronengold, J., Gazula, V. R., Chen, Y., Strumbos, J. G., Sigworth, F. J., . . . Kaczmarek, L. K. (2010). Fragile X mental retardation protein controls gating of the sodium-activated potassium channel Slack. *Nat Neurosci, 13*(7), 819-821. doi:10.1038/nn.2563

Caraiscos, V. B., Elliott, E. M., You-Ten, K. E., Cheng, V. Y., Belelli, D., Newell, J. G., . . . Orser, B. A. (2004). Tonic inhibition in mouse hippocampal CA1 pyramidal neurons is mediated by alpha5 subunit-containing gamma-aminobutyric acid type A receptors. *Proc Natl Acad Sci U S A, 101*(10), 3662-3667. doi:10.1073/pnas.0307231101

Cardin, J. A., Carlén, M., Meletis, K., Knoblich, U., Zhang, F., Deisseroth, K., . . . Moore, C. I. (2009). Driving fast-spiking cells induces gamma rhythm and controls sensory responses. *Nature, 459*(7247), 663-667. doi:10.1038/nature08002

Castrén, M., Pääkkönen, A., Tarkka, I. M., Ryynänen, M., & Partanen, J. (2003). Augmentation of auditory N1 in children with fragile X syndrome. *Brain Topogr, 15*(3), 165-171. Retrieved from https://www.ncbi.nlm.nih.gov/pubmed/12705812

Clarke, L. E., & Barres, B. A. (2013). Emerging roles of astrocytes in neural circuit development. *Nat Rev Neurosci, 14*(5), 311-321. doi:10.1038/nrn3484

Contractor, A., Klyachko, V. A., & Portera-Cailliau, C. (2015). Altered Neuronal and Circuit Excitability in Fragile X Syndrome. *Neuron, 87*(4), 699-715. doi:10.1016/j.neuron.2015.06.017

Crawford, D. C., Acuña, J. M., & Sherman, S. L. (2001). FMR1 and the fragile X syndrome: human genome epidemiology review. *Genet Med, 3*(5), 359-371. doi:10.109700125817-200109000-00006

Curia, G., Papouin, T., Séguéla, P., & Avoli, M. (2009). Downregulation of tonic GABAergic inhibition in a mouse model of fragile X syndrome. *Cereb Cortex, 19*(7), 1515-1520. doi:10.1093/cercor/bhn159

D'Hulst, C., De Geest, N., Reeve, S. P., Van Dam, D., De Deyn, P. P., Hassan, B. A., & Kooy, R. F. (2006). Decreased expression of the GABAA receptor in fragile X syndrome. *Brain Res, 1121*(1), 238-245. doi:10.1016/j.brainres.2006.08.115

D'Hulst, C., Heulens, I., Brouwer, J. R., Willemsen, R., De Geest, N., Reeve, S. P., . . . Kooy, R. F. (2009). Expression of the GABAergic system in animal models for fragile X syndrome and fragile X associated tremor/ataxia syndrome (FXTAS). *Brain Res, 1253*, 176-183. doi:10.1016/j.brainres.2008.11.075

D'Hulst, C., Heulens, I., Van der Aa, N., Goffin, K., Koole, M., Porke, K., . . . Kooy, R. F. (2015). Positron Emission Tomography (PET) Quantification of GABAA Receptors in the Brain of Fragile X Patients. *PLoS One, 10*(7), e0131486. doi:10.1371/journal.pone.0131486

Danaher, P., Warren, S., Dennis, L., D'Amico, L., White, A., Disis, M. L., . . . Fling, S. P. (2017). Gene expression markers of Tumor Infiltrating Leukocytes. *J Immunother Cancer, 5*, 18. doi:10.1186/s40425-017-0215-8

Darnell, J. C., Van Driesche, S. J., Zhang, C., Hung, K. Y., Mele, A., Fraser, C. E., . . . Darnell, R. B. (2011). FMRP stalls ribosomal translocation on mRNAs linked to synaptic function and autism. *Cell, 146*(2), 247-261. doi:10.1016/j.cell.2011.06.013

Deng, P. Y., Rotman, Z., Blundon, J. A., Cho, Y., Cui, J., Cavalli, V., . . . Klyachko, V. A. (2013). FMRP regulates neurotransmitter release and synaptic information transmission by modulating action potential duration via BK channels. *Neuron, 77*(4), 696-711. doi:10.1016/j.neuron.2012.12.018

Edbauer, D., Neilson, J. R., Foster, K. A., Wang, C. F., Seeburg, D. P., Batterton, M. N., . . . Sheng, M. (2010). Regulation of synaptic structure and function by FMRP-associated microRNAs miR-125b and miR-132. *Neuron, 65*(3), 373-384. doi:10.1016/j.neuron.2010.01.005

Erickson, C. A., Early, M., Stigler, K. A., Wink, L. K., Mullett, J. E., & McDougle, C. J. (2011). An open-label naturalistic pilot study of acamprosate in youth with autistic disorder. *J Child Adolesc Psychopharmacol, 21*(6), 565-569. doi:10.1089/cap.2011.0034

Ethridge, L. E., White, S. P., Mosconi, M. W., Wang, J., Byerly, M. J., & Sweeney, J. A. (2016). Reduced habituation of auditory evoked potentials indicate cortical hyper-excitability in Fragile X Syndrome. *Transl Psychiatry, 6*, e787. doi:10.1038/tp.2016.48

Ethridge, L. E., White, S. P., Mosconi, M. W., Wang, J., Pedapati, E. V., Erickson, C. A., . . . Sweeney, J. A. (2017). Neural synchronization deficits linked to cortical hyper-excitability and auditory hypersensitivity in fragile X syndrome. *Mol Autism, 8*, 22. doi:10.1186/s13229-017-0140-1

Exposito-Alonso, D., Osorio, C., Bernard, C., Pascual-Garcia, S., Del Pino, I., Marin, O., & Rico, B. (2020). Subcellular sorting of neuregulins controls the assembly of excitatory-inhibitory cortical circuits. *Elife, 9*. doi:10.7554/eLife.57000

Fazzari, P., Paternain, A. V., Valiente, M., Pla, R., Lujan, R., Lloyd, K., . . . Rico, B. (2010). Control of cortical GABA circuitry development by Nrg1 and ErbB4 signalling. *Nature, 464*(7293), 1376-1380. doi:10.1038/nature08928

Ferguson, B. R., & Gao, W. J. (2018). PV Interneurons: Critical Regulators of E/I Balance for Prefrontal Cortex-Dependent Behavior and Psychiatric Disorders. *Front Neural Circuits, 12*, 37. doi:10.3389/fncir.2018.00037

Ferron, L., Nieto-Rostro, M., Cassidy, J. S., & Dolphin, A. C. (2014). Fragile X mental retardation protein controls synaptic vesicle exocytosis by modulating N-type calcium channel density. *Nat Commun, 5*, 3628. doi:10.1038/ncomms4628

Filice, F., Janickova, L., Henzi, T., Bilella, A., & Schwaller, B. (2020). The Parvalbumin Hypothesis of Autism Spectrum Disorder. *Front Cell Neurosci, 14*, 577525. doi:10.3389/fncel.2020.577525

Frankland, P. W., Wang, Y., Rosner, B., Shimizu, T., Balleine, B. W., Dykens, E. M., . . . Silva, A. J. (2004). Sensorimotor gating abnormalities in young males with fragile X syndrome and Fmr1-knockout mice. *Mol Psychiatry, 9*(4), 417-425. doi:10.1038/sj.mp.4001432

Fu, Y., Kaneko, M., Tang, Y., Alvarez-Buylla, A., & Stryker, M. P. (2015). A cortical disinhibitory circuit for enhancing adult plasticity. *Elife, 4*, e05558. doi:10.7554/eLife.05558

Gantois, I., Vandesompele, J., Speleman, F., Reyniers, E., D'Hooge, R., Severijnen, L. A., . . . Kooy, R. F. (2006). Expression profiling suggests underexpression of the GABA(A) receptor subunit delta in the fragile X knockout mouse model. *Neurobiol Dis, 21*(2), 346-357. doi:10.1016/j.nbd.2005.07.017

Gao, F., Qi, L., Yang, Z., Yang, T., Zhang, Y., Xu, H., & Zhao, H. (2018). Impaired GABA Neural Circuits Are Critical for Fragile X Syndrome. *Neural Plast, 2018*, 8423420. doi:10.1155/2018/8423420

Gatto, C. L., Pereira, D., & Broadie, K. (2014). GABAergic circuit dysfunction in the Drosophila Fragile X syndrome model. *Neurobiol Dis, 65*, 142-159. doi:10.1016/j.nbd.2014.01.008

Gibson, J. R., Bartley, A. F., Hays, S. A., & Huber, K. M. (2008). Imbalance of neocortical excitation and inhibition and altered UP states reflect network hyperexcitability in the mouse model of fragile X syndrome. *J Neurophysiol, 100*(5), 2615-2626. doi:10.1152/jn.90752.2008

Goel, A., Cantu, D. A., Guilfoyle, J., Chaudhari, G. R., Newadkar, A., Todisco, B., . . . Portera-Cailliau, C. (2018). Impaired perceptual learning in a mouse model of Fragile X syndrome is mediated by parvalbumin neuron dysfunction and is reversible. *Nat Neurosci, 21*(10), 1404-1411. doi:10.1038/s41593-018-0231-0

Gonçalves, J. T., Anstey, J. E., Golshani, P., & Portera-Cailliau, C. (2013). Circuit level defects in the developing neocortex of Fragile X mice. *Nat Neurosci, 16*(7), 903-909. doi:10.1038/nn.3415

Hashemi, E., Ariza, J., Rogers, H., Noctor, S. C., & Martinez-Cerdeno, V. (2017). The Number of Parvalbumin-Expressing Interneurons Is Decreased in the Prefrontal Cortex in Autism. *Cereb Cortex, 27*(3), 1931-1943. doi:10.1093/cercor/bhw021

Hays, S. A., Huber, K. M., & Gibson, J. R. (2011). Altered neocortical rhythmic activity states in Fmr1 KO mice are due to enhanced mGluR5 signaling and involve changes in excitatory circuitry. *J Neurosci, 31*(40), 14223-14234. doi:10.1523/JNEUROSCI.3157-11.2011

Higashimori, H., Morel, L., Huth, J., Lindemann, L., Dulla, C., Taylor, A., . . . Yang, Y. (2013). Astroglial FMRP-dependent translational down-regulation of mGluR5 underlies glutamate transporter GLT1 dysregulation in the fragile X mouse. *Hum Mol Genet, 22*(10), 2041-2054. doi:10.1093/hmg/ddt055

Higashimori, H., Schin, C. S., Chiang, M. S., Morel, L., Shoneye, T. A., Nelson, D. L., & Yang, Y. (2016). Selective Deletion of Astroglial FMRP Dysregulates Glutamate Transporter GLT1 and Contributes to Fragile X Syndrome Phenotypes In Vivo. *J Neurosci, 36*(27), 7079-7094. doi:10.1523/JNEUROSCI.1069-16.2016

Ishibashi, M., Egawa, K., & Fukuda, A. (2019). Diverse Actions of Astrocytes in GABAergic Signaling. *Int J Mol Sci, 20*(12). doi:10.3390/ijms20122964

Jacobs, S., & Doering, L. C. (2010). Astrocytes prevent abnormal neuronal development in the fragile x mouse. *J Neurosci, 30*(12), 4508-4514. doi:10.1523/JNEUROSCI.5027-09.2010

Jin, S. X., Higashimori, H., Schin, C., Tamashiro, A., Men, Y., Chiang, M. S. R., . . . Yang, Y. (2021). Astroglial FMRP modulates synaptic signaling and behavior phenotypes in FXS mouse model. *Glia, 69*(3), 594-608. doi:10.1002/glia.23915

Koeppen, J., Nguyen, A. Q., Nikolakopoulou, A. M., Garcia, M., Hanna, S., Woodruff, S., . . . Ethell, I. M. (2018). Functional Consequences of Synapse Remodeling Following Astrocyte-Specific Regulation of Ephrin-B1 in the Adult Hippocampus. *J Neurosci, 38*(25), 5710-5726. doi:10.1523/JNEUROSCI.3618-17.2018

Kwak, H., Koh, W., Kim, S., Song, K., Shin, J. I., Lee, J. M., . . . Cheong, E. (2020). Astrocytes Control Sensory Acuity via Tonic Inhibition in the Thalamus. *Neuron, 108*(4), 691-706 e610. doi:10.1016/j.neuron.2020.08.013

Lee, E., Lee, J., & Kim, E. (2017). Excitation/Inhibition Imbalance in Animal Models of Autism Spectrum Disorders. *Biol Psychiatry, 81*(10), 838-847. doi:10.1016/j.biopsych.2016.05.011

Lin, R. C., Polsky, K., & Matesic, D. F. (1993). Expression of gamma-aminobutyric acid immunoreactivity in reactive astrocytes after ischemia-induced injury in the adult forebrain. *Brain Res, 600*(1), 1-8. doi:10.1016/0006-8993(93)90394-3

Lovelace, J. W., Ethell, I. M., Binder, D. K., & Razak, K. A. (2018a). Translation-relevant EEG phenotypes in a mouse model of Fragile X Syndrome. *Neurobiol Dis, 115*, 39-48. doi:10.1016/j.nbd.2018.03.012

Lovelace, J. W., Ethell, I. M., Binder, D. K., & Razak, K. A. (2018b). Translation-relevant EEG phenotypes in a mouse model of Fragile X Syndrome. *Neurobiol Dis*. doi:10.1016/j.nbd.2018.03.012

Lovelace, J. W., Rais, M., Palacios, A. R., Shuai, X. S., Bishay, S., Popa, O., . . . Razak, K. A. (2020). Deletion of Fmr1 from Forebrain Excitatory Neurons Triggers Abnormal Cellular, EEG, and Behavioral Phenotypes in the Auditory Cortex of a Mouse Model of Fragile X Syndrome. *Cereb Cortex, 30*(3), 969-988. doi:10.1093/cercor/bhz141

Lovelace, J. W., Wen, T. H., Reinhard, S., Hsu, M. S., Sidhu, H., Ethell, I. M., . . . Razak, K. A. (2016). Matrix metalloproteinase-9 deletion rescues auditory evoked potential habituation deficit in a mouse model of Fragile X Syndrome. *Neurobiol Dis, 89*, 126-135. doi:10.1016/j.nbd.2016.02.002

Lunden, J. W., Durens, M., Phillips, A. W., & Nestor, M. W. (2019). Cortical interneuron function in autism spectrum condition. *Pediatr Res, 85*(2), 146-154. doi:10.1038/s41390-018-0214-6

Marin, O. (2012). Interneuron dysfunction in psychiatric disorders. *Nat Rev Neurosci, 13*(2), 107-120. doi:10.1038/nrn3155

Maris, E., & Oostenveld, R. (2007). Nonparametric statistical testing of EEG- and MEG-data. *J Neurosci Methods, 164*(1), 177-190. doi:10.1016/j.jneumeth.2007.03.024

Mientjes, E. J., Nieuwenhuizen, I., Kirkpatrick, L., Zu, T., Hoogeveen-Westerveld, M., Severijnen, L., . . . Oostra, B. A. (2006). The generation of a conditional Fmr1 knock out mouse model to study Fmrp function in vivo. *Neurobiol Dis, 21*(3), 549-555. doi:10.1016/j.nbd.2005.08.019

Muller, T., Braud, S., Juttner, R., Voigt, B. C., Paulick, K., Sheean, M. E., . . . Birchmeier, C. (2018). Neuregulin 3 promotes excitatory synapse formation on hippocampal interneurons. *EMBO J, 37*(17). doi:10.15252/embj.201798858

Myrick, L. K., Deng, P. Y., Hashimoto, H., Oh, Y. M., Cho, Y., Poidevin, M. J., . . . Klyachko, V. A. (2015). Independent role for presynaptic FMRP revealed by an FMR1 missense mutation associated with intellectual disability and seizures. *Proc Natl Acad Sci U S A, 112*(4), 949-956. doi:10.1073/pnas.1423094112

Nguyen, A. Q., Sutley, S., Koeppen, J., Mina, K., Woodruff, S., Hanna, S., . . . Ethell, I. M. (2020). Astrocytic Ephrin-B1 Controls Excitatory-Inhibitory Balance in Developing Hippocampus. *J Neurosci, 40*(36), 6854-6871. doi:10.1523/JNEUROSCI.0413-20.2020

Niell, C. M., & Stryker, M. P. (2010). Modulation of visual responses by behavioral state in mouse visual cortex. *Neuron, 65*(4), 472-479. doi:10.1016/j.neuron.2010.01.033

Nomura, T., Musial, T. F., Marshall, J. J., Zhu, Y., Remmers, C. L., Xu, J., . . . Contractor, A. (2017). Delayed Maturation of Fast-Spiking Interneurons Is Rectified by Activation of the TrkB Receptor in the Mouse Model of Fragile X Syndrome. *J Neurosci, 37*(47), 11298-11310. doi:10.1523/JNEUROSCI.2893-16.2017

Nygaard, K. R., Maloney, S. E., & Dougherty, J. D. (2019). Erroneous inference based on a lack of preference within one group: Autism, mice, and the social approach task. *Autism Res, 12*(8), 1171-1183. doi:10.1002/aur.2154

Oliveira, J. F., Sardinha, V. M., Guerra-Gomes, S., Araque, A., & Sousa, N. (2015). Do stars govern our actions? Astrocyte involvement in rodent behavior. *Trends Neurosci, 38*(9), 535-549. doi:10.1016/j.tins.2015.07.006

Olmos-Serrano, J. L., Paluszkiewicz, S. M., Martin, B. S., Kaufmann, W. E., Corbin, J. G., & Huntsman, M. M. (2010). Defective GABAergic neurotransmission and pharmacological rescue of neuronal hyperexcitability in the amygdala in a mouse model of fragile X syndrome. *J Neurosci, 30*(29), 9929-9938. doi:10.1523/JNEUROSCI.1714-10.2010

Pacey, L. K., & Doering, L. C. (2007). Developmental expression of FMRP in the astrocyte lineage: implications for fragile X syndrome. *Glia, 55*(15), 1601-1609. doi:10.1002/glia.20573

Paxinos, G., & Franklin, K. B. (2004). *The mouse brain in stereotaxic coordinates*: Gulf professional publishing.

Penagarikano, O., Mulle, J. G., & Warren, S. T. (2007). The pathophysiology of fragile x syndrome. *Annu Rev Genomics Hum Genet, 8*, 109-129. doi:10.1146/annurev.genom.8.080706.092249

Pérez-Alcázar, M., Nicolás, M. J., Valencia, M., Alegre, M., Iriarte, J., & Artieda, J. (2008). Chirp-evoked potentials in the awake and anesthetized rat. A procedure to assess changes in cortical oscillatory activity. *Exp Neurol, 210*(1), 144-153. doi:10.1016/j.expneurol.2007.10.017

Purcell, D. W., John, S. M., Schneider, B. A., & Picton, T. W. (2004). Human temporal auditory acuity as assessed by envelope following responses. *J Acoust Soc Am, 116*(6), 3581-3593. Retrieved from https://www.ncbi.nlm.nih.gov/pubmed/15658709

Rais, M., Binder, D. K., Razak, K. A., & Ethell, I. M. (2018). Sensory Processing Phenotypes in Fragile X Syndrome. *ASN Neuro, 10*, 1759091418801092. doi:10.1177/1759091418801092

Rossignol, E. (2011). Genetics and function of neocortical GABAergic interneurons in neurodevelopmental disorders. *Neural Plast, 2011*, 649325. doi:10.1155/2011/649325

Rotschafer, S., & Razak, K. (2013). Altered auditory processing in a mouse model of fragile X syndrome. *Brain Res, 1506*, 12-24. doi:10.1016/j.brainres.2013.02.038

Sabanov, V., Braat, S., D'Andrea, L., Willemsen, R., Zeidler, S., Rooms, L., . . . Balschun, D. (2017). Impaired GABAergic inhibition in the hippocampus of Fmr1 knockout mice. *Neuropharmacology, 116*, 71-81. doi:10.1016/j.neuropharm.2016.12.010

Schneider, A., Leigh, M. J., Adams, P., Nanakul, R., Chechi, T., Olichney, J., . . . Hessl, D. (2013). Electrocortical changes associated with minocycline treatment in fragile X syndrome. *J Psychopharmacol, 27*(10), 956-963. doi:10.1177/0269881113494105

Selby, L., Zhang, C., & Sun, Q. Q. (2007). Major defects in neocortical GABAergic inhibitory circuits in mice lacking the fragile X mental retardation protein. *Neurosci Lett, 412*(3), 227-232. doi:10.1016/j.neulet.2006.11.062

Sinclair, D., Oranje, B., Razak, K., Siegel, S., & Schmid, S. (2017). Sensory processing in autism spectrum disorders and Fragile X syndrome—From the clinic to animal models. *Neuroscience & Biobehavioral Reviews, 76*, 235-253.

Sinclair, D., Oranje, B., Razak, K. A., Siegel, S. J., & Schmid, S. (2017). Sensory processing in autism spectrum disorders and Fragile X syndrome-From the clinic to animal models. *Neurosci Biobehav Rev, 76*(Pt B), 235-253. doi:10.1016/j.neubiorev.2016.05.029

Sohal, V. S., Zhang, F., Yizhar, O., & Deisseroth, K. (2009). Parvalbumin neurons and gamma rhythms enhance cortical circuit performance. *Nature, 459*(7247), 698-702. doi:10.1038/nature07991

Sun, Y., Ikrar, T., Davis, M. F., Gong, N., Zheng, X., Luo, Z. D., . . . Xu, X. (2016). Neuregulin-1/ErbB4 Signaling Regulates Visual Cortical Plasticity. *Neuron, 92*(1), 160-173. doi:10.1016/j.neuron.2016.08.033

Sutcliffe, J. S., Nelson, D. L., Zhang, F., Pieretti, M., Caskey, C. T., Saxe, D., & Warren, S. T. (1992). DNA methylation represses FMR-1 transcription in fragile X syndrome. *Hum Mol Genet, 1*(6), 397-400. Retrieved from https://www.ncbi.nlm.nih.gov/pubmed/1301913

Tallon-Baudry, C., Bertrand, O., Delpuech, C., & Pernier, J. (1996). Stimulus specificity of phase-locked and non-phase-locked 40 Hz visual responses in human. *J Neurosci, 16*(13), 4240-4249. Retrieved from https://www.ncbi.nlm.nih.gov/pubmed/8753885

Tan, C. X., Burrus Lane, C. J., & Eroglu, C. (2021). Role of astrocytes in synapse formation and maturation. *Curr Top Dev Biol, 142*, 371-407. doi:10.1016/bs.ctdb.2020.12.010

Telias, M., Segal, M., & Ben-Yosef, D. (2016). Immature Responses to GABA in Fragile X Neurons Derived from Human Embryonic Stem Cells. *Front Cell Neurosci, 10*, 121. doi:10.3389/fncel.2016.00121

Ullian, E. M., Christopherson, K. S., & Barres, B. A. (2004). Role for glia in synaptogenesis. *Glia, 47*(3), 209-216. doi:10.1002/glia.20082

Verkerk, A. J., Pieretti, M., Sutcliffe, J. S., Fu, Y. H., Kuhl, D. P., Pizzuti, A., . . . Zhang, F. P. (1991). Identification of a gene (FMR-1) containing a CGG repeat coincident with a breakpoint cluster region exhibiting length variation in fragile X syndrome. *Cell, 65*(5), 905-914. Retrieved from https://www.ncbi.nlm.nih.gov/pubmed/1710175

Volman, V., Behrens, M. M., & Sejnowski, T. J. (2011). Downregulation of parvalbumin at cortical GABA synapses reduces network gamma oscillatory activity. *J Neurosci, 31*(49), 18137-18148. doi:10.1523/JNEUROSCI.3041-11.2011

Wallingford, J., Scott, A. L., Rodrigues, K., & Doering, L. C. (2017). Altered Developmental Expression of the Astrocyte-Secreted Factors Hevin and SPARC in the Fragile X Mouse Model. *Front Mol Neurosci, 10*, 268. doi:10.3389/fnmol.2017.00268

Wang, J., Barstein, J., Ethridge, L. E., Mosconi, M. W., Takarae, Y., & Sweeney, J. A. (2013). Resting state EEG abnormalities in autism spectrum disorders. *J Neurodev Disord, 5*(1), 24. doi:10.1186/1866-1955-5-24

Wen, L., Lu, Y. S., Zhu, X. H., Li, X. M., Woo, R. S., Chen, Y. J., . . . Mei, L. (2010). Neuregulin 1 regulates pyramidal neuron activity via ErbB4 in parvalbumin-positive interneurons. *Proc Natl Acad Sci U S A, 107*(3), 1211-1216. doi:10.1073/pnas.0910302107

Wen, T. H., Afroz, S., Reinhard, S. M., Palacios, A. R., Tapia, K., Binder, D. K., . . . Ethell, I. M. (2018). Genetic Reduction of Matrix Metalloproteinase-9 Promotes Formation of Perineuronal Nets Around Parvalbumin-Expressing Interneurons and Normalizes Auditory Cortex Responses in Developing Fmr1 Knock-Out Mice. *Cereb Cortex, 28*(11), 3951-3964. doi:10.1093/cercor/bhx258

Zhang, N., Peng, Z., Tong, X., Lindemeyer, A. K., Cetina, Y., Huang, C. S., . . . Houser, C. R. (2017). Decreased surface expression of the δ subunit of the GABAA receptor contributes to reduced tonic inhibition in dentate granule cells in a mouse model of fragile X syndrome. *Exp Neurol, 297*, 168-178. doi:10.1016/j.expneurol.2017.08.008

Zhang, Y., Bonnan, A., Bony, G., Ferezou, I., Pietropaolo, S., Ginger, M., . . . Frick, A. (2014). Dendritic channelopathies contribute to neocortical and sensory hyperexcitability in Fmr1(-/y) mice. *Nat Neurosci, 17*(12), 1701-1709. doi:10.1038/nn.3864

Zhang, Y. Q., Bailey, A. M., Matthies, H. J., Renden, R. B., Smith, M. A., Speese, S. D., . . . Broadie, K. (2001). Drosophila fragile X-related gene regulates the MAP1B

homolog Futsch to control synaptic structure and function. *Cell, 107*(5), 591-603. Retrieved from https://www.ncbi.nlm.nih.gov/pubmed/11733059

Figure 4.1

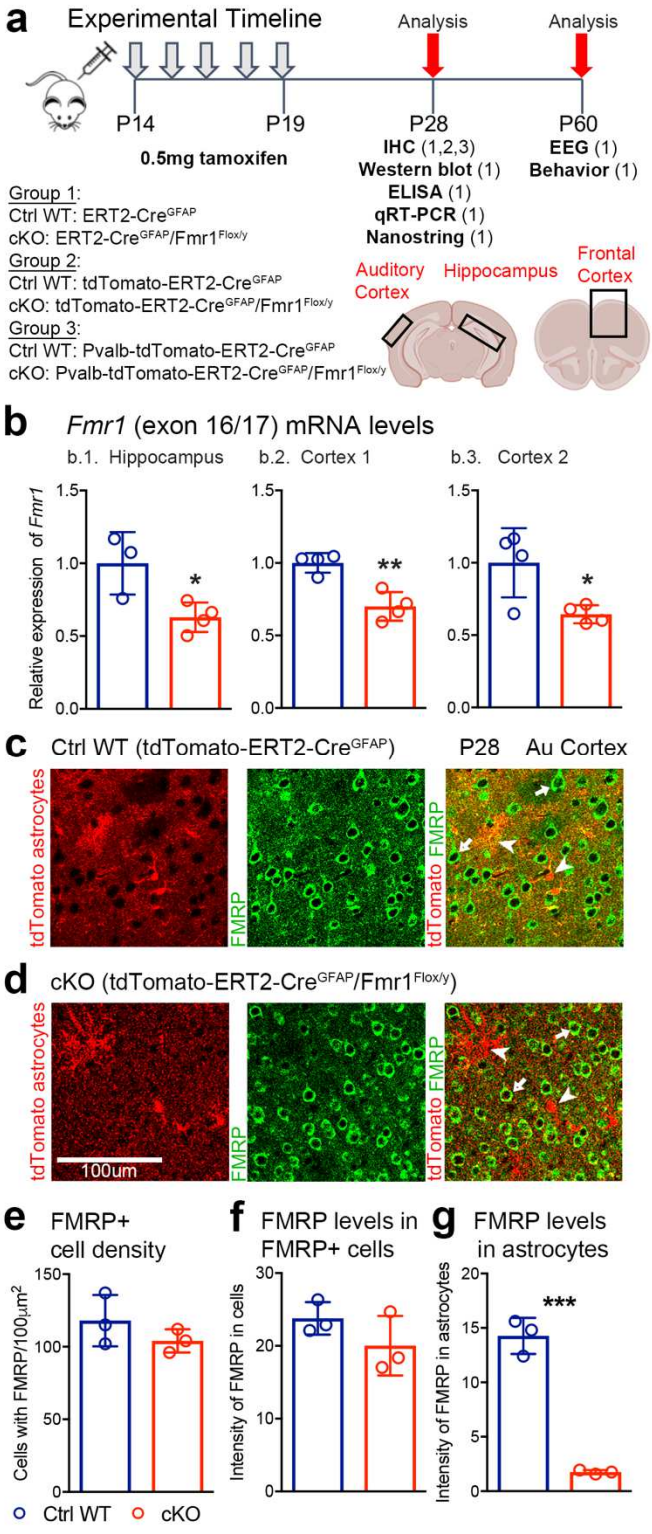
a
Experimental Timeline
Analysis
Analysis
P14
P19
P28
P60
0.5mg tamoxifen
IHC (1,2,3)
Western blot (1)
ELISA (1)
qRT-PCR (1)
Nanostring (1)
EEG (1)
Behavior (1)
Group 1:
Ctrl WT: ERT2-Cre^GFAP
cKO: ERT2-Cre^GFAP/Fmr1^Flox/y
Group 2:
Ctrl WT: tdTomato-ERT2-Cre^GFAP
cKO: tdTomato-ERT2-Cre^GFAP/Fmr1^Flox/y
Group 3:
Ctrl WT: Pvalb-tdTomato-ERT2-Cre^GFAP
cKO: Pvalb-tdTomato-ERT2-Cre^GFAP/Fmr1^Flox/y
Auditory Cortex
Hippocampus
Frontal Cortex
b
Fmr1 (exon 16/17) mRNA levels
b.1. Hippocampus
b.2. Cortex 1
b.3. Cortex 2
Relative expression of Fmr1
c
Ctrl WT (tdTomato-ERT2-Cre^GFAP)
P28
Au Cortex
tdTomato astrocytes
FMRP
tdTomato FMRP
d
cKO (tdTomato-ERT2-Cre^GFAP/Fmr1^Flox/y)
100um
e
FMRP+ cell density
Cells with FMRP/100μm²
f
FMRP levels in FMRP+ cells
Intensity of FMRP in cells
g
FMRP levels in astrocytes
Intensity of FMRP in astrocytes
Ctrl WT
cKO

Figure 4.1. Astrocyte-specific deletion of FMRP during P14-P28 period.
(A) Three transgenic mouse groups were used in this study: (1) ERT2-Cre^{GFAP} control (Ctrl WT) and ERT2-Cre^{GFAP}*Fmr1*$^{flox/y}$ condition KO (cKO); (2) tdTomatoERT2-Cre^{GFAP} Ctrl WT and tdTomatoERT2-Cre^{GFAP}*Fmr1*$^{flox/y}$ cKO; and (3) Pvalb-tdTomato-ERT2-Cre^{GFAP} Ctrl WT and Pvalb-tdvTomato-ERT2-Cre^{GFAP}*Fmr1*$^{flox/y}$ cKO. To achieve FMRP deletion in astrocytes tamoxifen (0.5 mg) was intraperitoneally (IP) injected at P14 for 5 days; experiments were performed at P28 and P60 (adult) on mouse groups 1, 2 or 3. Schematic representation of hippocampus, auditory cortex (AuC), and frontal cortex (FC) areas analyzed in these studies are outlined with the box in representative mouse coronal brain slices. (B) Analysis of *Fmr1* (exon 16/17) mRNA levels in the hippocampus (B.1.), cortex 1 (frontal cortical areas; B.2.), and cortex 2 (sensory cortical areas; B.3.) of Ctrl WT and cKO mice at P28 with qRT-PCR. Graphs show mean ± SEM (n= 3-4 mice/group, *p<0.05; **p<0.01, t-test). *Fmr1* mRNA levels were significantly reduced in all three brain areas of cKO mice compared to Ctrl WT. (C-D) Confocal images showing tdTomato astrocytes (red) and FMRP immunoreactivity (green) in neurons (arrow) and astrocytes (arrowhead) of AuC of Ctrl WT (C) and cKO (D) mice at P28. (E-G) Quantitative analysis of FMRP+ cell density (E), FMRP levels in FMRP+ cells (F) and FMRP levels in astrocytes (G). Graphs show mean ± SEM (n= 3 mice/group, ***p<0.001, t-test). While no significant differences were observed in FMRP+ cell density and FMRP intensity in FMRP+ cells between the genotypes, there was a significant decrease in FMRP levels in cKO astrocytes compared to Ctrl WT mice.

Figure 4.2

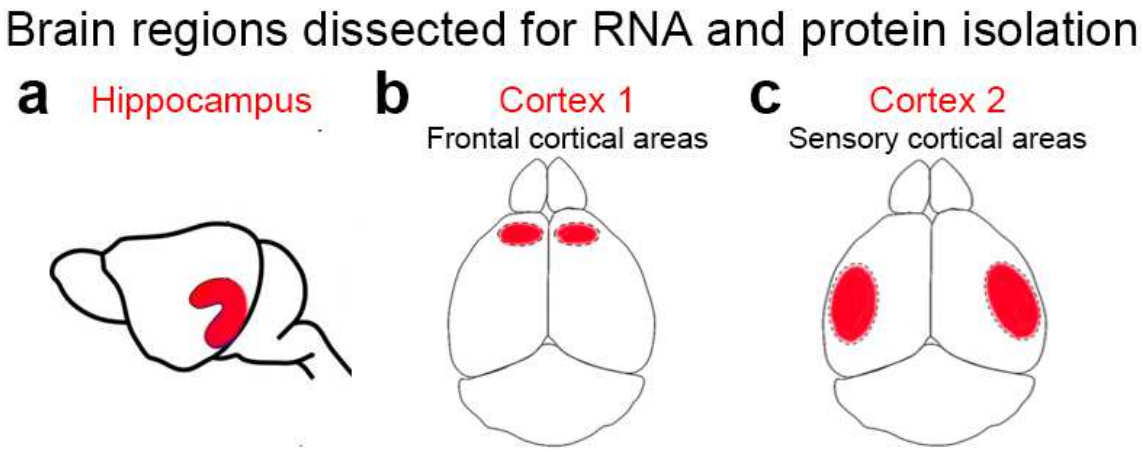

Figure 4.2. Schematic representation of the mouse brain regions used for RNA and protein analysis.
(A-C) Hippocampus (A), cortex1 (frontal cortical areas) (B), and cortex 2 (sensory cortical areas) (C) dissected for RNA and protein isolation (depicted by red regions).

Figure 4.3

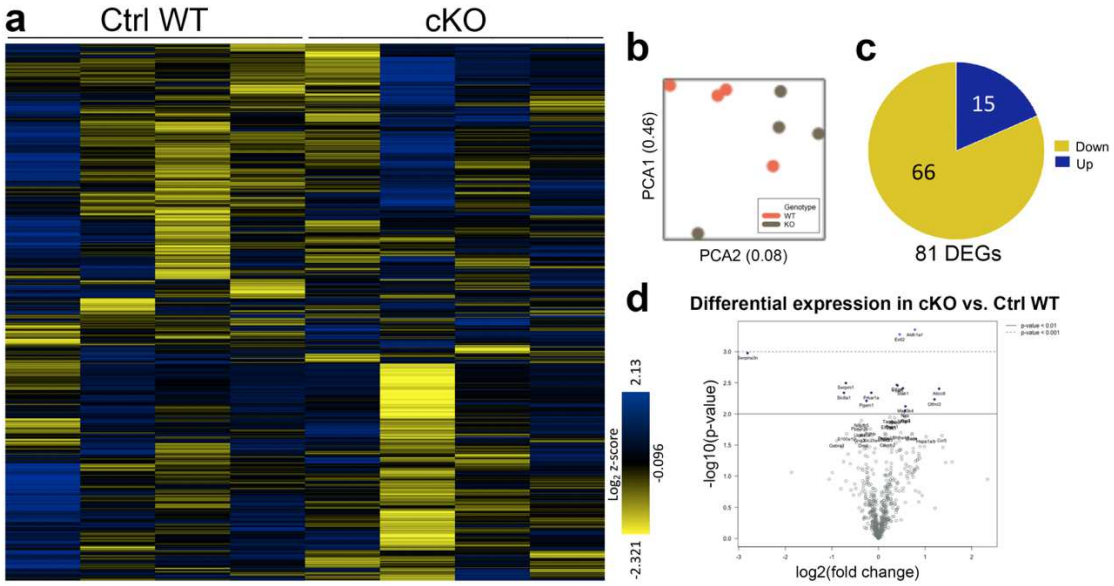

Figure 4.3. Postnatal deletion of *Fmr1* from astrocytes triggers a shift in gene expression in developing hippocampus of cKO mice.
(A) Hippocampal RNA was hybridized with NanoString "Glial Profiling" panel specific codesets, and RNA-conjugated probes were counted via NanoString Sprint Profiler technology. Resulting gene expression changes compared to calculated control z-scores are demonstrated in the heatmap. Gene expression is depicted from low expression (yellow) to high expression (blue). Heatmap is generated from normalized gene expression data using nSolver software. (B) Principal component analysis (PCA) plot of biological replicates from hippocampus of Ctrl WT and cKO mice. Numbers on axes represent percentage of variation in that component. PCA plot demonstrate that biological replicates within each genotype generally exhibit close clustering. (C) Fold change analysis of cKO genes compared to Ctrl WT identified 81 differentially expressed genes (DEGs) with *Fmr1* loss from astrocytes. Pie chart denotes number of up- and down-regulated DEGs. (D) Volcano plot depicts differential expression analysis of cKO and Ctrl WT groups. Top 25 most differentially expressed genes are identified based on fold change (x-axis) vs. p-value (y-axis). Two adjusted p-value cutoffs in the plot are indicated by lines as follows (from bottom to top): <0.01 and <0.001.

Figure 4.4

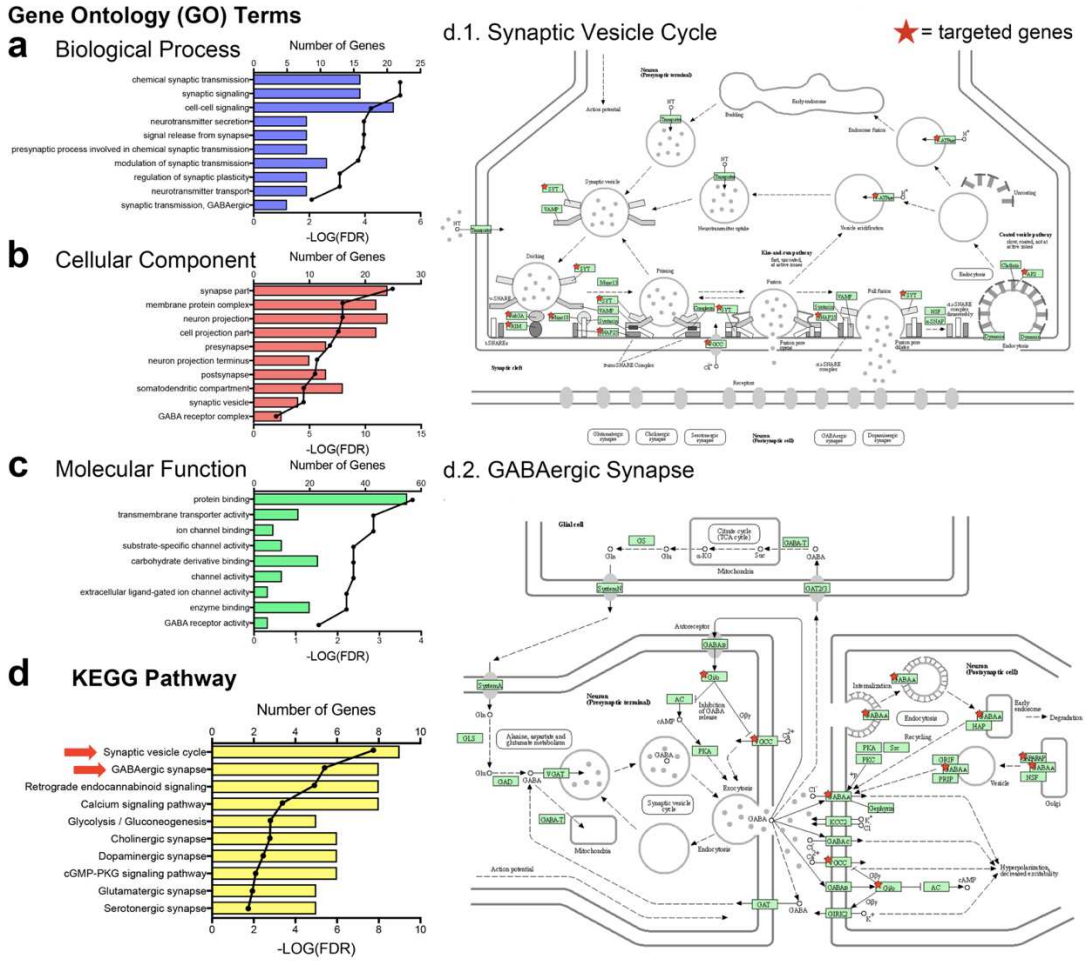
Gene Ontology (GO) Terms
a Biological Process
Number of Genes
chemical synaptic transmission
synaptic signaling
cell-cell signaling
neurotransmitter secretion
signal release from synapse
presynaptic process involved in chemical synaptic transmission
modulation of synaptic transmission
regulation of synaptic plasticity
neurotransmitter transport
synaptic transmission, GABAergic
-LOG(FDR)
b Cellular Component
Number of Genes
synapse part
membrane protein complex
neuron projection
cell projection part
presynapse
neuron projection terminus
postsynapse
somatodendritic compartment
synaptic vesicle
GABA receptor complex
-LOG(FDR)
c Molecular Function
Number of Genes
protein binding
transmembrane transporter activity
ion channel binding
substrate-specific channel activity
carbohydrate derivative binding
channel activity
extracellular ligand-gated ion channel activity
enzyme binding
GABA receptor activity
-LOG(FDR)
d KEGG Pathway
Number of Genes
Synaptic vesicle cycle
GABAergic synapse
Retrograde endocannabinoid signaling
Calcium signaling pathway
Glycolysis / Gluconeogenesis
Cholinergic synapse
Dopaminergic synapse
cGMP-PKG signaling pathway
Glutamatergic synapse
Serotonergic synapse
-LOG(FDR)
d.1. Synaptic Vesicle Cycle
= targeted genes
d.2. GABAergic Synapse

Figure 4.4. Postnatal deletion of *Fmr1* from astrocytes affects synaptic and GABAergic gene expression in developing hippocampus of cKO mice.
(A-C) Functional enrichment of 81 DEGs using the Database for Annotation, Visualization and Integrated Discovery (DAVID) shows functional GO analysis of Biological Process (A), Cellular Component (B), and Molecular Function (C). At the level of Biological Process (A), the genes that were dysregulated due to *Fmr1* loss in astrocytes enriched heavily to the synaptic transmission GO terms, including: "synaptic signaling" (SNAP25, SYT4, GABRA1, RAB3A, SYT1, STXBP1, GABRA3, CACNA1B, GABRG2, GNAI1, P2RX7, RIMS1, SYNGR1, KRAS, VDAC1, MAPT); "regulation of synaptic plasticity" (RIMS1, SNAP25, SYT4, SYNGR1, RAB3A, STXBP1, KRAS, MAPT); and "GABAergic synaptic transmission" (GABRA1, STXBP1, GABRG2). At the level of Cellular Component (B), the genes that were dysregulated due to *Fmr1* loss in astrocytes enriched heavily to the synapse part GO terms, including: "neuron projection" (SNAP25, CNTNAP2, SYT4, GABARAPL1, RAB3A, SYT1, STXBP1, ATP2B4, CACNA1B, FOS, GABRG2, SLC8A1, PPM1A, GRK3, SYNGR1, UCHL1, GNG3, GRIN3A, MAP2, GNB1, TIMP2, DMD, MAPT, AP2M1); "presynapse" (SNAP25, SYT4, RAB3A, SYT1, ABCC8, STXBP1, CACNA1B, P2RX7, RIMS1, SYNGR1, VDAC1, DNM1L, AP2M1); "postsynapse" (SYT4, GABRA1, GABRA3, GABRG2, SLC8A1, RIMS1, GRK3, GNG3, GRIN3A, ERBB3, MAP2, DMD, MAPT); and "GABA receptor complex" (GABRA1, GABRA3, GABRG2). At the level of Molecular Function (C), the genes that were dysregulated due to *Fmr1* loss in astrocytes enriched heavily to the protein binding GO terms, including: "transmembrane transporter activity" (SNAP25, GABRA1, ABCC8, GABRA3, ATP2B4, CACNA1B, AQP4, SLC2A5, ATP1B1, GABRG2, SLC8A1, P2RX7, GRIN3A, ATP6V1B2, VDAC1, ATP6V1D); "substrate-specific channel activity" (P2RX7, SNAP25, GABRA1, GRIN3A, ABCC8, GABRA3, CACNA1B, AQP4, VDAC1, GABRG2); "extracellular ligand-gated ion channel activity" (P2RX7, GABRA1, GRIN3A, GABRA3, GABRG2); and "GABA receptor activity" (GABRA1, GABRA3, GABRG2). Top x-axis represents number of DEGs mapping to the Gene Ontology (GO) term (FDR < 5%). (D) DAVID Kyoto Encyclopedia of Genes and Genomes (KEGG) Pathway analysis. Red arrows indicate the top 2 pathways most closely associated with the 81 DEGs: Synaptic Vesicle Cycle and GABAergic Synapse. Additional pathway maps highlight the targeted genes (red stars) that were dysregulated due to *Fmr1* loss in astrocytes involved in the Synaptic Vesicle Cycle Pathway (D.1.) and GABAergic Synapse Pathway (D.2.).

Figure 4.5

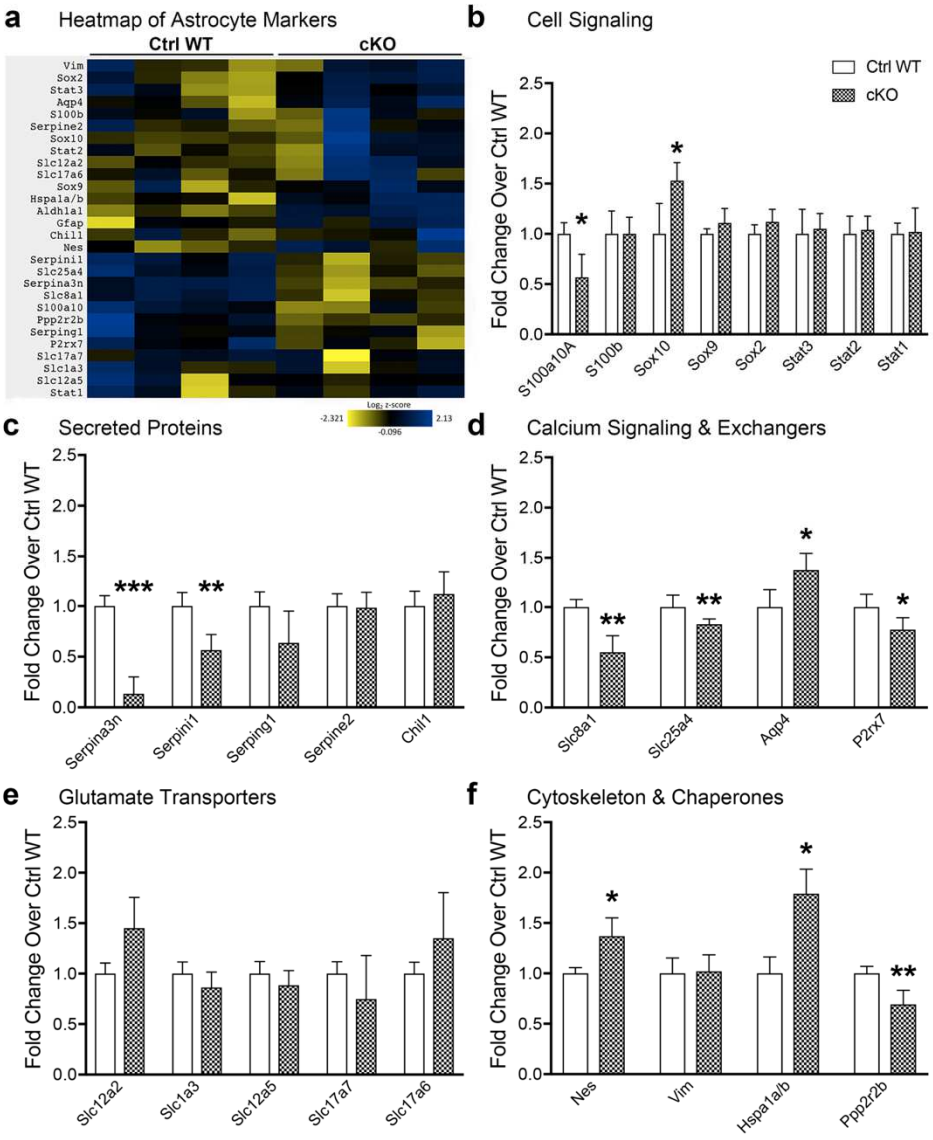

Figure 4.5. Postnatal deletion of *Fmr1* from astrocytes alters gene expression of some astrocytic markers in developing hippocampus of cKO mice.
(A) Heatmap of genes from the Glial Profiling NanoString Panel encoding astrocyte markers in the hippocampus of cKO and Ctrl WT mice. Heatmap shows normalized gene expression data from low expression (yellow) to high expression (blue) and is generated using nSolver software. (B-F) Quantitative analysis of mRNA levels of genes associated with cell signaling (B), secreted proteins (C), calcium signaling and exchangers (D), glutamate transporters (E), and cytoskeleton and chaperones (F). Graphs show mean ± SEM (n= 4 mice/group; *p<0.05; **p<0.01; ***p<0.001, t-test).

Figure 4.6

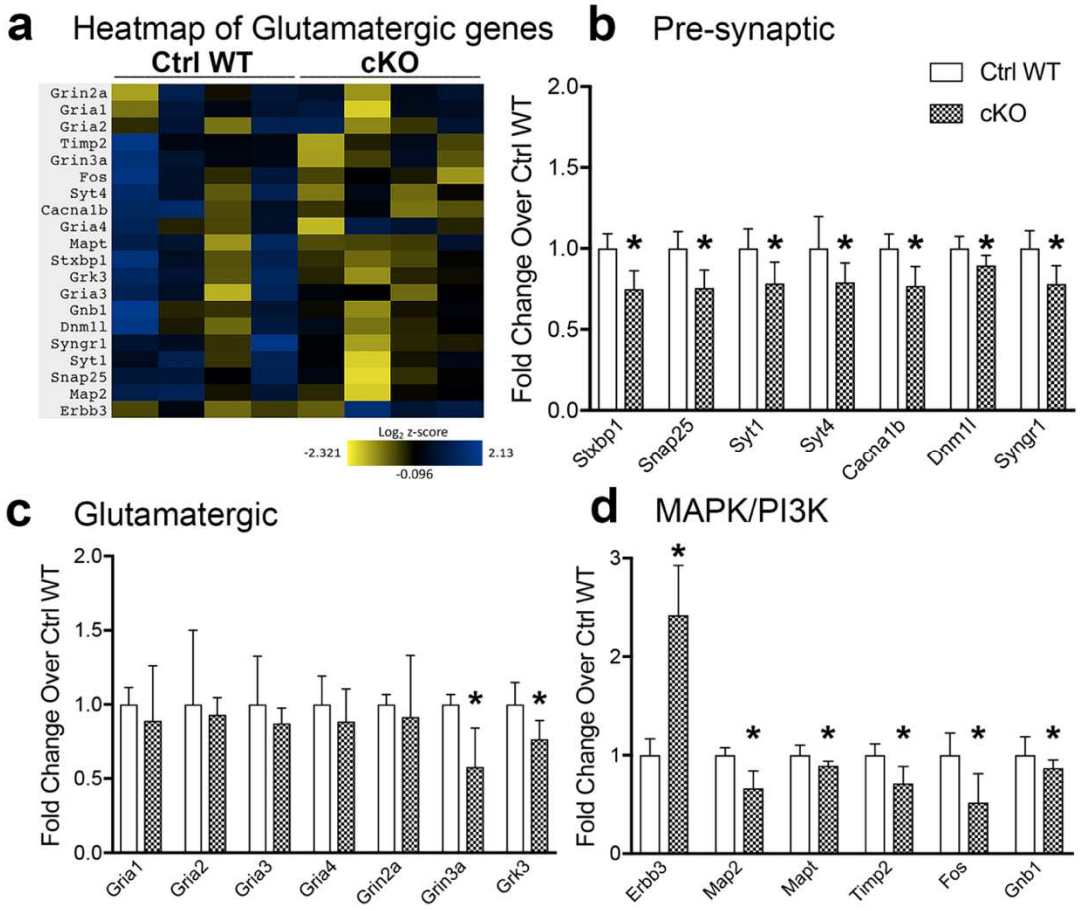

Figure 4.6. Postnatal deletion of *Fmr1* from astrocytes affects presynaptic glutamatergic gene expression in developing hippocampus of cKO mice.
(A) Heatmap of genes from the Glial Profiling NanoString Panel encoding glutamatergic genes in the hippocampus of cKO and Ctrl WT mice. Heatmap shows normalized gene expression data from low expression (yellow) to high expression (blue) and is generated using nSolver software. (B-D) Quantitative analysis of mRNA levels of genes associated with presynaptic (B), glutamatergic (C), and MAPK/PI3K signaling (D). Graphs show mean ± SEM (n= 4 mice/group; *p<0.05, t-test). Notably, there is a significant decrease in all presynaptic glutamatergic genes in the hippocampus of cKO mice compared to Ctrl WT. Furthermore, there is also a significant decrease in genes associated with MAPK/PI3K signaling such as, MAP2, MAPT, TIMP2, FOS, and GNB1.

Figure 4.7

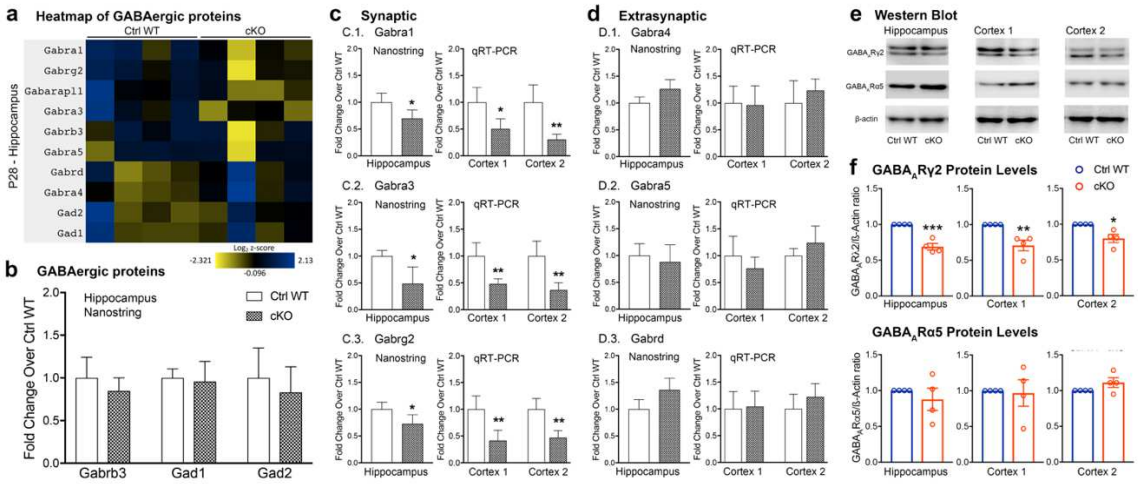

Figure 4.7. Postnatal deletion of *Fmr1* from astrocytes alters synaptic GABA$_A$ receptor levels in the developing hippocampus and cortex.
(A) Heatmap of genes from the Glial Profiling NanoString Panel encoding GABAergic proteins in the hippocampus of cKO and Ctrl WT mice. Heatmap shows normalized gene expression data from low expression (yellow) to high expression (blue) and is generated using nSolver software. (B-D) Quantitative analysis of mRNA levels of GABAergic genes. Analysis of mRNA expression in cortical samples was performed with qRT-PCR. Graphs show mean ± SEM (n= 4 mice/group; *p<0.05; **p<0.01, t-test). No significant differences were observed in mRNA levels of Gad1 and Gad2 (B); and GABA$_A$ receptor subunits: Gabrb3 (B), Gabra4 (D.1.), Gabra5 (D.2.), and Gabrd (D.3.) in the hippocampus (NanoString) and cortex (qRT-PCR) of cKO mice compared to Ctrl WT. However, there is a significant decrease in synaptic GABA$_A$ receptor subunits: Gabra1 (C.1.), Gabra3 (C.2.), and Gabrg2 (C.3.) in the hippocampus (NanoString) and cortex (qRT-PCR) of cKO mice compared to Ctrl WT. (E-F) Western blots showing GABA$_A$Rγ2 and GABA$_A$Rα5 protein levels in lysates from hippocampus and cortex of Ctrl WT and cKO mice. Graphs show mean ± SEM (n=4/group, *p<0.05; **p<0.01; ***p<0.001, t-test). Levels of synaptic GABA$_A$Rγ2 but not extrasynaptic GABA$_A$Rα5 subunit were significantly reduced in hippocampus and cortex of cKO mice compared to Ctrl WT.

Figure 4.8

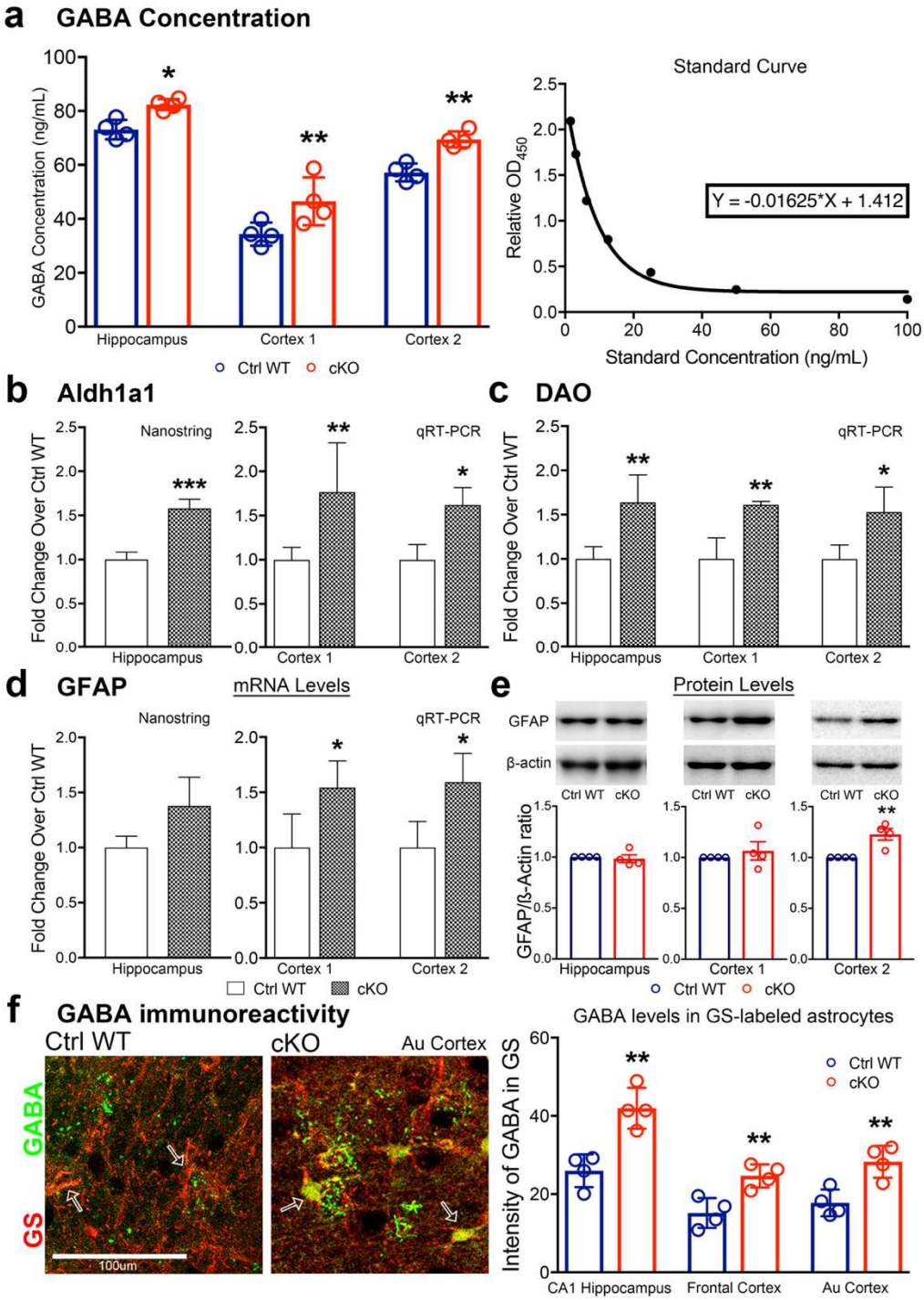
a
GABA Concentration
GABA Concentration (ng/mL)
Hippocampus
Cortex 1
Cortex 2
Ctrl WT
cKO
Standard Curve
Relative OD450
Y = -0.01625*X + 1.412
Standard Concentration (ng/mL)
b
Aldh1a1
Nanostring
qRT-PCR
Fold Change Over Ctrl WT
c
DAO
d
GFAP
mRNA Levels
e
Protein Levels
GFAP
β-actin
GFAP/β-Actin ratio
f
GABA immunoreactivity
Ctrl WT
cKO
Au Cortex
GABA
GS
100um
GABA levels in GS-labeled astrocytes
Intensity of GABA in GS
CA1 Hippocampus
Frontal Cortex
Au Cortex

Figure 4.8. Astrocytic GABA levels and expression of GABA-synthesizing enzymes are significantly upregulated following the developmental deletion of FMRP in astrocytes.

(A) GABA levels are upregulated in hippocampus and cortex of cKO mice compared to Ctrl WT at P28 in ELISA assay. Graph shows mean ± SEM (n=4 mice/group, *p<0.05; **p<0.01, t-test). Right panel shows standard curve. (B-D) Quantitative analysis of mRNA levels of Aldh1a1 (B), DAO (C), and GFAP (D). Graphs show mean ± SEM (n= 3-4 mice/group, *p<0.05; **p<0.01; ***p<0.001, t-test). There is a significant increase in the expression levels of astrocyte-specific GABA-synthesizing enzymes Aldh1a1 and DAO in the hippocampus and cortex of cKO mice compared to Ctrl WT. There is also a significant increase in GFAP mRNA levels in the cortex of cKO mice compared to Ctrl WT. (E) Western blots showing GFAP protein levels in lysates from hippocampus and cortex of Ctrl WT and cKO mice. No significant differences were observed in GFAP protein levels in the hippocampus. However, there is a trend for increase in cortical sample 1 and a significant increase in GFAP protein levels in cortical sample 2 of cKO mice compared to Ctrl WT. (F) Confocal images showing Glutamine Synthetase (GS, red) and GABA (green) immunoreactivity in superficial layer of AuC of Ctrl WT and cKO mice. Arrows indicate GS-labeled cell bodies of astrocytes. Quantitative analysis of the intensity of GABA immunoreactivity in GS-labeled astrocytes. Graphs show mean ± SEM (n= 4 mice/group, **p<0.01, t-test). GABA levels in GS-labeled astrocytes were significantly increased in the hippocampus and cortex of cKO mice compared to Ctrl WT.

Figure 4.9

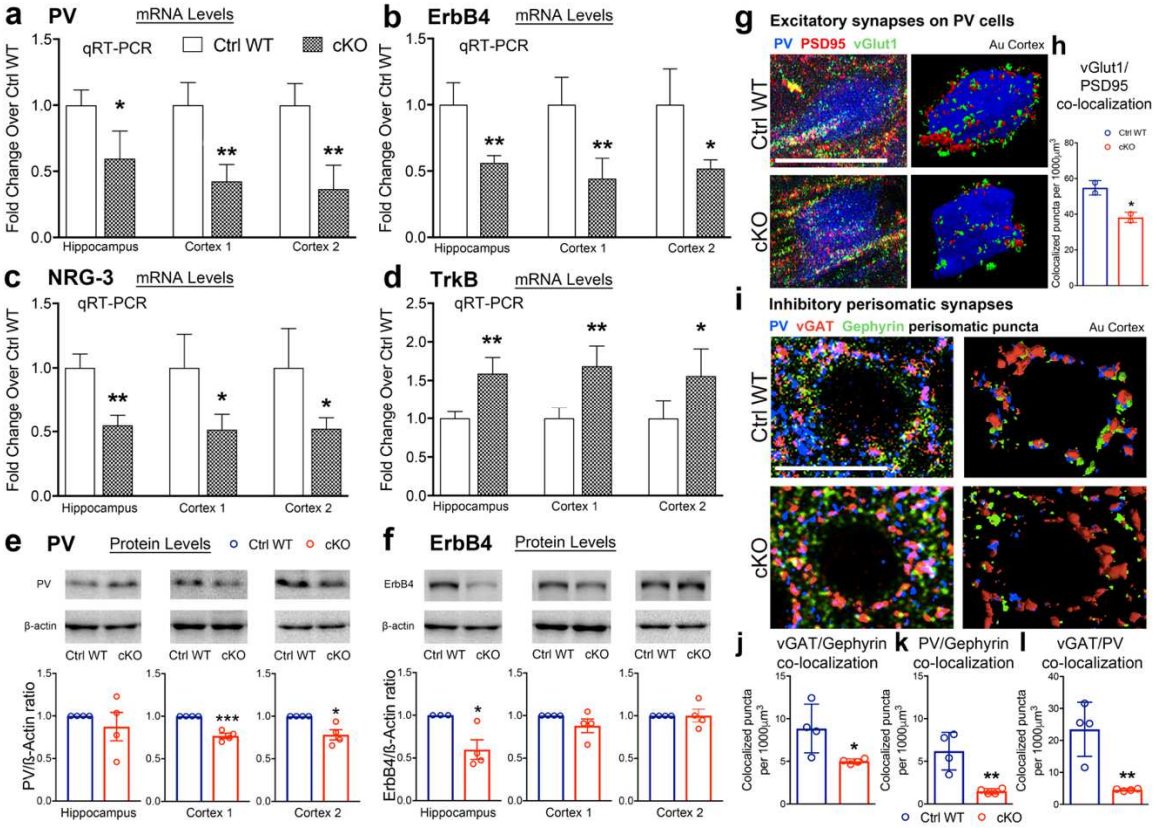
a PV mRNA Levels
qRT-PCR
Ctrl WT
cKO
Fold Change Over Ctrl WT
Hippocampus
Cortex 1
Cortex 2
b ErbB4 mRNA Levels
c NRG-3 mRNA Levels
d TrkB mRNA Levels
e PV Protein Levels
f ErbB4 Protein Levels
PV
ErbB4
β-actin
PV/β-Actin ratio
ErbB4/β-Actin ratio
g Excitatory synapses on PV cells
PV PSD95 vGlut1
Au Cortex
h vGlut1/ PSD95 co-localization
Colocalized puncta per 1000μm3
i Inhibitory perisomatic synapses
PV vGAT Gephyrin perisomatic puncta
j vGAT/Gephyrin co-localization
k PV/Gephyrin co-localization
l vGAT/PV co-localization

Figure 4.9. Developmental deletion of *Fmr1* from astrocytes affects expression of genes implicated in synaptic wiring and survival of PV interneuron.
(A-D) qRT-PCR analysis of PV, ERBB4, NRG3 and TRKB mRNA levels. Graphs show mean ± SEM (n= 3-4 mice/group, *p<0.05; **p<0.01, t-test). While PV (A), ERBB4 (B) and NRG3 (C) mRNA levels are significantly decreased, TRKB (D) mRNA levels are upregulated in the hippocampus and cortex of cKO mice compared to Ctrl WT. (E-F) Western blots showing PV, ErbB4 and beta-actin protein levels in lysates from hippocampus and cortex of Ctrl WT and cKO mice. Graphs show mean ± SEM (n=3-4/group, *p<0.05; ***p<0.001, t-test). PV levels normalized to beta-actin levels are significantly reduced in the cortical samples of cKO mice compared to Ctrl WT, however ErbB4 levels are only decreased in the hippocampus.
(G) Confocal images showing PV inhibitory interneurons expressing tdTomato (blue) immunolabelled with PSD95 (red) and vGlut1 (green) to visualize excitatory synaptic sites in superficial layer of AuC of Ctrl WT and cKO mice. Scale bar, 20 μm. (H) Quantitative analysis of vGlut1/PSD95 puncta colocalization on tdTomato-expressing PV interneurons. Graphs show mean ± SEM (n= 2 mice/group, *p<0.05, t-test). Preliminary data shows that colocalization of vGlut1 and PSD95 on PV interneurons is significantly reduced in AuC of cKO mice compared to Ctrl WT.
(I) Confocal images showing PV-positive pre-synaptic boutons (blue) immunolabelled with vGAT (red) and gephyrin (green) to visualize inhibitory synaptic sites in superficial layer of AuC of Ctrl WT and cKO mice. Scale bar, 20 μm. **(**J-L**)** Quantitative analysis of vGAT/Gephyrin (J), PV/Gephyrin (K), and vGAT/PV (L) colocalized puncta. Graphs show mean ± SEM (n= 4 mice/group, *p<0.05; **p<0.01, t-test). vGAT/Gephyrin, PV/Gephyrin, and vGAT/PV co-localization is significantly reduced in AuC of cKO mice compared to Ctrl WT.

Figure 4.10

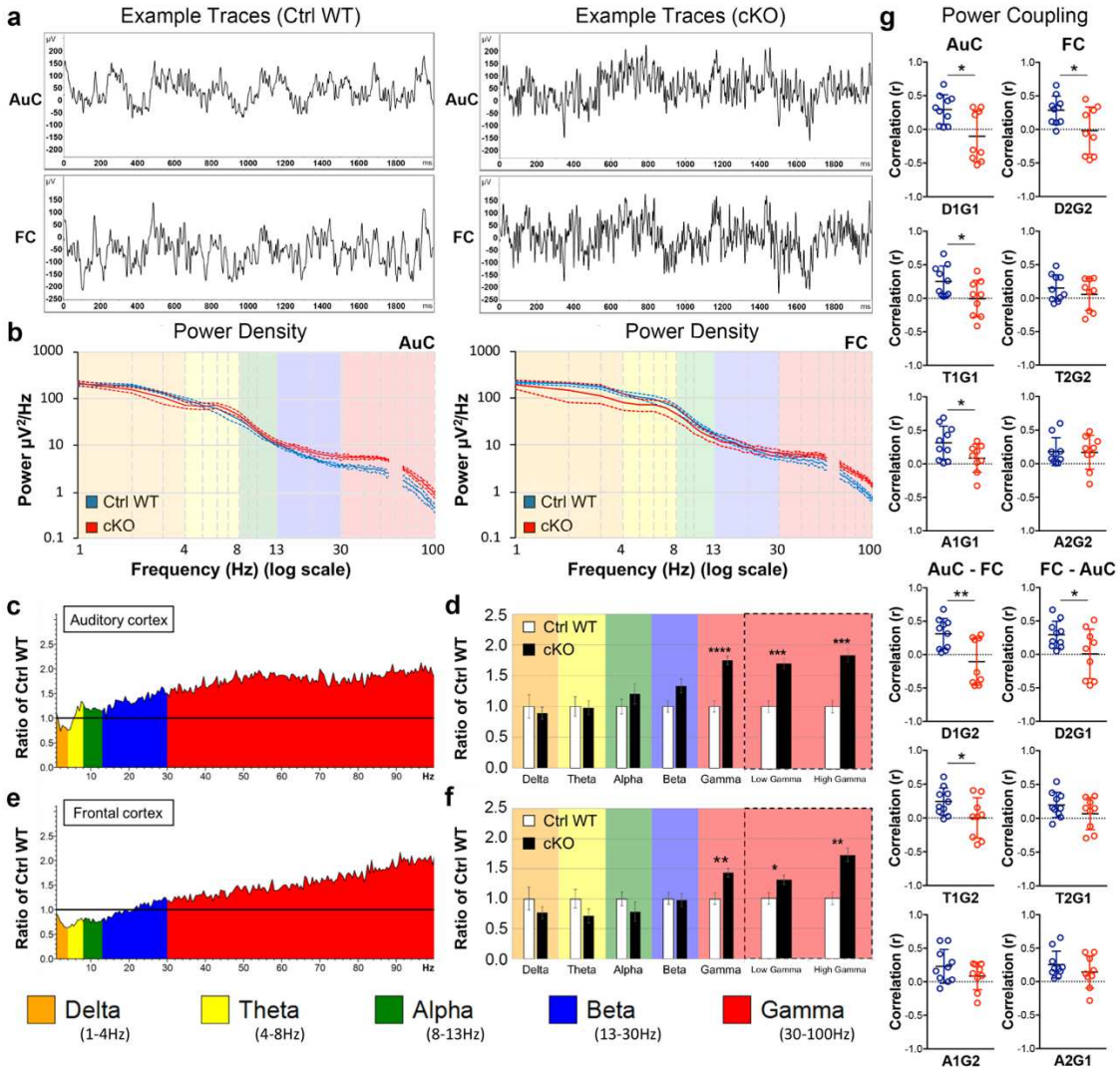
a
Example Traces (Ctrl WT)
Example Traces (cKO)
AuC
FC
b
Power Density
Power μV²/Hz
Frequency (Hz) (log scale)
Ctrl WT
cKO
c
Auditory cortex
Ratio of Ctrl WT
d
Delta
Theta
Alpha
Beta
Gamma
Low Gamma
High Gamma
e
Frontal cortex
f
g
Power Coupling
Correlation (r)
D1G1
D2G2
T1G1
T2G2
A1G1
A2G2
AuC - FC
FC - AuC
D1G2
D2G1
T1G2
T2G1
A1G2
A2G1
Delta (1-4Hz)
Theta (4-8Hz)
Alpha (8-13Hz)
Beta (13-30Hz)
Gamma (30-100Hz)

Figure 4.10. Characterization of baseline EEG power in the auditory and frontal cortex of adult cKO mice following developmental deletion of FMRP from astrocytes.
Five min of baseline EEG data (in the absence of auditory stimulation) from electrodes implanted in AuC and FC of Ctrl WT (n=10) and cKO (n=9) mice was recorded and FFT analysis was done to determine spectral power. (A) Examples of 2s segments of raw baseline EEG from AuC and FC of Ctrl WT and cKO mice. The enhanced high frequency oscillations can be visually observed in both AuC and FC of cKO mice. (B) Power density (μV^2/Hz) was calculated for each artifact-free segment using Fast Fourier Transform, followed by averaging of all segments for a given mouse. These individual averages then contributed to the grand average for each genotype (n=9-10 per genotype). Significant differences between genotypes are observed in AuC and FC at gamma frequencies (low: 30-55Hz, high: 65-100Hz). Frequencies from 55-65Hz were excluded in *all* analysis, as a 60Hz notch filter was utilized to eliminate line noise. (C, E) Average power in AuC (C) and FC (E) is expressed as the ratio of Ctrl WT levels. A value of 1 (horizontal black line) indicates no mean difference in power at that frequency between genotypes, whereas values >1 indicate cKO>Ctrl WT, and <1 indicates cKO<Ctrl WT. The elevated gamma power (red) can be visualized in AuC and FC of cKO relative to Ctrl WT mice. (D, F) Quantification of spectral power differences across genotypes. The values were divided into canonical frequency bands. MANCOVA analysis controlling for the effect of movement, revealed differences in the gamma range in AuC (D) and FC (F) of cKO mice after Bonferroni correction for multiple comparisons (*p<0.05, **p<0.01, ***p<0.001, ****p<0.0001). The gamma band was further subdivided into low and high gamma revealing genotype differences in both bands. (G) Power coupling of different oscillation frequencies. Graphs show Pearson's correlation (r) for AuC Delta/AuC Gamma (D1G1), AuC Theta/AuC Gamma (T1G1), and AuC Alpha/AuC Gamma (A1G1); FC Delta/FC Gamma (D2G2), FC Theta/FC Gamma (T2G2), and FC Alpha/FC Gamma (A2G2); AuC Delta/FC Gamma (D1G2), AuC Theta/FC Gamma (T1G2), and AuC Alpha/FC Gamma (A1G2); FC Delta/AuC Gamma (D2G1), FC Theta/AuC Gamma (T2G1), and FC Alpha/AuC Gamma (A2G1) power coupling (*p<0.05; **p<0.01, t-test).

Figure 4.11

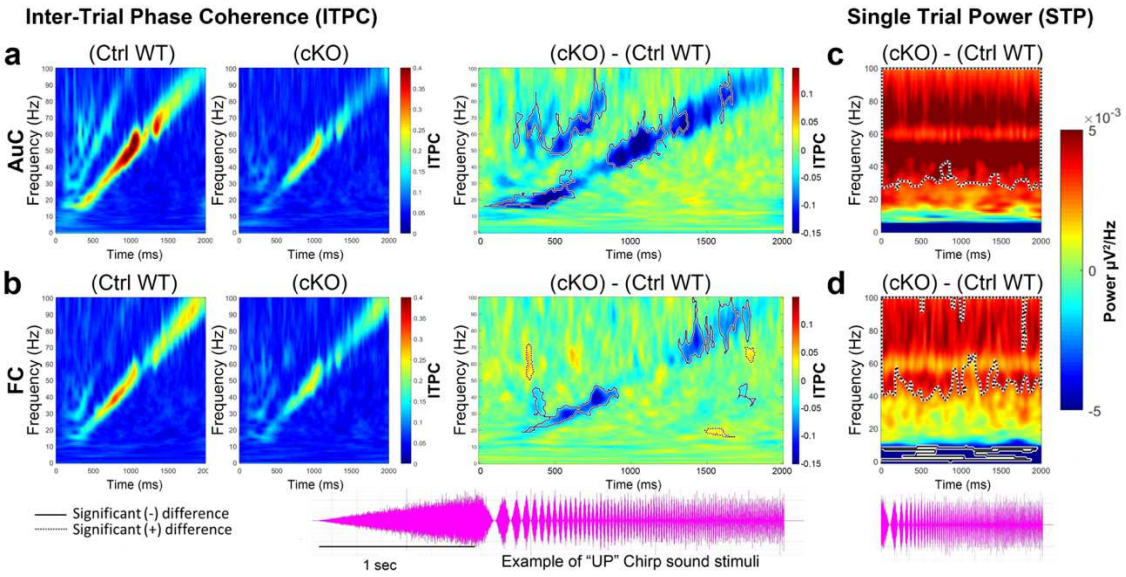
Inter-Trial Phase Coherence (ITPC)
Single Trial Power (STP)
a
(Ctrl WT)
(cKO)
(cKO) - (Ctrl WT)
c
(cKO) - (Ctrl WT)
AuC
Frequency (Hz)
Time (ms)
ITPC
b
(Ctrl WT)
(cKO)
(cKO) - (Ctrl WT)
d
(cKO) - (Ctrl WT)
FC
Power μV²/Hz
Significant (-) difference
Significant (+) difference
1 sec
Example of "UP" Chirp sound stimuli

Figure 4.11. Developmental deletion of *Fmr1* from astrocytes affects phase locking to time varying auditory stimuli (chirps), as well as non-phase locked single trial power (STP) in the auditory and frontal cortex of adult cKO mice.
The chirp stimulus (oscillogram shown at the bottom of this figure) is a 1s broadband noise whose amplitude is modulated linearly by a frequency sweep with frequencies increasing from 1 to 100 Hz. To reduce stimulus onset from overwhelming the early response, the chirp is preceded by a 1s slow ramp of broadband noise. The ability of the cortical neural generators of EEG to follow this temporally dynamic stimulus is quantified by measuring the inter-trial phase coherence (ITPC, also known as phase locking factor). Trains of chirp stimuli were presented to each mouse 300 times. For each mouse, ITPC was measured to determine the degree of phase locking across trials. (A-B) Grand average matrices were calculated for each genotype (left and middle panels), and then Ctrl WT (n=10) ITPC values were subtracted from cKO (n=9) values (right panels) for AuC (A) and FC (B). Blue areas indicating cKO<Ctrl WT, green areas no difference, and red cKO>Ctrl WT. Statistical cluster analysis reveals contiguous time x frequency regions that are significantly different between genotypes. Black solid contours (mean negative difference) and black dashed contours (mean positive difference) indicate clusters with significant differences. cKO mice express statistically significant decrease in ITPC at beta (13-30Hz) and gamma frequencies (30-100 Hz, blue). (C-D) For each mouse, single-trial power (STP) was measured to determine the average total non-phase locked power during chirp train presentation. Grand average matrices were calculated for each genotype, and then Ctrl WT (n=10) STP values were subtracted from cKO (n=9) values for AuC (C) and FC (D). Statistical cluster analysis reveals contiguous time x frequency regions that are significantly different between genotypes. Black dashed contour indicates these significant clusters. Consistent with the increase in gamma power changes in baseline EEGs, cKO mice express statistically significant increase in non-phase gamma power range (30-100Hz, red) throughout sound presentation in both AuC and FC.

Figure 4.12

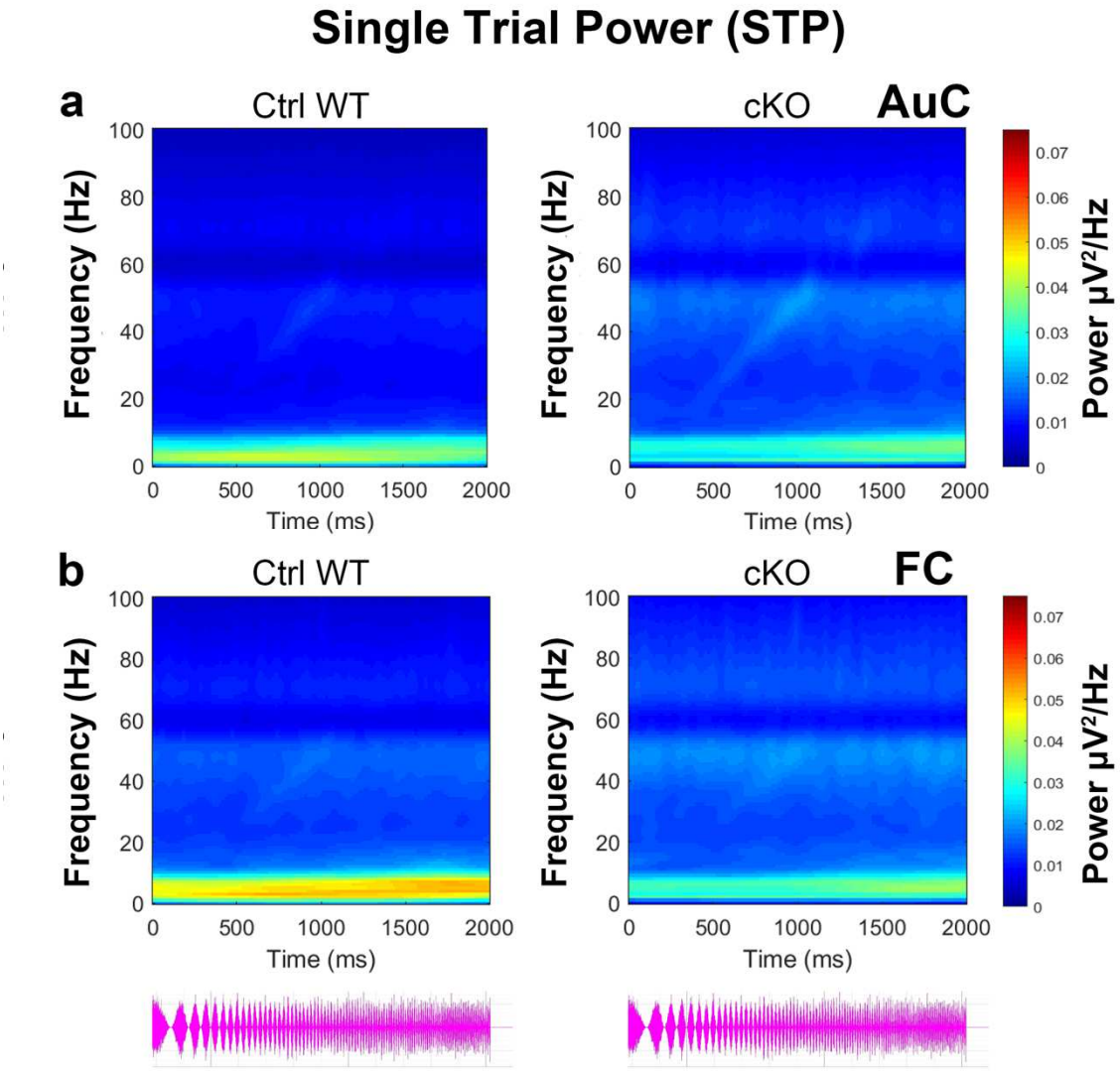

Figure 4.12. Background power during auditory "Up Chirp" stimuli.
(A-B) Grand average Ctrl WT and cKO Single Trial Power (STP) to up chirp in Auc (A) and FC (B). This is on-going 'background' power during auditory stimulation.

Figure 4.13

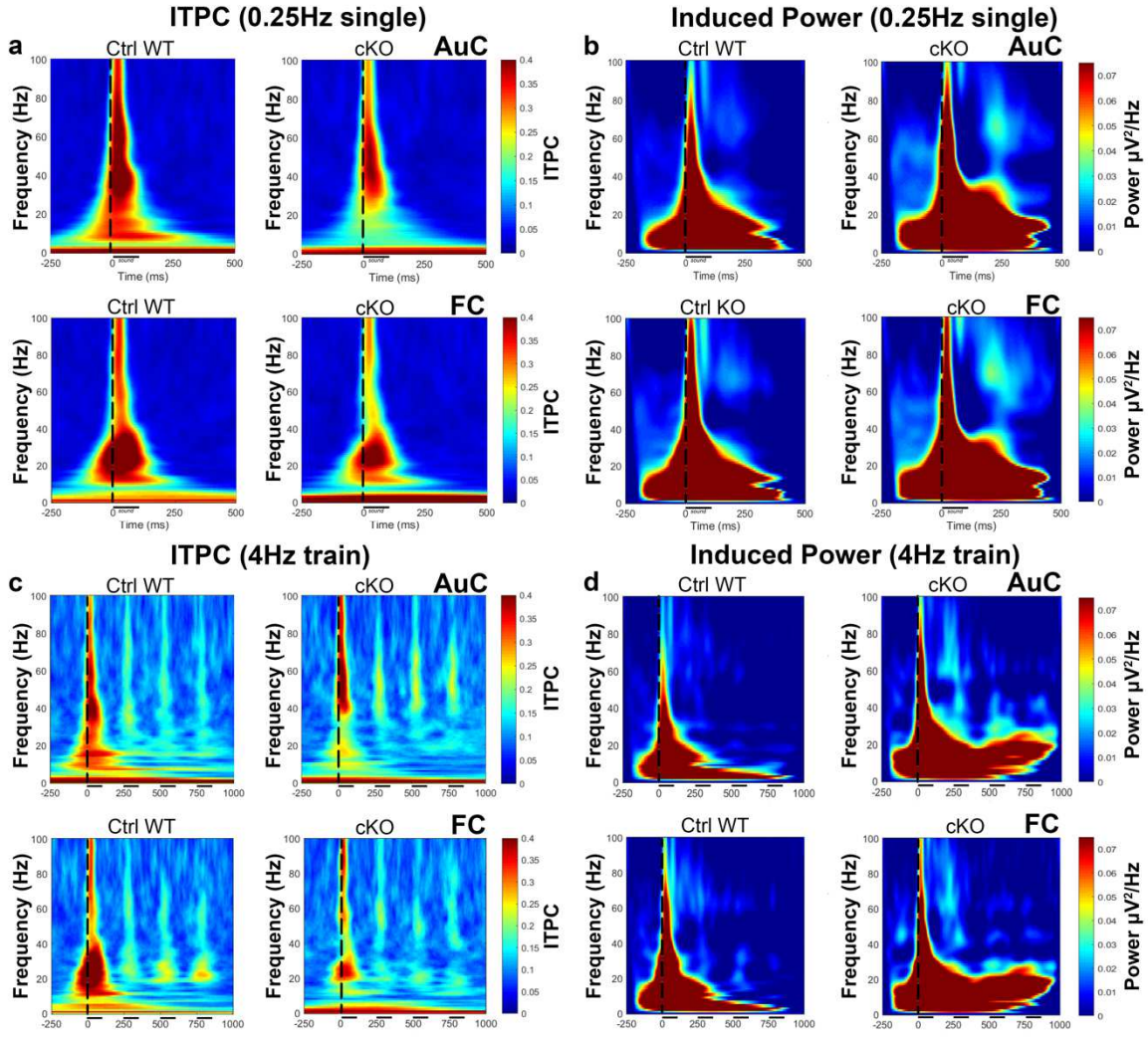

Figure 4.13. ITPC and induced (non–phase-locked) power in response to single sound presentations at 0.25Hz and 4Hz sound train.
(A-B) Ctrl WT and cKO grand average of ITPC (A) and induced power (B) during single-sound presentations at 0.25 Hz in Auc and FC. Black dashed line indicates onset of sound; black solid line indicates duration of 100ms broadband noise. (C-D) Ctrl WT and cKO grand average of ITPC (C) and induced power (D) during 4Hz sound train in Auc and FC. Only the first four noise bursts of each train were analyzed.

Figure 4.14

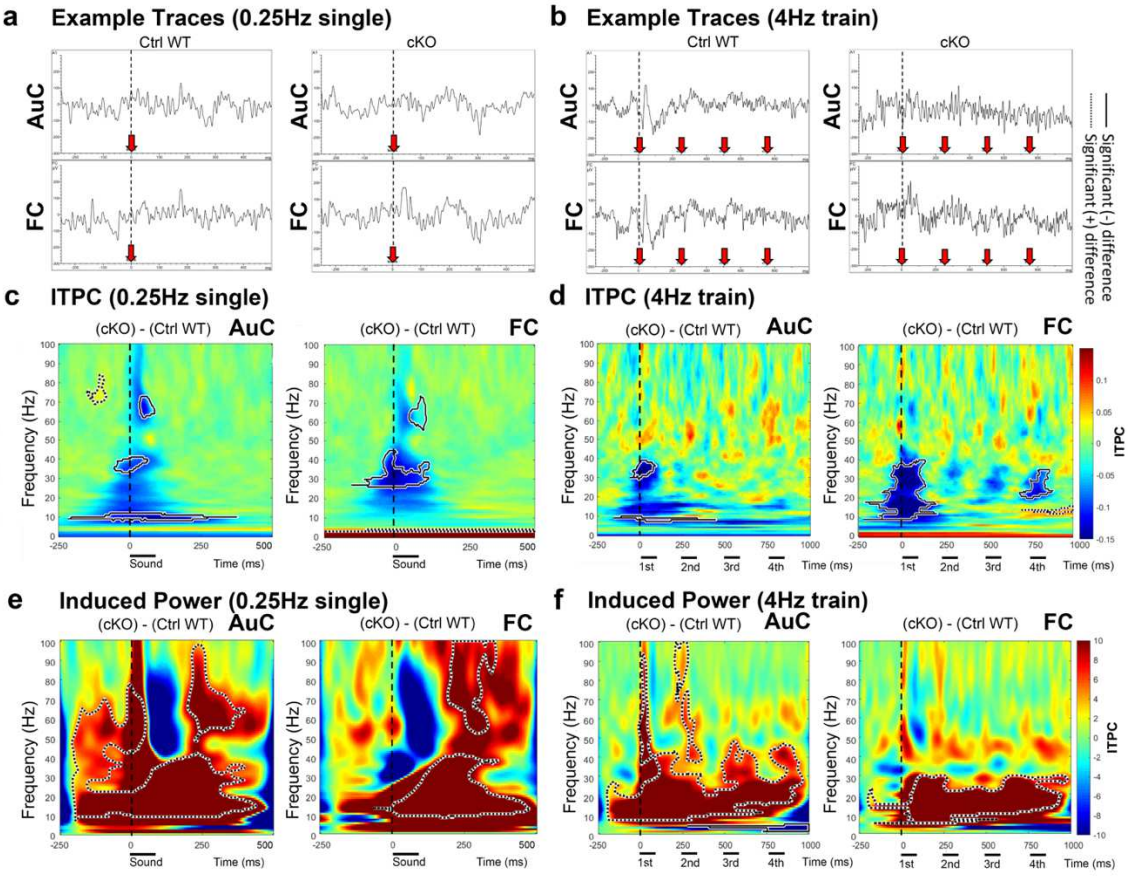
a Example Traces (0.25Hz single)
Ctrl WT
cKO
AuC
FC
b Example Traces (4Hz train)
Ctrl WT
cKO
AuC
FC
Significant (-) difference
Significant (+) difference
c ITPC (0.25Hz single)
(cKO) - (Ctrl WT) AuC
(cKO) - (Ctrl WT) FC
Frequency (Hz)
Sound
Time (ms)
d ITPC (4Hz train)
(cKO) - (Ctrl WT) AuC
(cKO) - (Ctrl WT) FC
1st
2nd
3rd
4th
Time (ms)
ITPC
e Induced Power (0.25Hz single)
(cKO) - (Ctrl WT) AuC
(cKO) - (Ctrl WT) FC
Frequency (Hz)
Sound
Time (ms)
f Induced Power (4Hz train)
(cKO) - (Ctrl WT) AuC
(cKO) - (Ctrl WT) FC
1st
2nd
3rd
4th
Time (ms)
ITPC

Figure 4.14. Developmental deletion of *Fmr1* from astrocytes affects ITPC and induced (baseline corrected) power in response to sound presentation in the auditory and frontal cortex of adult cKO mice.
(A-B) Example traces of responses in AuC and FC to single broadband noise presentation at 0.25Hz (A) and sound train presented at 4 Hz (B) for Ctrl WT and cKO mice. Red arrow indicates onset of 100ms broadband noise. (C-D) Grand average plot of ITPC during single sound presentation at 0.25Hz and sound presentations in 4Hz train were calculated for each genotype, and differences between genotypes (cKO – Ctrl WT) are presented here. Black solid lines indicate duration of 100ms broadband noise. In the AC, there is a decrease in ITPC in the cKO mice at ~8-13Hz (alpha frequencies), ~30-40Hz (low gamma frequencies), and ~60-70Hz (high gamma frequencies) during 0.25 Hz sound presentation. There is also a decrease in ITPC in the cKO mice at ~8-13Hz (alpha frequencies) throughout the first and second sound in the 4 Hz train, and at ~30-40Hz (low gamma frequencies) during the first sound in the 4 Hz train. In the FC, there is a decrease in ITPC in the cKO mice at ~30-40Hz (low gamma frequencies) and ~60-70Hz (high gamma frequencies) during 0.25 Hz sound presentation. **T**here is also a decrease in ITPC in the cKO mice at ~10-40Hz during the first sound in the train, and at ~20-40Hz (low gamma frequencies) during the fourth sound in the 4 Hz train. (E-F) Grand average difference plot of baseline corrected sound-induced power during single sound presentation at 0.25Hz and sound presentations in 4Hz train were calculated for each genotype, and differences between genotypes (cKO – Ctrl WT) are presented here. In both AuC and FC, increased induced power is observed in the cKO mice in response to the sound as well as after sound presentation, indicating increased onset and on-going activity. In addition, increased onset and on-going activity is also observed in AuC and FC of the cKO mice at ~10-40Hz during all four sounds in the 4 Hz train.

Figure 4.15

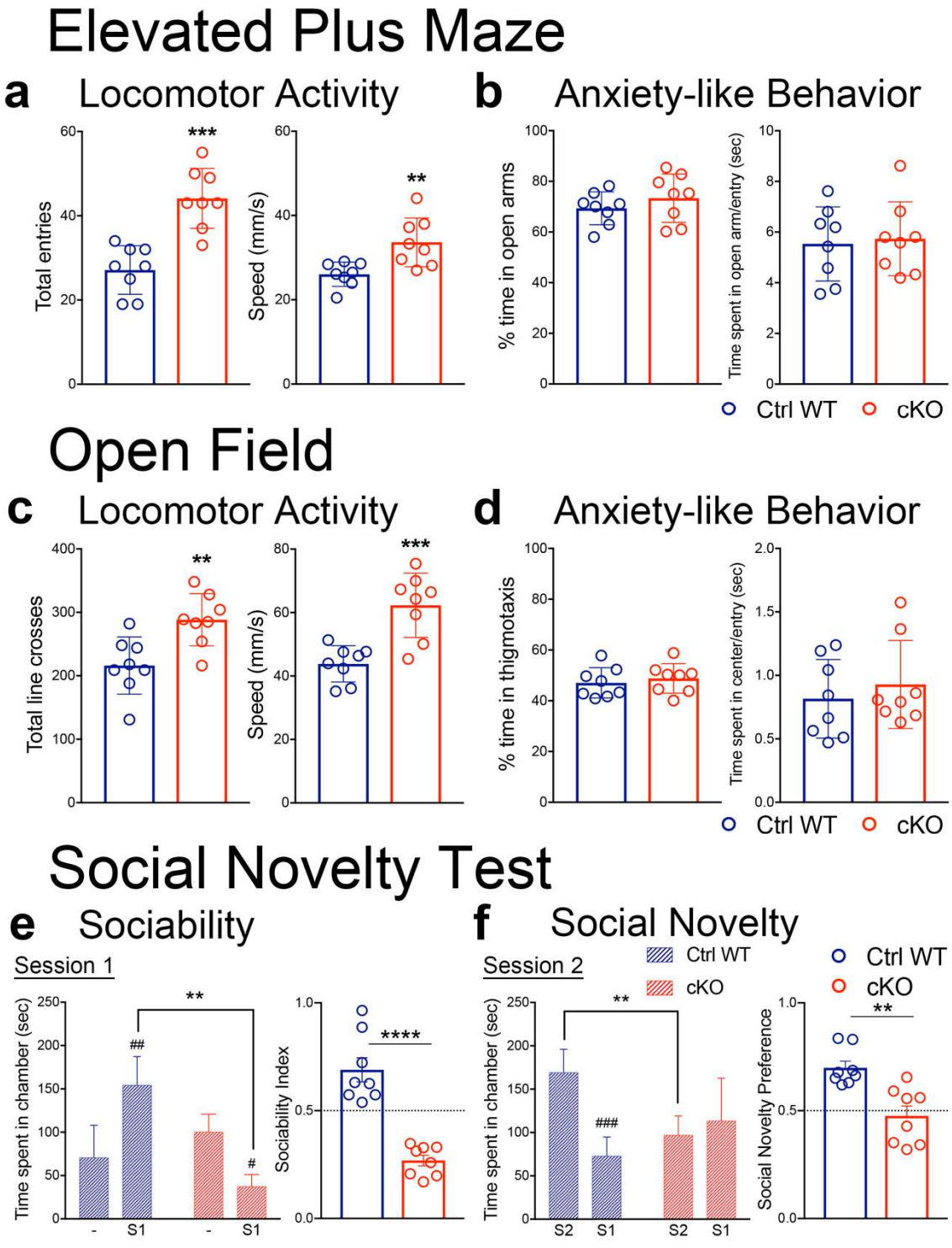
Elevated Plus Maze
a Locomotor Activity
b Anxiety-like Behavior
Total entries
Speed (mm/s)
% time in open arms
Time spent in open arm/entry (sec)
Ctrl WT
cKO
Open Field
c Locomotor Activity
d Anxiety-like Behavior
Total line crosses
Speed (mm/s)
% time in thigmotaxis
Time spent in center/entry (sec)
Ctrl WT
cKO
Social Novelty Test
e Sociability
f Social Novelty
Session 1
Session 2
Time spent in chamber (sec)
Sociability Index
Social Novelty Preference
Ctrl WT
cKO
S1
S2

Figure 4.15. Developmental deletion of *Fmr1* in astrocytes leads to increased locomotor activity and decreased socialization in adult cKO mice.
(A-B) Graphs demonstrate the performance of mice in the elevated plus maze. Locomotor activity is measured by total arm entries and speed (A). Anxiety-like behavior is measured by percentage of time in open arms and time spent in open arm per entry (B). Graphs show mean ± SEM (n=8 mice/group, **p<0.01; ***p<0.001, t-test).
(C-D) Graphs demonstrate the performance of mice in the open field. Locomotor activity is measured by total line crosses and speed (C). Anxiety-like behavior is measured by percentage of time in thigmotaxis and time spent in center per entry (D). Graphs show mean ± SEM (n=8 mice/group, **p<0.01; ***p<0.001, t-test). cKO exhibit higher locomotor activity than Ctrl WT mice (A, C). No changes in anxiety-like behaviors are observed (B, D).
(E-F) Graphs demonstrate the sociability (E) and social novelty preference (F) of mice in the social novelty test. Session 1: preference between an empty chamber and a chamber with S1 mouse during sociability test. Session 2: preference between a chamber with a novel mouse S2 and a chamber with a familiar mouse S1 during social novelty test. Left panels, graphs show time spent in the chambers (mean ± SEM, n=8 mice/group, *p<0.05; **p<0.01, ***p<0.001, two-way ANOVA, Bonferroni *post hoc* test). Right panels, graphs show sociability index (E) or social novelty preference index (F) (**p<0.01, ****p<0.001, t-test). In Session 1, Ctrl WT mice prefer spending time with S1 mouse compared with time in the empty chamber. cKO mice show impaired sociability, reduced sociability index and spend significantly more time in the empty chamber than with S1 mouse. In Session 2, Ctrl WT mice spend significantly more time with novel S2 mouse than with familiar S1 mouse, indicating normal social novelty. cKO mice spend the same amount of time in S1 and S2 chambers, and show reduced social novelty index, indicating impaired social novelty preference.

Table 4.1. Summary table showing: (1) *Fmr1* (exon 16/17) mRNA levels in hippocampus and cortex of Ctrl WT and cKO mice at P28 (mean ± SEM); and (2) FMRP levels in tdTomato labeled astrocytes in the auditory cortex of Ctrl WT and cKO mice at P28 (mean ± SEM). Statistical analysis of differences between cKO and Ctrl WT mice was performed using t-test (unpaired, two-tailed): **p*<0.05, ***p*<0.01, ****p*<0.001. (**H** = hippocampus; **C1** = Cortex 1; **C2** = Cortex 2; **AuC** = auditory cortex)

	Ctrl WT	**cKO**
Fmr1 mRNA levels (**H**)	1 ± 0.12	0.63 ± 0.05 t(5) = 3.095 **p*=0.0270
Fmr1 mRNA levels (**C1**)	1 ± 0.03	0.70 ± 0.05 t(6) =5.005 ***p*=0.0024
Fmr1 mRNA levels (**C2**)	1 ± 0.12	0.64 ± 0.03 t(6) =2.874 **p*=0.0283
FMRP levels in astrocytes (**AuC**)	14.3 ± 0.96	1.76 ± 0.11 t(4) =12.93 ****p*=0.0002

Table 4.2. Summary table showing synaptic $GABA_A$ receptor mRNA and protein levels in the developing hippocampus and cortex of Ctrl WT and cKO mice (mean ± SEM). Statistical analysis of differences between cKO and Ctrl WT mice was performed using t-test (unpaired, two-tailed): **p*<0.05, ***p*<0.01, ****p*<0.001. (**H** = hippocampus; **C1** = Cortex 1; **C2** = Cortex 2)

	Ctrl WT	**cKO**
Gabra1 mRNA (**H**)	1 ± 0.07	0.69 ± 0.07 t(6) = 2.982; **p*=0.0246
Gabra1 mRNA (**C1**)	1 ± 0.14	0.50 ± 0.09 t(6) =2.958; **p*=0.0254
Gabra1 mRNA (**C2**)	1 ± 0.16	0.31 ± 0.05 t(6) =4.085; ***p*=0.0065
Gabra3 mRNA (**H**)	1 ± 0.05	0.49 ± 0.16 t(6) =3.12; **p*=0.0206
Gabra3 mRNA (**C1**)	1 ± 0.12	0.48 ± 0.05 t(6) =3.931; ***p*=0.0077
Gabra3 mRNA (**C2**)	1 ± 0.14	0.37 ± 0.07 t(6) =4.115; ***p*=0.0062
Gabrg2 mRNA (**H**)	1 ± 0.06	0.73 ± 0.08 t(6) =2.544; **p*=0.0438
Gabrg2 mRNA (**C1**)	1 ± 0.12	0.42 ± 0.09 t(6) =3.726; ***p*=0.0098
Gabrg2 mRNA (**C2**)	1 ± 0.10	0.47 ± 0.07 t(6) =4.409; ***p*=0.0045
$GABA_AR\gamma2$ protein (**H**)	1 ± 0	0.68 ± 0.04 t(6) =6.961; ****p*=0.0004
$GABA_AR\gamma2$ protein (**C1**)	1 ± 0	0.70 ± 0.07 t(6) =3.917; ***p*=0.0078
$GABA_AR\gamma2$ protein (**C2**)	1 ± 0	0.80 ± 0.05 t(6) =3.48; **p*=0.0131

Table 4.3. Summary table showing: (1) total GABA levels; (2) expression levels of GABA-synthesizing enzymes; and (3) GABA levels in GS-labeled astrocytes in developing hippocampus and cortex of Ctrl WT and cKO mice (mean ± SEM). Statistical analysis of differences between cKO and Ctrl WT mice was performed using t-test (unpaired, two-tailed): *p<0.05, **p<0.01, ***p<0.001. (**H** = hippocampus; **C1** = Cortex 1; **C2** = Cortex 2; **AuC** = auditory cortex; **FC** = frontal cortex)

	Ctrl WT	**cKO**
GABA Concentration (**H**)	73 ± 1.8	82 ± 1.0 t(6) = 4.504; **p=0.0041
GABA Concentration (**C1**)	34 ± 2.1	47 ± 4.4 t(6) =2.472; *p=0.0483
GABA Concentration (**C2**)	57 ± 1.6	69 ± 1.5 t(6) =5.544; **p=0.0015
Aldh1a1 mRNA (**H**)	1 ± 0.04	1.58 ± 0.05 t(6) =8.661; ***p=0.0001
Aldh1a1 mRNA (**C1**)	1 ± 0.07	1.77 ± 0.28 t(6) =2.665; *p=0.0373
Aldh1a1 mRNA (**C2**)	1 ± 0.08	1.62 ± 0.09 t(6) =4.724; **p=0.0032
DAO mRNA (**H**)	1 ± 0.08	1.64 ± 0.16 t(5) =3.259; *p=0.0225
DAO mRNA (**C1**)	1 ± 0.12	1.61 ± 0.02 t(6) =5.06; **p=0.0023
DAO mRNA (**C2**)	1 ± 0.08	1.53 ± 0.14 t(6) =3.263; *p=0.0172
GFAP mRNA (**H**)	1 ± 0.05	1.38 ± 0.13 t(6) =2.714; *p=0.0349
GFAP mRNA (**C1**)	1 ± 0.15	1.54 ± 0.12 t(6) =2.787; *p=0.0317
GFAP mRNA (**C2**)	1 ± 0.12	1.59 ± 0.13 t(6) =3.373; *p=0.0150
GFAP protein (**H**)	1 ± 0	0.98 ± 0.04 p=0.6773
GFAP protein (**C1**)	1 ± 0	1.07 ± 0.09 p=0.5000
GFAP protein (**C2**)	1 ± 0	1.23 ± 0.05 t(6) =4.003; **p=0.0071
GABA levels in astrocytes (**CA1 H**)	26 ± 2.1	42 ± 2.6 t(6) =4.772; **p=0.0031

GABA levels in astrocytes (**FC**)	15 ± 1.9	25 ± 1.5 t(6) =3.928; ***p*=0.0077
GABA levels in astrocytes (**AuC**)	18 ± 1.7	28 ± 1.5 t(6) =4.633; ***p*=0.0036

Table 4.4. Summary table showing: (1) PV, Erb4, NRG-3, and TrkB mRNA levels; and (2) PV and ErbB4 protein levels in developing hippocampus and cortex of Ctrl WT and cKO mice (mean ± SEM). Statistical analysis of differences between cKO and Ctrl WT mice was performed using t-test (unpaired, two-tailed): *p<0.05, **p<0.01, ***p<0.001. (**H** = hippocampus; **C1** = Cortex 1; **C2** = Cortex 2)

	Ctrl WT	**cKO**
PV mRNA (**H**)	1 ± 0.07	0.59 ± 0.10 t(5) = 2.973; *p=0.0311
PV mRNA (**C1**)	1 ± 0.09	0.42 ± 0.06 t(6) =5.366; **p=0.0017
PV mRNA (**C2**)	1 ± 0.08	0.36 ± 0.09 t(6) =5.18; **p=0.0021
ErbB4 mRNA (**H**)	1 ± 0.09	0.56 ± 0.03 t(5) =5.023; **p=0.0040
ErbB4 mRNA (**C1**)	1 ± 0.10	0.44 ± 0.08 t(6) =4.326; **p=0.0050
ErbB4 mRNA (**C2**)	1 ± 0.13	0.52 ± 0.03 t(6) =3.459; *p=0.0135
NRG-3 mRNA (**H**)	1 ± 0.06	0.55 ± 0.04 t(5) =6.524; **p=0.0013
NRG-3 mRNA (**C1**)	1 ± 0.13	0.51 ± 0.06 t(6) =3.404; *p=0.0144
NRG-3 mRNA (**C2**)	1 ± 0.15	0.52 ± 0.04 t(6) =3.03; *p=0.0231
TrkB mRNA (**H**)	1 ± 0.05	1.59 ± 0.10 t(5) =4.531; **p=0.0062
TrkB mRNA (**C1**)	1 ± 0.07	1.69 ± 0.13 t(6) =4.643; **p=0.0035
TrkB mRNA (**C2**)	1 ± 0.12	1.56 ± 0.18 t(6) =2.637; *p=0.0387
PV protein (**H**)	1 ± 0	0.87 ± 0.17 p=0.4814
PV protein (**C1**)	1 ± 0	0.76 ± 0.03 t(6) =7.51; ***p=0.0003
PV protein (**C2**)	1 ± 0	0.78 ± 0.06 t(6) =3.602; *p=0.0113
ErbB4 protein (**H**)	1 ± 0	0.59 ± 0.11 t(6) =2.965; *p=0.0314
ErbB4 protein (**C1**)	1 ± 0	0.88 ± 0.08 p=0.1890

ErbB4 protein (**C2**)	1 ± 0	1.002 ± 0.07 *p*=0.9783

Table 4.5. Summary table showing: (1) vGlut1/PSD95 co-localization onto tdTomato-expressing PV inhibitory interneurons; and (2) vGAT/Gephyrin, PV/Gephyrin and vGAT/PV puncta co-localization in developing auditory cortex of Ctrl WT and cKO mice (mean ± SEM). Statistical analysis of differences between cKO and Ctrl WT mice was performed using t-test (unpaired, two-tailed): *p<0.05, **p<0.01.
(**AuC** = auditory cortex)

	Ctrl WT	**cKO**
vGlut1/PSD95 co-localization onto PV (**AuC**)	54.8 ± 2.87	38.2 ± 2.03 t(2) =4.727; *p=0.0420
vGAT/Gephyrin co-localization (**AuC**)	8.85 ± 1.43	5.01 ± 0.14 t(6) =2.672; *p=0.0369
PV/Gephyrin co-localization (**AuC**)	6.19 ± 1.10	1.49 ± 0.15 t(6) =4.227; **p=0.0055
vGAT/PV co-localization (**AuC**)	23.5 ± 4.24	4.58 ± 0.17 t(6) =4.459; **p=0.0043

Table 4.6. Summary table showing statistical analysis of differences in the gamma, low gamma, and high gamma bands in auditory cortex and frontal cortex of adult Ctrl WT and cKO mice. Statistical analysis was performed using MANCOVA. When multiple comparisons for MANCOVA were made, genotype comparisons were corrected using Bonferroni adjustments. The divisor for Bonferroni correction for multiple comparisons (for 6 frequency bands) was set to 6, $\alpha = 0.05/6 = 0.0083$.
(**AuC** = auditory cortex; **FC** = frontal cortex)

	cKO vs. Ctrl WT
AuC Gamma	$F(1,16) = 38.383$; ****$p<0.00001$; $\eta^2 = 0.706$
AuC Low Gamma	$F(1,16) = 33.882$; ***$p=0.00003$; $\eta^2 = 0.679$
AuC High Gamma	$F(1,16) = 27.222$; ***p=0.00004; $\eta^2 = 0.630$
FC Gamma	$F(1,16) = 22.283$; **$p=0.00023$; $\eta^2 = 0.582$
FC Low Gamma	$F(1,16) = 10.708$; *$p=0.005$; $\eta^2 = 0.401$
FC High Gamma	$F(1,16) = 16.739$; **$p=0.001$; $\eta^2 = 0.511$

Table 4.7. Summary table showing Pearson's correlation (r) of power coupling of different oscillation frequencies in auditory cortex and frontal cortex of adult Ctrl WT and cKO mice (mean ± SEM). Statistical analysis of differences between cKO and Ctrl WT mice was performed using t-test (unpaired, two-tailed): *p<0.05, **p<0.01. (**AuC** = auditory cortex; **FC** = frontal cortex)

	Ctrl WT	**cKO**
AuC Delta/Gamma D1G1	0.29 ± 0.07	-0.10 ± 0.13 t(17) = 2.855; *p=0.0110
AuC Theta/Gamma T1G1	0.25 ± 0.07	-0.005 ± 0.09 t(17) =2.224; *p=0.0400
AuC Alpha/Gamma A1G1	0.31 ± 0.08	0.08 ± 0.06 t(17) =2.161; *p=0.0452
FC Delta/Gamma D2G2	0.29 ± 0.06	-0.017 ± 0.12 t(17) =2.294; *p=0.0348
AuC Delta/FC Gamma D1G2	0.31 ± 0.07	-0.106 ± 0.11 t(17) =3.123; **p=0.0062
AuC Theta/FC Gamma T1G2	0.24 ± 0.06	0.0007 ± 0.09 t(17) =2.11; *p=0.0499
FC Delta/AuC Gamma D2G1	0.29 ± 0.06	0.008 ± 0.12 t(17) =2.127; *p=0.0483

Table 4.8. Summary table showing locomotor activity and anxiety-like behaviors of adult Ctrl WT and cKO mice using elevated plus maze (EP) and open-field (OF) behavior tests (mean ± SEM). Statistical analysis of differences between cKO and Ctrl WT mice was performed using t-test (unpaired, two-tailed): $**p<0.01$, $***p<0.001$.

	Ctrl WT	**cKO**
Total entries (EP)	27 ± 2.0	44 ± 2.5 t(14) =5.247; ***p=0.0001
Speed (EP)	26 ± 1.0	34 ± 2.1 t(14) =3.319; **p=0.0051
Time spent in open arm/entry (EP)	5.5 ± 0.5	5.7 ± 0.5 p=0.7845
% Time in open arms (EP)	69 ± 2.3	73 ± 3.4 p=0.3423
Total line crosses (OF)	216 ± 16	288 ± 14 t(14) =3.346; **p=0.0048
Speed (OF)	44 ± 2.2	62 ± 3.3 t(14) =4.477; ***p=0.0005
Time spent in center/entry (OF)	0.82 ± 0.11	0.93 ± 0.12 p=0.5034
% Time in thigmotaxis (OF)	47 ± 2.1	49 ± 2.1 p=0.5596

Table 4.9. Summary table showing sociability (Session 1) and social novelty preference (Session 2) of adult Ctrl WT and cKO mice using the social novelty behavior test (mean ± SEM). Statistical analysis of differences between cKO and Ctrl WT mice was performed using two-way ANOVA followed by Bonferroni multiple comparison post-test for "time spent in chamber" comparisons; and using t-test (unpaired, two-tailed) for sociability and social novelty preference index comparisons: *p<0.05, **p<0.01, ***p<0.001, ****p< 0.0001 for genotype comparison; $^{\#}p$<0.05, $^{\#\#}p$<0.01, $^{\#\#\#}p$<0.001, $^{\#\#\#\#}p$<0.0001 for chamber comparison.

	Ctrl WT	**cKO**
Time spent in empty chamber	71 ± 13	100 ± 7.2
Time spent with stranger mouse (S1)	154 ± 12 $^{\#\#}p$=0.0090	38 ± 4.8 **p=0.0012 $^{\#}p$=0.0408
Sociability index	0.69 ± 0.05	0.27 ± 0.02 t(14) = 6.914; ****p<0.0001
Time spent with novel mouse (S2)	169 ± 9	97 ± 8 **p=0.0031
Time spent with familiar mouse (S1)	73 ± 8 $^{\#\#\#}p$=0.0005	114 ± 17
Social novelty preference index	0.70 ± 0.03	0.48 ± 0.05 t(14) = 4.059; **p=0.0012

Table 4.10. List of primer sequences used for qRT-PCR

Gene	Forward primer sequence (5′–3′)	Reverse primer sequence (5′–3′)
Fmr1 (exon 16/17)	CCGAACAGATAATCGTCCACG	ACGCTGTCTGGCTTTTCCTTC
Gabra1	CAGAAAAGCCAAAGAAAGTAAAGGA	TGGTTGCTGTAGGAGCATATGTG
Gabra3	GCTGCTCAGACTGGTAGATAATGG	GGGCATTCAGCGTGTATTGTT
Gabrg2	CCTGCCCCCTGGAGTTCT	ACTGCGCTTCCATTGATAAACA
Gabra4	GGCAGACTGTATCAAGCGAGACT	GGTGGAAGTAAACCGTCATAACAA
Gabra5	GCAGACAGTAGGCACTGAGAACA	GGAAGTGAGCAGTCATGATCGTAT
Gabrd	TGACCATATCTCAGAGGCAAACA	CCGCCAGCTCTGATGCA
Aldh1a1	TGTTAGCTGATGCCGACTTG	TTCTTAGCCCGCTCAACACT
DAO	CTGCTAACCATGTTCATGC	GTGTTTGAAGGTCCAGTGC
GFAP	CAACGTTAAGCTAGCCCTGGACAT	CTCACCATCCCGCATCTCCACAGT
PV	GGCCTGAAGAAAAAGAACCCG	ATCTTGCCGTCCCCATCCTT
ErbB4	CACGAACACAAGGATAACATCGG	ACATTGCGGGCTGCCAG
TrkB	CCGGCTTAAAGTTTGTGGCTTAC	GGATCAGGTCAGACAAAGTCAAG
NRG-3	CTACCAAGGAGTCCGTTGTGA	TTGACTCCATTATTTTCTTCA
GAPDH	ACTCCACTCACGGCAAATTC	TCTCCATGGTGGTGAAGACA

Chapter 5 – Conclusions and Future Studies

Hyperarousal and anxiety in humans with FXS may be linked to strong reactions to sensory stimuli. There is an abundance of evidence describing sensory cortical dysfunctions in the *Fmr1* KO mice and in humans with FXS. The common underlying phenotype is "sensory hypersensitivity", including hypersensitivity to visual, auditory or tactile stimuli that may lead to behavioral alterations such as poor eye contact, avoidance of noisy places, anxiety and impaired social reciprocity. These alterations in sensory processing appear to be a universal problem in individuals with FXS, as they cause impairment in processing and encoding of many types of sensory information, which may affect more complex social behaviors. Moreover, sensory processing disorders could occur because of dysfunction at multiple levels of each sensory system. The *Fmr1* KO mice also display deficiencies in sensory processing that may help to understand the mechanism of sensory hypersensitivity in FXS. Mechanisms underlying the sensory hypersensitivity may be relatively more tractable compared to more complex social behaviors typically studied in FXS. Therefore, it is of critical importance to use sensory hypersensitivity as a robust, reliable, and translatable phenotype to integrate pre-clinical and clinical investigations at multiple levels of analysis to facilitate drug discovery in FXS.

Indeed, studies of mouse sensory hypersensitivity neurobehavioral phenotypes have led to a better understanding of circuit level pathophysiology in FXS. The heightened sensory activity seen in humans with FXS may stem from a concurrence of dysfunctional intrinsic excitability and/or impaired inhibition due to a loss or abnormal

development of inhibitory neurons, abnormal dendrite morphology, or reduced GABAergic activity. The molecular and cellular mechanisms of circuit hyperexcitability are beginning to be understood. *Fmr1* KO mouse somatosensory and auditory cortex show weakened inhibitory interneuron activity and more excitable pyramidal neurons that may underlie changes in sensory and high order cognitive behaviors seen in *Fmr1* KO mice. Disrupted cytoarchitecture of sensory circuits in *Fmr1* KO mice during early development may impair the ability of mice to integrate sensory experiences leading to abnormal sensory circuit development, learning and high order cognitive skills that persists into adulthood.

FXS is a neurodevelopmental disorder, but the mechanisms of impaired development of functional neural response selectivity to sensory stimuli are still unclear. The predominant focus of published work in the FXS field has been on characterizing the changes in dendritic spine properties and synaptic or intrinsic properties of neurons. However, the consequence of these synaptic changes to development of behaviorally relevant neural response properties in FXS are not known. Therefore, it is not clear if the observed sensory hypersensitivity in humans with FXS is due to an altered regulation of developmental processes during critical plasticity period that persists into adulthood. The majority of studies using *Fmr1* KO mice focus on the neuronal responses and behaviors during a specific developmental window or in adult mice, while neglecting to look at any long-term changes in *Fmr1* KO mice from early development into adulthood and the long-term impact of early treatment to reverse FXS-associated behavioral deficits. Is the loss of FMRP only detrimental during a critical plasticity period or are the changes

attributed to the on-going absence of FMRP? A recent finding, that eliminating FMRP in only the prefrontal cortex of adult mice can lead to abnormal learning, suggests FMRP continues to plays a role in neural function even after critical plasticity period ends (Siegel et al., 2017). In addition, some phenotypes are reversed in the adult animal models by acute pharmacological treatments. However, it is not clear whether the acute effects are long-lasting. Moreover, chronic treatments may result in drug tolerance. Further studies are needed to determine developmental versus adult effects of FMRP loss on cortical responses in order to identify specific time windows, which can be targeted therapeutically.

Questions on whether the animal models are appropriate to study human neurological disorders have arisen due to the inability to translate preclinical therapeutic success to the clinic (Dahlhaus, 2018). Indeed it is important to compare multiple model systems for any neurological disorder. Regardless of the animal model studied (even in non-human primates), the manifestation of cognitive and social symptoms will depend on underlying circuits that are quite different across species. The development of these circuits is also difficult to probe. Sensory processing circuits and mechanisms are more likely to show relatively more similarities. This is seen in FXS studies that show very similar baseline and sound evoked EEG phenotypes in mice and humans (Ethridge et al., 2017; Lovelace et al., 2016; Schneider et al., 2013; Sinclair, Oranje, Razak, Siegel, & Schmid, 2017; Wang et al., 2017). In addition, few studies of FXS (in humans and mice) have quantified developmental trajectories and roles of FMRP. Again, when additional model systems are studied, it is imperative to analyze changes in circuit function over

development. Therefore, my findings conclude that development of sensory hypersensitivity may be used as a neurobehavioral probe to more successfully evaluate and translate drug treatments from pre-clinical models to humans, as well as underlying mechanisms of FXS-associated deficits.

References

Dahlhaus, R. (2018). Of Men and Mice: Modeling the Fragile X Syndrome. *Front Mol Neurosci, 11*, 41. doi:10.3389/fnmol.2018.00041

Ethridge, L. E., White, S. P., Mosconi, M. W., Wang, J., Pedapati, E. V., Erickson, C. A., . . . Sweeney, J. A. (2017). Neural synchronization deficits linked to cortical hyper-excitability and auditory hypersensitivity in fragile X syndrome. *Mol Autism, 8*, 22. doi:10.1186/s13229-017-0140-1

Lovelace, J. W., Wen, T. H., Reinhard, S., Hsu, M. S., Sidhu, H., Ethell, I. M., . . . Razak, K. A. (2016). Matrix metalloproteinase-9 deletion rescues auditory evoked potential habituation deficit in a mouse model of Fragile X Syndrome. *Neurobiol Dis, 89*, 126-135. doi:10.1016/j.nbd.2016.02.002

Schneider, A., Leigh, M. J., Adams, P., Nanakul, R., Chechi, T., Olichney, J., . . . Hessl, D. (2013). Electrocortical changes associated with minocycline treatment in fragile X syndrome. *J Psychopharmacol, 27*(10), 956-963. doi:10.1177/0269881113494105

Siegel, J. J., Chitwood, R. A., Ding, J. M., Payne, C., Taylor, W., Gray, R., . . . Johnston, D. (2017). Prefrontal Cortex Dysfunction in Fragile X Mice Depends on the Continued Absence of Fragile X Mental Retardation Protein in the Adult Brain. *J Neurosci, 37*(31), 7305-7317. doi:10.1523/JNEUROSCI.0571-17.2017

Sinclair, D., Oranje, B., Razak, K. A., Siegel, S. J., & Schmid, S. (2017). Sensory processing in autism spectrum disorders and Fragile X syndrome-From the clinic to animal models. *Neurosci Biobehav Rev, 76*(Pt B), 235-253. doi:10.1016/j.neubiorev.2016.05.029

Wang, J., Ethridge, L. E., Mosconi, M. W., White, S. P., Binder, D. K., Pedapati, E. V., . . . Sweeney, J. A. (2017). A resting EEG study of neocortical hyperexcitability and altered functional connectivity in fragile X syndrome. *J Neurodev Disord, 9*, 11. doi:10.1186/s11689-017-9191-z